

1-1-1989

PH-dependent structural reorganization of phosphatidylcholine bilayer membranes by poly(2-ethylacrylic acid)/

Keith A. Borden

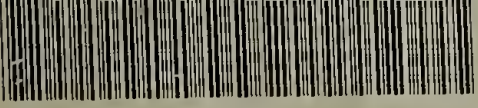
University of Massachusetts Amherst

Follow this and additional works at: https://scholarworks.umass.edu/dissertations_1

Recommended Citation

Borden, Keith A., "PH-dependent structural reorganization of phosphatidylcholine bilayer membranes by poly(2-ethylacrylic acid)/" (1989). *Doctoral Dissertations 1896 - February 2014*. 746.
https://scholarworks.umass.edu/dissertations_1/746

This Open Access Dissertation is brought to you for free and open access by ScholarWorks@UMass Amherst. It has been accepted for inclusion in Doctoral Dissertations 1896 - February 2014 by an authorized administrator of ScholarWorks@UMass Amherst. For more information, please contact scholarworks@library.umass.edu.



312066007581431

pH-DEPENDENT STRUCTURAL REORGANIZATION OF
PHOSPHATIDYLCHOLINE BILAYER MEMBRANES BY
POLY(2-ETHYLACRYLIC ACID)

A Dissertation Presented

by

KEITH A. BORDEN

Submitted to the Graduate School of the
University of Massachusetts in partial fulfillment
of the requirements for the degree of

DOCTOR OF PHILOSOPHY

May 1989

Polymer Science and Engineering

© Copyright by Keith Alan Borden 1989

All Rights Reserved

pH-DEPENDENT STRUCTURAL REORGANIZATION OF
PHOSPHATIDYLCHOLINE BILAYER MEMBRANES BY
POLY(2-ETHYLACRYLIC ACID)

A Dissertation Presented

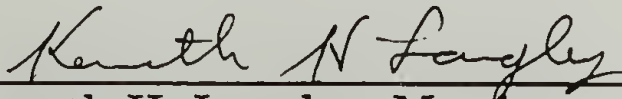
by

KEITH A. BORDEN

Approved as to style and content by:



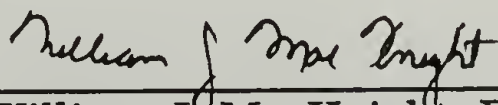
David A. Tirrell, Chairperson of Committee



Kenneth H. Langley, Member



David A. Hoagland, Member



William J. MacKnight, Department Head
Polymer Science and Engineering

This dissertation is dedicated to my parents, Warne and Sandra Borden.

ACKNOWLEDGEMENTS

First and foremost I must thank my research advisor, Professor David Tirrell, for his guidance and support. His wit, his subtle means of persuasion, and his persistent efforts to keep me on track were greatly appreciated.

I am grateful to Professors Kenneth Langley and David Hoagland for serving as dissertation committee members. I would also like to thank Dr. Julia S. Tan and Dr. Peter A. Martic of the Eastman Kodak Research Laboratories for their invaluable contributions to this work. I am indebted to the Eastman Kodak Co. for allowing me to work in the laboratories of the Life Sciences Division and for the financial support they provided. I am also indebted to Connie L. Voycheck of the Eastman Kodak Laboratories, who was instrumental in obtaining the electron micrographs presented in this work. The contributions of Karen I. Winey to this work are also gratefully acknowledged. I would like to thank Rajan, Glenn, and Sharon for their efforts in helping me get started as a research scientist.

Special thanks go to everyone in the Polymer Science and Engineering Department and their friends who participated in the weekly Ultimate Frisbee games for the past four years. This activity was one of the most enjoyable aspects of my graduate career. I will miss the camaraderie.

For all of their love and support, and the good times we have together which keep me going, I would like to thank my entire family; my grandparents, my aunts and uncles, my cousins, my in-laws, and especially mom, dad, Scott, Kelli, Kevin, Stephen, Sean, Kurt, and Stacy. Lastly, I thank Robyn for all she has done to help me through my graduate career.

ABSTRACT

pH-DEPENDENT STRUCTURAL REORGANIZATION OF PHOSPHATIDYLCHOLINE BILAYER MEMBRANES BY POLY(2-ETHYLACRYLIC ACID)

MAY 1989

KEITH ALAN BORDEN, B.S., CARNEGIE-MELLON UNIVERSITY

Ph.D., UNIVERSITY OF MASSACHUSETTS

Directed by: Professor David A. Tirrell

The mechanism of the pH-dependent polyelectrolyte-induced structural reorganization of phospholipid vesicles was investigated. The study focused on the pH-dependent interaction of poly(2-ethylacrylic acid) (PEAA) with vesicles formed from L- α -dipalmitoylphosphatidylcholine (DPPC). The relationship between the conformational properties of the PEAA and the structural reorganization process was discerned through the use of fluorescence spectroscopy, potentiometric titration, and turbidity measurements. The pH-dependent interaction was characterized with the techniques of transmission electron microscopy, differential scanning calorimetry, and several photophysical techniques including fluorescence polarization, fluorescence lifetime measurements, and intramolecular excimer formation.

Experiments have shown that it is the pH-dependent conformational collapse of the PEAA chain which leads to the structural reorganization of the DPPC vesicles. Transmission electron microscopy shows the reorganization products to be disk-like mixed micelles with average dimensions of 54 Å thickness and 160 Å diameter. The composition of the

PEAA/DPPC mixed micelles was determined to be 40-80 mol DPPC/mol PEAA (PEAA $M_n = 20,000$ g/mol). The reorganization phenomenon is a two stage process. Initial reduction of pH leads to the interaction of the PEAA in an expanded coil conformation with the surface of the DPPC vesicle. Subsequent lowering of pH results in the conformational collapse of the PEAA chain with concomitant formation of PEAA/DPPC mixed micelles.

TABLE OF CONTENTS

| | page |
|-----------------------------------------------------------------------------------------------------------------|------|
| ACKNOWLEDGMENTS..... | v |
| ABSTRACT | vi |
| LIST OF TABLES | xi |
| LIST OF FIGURES | xii |
| Chapter | |
| I. INTRODUCTION | 1 |
| A. Responsive Systems..... | 1 |
| B. Phospholipid Vesicles..... | 2 |
| C. Interaction of Poly(carboxylic acid)s with Phospholipid Vesicles. | 5 |
| D. Conformational Behavior of Poly(carboxylic acid)s..... | 8 |
| E. Use of Fluorescence Spectroscopy to Monitor Conformational Transitions..... | 9 |
| F. Fluorescence Polarization of Probe Molecules in Surfactant Bilayers..... | 13 |
| G. Fluorescence Energy Transfer..... | 15 |
| H. Other Fluorescence Spectroscopic Techniques..... | 15 |
| I. Overview..... | 20 |
| II. EXPERIMENTAL SECTION | 27 |
| A Routine Measurements | 27 |
| B Materials | 27 |
| C Methods..... | 30 |
| 1. Synthesis of poly(2-ethylacrylic acid) {PEAA}..... | 30 |
| a. Synthesis of 2-ethylacrylic acid..... | 30 |
| b. Polymerization of 2-ethylacrylic acid..... | 30 |
| 2. Synthesis of poly(2-ethylacrylic acid) with a pyrene chromophore. | 31 |
| a. Synthesis of poly(2-ethylacrylic acid-co-1- pyreneacrylic acid) {PEAA-py1}. | 31 |
| b. Synthesis of poly(2-ethylacrylic acid-co- 2-(4-(1-pyrene)butanoyl)aminopropenoic acid) {PEAA-py2}..... | 32 |
| 3. Synthesis of poly(2-ethylacrylic acid) containing tryptophan {PEAA-trp}. | 33 |

| | | |
|----------------------------------|----------------------------------------------------------------------------------------------------|-----|
| 4. | Preparation of vesicle samples..... | 34 |
| | a. Multilamellar vesicles. | 34 |
| | b. Sonicated vesicles..... | 34 |
| 5. | Preparation of samples for fluorescence spectroscopy..... | 34 |
| | a. Fluorescence studies with pyrene..... | 34 |
| | b. Fluorescence studies with PEAA-bound pyrene {PEAA-py}. | 35 |
| | c. Fluorescence studies with 1,3-bis- (1-pyrene)propane {Py ₂ C ₃ }. | 36 |
| | d. Fluorescence polarization studies with DPH. | 36 |
| | e. Fluorescence polarization studies with DPHPC..... | 38 |
| | f. Fluorescence polarization studies with PyPC. | 38 |
| | g. Fluorescence polarization studies with Py-DPPE. | 38 |
| | h. Fluorescence energy transfer studies with PEAA-trp and AMC..... | 39 |
| 6. | Potentiometric titration..... | 39 |
| 7. | Electron microscopy | 40 |
| 8. | Differential scanning calorimetry..... | 40 |
| 9. | Determination of PEAA-DPPC mixed micelle composition..... | 41 |
| | a. Samples with PEAA and sonicated DPPC vesicles..... | 41 |
| | b. Samples with PEAA and multilamellar DPPC vesicles..... | 41 |
| 10. | Binding of PEAA to DPPC Vesicles..... | 42 |
| | a. Binding as a function of solution pH..... | 42 |
| | b. Binding as a function of DPPC concentration. | 43 |
| III. RESULTS AND DISCUSSION..... | | 44 |
| A. | Goals and Accomplishments..... | 44 |
| B. | Morphological Characterization of the PEAA-DPPC System..... | 44 |
| C. | Conformational Behavior of PEAA in Aqueous Solution..... | 55 |
| D. | Conformational Behavior of PEAA in DPPC Suspensions..... | 69 |
| E. | Potentiometric Titration of PEAA and PEAA-py Solutions..... | 89 |
| F. | The pH-Dependent Binding of PEAA and DPPC..... | 102 |
| G. | Concentration-Dependent Binding of PEAA-py to DPPC Vesicles..... | 112 |

| | |
|---------------------------------------------------------------------------------------------------------------------------------------------------------------|-----|
| H. Fluorescence Polarization Experiments..... | 118 |
| 1. Use of Diphenylhexatriene | 120 |
| 2. Use of 3-Palmitoyl-2-(3-(diphenylhexatrienyl) propanoyl-L- α - phosphatidylcholine (DPHPC) | 124 |
| 3. Use of 3-Palmitoyl-2-(1-pyrenedecanoyl)-L- α - phosphatidylcholine (PyPC)..... | 126 |
| 4. Use of N-(1-pyrenesulfonyl)dipalmitoyl-L- β - phosphatidylethanolamine (Py-DPPE) | 131 |
| I. Monitoring Bilayer Properties with an Intramolecular Excimer Forming Probe : Use of 1,3-bis-(1-pyrene)propane (Py ₂ C ₃)..... | 133 |
| J. Fluorescence Behavior of Pyrene in PEAA/DPPC Mixtures..... | 137 |
| K. Fluorescence Energy Transfer in the PEAA + DPPC System..... | 141 |
| L. Differential Scanning Calorimetry of the PEAA + DPPC System. | 145 |
| M. Characterization of PEAA/DPPC Mixed Micelles..... | 151 |
| 1. Comparison to Other DPPC Mixed Micelles..... | 151 |
| 2. Phase Transition Behavior..... | 156 |
| 3. Composition of the PEAA/DPPC Mixed Micelles..... | 157 |
| IV. CONCLUSIONS | 165 |
| V. FUTURE WORK | 168 |
| REFERENCES..... | 171 |
| BIBLIOGRAPHY..... | 177 |

LIST OF TABLES

| | page |
|---------------------------------------------------------------------------------------------------------------------------------------------------------------------------------------------------------------------|------|
| Table 3.1 Polarization of DPH fluorescence and the ratio of monomer to excimer fluorescence of Py_2C_3 in aqueous solutions of various micelle forming molecules..... | 153 |
| Table 3.2 Polarization of fluorescence from DPH, DPHPC and Py-DPPE, and the ratio of monomer to excimer fluorescence of Py_2C_3 in aqueous solutions of various DPPC mixed micellar structures..... | 154 |

LIST OF FIGURES

| | page |
|-------------|-----------------------------------------------------------------------------------------------------------------------------------|
| Figure 1.1 | Formation of vesicular structures via the dispersion of phospholipid molecules in aqueous solution..... 3 |
| Figure 1.2 | Phase transitions in phospholipid bilayers as detected by differential scanning calorimetry (DSC)..... 4 |
| Figure 1.3 | Disruption of phospholipid vesicles through the pH-dependent interaction of poly(2-ethylacrylic acid) (PEAA)..... 6 |
| Figure 1.4 | Detection of the PEAA-induced reorganization of DPPC vesicles through the use of optical density measurements. 7 |
| Figure 1.5 | The pH-induced conformational transition of PEAA.10 |
| Figure 1.6 | Use of a hydrophobic fluorescent probe to monitor the conformational transition of hydrophobic polyelectrolytes.11 |
| Figure 1.7 | Spectral overlap between donor emission (E_D) and acceptor adsorption (A_A) required for resonance energy transfer.....16 |
| Figure 1.8 | Conformational transition within a hydrocarbon chain required for the formation of intramolecular excimers.....18 |
| Figure 1.9 | Vibrational fine structure in the fluorescence emission spectrum of pyrene.....19 |
| Figure 1.10 | Possible mechanistic schemes for the pH-dependent interaction of PEAA and DPPC.....21 |
| Figure 1.11 | Use of fluorescent probes to monitor the pH-dependent interaction between PEAA and DPPC.23 |
| Figure 1.12 | Chemical structures of the various fluorescent probes used to study the pH-dependent interaction between PEAA and DPPC.....25 |
| Figure 1.13 | Application of the resonance energy transfer experiment to the PEAA-DPPC system.....26 |

| | | |
|-------------|-------------------------------------------------------------------------------------------------------------------------------------------------------------------------------------------------------------------------------------------|----|
| Figure 3.1 | Sequence of events in the pH-dependent interaction between PEAA and DPPC. | 45 |
| Figure 3.2 | Negative-stain electron micrograph of DPPC (1 mg/ml) suspended in phosphate-buffered (0.02 M) aqueous PEAA (1 mg/ml), pH 5.7..... | 47 |
| Figure 3.3 | Negative-stain electron micrograph of DPPC (1 mg/ml) suspended in phosphate-buffered (0.02 M) aqueous PEAA (1 mg/ml), pH 7.6..... | 49 |
| Figure 3.4 | Negative-stain electron micrograph of a PEAA-free phosphate-buffered (0.02 M) aqueous suspension of DPPC (1 mg/ml), pH 7.1..... | 50 |
| Figure 3.5 | Negative-stain electron micrograph of DPPC (1 mg/ml) suspended in phosphate-buffered (0.02 M) aqueous PEAA (1 mg/ml), pH 7.1..... | 51 |
| Figure 3.6 | Negative-stain electron micrograph of DPPC (1 mg/ml) suspended in phosphate-buffered (0.02 M) aqueous PEAA (1 mg/ml), pH 6.4..... | 53 |
| Figure 3.7 | Negative-stain electron micrograph of DPPC (1 mg/ml) suspended in phosphate-buffered (0.02 M) aqueous PEAA (1 mg/ml), pH 6.4, temperature of sample maintained at 25 °C (below the main phase transition temperature of DPPC, 41 °C)..... | 54 |
| Figure 3.8 | Fluorescence emission spectra for pyrene (5×10^{-6} M) in phosphate-buffered (0.02 M) solutions of PEAA (1 mg/ml). | 56 |
| Figure 3.9 | Fluorescence intensity (374 nm) emitted by pyrene (5×10^{-6} M) in phosphate buffered (0.02 M) solutions of PEAA (1 mg/ml) as a function of pH..... | 57 |
| Figure 3.10 | Fluorescence excitation spectra for pyrene (5×10^{-6} M) in phosphate-buffered (0.02 M) solutions of PEAA (1 mg/ml). | 59 |
| Figure 3.11 | Origin of solvent-induced spectral shifts for nonpolar fluorophores..... | 61 |
| Figure 3.12 | Fluorescence emission spectra for PEAA-py2 copolymer (1 mg/ml) in phosphate-buffered (0.40 M) aqueous solution. | 63 |

| | | |
|-------------|-------------------------------------------------------------------------------------------------------------------------------------------------------------------------------------------|----|
| Figure 3.13 | Fluorescence intensity (377 nm) emitted by PEAA-py2 (1 mg/ml) in phosphate-buffered (0.40M) aqueous solution as a function of pH..... | 64 |
| Figure 3.14 | Wavelength of maximum intensity in the emission spectrum of PEAA-py2 (1 mg/ml) in phosphate-buffered (0.40M) aqueous solution as a function of pH..... | 66 |
| Figure 3.15 | Fluorescence excitation spectra for PEAA-py2 copolymer (1 mg/ml) in phosphate-buffered (0.40 M) aqueous solution..... | 67 |
| Figure 3.16 | Wavelength of maximum intensity in the excitation spectrum of PEAA-py2 (1 mg/ml) in phosphate-buffered (0.40M) aqueous solution as a function of pH..... | 68 |
| Figure 3.17 | Second derivative excitation spectra for PEAA-py2 copolymer (1 mg/ml) in phosphate-buffered (0.40 M) aqueous solution..... | 70 |
| Figure 3.18 | Fluorescence intensity (377 nm) emitted by PEAA-py1 copolymer (1 mg/ml) in 0.02 M, 0.10 M, and 0.40 M phosphate-buffered solutions as a function of pH. | 71 |
| Figure 3.19 | Fluorescence intensity (377 nm) emitted by PEAA-py2 copolymer (1 mg/ml) in phosphate-buffered (0.40 M) aqueous solution and suspensions of DPPC (1 mg/ml) as a function of pH. | 72 |
| Figure 3.20 | Effect of optical density on intensity of fluorescence emitted by PEAA-py2 in suspensions of DPPC. | 74 |
| Figure 3.21 | Fluorescence emission spectra for PEAA-py2 copolymer (1 mg/ml) in phosphate-buffered (0.40 M) suspensions of DPPC (1 mg/ml)..... | 76 |
| Figure 3.22 | Wavelength of maximum intensity in the emission spectrum of PEAA-py2 (1 mg/ml) in phosphate-buffered (0.40M) aqueous solution and suspensions of DPPC (1 mg/ml) as a function of pH. | 77 |
| Figure 3.23 | Fluorescence excitation spectra for PEAA-py2 copolymer (1 mg/ml) in phosphate-buffered (0.40 M) suspensions of DPPC (1 mg/ml)..... | 79 |

| | | |
|-------------|-----------------------------------------------------------------------------------------------------------------------------------------------------------------------------------|----|
| Figure 3.24 | Wavelength of maximum intensity in the excitation spectrum of PEAA-py2 (1 mg/ml) in phosphate-buffered (0.40M) aqueous solution and suspensions of DPPC as a function of pH. | 80 |
| Figure 3.25 | Second derivative excitation spectra for PEAA-py2 copolymer (1 mg/ml) in phosphate-buffered (0.40 M) suspensions of DPPC (1 mg/ml). | 81 |
| Figure 3.26 | Excitation spectra and their second derivatives for PEAA-py2 (1 mg/ml) in sedimented and un-sedimented suspensions of DPPC (1 mg/ml) at pH 6.93. | 83 |
| Figure 3.27 | Emission intensity (378 nm) and optical density (600 nm) for phosphate-buffered (0.02 M) mixtures of PEAA-py1 (0.1 mg/ml) and DPPC (0.1 mg/ml). | 85 |
| Figure 3.28 | Optical density (600 nm) of 0.02 M, 0.10 M, and 0.40 M phosphate-buffered mixtures of PEAA-py1 (1 mg/ml) and DPPC (1 mg/ml). | 87 |
| Figure 3.29 | Optical density (600 nm) for PEAA (1 mg/ml) in phosphate-buffered (0.02 M) suspensions of multilamellar and sonicated DPPC vesicles (1 mg/ml). | 88 |
| Figure 3.30 | The pH of a solution containing PEAA-py2 (1 mg/ml) and 0.40 M NaCl as a function of added 0.100 N HCl. | 90 |
| Figure 3.31 | Degree of ionization of PEAA-py2 (1 mg/ml) in 0.40 M NaCl solution as a function of pH. | 92 |
| Figure 3.32 | Fluorescence emission intensity (377 nm) for phosphate-buffered (0.40 M) solutions of PEAA-py2 and degree of ionization of PEAA-py2 in 0.40 M NaCl solutions. | 93 |
| Figure 3.33 | Degree of ionization of PEAA-py2 in aqueous solution and suspensions of DPPC (1 mg/ml). | 94 |
| Figure 3.34 | Determination of the fraction of collapsed coils (f_c) in the conformational transition region of PEAA. | 96 |
| Figure 3.35 | Fraction of collapsed coils of PEAA-py2 (1 mg/ml) in aqueous solution and suspensions of DPPC (1 mg/ml) as a function of pH. | 97 |

| | | |
|-------------|-------------------------------------------------------------------------------------------------------------------------------------------------------------------------------------------------|-----|
| Figure 3.36 | Fraction of collapsed coils and emitted fluorescence intensity (377 nm) for aqueous solutions of PEAA-py2 (1 mg/ml) as a function of pH..... | 99 |
| Figure 3.37 | Degree of ionization of PEAA (1 mg/ml) in aqueous solution as a function of pH for samples at 25 °C and 55 °C..... | 101 |
| Figure 3.38 | Supernatant concentrations of PEAA-py2 and DPPC as a function of pH for 0.02M phosphate-buffered samples after centrifugation. | 103 |
| Figure 3.39 | Supernatant concentrations of PEAA-py2 and DPPC as a function of pH for 0.40 M phosphate-buffered samples after centrifugation. | 105 |
| Figure 3.40 | Fraction of added PEAA-py2 bound to DPPC aggregates as function of pH for phosphate-buffered (0.02 M and 0.40 M) mixtures of PEAA-py2 (0.5 mg/ml) and DPPC (0.5 mg/ml)..... | 106 |
| Figure 3.41 | Fraction of DPPC bound PEAA-py2 and degree of ionization of PEAA-py2 as a function of pH in aqueous suspensions of DPPC. | 108 |
| Figure 3.42 | Fraction of added PEAA-py2 bound to DPPC aggregates as function of the degree of ionization of PEAA-py2 for 0.02 M and 0.40 M ionic strength solutions of PEAA-py2 and DPPC..... | 110 |
| Figure 3.43 | Fraction of added PEAA-py2 bound to DPPC aggregates as function of pH for phosphate-buffered (0.40 M) suspensions of PEAA-py2 (0.5 mg/ml) and DPPC (0.5 mg/ml and 1.75 mg/ml). | 111 |
| Figure 3.44 | Wavelength of maximum intensity in the emission spectrum of PEAA-py2 (0.5 mg/ml) in phosphate-buffered (0.40M) aqueous suspensions of DPPC (0.5 mg/ml and 1.75 mg/ml) as a function of pH. | 113 |
| Figure 3.45 | Fraction of PEAA-py2 bound to DPPC vesicles in 0.02 M phosphate-buffered suspensions at pH 7.1 as a function of the ratio of added DPPC to PEAA-py2..... | 114 |
| Figure 3.46 | Fraction of PEAA-py2 bound to DPPC vesicles in 0.40 M phosphate-buffered suspensions at pH 7.1, pH 8.6, and pH 10.3 as a function of the ratio of added DPPC to PEAA-py2..... | 116 |

| | | |
|-------------|----------------------------------------------------------------------------------------------------------------------------------------------------------------------------------------------------------------------------------------------------------------|-----|
| Figure 3.47 | Excitation spectra and their second derivatives for PEAA-py2 (0.5 mg/ml) in phosphate-buffered (0.40 M) aqueous solution and suspensions of DPPC (0.5 mg/ml) at pH 10.3..... | 117 |
| Figure 3.48 | Wavelength of maximum intensity in the emission spectrum of PEAA-py2 (0.5 mg/ml) in phosphate-buffered (0.40M) aqueous suspensions of DPPC at pH 7.1 as a function of the ratio of added DPPC to PEAA-py2. | 119 |
| Figure 3.49 | Polarization of fluorescence (430 nm) from 3.4×10^{-7} M DPH in 0.02 M phosphate-buffered suspensions of sonicated DPPC vesicles (0.25 mg/ml) and with mixtures of PEAA (0.25 mg/ml) as a function of pH..... | 121 |
| Figure 3.50 | Polarization of fluorescence (430 nm) from 3.4×10^{-7} M DPHPC in 0.02 M phosphate-buffered mixtures of PEAA (0.25 mg/ml) and sonicated DPPC vesicles (0.25 mg/ml) as a function of pH..... | 125 |
| Figure 3.51 | Polarization of fluorescence (398 nm) from 3.4×10^{-7} M PyPC in 0.02 M phosphate buffered suspensions of sonicated DPPC vesicles (0.25 mg/ml) and with mixtures of PEAA (0.25 mg/ml) as a function of pH..... | 127 |
| Figure 3.52 | Fluorescence lifetime of PyPC in 0.02 M phosphate-buffered suspensions of sonicated DPPC vesicles and with mixtures of PEAA as a function of pH..... | 128 |
| Figure 3.53 | Polarization of fluorescence (380 nm) from 4.5×10^{-7} M Py-DPPE in 0.02 M phosphate-buffered suspensions of sonicated DPPC vesicles (0.25 mg/ml) and with mixtures of PEAA (0.25 mg/ml) as a function of pH..... | 132 |
| Figure 3.54 | Fluorescence emission spectra for 9×10^{-7} M Py ₂ C ₃ in 0.02 M phosphate-buffered mixtures of PEAA (1 mg/ml) and sonicated DPPC vesicles (1 mg/ml)..... | 135 |
| Figure 3.55 | Ratio of monomer intensity (396 nm) to excimer intensity (488 nm) (I_M/I_E) for 9×10^{-7} M Py ₂ C ₃ in 0.02 M phosphate-buffered mixtures of PEAA (1 mg/ml) and sonicated DPPC vesicles (1 mg/ml) as a function of pH..... | 136 |
| Figure 3.56 | Ratio of peak 1 (373 nm) and peak 3 (384 nm) intensities for 5×10^{-6} M pyrene in 0.02 M phosphate-buffered mixtures of PEAA (1 mg/ml) and DPPC (1 mg/ml) as a function of pH..... | 138 |

| | | |
|-------------|---------------------------------------------------------------------------------------------------------------------------------------------------------------------------------------------------------------------------------------|-----|
| Figure 3.57 | Fluorescence lifetime of pyrene in PEAA, DPPC vesicles, and mixtures of PEAA and DPPC as a function of pH..... | 140 |
| Figure 3.58 | Determination of the extent of resonance energy transfer (I_F/I_0) in mixtures of PEAA-trp, DPPC, and AMC..... | 142 |
| Figure 3.59 | Extent of energy transfer (I_F/I_0) as a function of pH in 0.02 M phosphate-buffered mixtures of PEAA-trp (1 mg/ml) and sonicated DPPC vesicles (1 mg/ml) containing AMC (3×10^{-5} M)..... | 144 |
| Figure 3.60 | DSC thermograms of DPPC (1 mg/ml) in 0.02 M phosphate-buffered solutions of PEAA (1 mg/ml)..... | 147 |
| Figure 3.61 | DSC thermograms of DPPC (1 mg/ml) in 0.02 M phosphate-buffered solutions of PMAA (1 mg/ml)..... | 148 |
| Figure 3.62 | Polarization of DPH fluorescence (430 nm) in 0.02 M phosphate-buffered (pH 6) suspensions of sonicated DPPC vesicles and PEAA/DPPC mixed micelles as a function of temperature..... | 158 |
| Figure 3.63 | Optical density (600 nm) of a 0.02 M phosphate-buffered (pH 6) suspension of DPPC vesicles as a function of the volume of added PEAA and the determination of the concentration of PEAA required to solubilize the DPPC vesicles..... | 160 |
| Figure 3.64 | Concentration of PEAA required for solubilization of DPPC vesicles as a function of DPPC concentration..... | 161 |
| Figure 3.65 | Optical density (600 nm) of 0.02 M phosphate-buffered mixtures of PEAA and sonicated DPPC vesicles as a function of pH at subsolubilizing concentrations of PEAA..... | 163 |

CHAPTER I

INTRODUCTION

A. Responsive Systems.

A fundamental property of biological membranes is the ability to respond to chemical and physical stimuli. Many critical cellular functions are mediated by the responsive characteristics of the cell membrane. Recently, researchers have sought to mimic the responsive nature of biological membranes through the development of physical systems which are sensitive to environmental stimuli. Systems of this type are important due to their potential application in areas of medical diagnostics, therapeutics, information storage and transfer, sensing, imaging, and chemical reaction control. Several research groups have reported on the successful development of systems which are sensitive to changes in temperature, pH, and redox potential [1-14]. Most of these systems are based on synthetic bilayer membranes formed from aqueous dispersions of surfactants. One approach has been to prepare surfactant molecules which carry functional groups sensitive to the environmental stimulus of interest and to integrally incorporate these surfactants into the bilayer membrane. A different approach to forming a responsive system has exploited the conditional interaction of macromolecules with surfactant bilayer membranes.

B. Phospholipid Vesicles.

Phospholipids are double chain surfactant molecules which are important constituents of cell membranes. Accordingly, in the attempt to understand the physical chemistry of biological membranes, an enormous number of research papers have been published on the study of model phospholipid bilayer membranes. Additionally, many of the responsive systems mentioned previously have employed phospholipids as the bilayer membrane forming component [1-5, 8, 13, 14]. Phospholipids are amphiphilic in nature as a result of their long nonpolar hydrocarbon tails and polar phosphodiester headgroups. When these compounds are dispersed in aqueous solution they form closed bilayer structures with an internal aqueous compartment (see Figure 1.1) [15-17]. In the vesicle structure the long hydrocarbon chains form a hydrophobic core, while the hydrophilic headgroups contact the aqueous medium. Dispersion of phospholipids in water with shaking or vortex agitation results in the formation of multilamellar vesicles, which exhibit an onion-like layering of bilayers. Multilamellar vesicles are relatively large (sizes range from 10^3 to 10^5 Å in diameter); consequently these preparations appear turbid due to scattering of incident light.

Pure phospholipids undergo a reversible order-to-disorder transition with an increase in temperature through a characteristic melting temperature (T_m) (see Figure 1.2) [18]. The transition has been associated with the order and alignment of the hydrocarbon chains within the bilayer structure [18, 19]. In the ordered gel state (denoted as L_{β}') the hydrocarbon chains assume an all-trans configuration, while in the disordered fluid

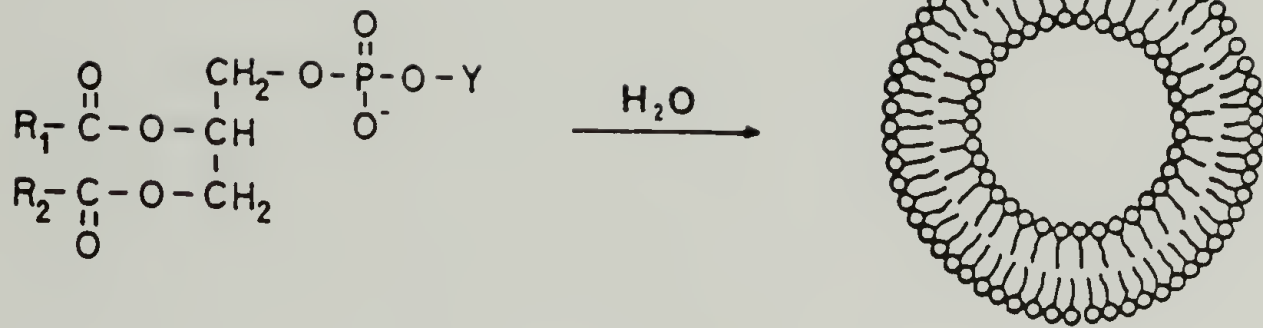


Figure 1.1 Formation of vesicular structures via the dispersion of phospholipid molecules in aqueous solution.

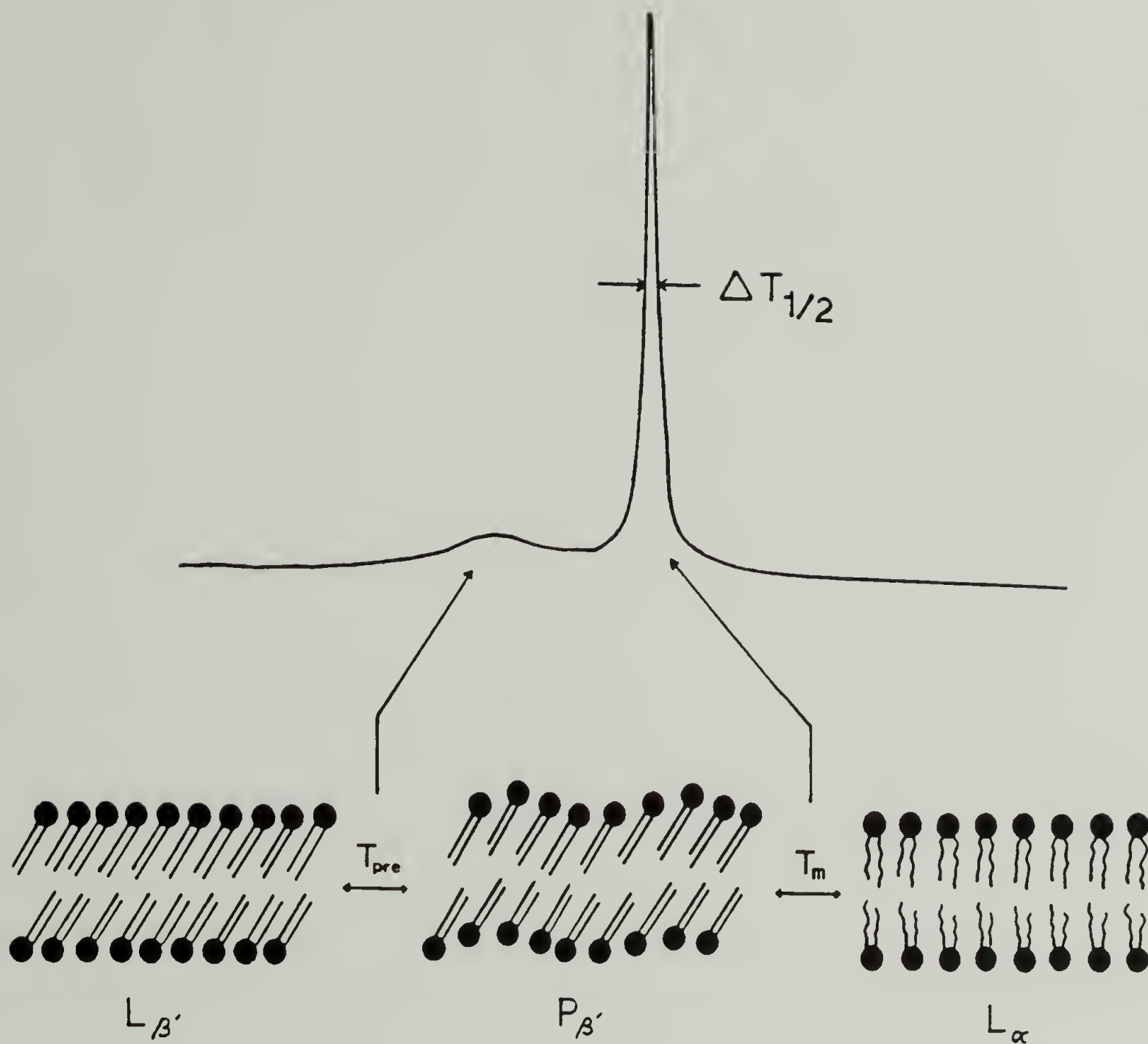


Figure 1.2 Phase transitions in phospholipid bilayers as detected by differential scanning calorimetry (DSC). The main melting transition (T_m) is associated with a change in the hydrocarbon chain conformation from an ordered all-trans state ($L_{\beta'}$) to a disordered fluid-like state (L_{α}). Some phospholipids exhibit a minor thermal transition known as a pretransition, which results in the formation of a periodic lamellar phase ($P_{\beta'}$). From M.J. Janiak, D.M. Small, G.G. Shipley, *Biochemistry*, 1976, 15, 4575.

state (denoted as L_α) the chains contain several gauche rotamers. In multilamellar vesicles, the melting transition occurs over a very narrow temperature range (transition peak width at half-height, $\Delta T_{1/2} < 0.5$ °C), which is indicative of a highly cooperative process [18]. Because the hydrocarbon chains are in close proximity, when one chain undergoes a trans to gauche rotation it induces a similar rotation in neighboring chains. The cooperative unit in phospholipid vesicles can include several hundred molecules. Some phospholipids exhibit a minor phase transition at temperatures below the main melting transition (see Figure 1.2). Known as the pre-transition, it is accompanied by a change to a periodic lamellar phase (denoted as P_β') and leads to a rippled surface texture [20, 21].

C. Interaction of Poly(carboxylic acid)s with Phospholipid Vesicles.

Tirrell and coworkers discovered that initially pH-insensitive phospholipid vesicles became highly responsive to solution pH through the addition of a hydrophobic poly(carboxylic acid) [13, 14]. They found that the pH-dependent interaction of poly(2-ethylacrylic acid) (PEAA) with phospholipid vesicles led to the disruption of the vesicle's structural organization and resulted in the concomitant release of contents entrapped in the internal aqueous cavity (see Figure 1.3). Reorganization of dipalmitoylphosphatidylcholine (DPPC) vesicles in aqueous solutions of PEAA was observed to occur when the solution pH was lowered below 7. The reorganization is characterized by clarification of the highly turbid vesicle suspension, which suggests the formation of small PEAA-DPPC mixed micellar structures. This phenomenon is shown in Figure 1.4 as a

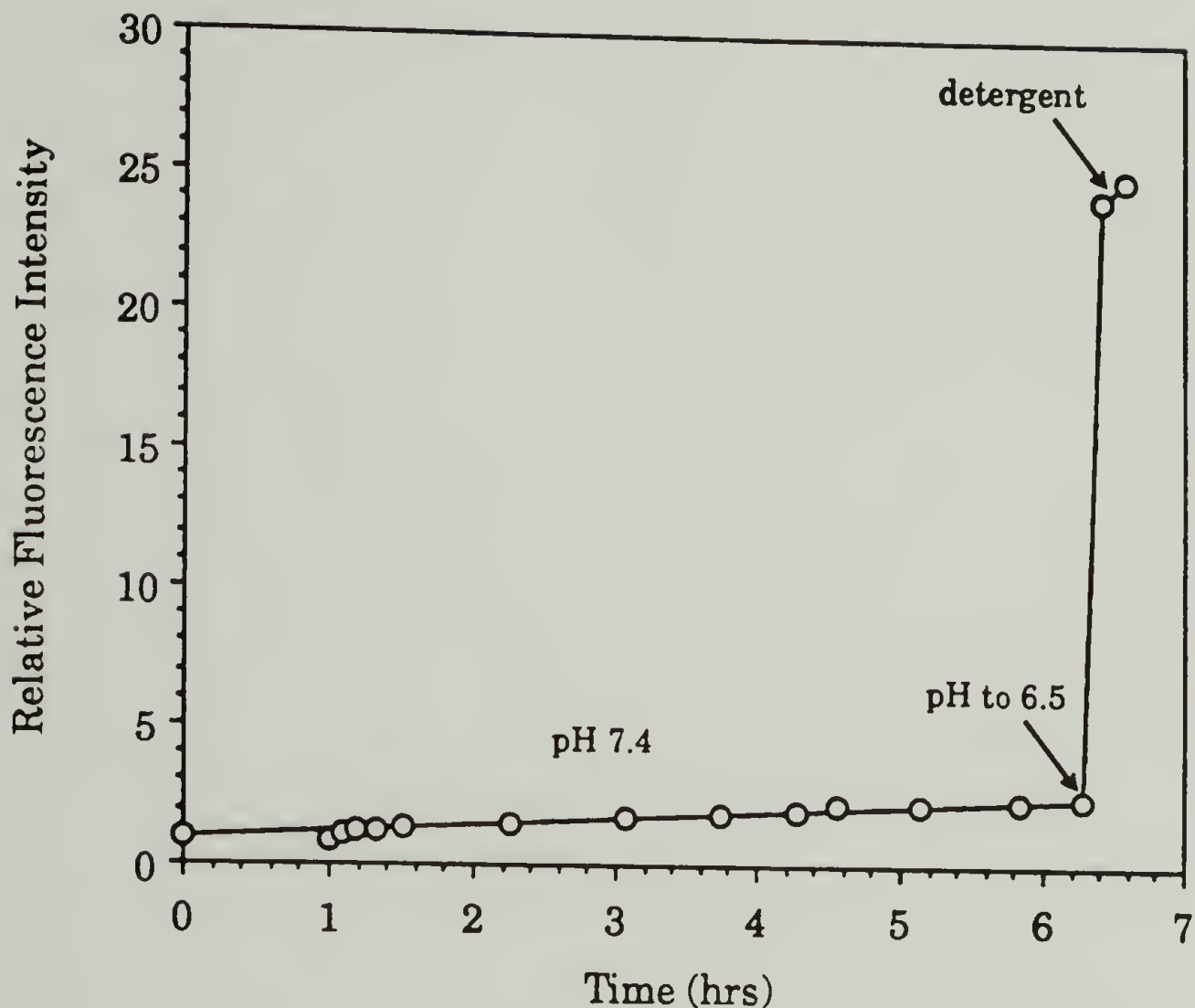


Figure 1.3 Disruption of phospholipid vesicles through the pH-dependent interaction of poly(2-ethylacrylic acid) (PEAA). Vesicle disruption is detected by monitoring the efflux of entrapped 6-carboxyfluorescein from egg yolk phosphatidylcholine (EYPC) vesicles suspended in 50 mM Tris-HCl, 100 mM NaCl solution containing 0.03 wt. % PEAA at 25 °C. There is little efflux of dye in mixtures of EYPC and PEAA at pH 7.4, however acidification of the suspension to pH 6.5 results in near quantitative release of entrapped dye (addition of detergent produces little additional liberation of dye). From D.A. Tirrell, D.Y. Takigawa, K. Seki, *Ann. N.Y. Acad. Sci.*, 1985, 446, 237.

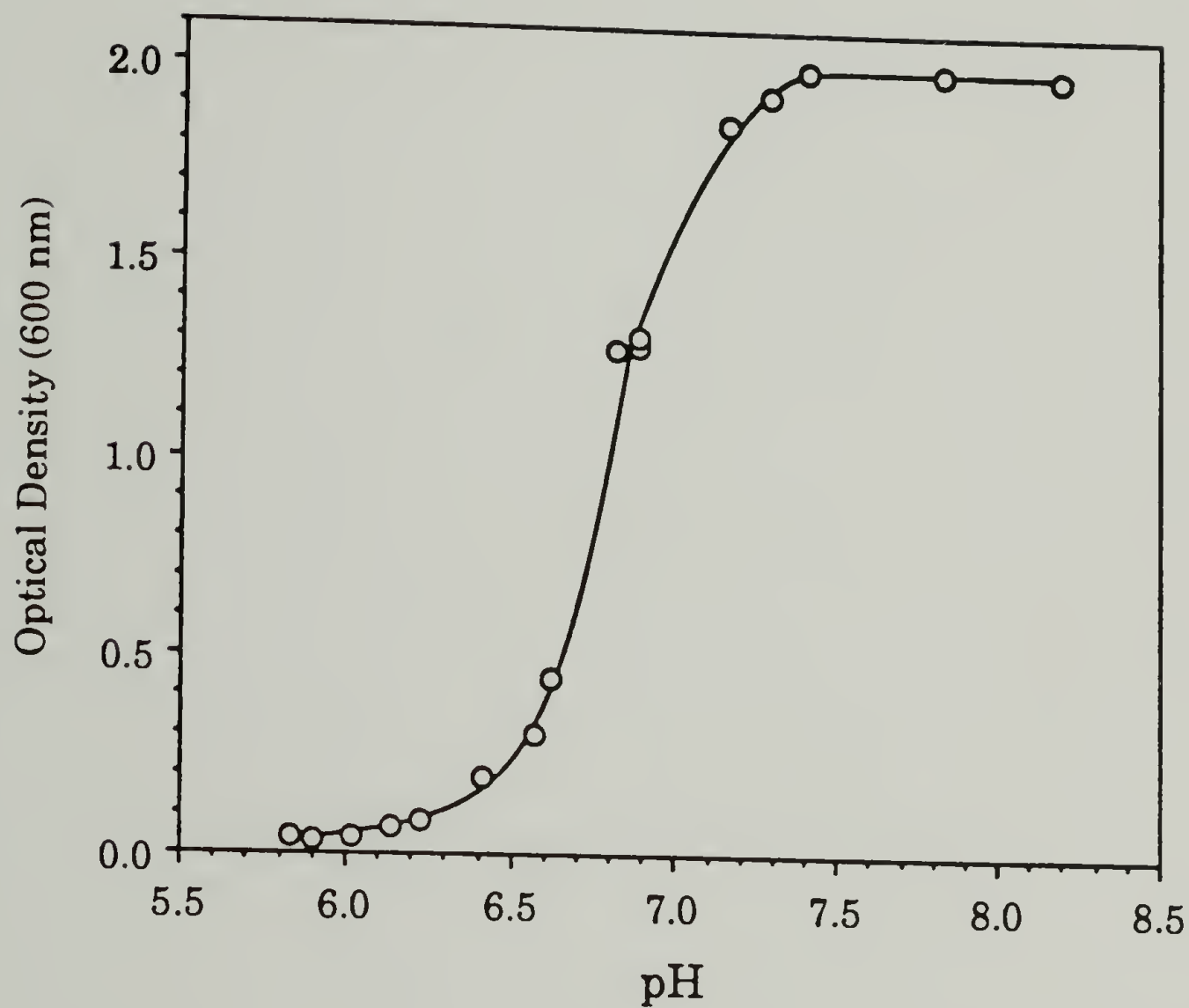


Figure 1.4 Detection of the PEAA-induced reorganization of DPPC vesicles through the use of optical density measurements. The optical density (600 nm) of 0.02 M phosphate buffered suspensions of DPPC and PEAA (1 mg/ml each) was measured.

plot of optical density versus pH for mixtures of PEAA and DPPC. The researchers also investigated the interaction of poly(acrylic acid) (PAA) and poly(2-methylacrylic acid) (PMAA) with DPPC vesicles [13]. They found that PAA and PMAA do exhibit pH-dependent complexation with DPPC vesicles, but do not cause the same catastrophic structural reorganization demonstrated with PEAA. Calorimetric studies revealed that the critical pH for interaction with DPPC vesicles depended on the chemical structure and stereochemistry of the poly(carboxylic acid). For example the critical pH values for PAA, PMAA, and PEAA were determined to be 4.6, 5.3, and 6.9, respectively. This trend of increasing critical pH values with increasing length of the alkyl substituent parallels the trend of increasing apparent pK_a values for this series of polymers [22-28]. Alteration of the polymer stereochemistry resulted in small changes in the critical interaction pH. For heterotactic PEAA the observed critical pH was 6.9, while for highly syndiotactic PEAA it was 7.1 [13].

D. Conformational Behavior of Poly(carboxylic acid)s.

It is believed that the observed pH-dependent PEAA-induced reorganization of DPPC vesicles is related to the conformational behavior of the PEAA. It is known from potentiometric titration, spectrophotometric titration, ^1H nuclear magnetic resonance, viscometry, and quasi-elastic light scattering [22-24, 29] that PEAA undergoes a conformational change with variation in solution pH. At high solution pH PEAA is highly ionized and exists as an expanded coil. As the solution pH is lowered through a characteristic critical value, the PEAA collapses to a compact coil

conformation (see Figure 1.5). PMAA also demonstrates this type of pH-induced conformational transition, while PAA does not [25-28, 30-35]. It is presumed that hydrophobic interactions between the alkyl side chains in PMAA and PEAA lead to deviation from the continuous chain expansion with increasing chain ionization one finds for polyelectrolytes such as PAA. Hydrophobic interactions between the alkyl side chains cause the polyelectrolyte to remain in the collapsed coil conformation until the charge-charge repulsion energy outweighs the energy of unfavorable alkyl group-water interactions. It was shown that PMAA can solubilize simple hydrocarbons in a collapsed coil conformation at low pH, but cannot in an expanded coil conformation at high pH [36]. It is postulated that PEAA acts in an analogous manner to solubilize phospholipid molecules in the hydrophobic domains of the collapsed polymer coil with the resultant formation of polymer-phospholipid mixed micelles. Even though PMAA also forms a compact coil structure at low pH, it appears the domains are not hydrophobic enough to solubilize DPPC.

E. Use of Fluorescence Spectroscopy to Monitor Conformational Transitions.

The emitted fluorescence intensity of a hydrophobic fluorescent probe molecule has been used to follow the conformational transition in polyelectrolytes. An investigation of this type was carried out by Thomas and coworkers in which pyrene was used to monitor the conformational behavior of PMAA [37] (see Figure 1.6). After a chromophore, such as pyrene, absorbs radiation to form an excited state, there are several competing processes by which the molecule may return to the ground

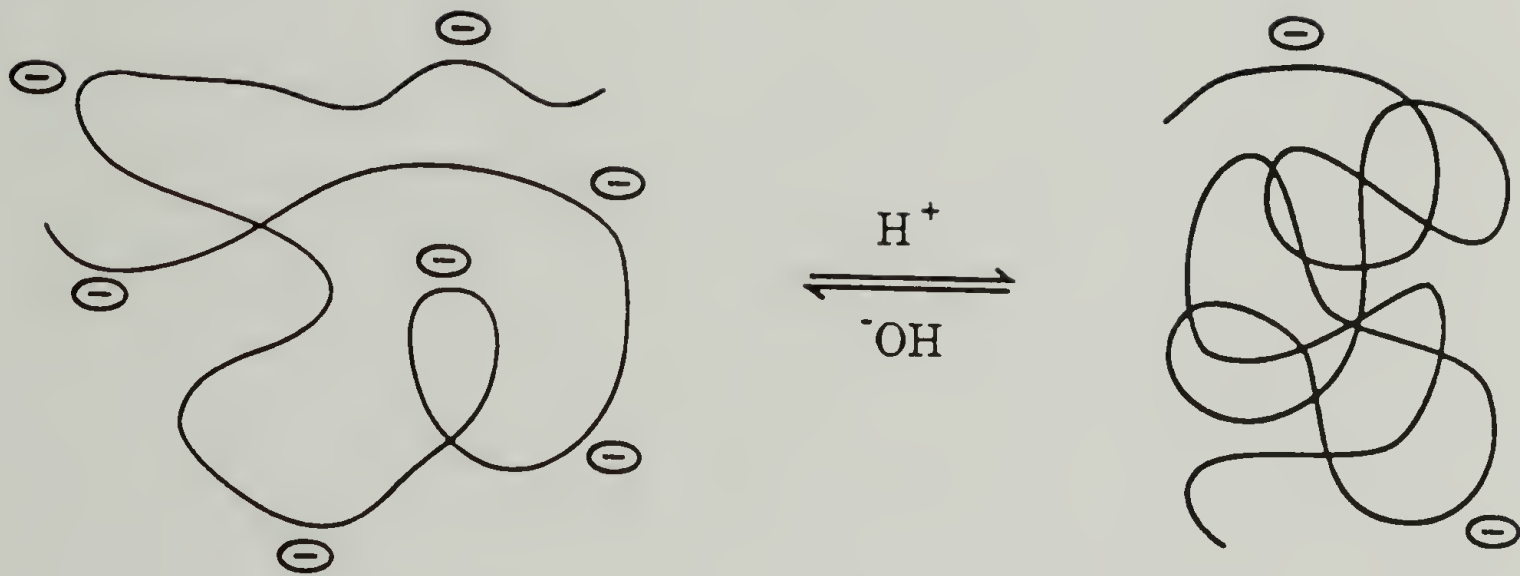


Figure 1.5 The pH-induced conformational transition of PEAA.

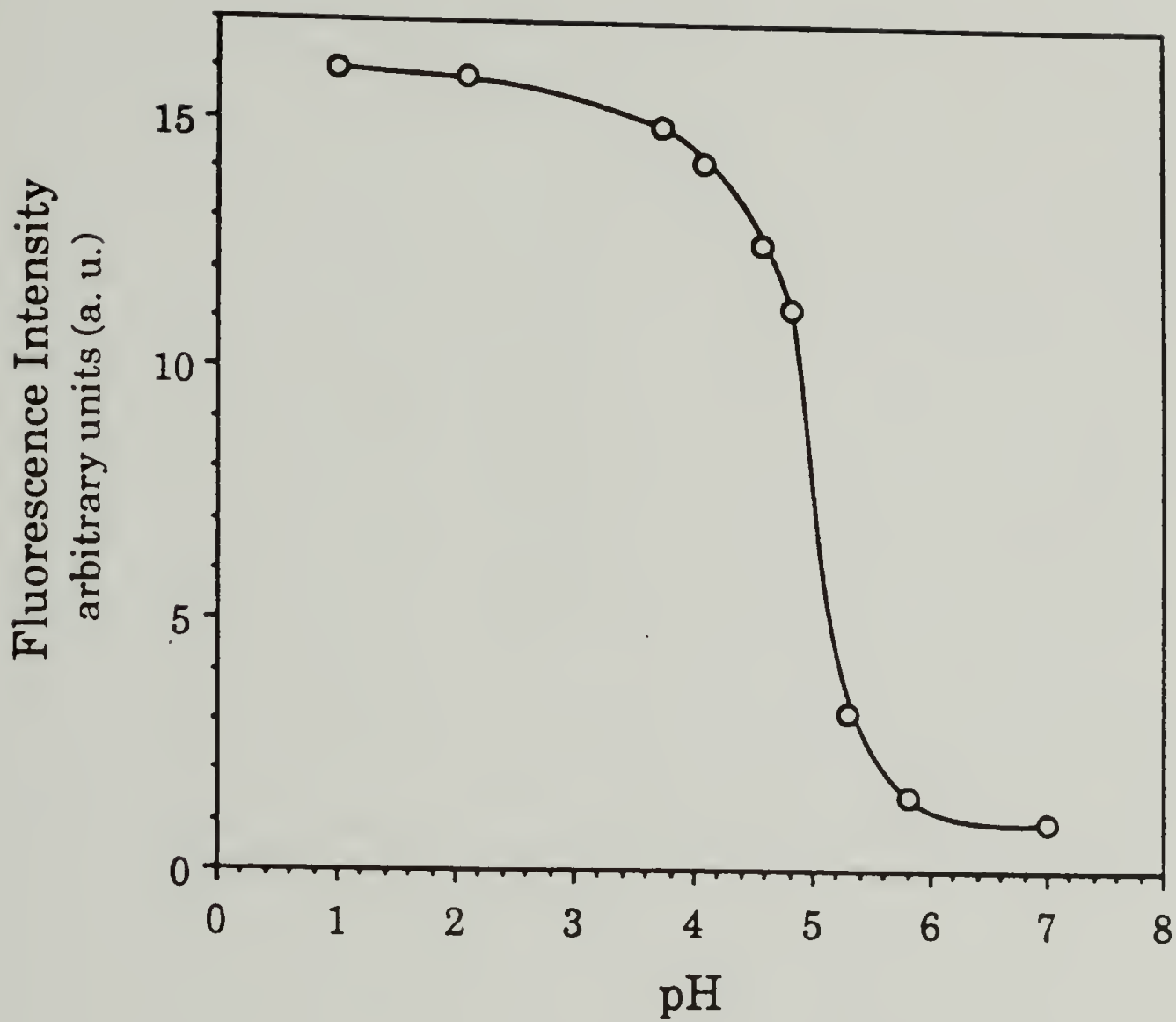


Figure 1.6 Use of a hydrophobic fluorescent probe to monitor the conformational transition of hydrophobic polyelectrolytes. The intensity emitted by 10^{-5} M pyrene in aqueous solutions of PMAA was measured (excitation wavelength 337 nm, emission wavelength 373 nm). From T. Chen and J.K. Thomas, *J. Polym. Sci. Polym. Chem. Ed.*, 1979, 17, 1103.

state [38-40]. These processes include the emission of radiation and the radiationless loss of energy. The intensity of emitted radiation is influenced by the relative rates of the emission and radiationless processes. Any factor which increases the extent of radiationless loss of energy will consequently decrease the intensity of emitted radiation. For pyrene, it has been found that an increase in solvent polarity results in an increase in the extent of radiationless loss of energy [37]. In aqueous solution at low pH, PMAA adopts a collapsed conformation with hydrophobic domains, which can solubilize hydrophobic pyrene molecules. The hydrophobic domains of PMAA are less polar than water, therefore measurement of the pyrene emission intensity for PMAA solutions at a range of pH values provides a convenient means of monitoring the pH-dependent conformational transition of PMAA. Thomas observed a dramatic change in pyrene fluorescence intensity over a narrow pH range with a characteristic critical pH for the conformational transition corresponding to the midpoint of the change in intensity. They found PMAA to undergo the conformational transition at pH 5, which is in accordance with results derived from techniques such as potentiometric titration, viscometry, and NMR [25-28, 30-36].

Thomas and coworkers have demonstrated that covalent attachment of pyrene to PMAA results in similar sensitive detection of the conformational transition [41]. In addition to the change in fluorescence intensity, Thomas and coworkers found that increased pyrene-water contacts resulted in a decrease in the excited state lifetime. They found the lifetime changed from 280 nsec in deaerated PMAA solutions below pH 5 to 140 nsec in deaerated PMAA solutions above pH 7. The midpoints of the changes in intensity and lifetime coincide. Pyrene solubilized in the hydrophobic domains of

collapsed PMAA becomes exposed to the aqueous medium when the PMAA undergoes the conformational transition to an expanded coil. The contacts with water result in pyrene exhibiting a decreased fluorescence quantum yield and lifetime.

F. Fluorescence Polarization of Probe Molecules in Surfactant Bilayers.

The polarization of fluorescence emitted by a probe molecule has frequently been used to characterize the physical state of biological membranes and synthetic vesicles. This type of experiment is performed by measuring the fluorescence polarization of a probe incorporated into the bilayer membrane as a function of some varying parameter. When a fluorescent molecule is excited with polarized light, the emission is also polarized as a result of the process of photoselection of molecules oriented in the direction of the polarized excitation. Steady state values of the polarization (P) and anisotropy (r) are defined as:

$$P = \frac{I_{||} - I_{\perp}}{I_{||} + I_{\perp}} \quad (\text{Eq. 1.1}) \quad \text{and} \quad r = \frac{I_{||} - I_{\perp}}{I_{||} + 2I_{\perp}} \quad (\text{Eq. 1.2})$$

where $I_{||}$ and I_{\perp} are the fluorescence intensities detected through a polarizer oriented parallel and perpendicular to the direction of the polarization of the excitation beam. The polarization and anisotropy values can be interconverted with the following equations:

$$P = \frac{3r}{2 + r} \quad (\text{Eq. 1.3}) \quad \text{and} \quad r = \frac{2P}{3 - P} \quad (\text{Eq. 1.4})$$

The measurement of polarization or anisotropy reveals the average angular displacement of the fluorescent molecule which occurs between the absorption and emission processes [39]. Any process which leads to an increase in the average angular displacement during the excited state lifetime of the fluorophore will result in depolarization of the emitted light. A common cause of fluorescence depolarization is the rotational diffusion of the fluorophore, which is dependent on the viscosity of the fluorophore environment, and on the size and shape of the fluorescent species. If it is assumed that the only process causing depolarization is rotational diffusion, then the extent of depolarization is described by the equation:

$$\frac{r_0}{r} = 1 + \frac{\tau}{\phi} \quad (\text{Eq. 1.5})$$

where r is the steady state anisotropy, r_0 is the limiting anisotropy observed in the absence of rotational diffusion, τ is the excited state lifetime, and ϕ is the rotational correlation time of the probe. A similar equation can be presented for the steady state polarization. For fluorescent probe molecules incorporated into vesicles, there are contributions to ϕ from the Brownian rotation of the vesicle and the lateral diffusion of the probe. Rotational diffusion of typical probes used in polarization studies results in rotational correlation times on the order of nanoseconds, while Brownian rotation of vesicles and lateral probe diffusion each exhibit rotational correlation times on the order of microseconds [42]. Therefore, in vesicle systems the latter two processes make negligible contributions to the depolarization of fluorescence.

G. Fluorescence Energy Transfer.

A molecule in an excited electronic state may transfer its excitation energy to a second molecule capable of an electronic transition at a frequency corresponding to the transferred energy [38-40]. This process is known as resonance energy transfer and involves donor and acceptor species with overlapping emission and absorption spectra (see Figure 1.7). The rate of energy transfer between the donor and acceptor ($N_{D \rightarrow A}$) is given by:

$$N_{D \rightarrow A} = \frac{1}{\tau_0} \left(\frac{R_0}{R} \right)^6 \quad (\text{Eq. 1.6})$$

where τ_0 is the donor excited state lifetime, R_0 is the distance at which the transfer is 50% efficient, and R is the distance between the donor and acceptor in the system under study. There is an inverse sixth order relationship between the donor-acceptor separation and the observed extent of resonance transfer. Therefore, the resonance energy transfer experiment provides a highly sensitive means of monitoring the interaction between two species.

H. Other Fluorescence Spectroscopic Techniques.

Another approach to the characterization of surfactant bilayer membranes involves the use of fluorescent probe molecules which form intramolecular excimers. During its lifetime a molecule in an excited state

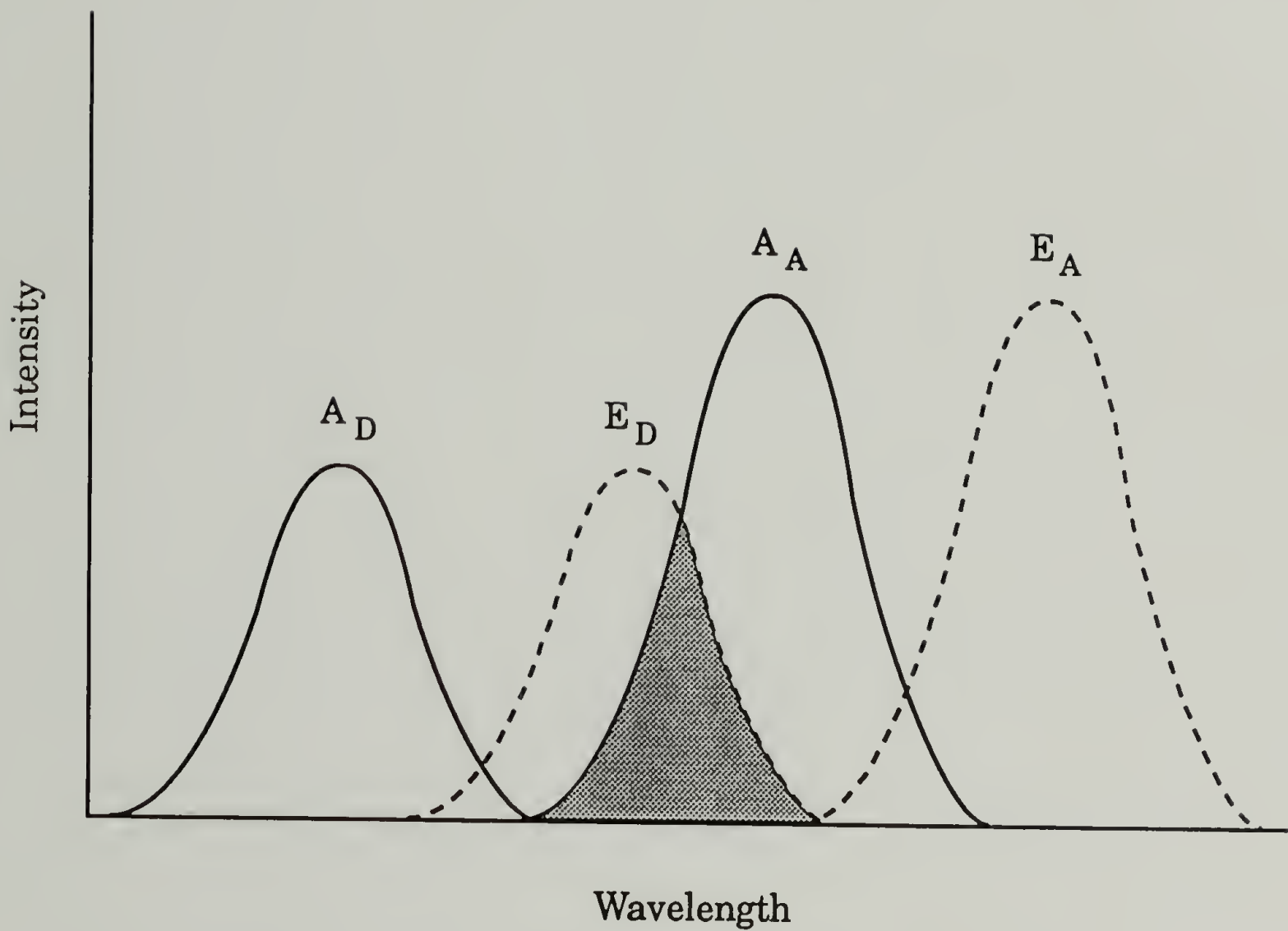


Figure 1.7 Spectral overlap between donor emission (E_D) and acceptor adsorption (A_A) required for resonance energy transfer. From A.J. Pesce, C.-G. Rosen, T.L. Pasby, Fluorescence Spectroscopy, Marcel Dekkar, New York, NY, 1971.

may interact with an unexcited molecule of the same species to form an excited dimer complex [38-40]. These excimers exhibit their own characteristic fluorescence behavior. The formation of excimers is a function of the concentration, the excited state lifetime, and the rate of diffusion of the fluorescent species. Attachment of the fluorescent moieties to the same molecule removes the concentration dependence of excimer formation. The intramolecular excimer formation involves a conformational rotation within the bridging segment of the molecule (see Figure 1.8), typically a hydrocarbon chain, and is dependent on the viscous resistance of the surrounding medium. Monomer fluorescence competes with the intramolecular excimer fluorescence, so that the ratio of the monomer and excimer emission intensity is a function of the microviscosity of the probe environment. Dipyranyl and dinaphthyl compounds have been employed in studies to determine the microviscosities of vesicles and biological membranes and to monitor changes in membrane fluidity [43-45].

The fluorescence emission spectrum of pyrene displays five readily distinguishable sharp peaks (see Figure 1.9). The intensity of peak 3 (383 nm) has been found to have little solvent dependence, while the intensity of peak 1 (373 nm) shows a large variance with solvent [46, 47]. Peak 1 has been assigned to the transition from the zero-point vibrational level of the excited state to the zero-point vibrational level of the ground state (the 0-0 band). For pyrene, the 0-0 band is a symmetry-forbidden transition, and in the absence of solvent interactions this transition is not observed. Solvent interactions modify the symmetry of the electronic state of the pyrene, and permit a weak 0-0 transition. The intensity of this weak 0-0 transition varies with the nature of the solvent and the solvent-fluorophore

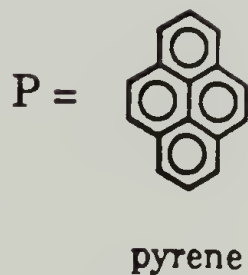
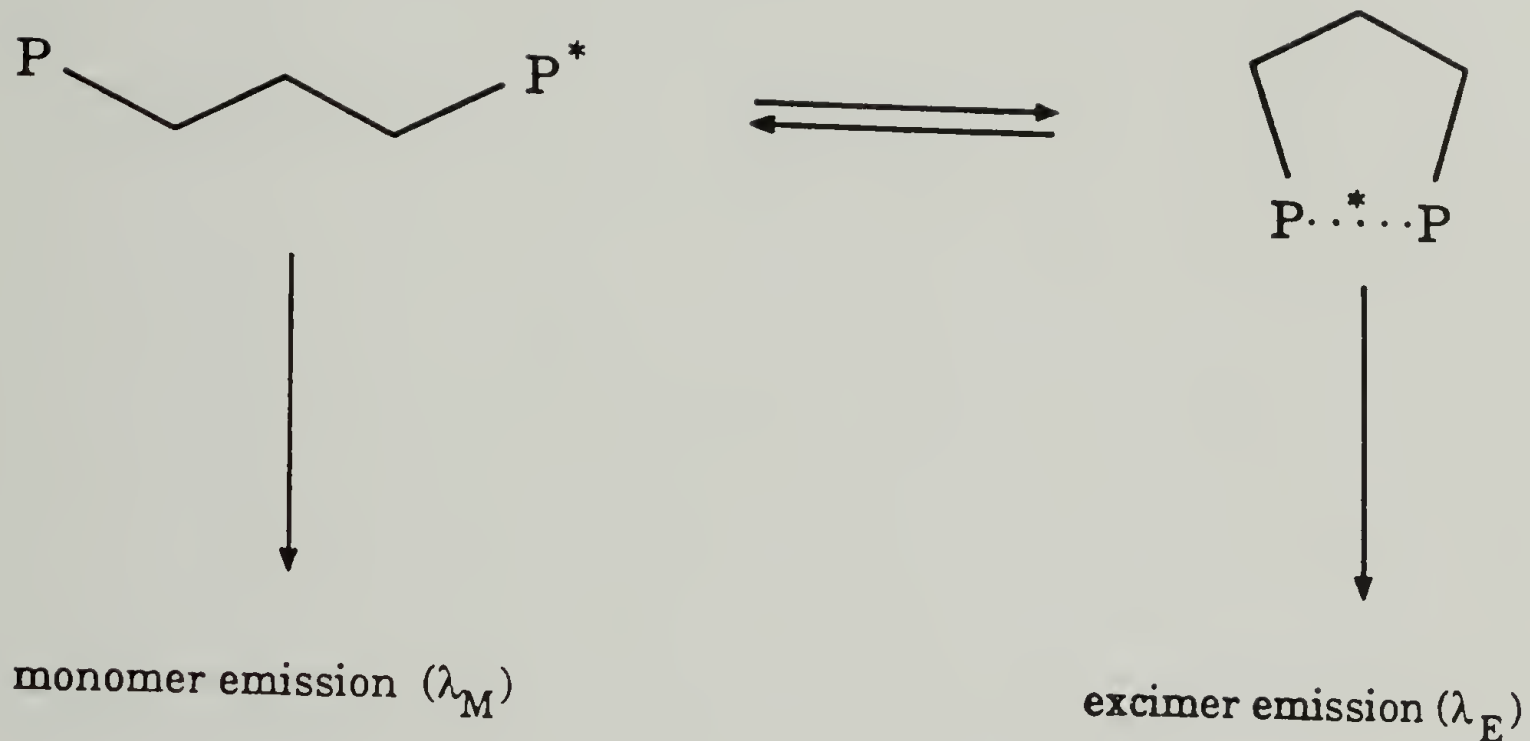


Figure 1.8 Conformational transition within a hydrocarbon chain required for the formation of intramolecular excimers. If chain rotation does not occur during the excited state lifetime, then only monomer emission (λ_M) is observed. Chain rotation allows the formation of the excited state complex and subsequent emitted fluorescence (λ_E).

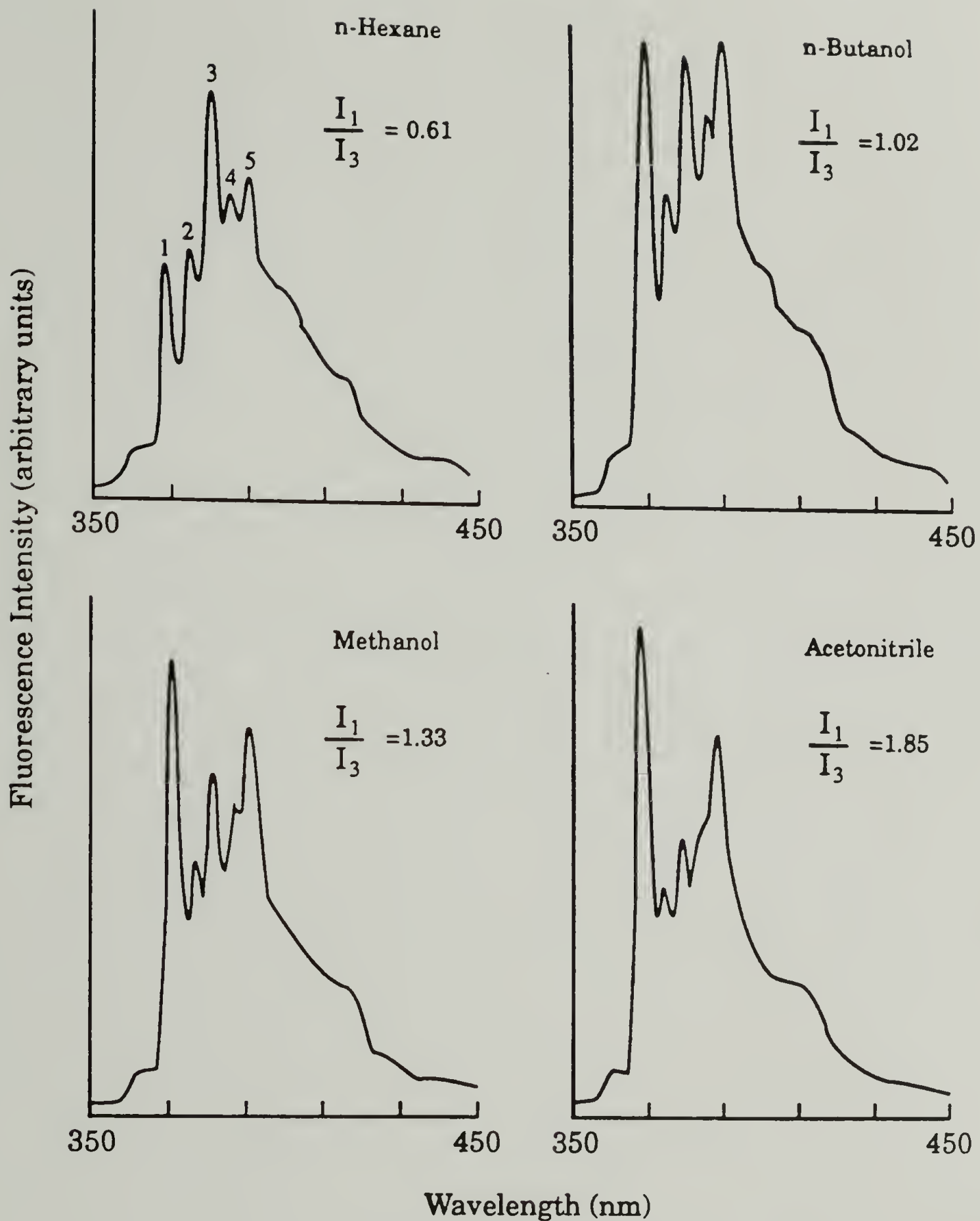


Figure 1.9 Vibrational fine structure in the fluorescence emission spectrum of pyrene. The relative intensities of peak 1 and peak 3 are sensitive to solvent. From K. Kalyanasundaram and J.K. Thomas, *J. Am. Chem. Soc.*, 1977, 99, 2039.

interactions. The intensity of peak 1 has been found to increase as the polarity of the solvent increases. Measurement of the peak 1/peak 3 ratio has been used as the basis of the pyrene scale of solvent polarity [48]. The polarity dependence of pyrene fluorescence has been used to characterize the structural organization of micelles and surfactant bilayer membranes [49].

I. Overview.

The work of Tirrell and coworkers has shown that a polyelectrolyte and double chain surfactant bilayer combine to form a system that is responsive to small changes in solution pH [13-14]. It is known that the polyelectrolyte, PEAA, exhibits a pH-dependent conformational transition, however it is not clear how this phenomenon is related to the PEAA-induced structural reorganization of DPPC vesicles. One can imagine two different mechanistic schemes for the pH-dependent interaction of PEAA and DPPC and the consequent vesicle structural reorganization (see Figure 1.10). One possibility is that at high solution pH the PEAA exists in the highly ionized expanded conformation and there is no interaction with the DPPC vesicle. When the pH is lowered the PEAA collapses to a tight coil, and further reduction in the solution pH causes the collapsed PEAA to partition into the DPPC vesicle resulting in the formation of PEAA-DPPC mixed micelles. The other possible scheme is that with initial reduction in solution pH the PEAA in an expanded conformation is driven to complex with the vesicle surface. At this point an additional decrease in pH results in a PEAA

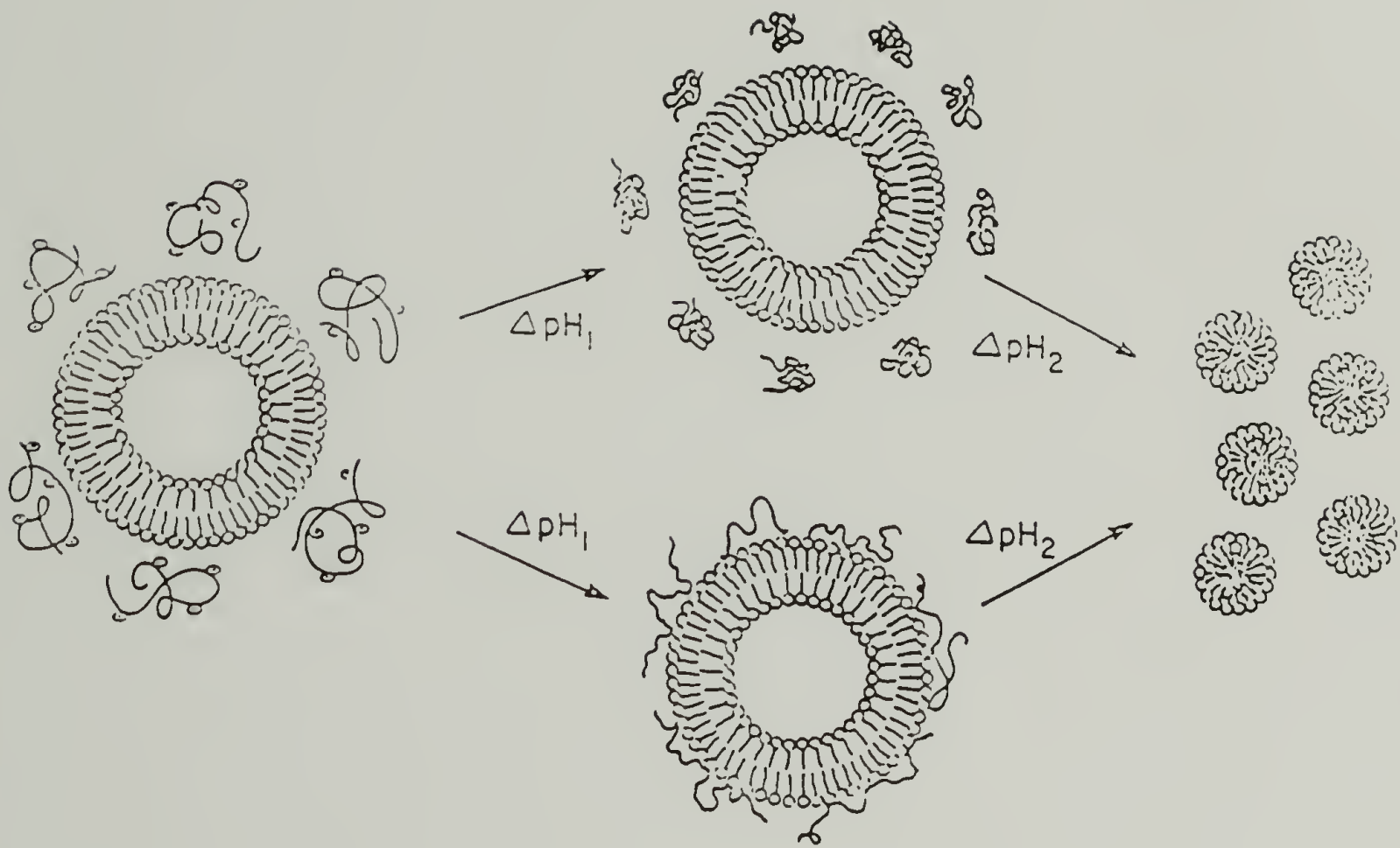


Figure 1.10 Possible mechanistic schemes for the pH-dependent interaction of PEAA and DPPC.

conformational transition to a collapsed coil with the resultant structural reorganization of the DPPC vesicle. In order to distinguish between these two possible schemes one must be able to simultaneously monitor the conformational transition of the polymer and the vesicle reorganization. This may be accomplished by using fluorescence spectroscopy to follow the conformational behavior of pyrene-tagged PEAA and the change in sample optical density to follow the DPPC vesicle reorganization. Information on the sequence of events can be obtained through comparison of the critical pH values for each of these processes.

Fluorescence spectroscopy may also be utilized to investigate the pH-dependent interaction of PEAA and DPPC vesicles through the incorporation of fluorescent probe molecules into the vesicles. One would then measure the fluorescent properties of the probe as a function of pH. The general technique is presented schematically in Figure 1.11. There are several locations within the surfactant bilayer where a probe may be placed. A hydrophobic probe may be simply imbibed into the hydrophobic internal portion of the bilayer. Another possibility is to covalently attach a probe to a surfactant molecule, either in the headgroup region or the hydrocarbon chain region. The fluorescent probes that would be useful in the study of the PEAA-DPPC system include pyrene, 1,6-diphenylhexatriene (DPH), 1,3-bis-(1-pyrene)propane (Py₂C₃), 3-palmitoyl-2-(3-(diphenylhexatrienyl)propanoyl-L- α -phosphatidylcholine (DPHPC), N-(1-pyrenesulfonyl)dipalmitoyl-L- β -phosphatidylethanolamine, triethylammonium salt (Py-DPPE), and 3-palmitoyl-2-(1-pyrenedecanoyl)-L- α -phosphatidylcholine (PyPC) (see Figure 1.12). Changes in the fluorescence polarization of probes DPH, DPHPC, PyPC, and Py-DPPE incorporated into DPPC vesicles can be measured to detect the effects of

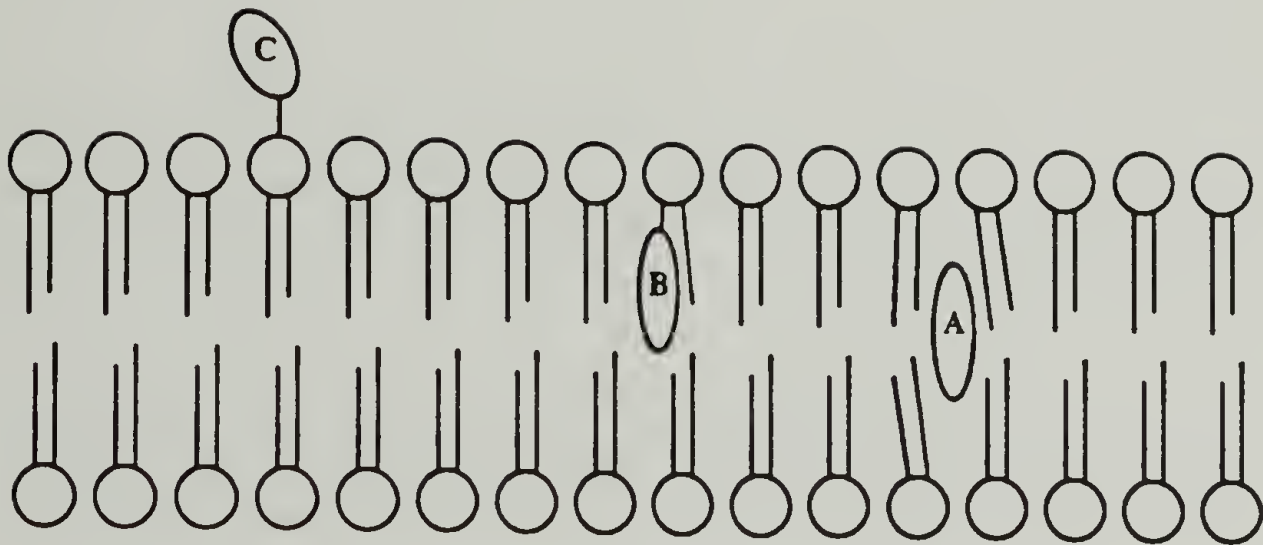
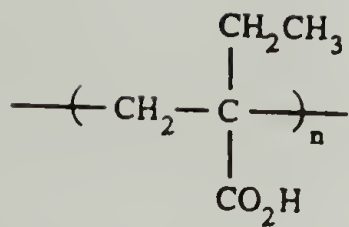


Figure 1.11 Use of fluorescent probes to monitor the pH-dependent interaction between PEAA and DPPC. Probes may be imbedded into the phospholipid bilayer (A), attached to the acyl chain of the phospholipid (B), or attached to the headgroup (C).

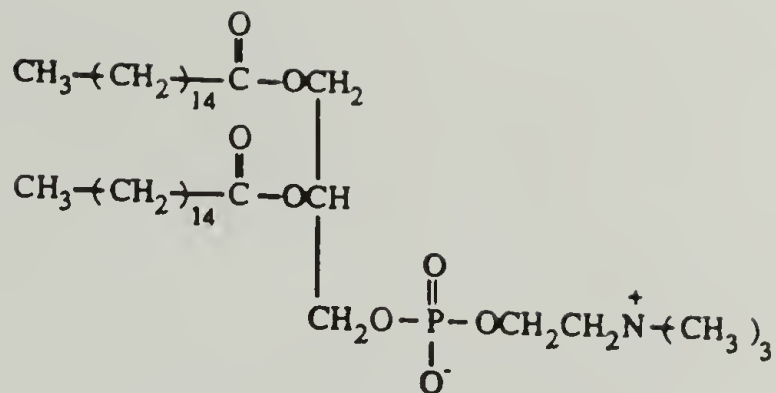
PEAA interaction. Pyrene and the intramolecular excimer forming probe Py₂C₃ can provide information on changes in the polarity and fluidity of the environment in which they reside.

The resonance energy transfer experiment provides a very sensitive means of detecting proximate interaction of two entities. This technique may be adapted to the PEAA-DPPC system through the covalent attachment of a donor species to PEAA and the incorporation of an acceptor species into DPPC vesicles (see Figure 1.13). A convenient donor-acceptor pair for resonance energy transfer studies is tryptophan-anthracene. In the PEAA-DPPC system this donor-acceptor pair will be present as PEAA-tryptophan and 9-anthracenemethyl 3 β -hydroxy-22, 23-bisnor-5-cholenate (AMC), which is incorporated into the DPPC bilayer.

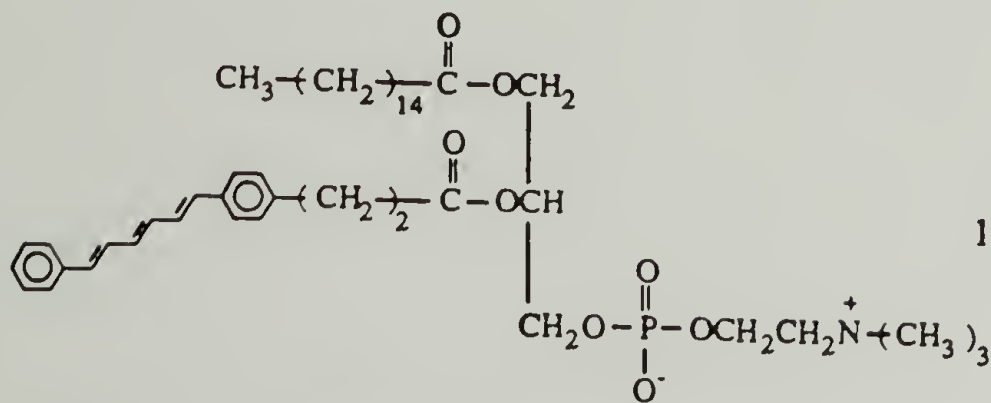
In addition to the fluorescence techniques described in the preceding sections, the techniques of differential scanning calorimetry, potentiometric titration, and transmission electron microscopy will be employed for the characterization of the pH-dependent interaction of PEAA and DPPC.



Poly(2-ethylacrylic acid) (PEAA)

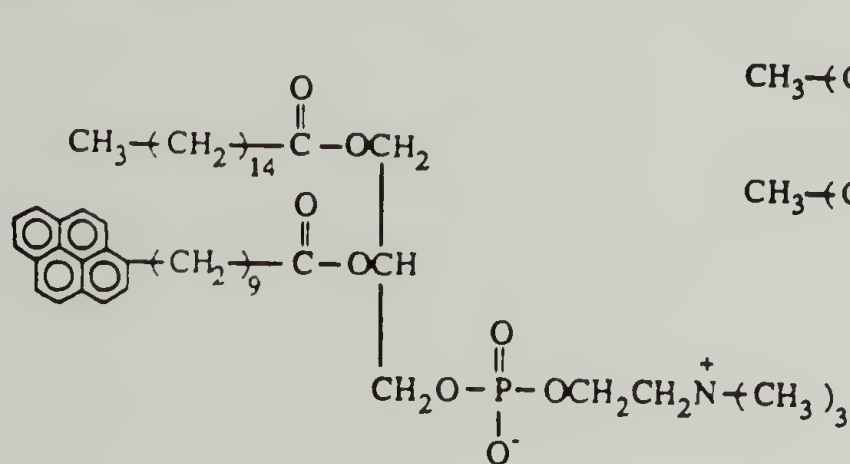


Dipalmitoylphosphatidylcholine (DPPC)

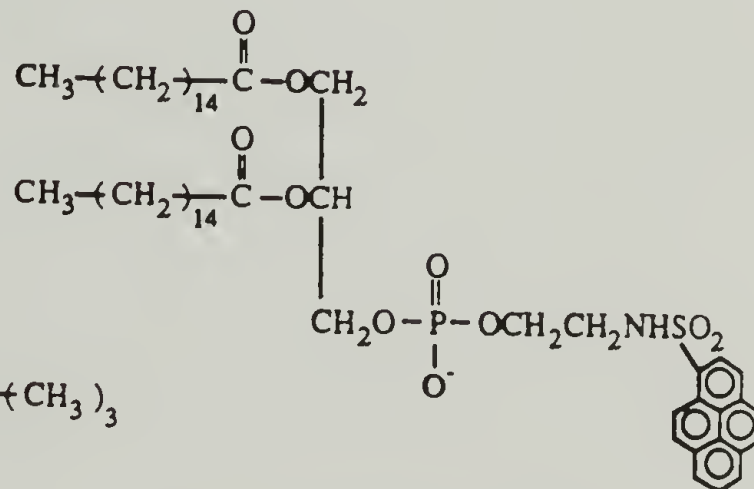


1,6-Diphenyl-1,3,5-hexatriene (DPH)

3-palmitoyl-2-(3-(diphenylhexatrienyl)propanoyl)-phosphatidylcholine (DPHPC)



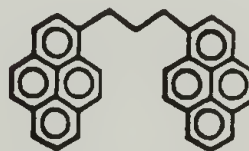
3-palmitoyl-2-(1-pyrenedecanoyl)-phosphatidylcholine (PyPC)



N-(1-pyrenesulfonyl)dipalmitoyl-phosphatidylethanolamine (Py-DPPE)

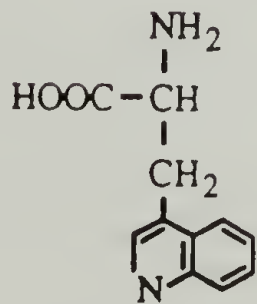
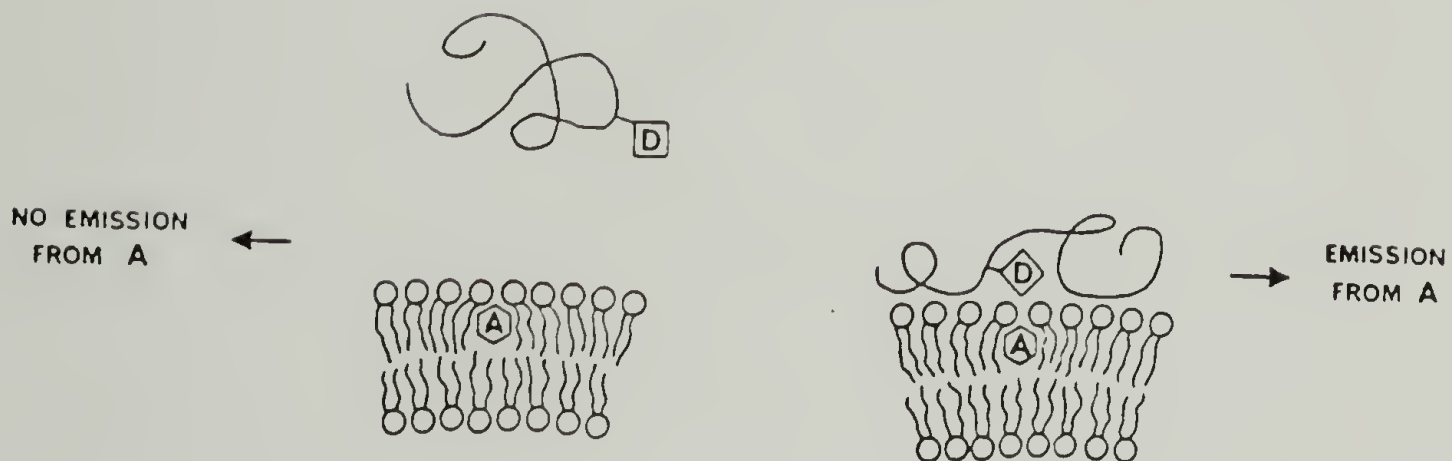
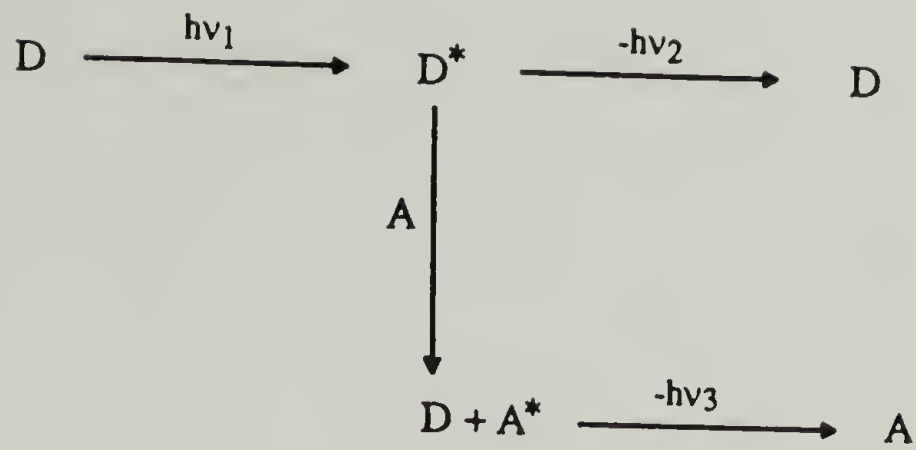


pyrene

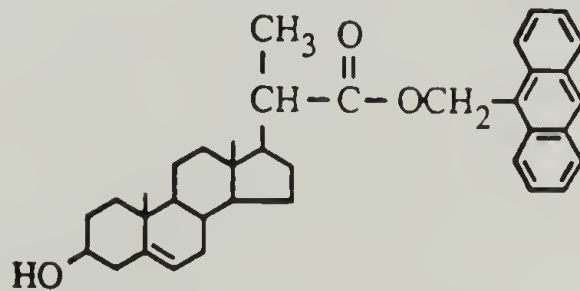


1,3-bis(1-pyrene)propane

Figure 1.12 Chemical structures of the various fluorescent probes used to study the pH-dependent interaction between PEAA and DPPC.



D = Donor (Tryptophan)



A = Acceptor (AMC)

Figure 1.13 Application of the resonance energy transfer experiment to the PEAA-DPPC system.

CHAPTER II

EXPERIMENTAL SECTION

A. Routine Measurements.

Optical density and absorbance measurements were obtained with a Beckmann DU-7 UV/VIS spectrometer.

Infrared spectra were recorded either on a Perkin-Elmer 283 or a Perkin-Elmer 1320 infrared spectrophotometer.

Proton nuclear magnetic resonance spectra were recorded either at 80 MHz on a Varian CFT-20, at 200 MHz on a Varian XL-200, or at 300 MHz on a Varian XL-300 spectrometer. Chemical shifts are reported as parts per million downfield from tetramethylsilane.

Elemental analysis measurements of the polymers were determined at the Microanalysis Laboratory at the University of Massachusetts at Amherst.

Inherent viscosity measurements were determined with a Cannon-Ubbelohde semi-micro viscometer (model 50-717).

B. Materials.

All reagents and their sources are listed below. The reagents were used as received unless indicated otherwise.

Acetone, ACS certified grade (F)

Ammonium thiocyanate (F)

9-Anthracenemethyl 3 β -hydroxy-22, 23-bisnor-5-cholenate, {AMC} (MP)

Azobisisobutyronitrile, {AIBN} (A), recrystallized from diethyl ether,
(lit. m.p. 100 °C ,dec.).

1,3-Bis-(1-pyrene)propane, {Py₂C₃}, (MP)

Carbon tetrachloride, ACS reagent grade (F)

Cellulose dialysis tubing, MW 1000 cutoff (F), rinsed with distilled water
prior to use.

Chloroform, HPLC grade (F)

Dicyclohexylcarbodiimide, 99% (A)

Diethyl ethylmalonate,99% (A)

Diethylamine, 98% (A)

Dimethylformamide, ACS reagent grade (F)

p-Dioxane, ACS reagent grade (F)

1,6-Diphenylhexatriene, {DPH} 98% (A), recrystallized from 50/50
hexane/acetone (lit. m.p. 199-203 °C).

Ethanol, absolute (P)

Ethyl acetate, ACS reagent grade (F)

Ferric chloride (F)

Formaldehyde (37% w/w in water) (F)

Hexane, ACS reagent grade (F)

Hydrochloric acid, 0.100 ± 0.001N volumetric standard solution (F)

L- α -Dipalmitoylphosphatidylcholine, 99% (S)

Lysophosphatidylcholine, palmitoyl, 99% (S)

Malonic acid, 99% (A)

Methanol, ACS certified grade (F)

Methylene chloride, ACS reagent grade (F)

N-(1-pyrenesulfonyl)dipalmitoyl-L- β -phosphatidylethanolamine,
triethylammonium salt, {Py-DPPE} (MP)

N-Hydroxysuccinimide, 97% (A)
Oxalyl chloride, 99+% (A)
3-Palmitoyl-2-(3-(diphenylhexatrienyl)propanoyl)-L- α -phosphatidylcholine,
{DPHPC} (MP)
3-Palmitoyl-2-(1-pyrenedecanoyl)-L- α -phosphatidylcholine, {PyPC} (MP)
Phosphorus pentachloride (A)
Pyrene, 99+% (A)
Pyrenebutanoic acid, 97% (A)
Pyrenecarboxaldehyde, 98+% (A)
4-Pyrrolidinopyridine, 98% (A), recrystallized from petroleum ether
(lit. m.p. 55-57 °C).
(D,L)-Serine methyl ester hydrochloride, 99% (A)
Sodium cholate, 97% (A)
Sodium deoxycholate, 98% (A)
Sodium dodecyl sulfate, electrophoresis grade (B)
Sodium hydroxide, 0.100 \pm 0.001N volumetric standard solution (F)
Triton X-100, scintillation grade (Am)
(D,L)-Tryptophan, 99+% (A)

Sources

(A) Aldrich Chemical Co. (Milwaukee, WI)
(Am) Amersham Corporation (Arlington Heights, IL)
(B) J.T. Baker (Phillipsburg, NJ)
(F) Fisher Scientific (Boston, MA)
(MP) Molecular Probes (Eugene, OR)
(P) Pharmco Products (Dayton, NJ)
(S) Sigma Chemical Co. (St. Louis, MO)

C. Methods.

1. Synthesis of poly(2-ethylacrylic acid) {PEAA}.

a. Synthesis of 2-ethylacrylic acid. 2-Ethylacrylic acid was synthesized by the procedure reported by Ferritto, Ponticello and Tirrell [50]. Ethyl ethylacrylate (IR, neat : 3300-2550 cm^{-1} , 1725 cm^{-1}) was purified by distillation prior to hydrolysis to 2-ethylacrylic acid (IR, neat : 3300-2550 cm^{-1} , 1695 cm^{-1}).

b. Polymerization of 2-ethylacrylic acid. 2-Ethylacrylic acid was placed in a round bottom flask with 0.5 mol % (based on monomer) azobis(isobutyronitrile) {AIBN}. The flask was fitted with a stopcock tubing connector and then the flask was subjected to three freeze-degas-thaw cycles. The flask was placed in an oil bath at 60 °C for 48 hrs. During the initial period of the polymerization the sample was stirred. After polymerization, the reaction mixture was ground up with mortar and pestle, suspended in distilled water (pH 6-7), filtered and washed with additional distilled water. An aqueous slurry of the solid was placed in cellulose dialysis tubing (1000 MW cutoff), and dialyzed against distilled water for one week (dialysate changed 2-3 times per day). The polymer was filtered and dried under vacuum. Yield, 25-30%. Anal. calcd. for $[\text{C}_5\text{H}_8\text{O}_2]_n$: C, 59.98%, H, 8.05%, O, 31.96%. Found : C, 59.31%, H, 7.98%, O, 31.5%. Gel permeation chromatography of the polymer was carried out as described by Schroeder and Tirrell [51] from which \overline{M}_n was determined to be 20,000 g/mol. PEAA produced by radical polymerization in bulk at 60 °C

has been shown to have a stereoirregular structure with 16% isotactic, 40% syndiotactic, and 44% heterotactic triads [13].

2. Synthesis of poly(2-ethylacrylic acid) with a pyrene chromophore.

a. Synthesis of poly(2-ethylacrylic acid-co-1-pyreneacrylic acid) {PEAA-py1}.

1. Synthesis of 1-pyreneacrylic acid [52]. 1-Pyrene-carboxaldehyde (2.53 g, 0.011 mol) and malonic acid (1.04 g, 0.01 mol) were added to a round bottom flask containing pyridine (25 ml) and piperidine (0.5 ml). The flask was fitted with a reflux condenser and the mixture was heated to 100 °C for 2 hrs. After cooling to room temperature, the solution was acidified to pH < 4 through the addition of dilute HCl, which caused the product to precipitate. The crude product was recrystallized from 80/20 methanol/acetone to give bright yellow-gold needles (lit. m.p. 280 °C [52]). Yield 1.90 g, 70%. ¹H NMR (90 MHz, DMSO) δ: 6.9, doublet (1H), 8.1-8.6, multiplet (9 H), 8.7, doublet (1 H). IR (KBr pellet) cm⁻¹: 3420, 3040, 1675, 1600, 1420, 1320, 1280, 840.

2. Copolymerization of 2-ethylacrylic acid and 1-pyreneacrylic acid. The copolymerization was carried out via the method described for the homopolymerization of PEAA, with the 1-pyreneacrylic acid (2 mol % relative to 2-ethylacrylic acid) suspended in the 2-ethylacrylic acid. Yield 25-30%. Anal. calcd. for [C₅H₈O₂]_n: C, 59.98%, H, 8.05%, O, 31.96%. Found: C, 59.21%, H, 8.08 %, O, 31.7%. GPC analysis gives $\overline{M}_n = 20,000$ g/mol. η_{inh} (0.2% in DMF, 35 °C), 0.63 dl/g. The copolymer contains 0.002 mol % pyrene

(based on PEAA monomer repeat unit). The concentration of pyrene, c_{py} , was calculated from the equation:

$$c_{py} = \frac{A_{343}}{\epsilon_{343} l} \quad (\text{Eq. 2.1})$$

where A_{343} is the measured absorbance at 343 nm, l is the cell pathlength (in cm), and ϵ_{343} is the reported molar extinction coefficient (in $M^{-1}cm^{-1}$) of 1-ethylpyrene in CH_3OH [53]. The copolymer composition was calculated as the ratio of the concentrations of pyrene and polymer repeat units. UV/VIS (0.65 mg/ml PEAA-py1 in CH_3OH): A_{343} , 0.0047, $\log \epsilon_{343}$, 4.6 [53].

b. Synthesis of poly(2-ethylacrylic acid-co-

2-(4-(1-pyrene)butanoyl)aminopropenoic acid) {PEAA-py2}.

1. Synthesis of 2-(4-(1-pyrene)butanoyl)aminopropenoic acid.

This compound was prepared via the synthetic procedure reported by Turro and Arora [54].

2. Copolymerization of 2-ethylacrylic acid and

2-(4-(1-pyrene)butanoyl)aminopropenoic acid. The copolymerization was carried out via the method described for the homopolymerization of PEAA, with the pyrene monomer (0.1 mol % relative to 2-ethylacrylic acid) suspended in the 2-ethylacrylic acid. Yield 28%. Anal. calcd. for $[C_{15}H_{18}O_2]_n$: C, 59.98%, H, 8.05%, O, 31.96%. Found: C, 59.75%, H, 7.89%, O, 30.9%. η_{inh} (0.2% in DMF, 35 °C), 0.65 dl/g. The copolymer contains

0.04 mol% pyrene (based on PEAA monomer repeat unit). The copolymer composition was determined as described for PEAA-py1. UV/VIS (3.6 mg/ml PEAA-py2 in CH₃OH) : A₃₄₃, 0.56.

3. Synthesis of poly(2-ethylacrylic acid) containing tryptophan {PEAA-trp}.

PEAA, $\overline{M}_n = 20,000$ g/mol, (1.0 g, 0.01 mol repeat unit) was dissolved in 100 ml freshly distilled dimethylformamide (DMF). Dicyclohexylcarbodiimide (0.21 g, 1 mmol) was added to the solution, followed by the addition of N-hydroxysuccinimide (0.115 g, 1 mmol), and 4-pyrrolidinopyridine (0.015g, 0.1 mmol). The reaction mixture was stirred at 22 °C for 15 hrs. Tryptophan (0.20 g, 1 mmol) was added to the reaction mixture and stirred at 22 °C for 8 hrs. The reaction mixture was added to ethyl acetate in order to precipitate the polymer. The precipitate was filtered and then dissolved in alkaline distilled water (pH 8-9). The resulting solution was then filtered. The volume of the filtrate was reduced to ~20 ml on a rotary evaporator. The solution was placed in cellulose dialysis tubing (1000 MW cutoff) and dialyzed against alkaline distilled water (pH 8-9) for 2 days (the dialysate was changed 2-3 times per day). The polymer was precipitated with the addition of HCl, filtered, and then dried under vacuum. The polymer was found to contain 1 mol % tryptophan (based on PEAA repeat unit). The composition of the polymer was determined as described for PEAA-py1, through the use of the reported value of the molar extinction coefficient of tryptophan at 280 nm in water [55]. UV/VIS (1 mg/ml PEAA-trp in H₂O): A₂₈₀ , 0.660, $\log \epsilon_{280} = 3.8$ [55].

4. Preparation of vesicle samples.

a. Multilamellar vesicles. Dipalmitoylphosphatidylcholine (DPPC) was dissolved in a minimum volume of chloroform, and the chloroform was removed through rotary evaporation to leave a thin film on the vial surface. A volume of phosphate buffer (NaH_2PO_4 - Na_2HPO_4 mixture) was added to the vial. The vial was placed in a water bath at 50-60 °C, and then subjected to several cycles of heating and vortexing to form the multilamellar vesicles.

b. Sonicated vesicles. Phosphate buffer was added to a vial containing a thin film of DPPC, and the resulting suspension was sonicated with a Branson Model 185 Cell Disruptor fitted with a 1/8 inch diameter titanium microtip at a power of 30 watts for 10-15 minutes at 50-60 °C. The sonicated suspension was then centrifuged for 30 minutes in a IEC Model CL clinical centrifuge with a 4 x 50 ml swinging bucket rotor (3350 rpm maximum) at setting 5 (~2500 rpm) to sediment titanium particles and large multilamellar vesicles. Small sonicated vesicles remained in the supernatant.

5. Preparation of samples for fluorescence spectroscopy.

a. Fluorescence studies with pyrene. A stock solution of pyrene (2×10^{-3} M) in acetone was prepared. Pyrene was dispersed in a stock solution of phosphate buffered PEAA (4 mg/ml) by stirring at room temperature for 2-3 hours. Aliquots of 0.500 ml from the PEAA stock solution were dispensed into vials. A total of 1.5 ml of NaH_2PO_4 and NaCl

solutions were added to the vials to give constant ionic strength solutions at various solution pH with 1 mg/ml PEAA. For studies with DPPC, the pyrene was dispersed in a stock suspension of phosphate buffered DPPC (4 mg/ml) vesicles and stirred at 50-60 °C overnight for at least 12 hours. Into vials was placed 0.500 ml of the DPPC stock, 0.500 ml of PEAA stock (4 mg/ml, no added pyrene), and 1.000 ml of the NaH₂PO₄ /NaCl solutions to yield samples of constant ionic strength at various pH values. The samples were then placed in a water bath at 50-60 °C for 1 hr. Pyrene concentration in all the samples was 5 x 10⁻⁶ M. Fluorescence spectra were recorded on a Perkin-Elmer MPF-66 fluorescence spectrometer equipped with a thermostatted sample compartment. The temperature was regulated to ± 0.2 °C with a Brinkmann Lauda RM-6 circulating bath. Correction factors for the wavelength-dependent intensity of the xenon lamp of the MPF-66 were generated using Rhodamine B (3 g/l in ethylene glycol) as a quantum counter over an excitation wavelength range from 200 nm to 600 nm. Correction factors for the wavelength-dependent efficiency of the MPF-66 detection system were generated from the Rhodamine B calibrated spectral output of the xenon lamp. Fluorescence spectra were automatically corrected with the Perkin-Elmer CLS software supplied with the MPF-66. Emission spectra were recorded at 23.0 ± 0.2 °C on aerated samples using 337 nm excitation with 3 nm excitation and emission slit widths. Excitation spectra were recorded at 23.0 ± 0.2 °C on aerated samples using 374 nm emission wavelength with 1 nm excitation and 2 nm emission slit widths.

b. Fluorescence studies with PEAA-bound pyrene {PEAA-py}.

Samples were prepared with stock solutions of PEAA-py and DPPC as

described for the pyrene studies in Section II.C. Emission spectra were recorded at 23.0 ± 0.2 °C on aerated samples using 345 nm excitation with 3 nm excitation and emission slit widths. Excitation spectra were recorded at 23.0 ± 0.2 °C on aerated samples with 378 nm emission and 3 nm slit widths.

c. Fluorescence studies with 1,3-bis-(1-pyrene)propane (Py₂C₃). A stock solution of Py₂C₃ (1.4×10^{-3} M) in acetone was prepared. Aliquots of the stock solution were added to degassed, argon flushed samples containing PEAA and sonicated DPPC (1 mg/ml each, prepared as described in Section II.C.) at 50-60 °C. The molar ratio of probe to DPPC was 1 to 1500. The samples were protected from light, heated at 50-60 °C for several hours, cooled to room temperature and bubbled through with argon for 10 minutes before measuring the fluorescence. Emission spectra were recorded as described in Section II.C. at 23.0 ± 0.2 °C on samples under an argon blanket with 331 nm excitation wavelength, 3 nm excitation and emission slit widths. Excitation spectra were obtained under similar conditions with 396 nm and 488 nm emission wavelengths, and 3 nm slit widths. The monomer to excimer ratio (I_M/I_E) was calculated from the ratio of the measured emission intensities at 396 nm and 488 nm. Scattered light can contribute to the measured monomer and excimer peak intensities, therefore identical intensity measurements were made on pure DPPC samples (O.D.< 0.25). Scattered light was less than 2% of the measured monomer or excimer intensities.

d. Fluorescence polarization studies with DPH. A stock solution of DPH in acetone (1.0×10^{-3} M) was prepared. Samples containing PEAA

and sonicated DPPC vesicles (0.25 mg/ml each) were prepared as described in Section II.C. Optical densities of the samples for all fluorescence polarization studies were < 0.10 (measured at 600 nm) to eliminate complications due to scattering. Aliquots of the DPH stock solution (DPH to DPPC molar ratio of 1 to 1000) were added to the degassed, nitrogen or argon flushed samples at 50-60 °C. The samples were protected from light and heated overnight at 50-60 °C. The samples were then cooled to room temperature and the emission spectra were recorded with a Perkin-Elmer MPF-66 fluorescence spectrometer fitted with a polarization accessory at 23.0 ± 0.2 °C on deaerated samples with 360 nm excitation, 5 nm excitation slit width, and 10 nm emission slit width for each of the four possible polarizer settings. The four possible settings are denoted as VV, VH, HH, and HV. In this notation V stands for vertical polarizer orientation and H stands for horizontal orientation. The first letter corresponds to the excitation beam and the second letter to the emission beam. The intensity at 430 nm was used for the calculation of the polarization. For each polarizer setting the intensity measurement was made 6-10 times, and the values were averaged to calculate the steady state polarization. The polarization was calculated from the equation:

$$P = \frac{k - 1}{k + 1} \quad (\text{Eq. 2.2}) \quad \text{with} \quad k = \frac{I_{VV} \times I_{HH}}{I_{VH} \times I_{HV}} \quad (\text{Eq. 2.3})$$

where I_{VV} , I_{HH} , I_{VH} , I_{HV} are the average emission intensities measured at each polarizer combination. This calculation takes into account the correction factor for effects of selective instrument polarization.

e. Fluorescence polarization studies with DPHPC. Samples containing PEAA and sonicated DPPC vesicles were prepared as described in Section II.C. DPHPC was dissolved in ethanol (6.4×10^{-4} M) and aliquots of the stock solution were added to the samples to yield a DPHPC to DPPC ratio of 1:1000. Sample treatment was as described in Section II.C. Emission spectra were obtained at 23.0 ± 0.2 °C on deaerated samples using 363 nm excitation with 4 nm excitation slit width and 10 nm emission slit width. The maximum emission intensity of the 430 nm peak was used for the polarization calculation. The precise position of the peak maximum varied with each polarizer setting, therefore the intensity corresponding to the peak maximum was recorded.

f. Fluorescence polarization studies with PyPC. Samples were prepared as described in Section II.C. A stock solution of PyPC in ethanol (6×10^{-4} M) was used, and the molar ratio of PyPC to DPPC in the samples was 1 to 1000. Emission spectra were recorded at 23.0 ± 0.2 °C on deaerated samples with 347 nm excitation using 4 nm excitation and 10 nm emission slit widths. The emission intensity at 398 nm was measured for determining the polarization.

g. Fluorescence polarization studies with Py-DPPE. Sample preparation and treatment were as described in Section II.C. Aliquots from a stock solution of Py-DPPE in ethanol (6×10^{-4} M) were added to samples to give a molar ratio of Py-DPPE to DPPC of 1 to 1000. Emission spectra were obtained at 23.0 ± 0.2 °C on deaerated samples using 350 nm excitation with 4 nm excitation and 10 nm emission slit widths. The emission intensity at 380 nm was used in the polarization calculation.

h. Fluorescence energy transfer studies with PEAA-trp and AMC. PEAA-trp and sonicated DPPC vesicle samples were prepared in nitrogen purged phosphate buffer following the procedures described in Section II.C. AMC (5.0×10^{-2} M in acetone) was dispersed in the DPPC vesicle suspension at 50-60°C with vortex agitation. The molar ratio of AMC to DPPC was 1 to 45. Samples containing PEAA-trp, DPPC, and AMC at various pH values were prepared following the procedure described previously. The PEAA-trp and DPPC concentrations were each 1 mg/ml in the samples. Emission spectra were recorded using 290 nm excitation for the tryptophan with 5 nm excitation and emission slit widths. The extent of energy transfer was calculated for each sample from the anthracene emission intensity at 395 nm as I_F/I_0 , where I_F is the sample emission intensity and I_0 is the emission intensity for an otherwise identical sample containing no PEAA-trp (See Figure 3.58 for graphical definition of I_F and I_0).

6. Potentiometric titration.

PEAA (3.0 ± 0.1 mg) was dissolved in 0.500 ml of 0.100 ± 0.001 N standardized NaOH. Next, a combination of NaCl (1.5 M stock solution), DPPC multilamellar vesicles (stock solution of 7.5 mg/ml) and/or distilled deionized water was added as required to give samples having ionic strengths of 0.02 M, 0.10 M, or 0.40 M with and without DPPC vesicles (at 1 mg/ml). The final volume of the sample was 3.000 ml. The sample was immersed in a jacketed beaker water bath maintained at 55.0 ± 0.2 °C, argon was slowly bubbled through for 10 minutes, and an argon blanket

was maintained above the sample throughout the titration. The titration was carried out with the injection of 5, 10 or 20 μl aliquots of $0.100 \pm 0.001\text{N}$ standardized HCl from a 25 μl syringe (uncalibrated) to the stirred sample. The solution pH was measured to 0.01 pH units after each injection with a Corning Model 155 ion analyzer equipped with a Corning X-EL combination semi-micro electrode. The pH meter was calibrated before each titration run with standardized buffers at pH 4, pH 10, and pH 7.

7. Electron microscopy.

PEAA and DPPC mixtures (1 mg/ml each) were prepared in 0.02 M phosphate buffer following the procedure described in Section II.C. After heating and vortex agitation the samples were cooled to room temperature (22 °C). Formvar and carbon-coated copper grids were treated with 5 μl of the PEAA-DPPC mixture. After 30 seconds, excess liquid was wicked away by using the edge of a filter paper. The samples were stained for 30 seconds with 5 μl of 2% aqueous phosphotungstic acid, the pH of which was adjusted to correspond to that of the sample. Again, the excess liquid was wicked away. The grids were then examined using a JEOL 100S transmission electron microscope operating at 80 kV.

8. Differential scanning calorimetry.

Mixtures of PEAA and DPPC (1 mg/ml each) in phosphate buffer were prepared as described in Section II.C. The sample was degassed under vacuum and then transferred via a calibrated syringe fitted with a Chaney adaptor to the calorimeter (0.90 ml added). The thermogram was

recorded on a Microcal MC-1 scanning calorimeter at a heating rate of 15 °C/hr. The power axis (y-axis) was calibrated by supplying a pulse of 2.21 mcal/min to the reference cell of the calorimeter after recording each thermogram. The first heatings of the samples are reported. Second runs were identical to first heatings with the exception of small increases in transition widths.

9. Determination of PEAA-DPPC mixed micelle composition.

a. Samples with PEAA and sonicated DPPC vesicles. Stock suspensions of sonicated DPPC vesicles were prepared in $\text{NaH}_2\text{PO}_4 + \text{Na}_2\text{HPO}_4$ buffer (pH 6, ionic strength 0.02 M) at concentrations of 2, 5, 10, 15, and 20 mg/ml as described in Section II.C. A stock solution of PEAA-py2 (20 mg/ml) in $\text{NaH}_2\text{PO}_4 + \text{Na}_2\text{HPO}_4$ buffer (pH 6, ionic strength 0.02 M) was prepared. For each concentration of DPPC, the optical density of the suspension was measured after successive addition of small amounts of PEAA solution. The samples were heated to 50-60 °C for a few minutes after each PEAA addition, and then cooled to room temperature prior to the optical density measurement.

b. Samples with PEAA and multilamellar DPPC vesicles. Stock solutions of PEAA-py2 (4 mg/ml and 9 mg/ml) and multilamellar DPPC vesicles (2 mg/ml and 4 mg/ml) were prepared in $\text{NaH}_2\text{PO}_4 + \text{Na}_2\text{HPO}_4$ buffer (pH 6, ionic strength 0.02 M) as described in Section II.C. Aliquots with 0.2 mg DPPC from the stock solution were dispensed into a series of vials. Aliquots of the PEAA-py2 stock solution were added to the vials to give a range of PEAA-py2 to DPPC weight ratios from 0:1 to 2.5:1.

Phosphate buffer (pH 6, ionic strength 0.02 M) was added to each vial to bring the final volume to 2.000 ml. The samples were heated at 50-60 °C for several hours, cooled to room temperature, vortexed and immediately placed in the UV/VIS spectrophotometer for measurement of the optical density at 600 nm. This procedure was repeated for series of samples containing 0.25 mg/ml, 0.5 mg/ml, 1 mg/ml, and 2 mg/ml DPPC.

10. Binding of PEAA to DPPC vesicles.

a. Binding as a function of solution pH. Phosphate buffered mixtures of PEAA-py2 (0.5 mg/ml) and DPPC multilamellar vesicles (0.5 mg/ml) at various solution pH and constant ionic strength (0.02 M and 0.40 M) were prepared following the procedures described in Sections 4.a. and 5.a. (total volume of sample was 2.00 ml). The samples were placed in a water bath at 55 °C for 2 hours. After cooling to room temperature, the samples were centrifuged for 1.5 hours at ~2500 rpm in an IEC Model CL centrifuge to sediment the vesicles. After cooling to room temperature, 0.300ml of the supernatant was withdrawn for the analysis of PEAA-py. Also, 0.200 ml of the supernatant was withdrawn for the analysis of DPPC. For the PEAA-py analysis, 0.700 ml of 0.100 ± 0.001 N standardized NaOH was added to the tube containing the withdrawn supernatant and vortexed. Next, 1.000 ml CH₃OH was added, followed by vortex agitation and heating to 55 °C for several minutes. After cooling to room temperature, the fluorescence emission spectrum was recorded using an excitation wavelength of 345 nm with 2 nm excitation and 1.5 nm emission slit widths. The emission intensity at 378 nm was used for the determination of

unbound PEAA-py. Calibration curves were established by repeating this procedure on a series of 2.00 ml samples only containing aliquots from the PEAA-py₂ stock solution and phosphate buffer.

The analysis for DPPC was carried out as described by Stewart [56]. To the withdrawn supernatant was added 2.000 ml of 0.1 N ammonium ferrioxalate. This mixture was then vortexed. Next, 2.000 ml of CHCl₃ was added, followed by vortex agitation. After settling for a few minutes, the CHCl₃ phase was withdrawn and the absorbance at 488 nm was measured. Calibration curves were prepared by repeating this procedure on a series of 2.00 ml samples only containing aliquots from the DPPC vesicle stock solution and phosphate buffer.

b. Binding as a function of DPPC concentration. Mixtures of PEAA-py₂ and DPPC at pH 7.1 were prepared in phosphate buffer at constant ionic strength with varying ratios of PEAA-py₂ to DPPC (PEAA-py₂ concentration was constant at 0.5 mg/ml). The samples were heated to 55 °C for 2 hours and then cooled to room temperature. The samples were centrifuged for 1.5 hours at ~2500 rpm in an IEC Model CL centrifuge. After cooling to room temperature the samples were analyzed for PEAA-py₂ and DPPC as described in the previous section. The concentration dependent binding experiment was repeated for samples having solution pH values of 8.6 and 10.3.

CHAPTER III

RESULTS AND DISCUSSION

A. Goals and Accomplishments.

We sought to gain an understanding of the mechanism of the pH-dependent PEAA-induced structural reorganization of DPPC vesicles. We have found that the sensitivity of this system to solution pH is due to the pH-dependent ionization behavior of the PEAA. The critical pH for vesicle reorganization was found to correspond to the critical pH for the conformational transition of PEAA. Various fluorescence techniques, as well as electron microscopy and differential scanning calorimetry, have shown that there are two main stages to the pH-dependent PEAA-DPPC interaction. As the solution pH is reduced there is increasing complexation of the PEAA with the surface of the vesicle. When the solution pH is lowered through the conformational critical pH of PEAA, the PEAA adopts a compact coil conformation and interacts to cause a breakdown in the enclosed bilayer structure of the vesicle. This two stage interaction is schematically depicted in Figure 3.1.

B. Morphological Characterization of the PEAA-DPPC System.

Transmission electron microscopy was applied in order to resolve questions about the size and morphology of the reorganization products and intermediates. Simple turbidity measurements (see Chapter I, Section C) indicate that there is a substantial reduction in the size of the initial DPPC

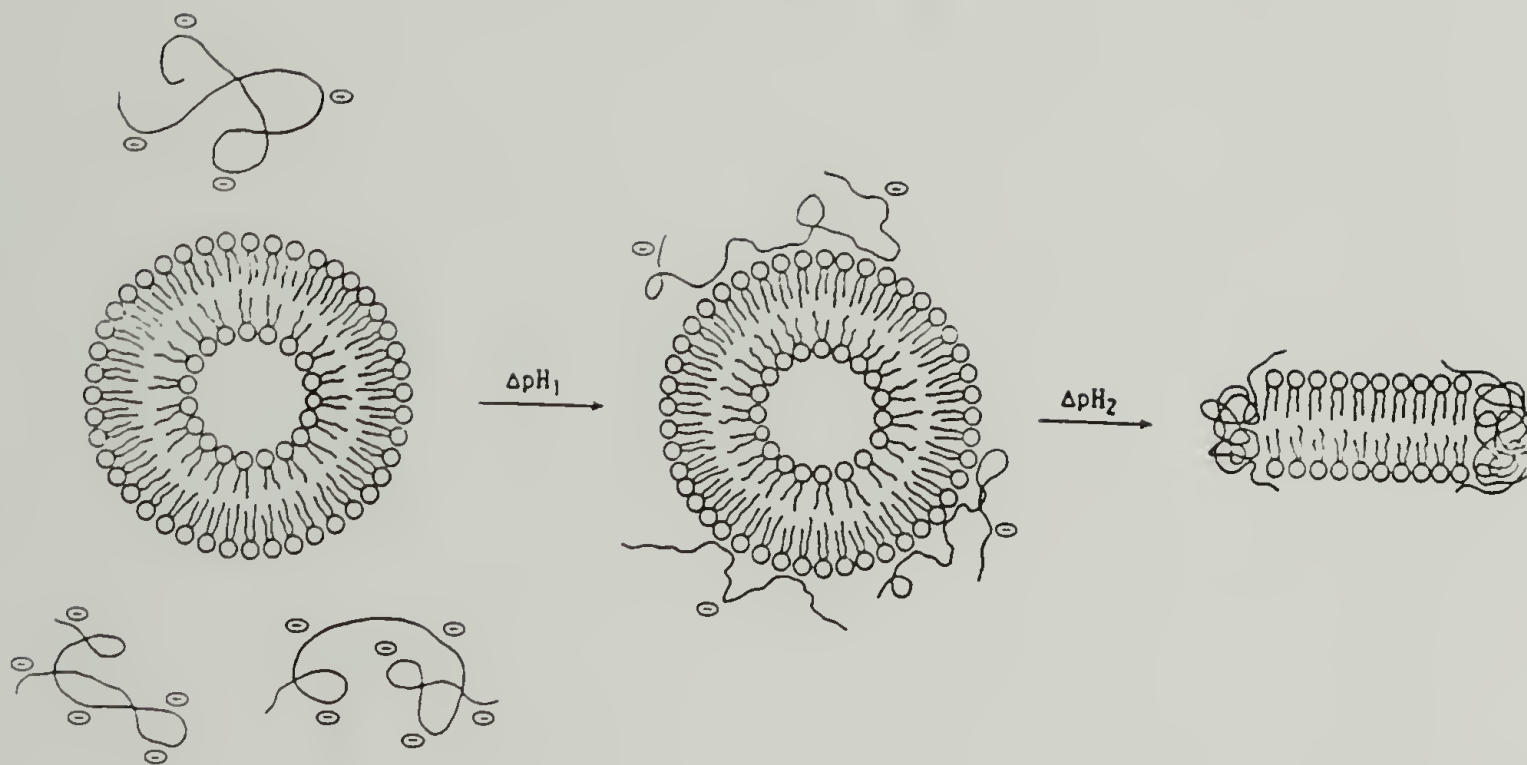


Figure 3.1 Sequence of events in the pH-dependent interaction between PEAA and DPPC.

vesicles as a result of the pH-dependent interaction of PEAA. This is observed as a complete clarification of the initially milky white vesicle suspension. In mixtures of PEAA (0.05 mg/ml) and DPPC (0.05 mg/ml), quasi-elastic light scattering measurements reveal a change in the average hydrodynamic radius, R_H , from ~ 90 nm to 5.5 nm when the solution pH is lowered below pH 6.5 [57]. The small particle size observed in PEAA-DPPC mixtures below pH 6.5 seems to be inconsistent with a vesicular structure. The reorganization products are presumed to be small PEAA-DPPC mixed micelles. These PEAA-DPPC mixed micelles appear as disk-like structures in negative stain electron micrographs. The micrograph obtained at pH 5.7 (see Figure 3.2) shows the presence of extended stacks of disk-like structures having average dimensions of 54 ± 6 Å in thickness and 160 ± 50 Å in diameter. Quasi-elastic light scattering measurements detect the presence of only single disk species in solution with an R_H of 5.5 nm and a diffusion coefficient of 4.0×10^{-7} cm²/sec [57]. The calculated diffusion coefficient for an oblate ellipsoid with major and minor axes of 16.0 nm and 5.5 nm, respectively, is 3.6×10^{-7} cm²/sec [57]. The average hydrodynamic radius implied by the microscopic images, assuming no aggregation of the disks prior to drying, is within 10% of the actual measured value. These results suggest that the stacking observed in the micrograph is an artifact of the drying and staining procedures required for visualization. Similar disk-like structures have been observed as the recombinant products from the interaction of phospholipid vesicles with apolipoproteins, bile salts, detergents, and amphiphilic proteins [58-63]. Characteristics shared by all the disk-forming agents include the presence of hydrophobic domains within a water-soluble molecule, and the ability to form hydrogen bonds with the phosphate headgroup of the phospholipid.



Figure 3.2 Negative-stain electron micrograph of DPPC (1 mg/ml) suspended in phosphate-buffered (0.02 M) aqueous PEAA (1 mg/ml), pH 5.7.

Electron micrographs were obtained over a range of pH values for the PEAA-DPPC system and reveal several interesting features of the interaction process. Micrographs of PEAA-DPPC samples at pH 7.6 (see Figure 3.3) show large vesicular structures which are identical to those observed for similar samples containing only DPPC (see Figure 3.4). We detect no interaction of PEAA with DPPC vesicles at pH 7.6. In micrographs taken of samples at pH 7.1 (see Figure 3.5) we see large intact vesicular structures which display a banded ripple-like surface texture with a periodicity of 140-150 Å. This rippled surface texture is reminiscent of the P_{β}' "ripple" phase of phosphatidylcholine vesicles observed in freeze fracture electron micrographs. Freeze fracture studies have reported the periodicity of the ripple phase of DPPC to be 150 ± 20 Å [20, 21]. While the ripple phase is characteristically manifested in phosphatidylcholine vesicles as a thermal transition (see Figure 1.2, for DPPC T_{pre} is 35 °C), it appears that we may be able to induce a rippled structure through polyelectrolyte adsorption. This effect would be analogous to the induction of the ripple phase in dipalmitoylphosphatidic acid (DPPA) vesicles through changes in pH, addition of Ca^{2+} ions, and the addition of poly(lysine) [64]. In the bilayer structure, phospholipid molecules pack closely together to minimize interchain van der Waals interaction energy [65]. The large headgroup of phosphatidylcholines (~15% larger cross-sectional area than the acyl chain region [66]) prevents acyl chains that are perpendicular to the bilayer normal from coming close enough to minimize the van der Waals energy. In the L_{β}' gel phase the acyl chains are tilted with respect to the bilayer normal, which reduces the interchain separation while maintaining the headgroup separation. At the pretransition temperature there is a substantial increase in the interfacial area per phospholipid

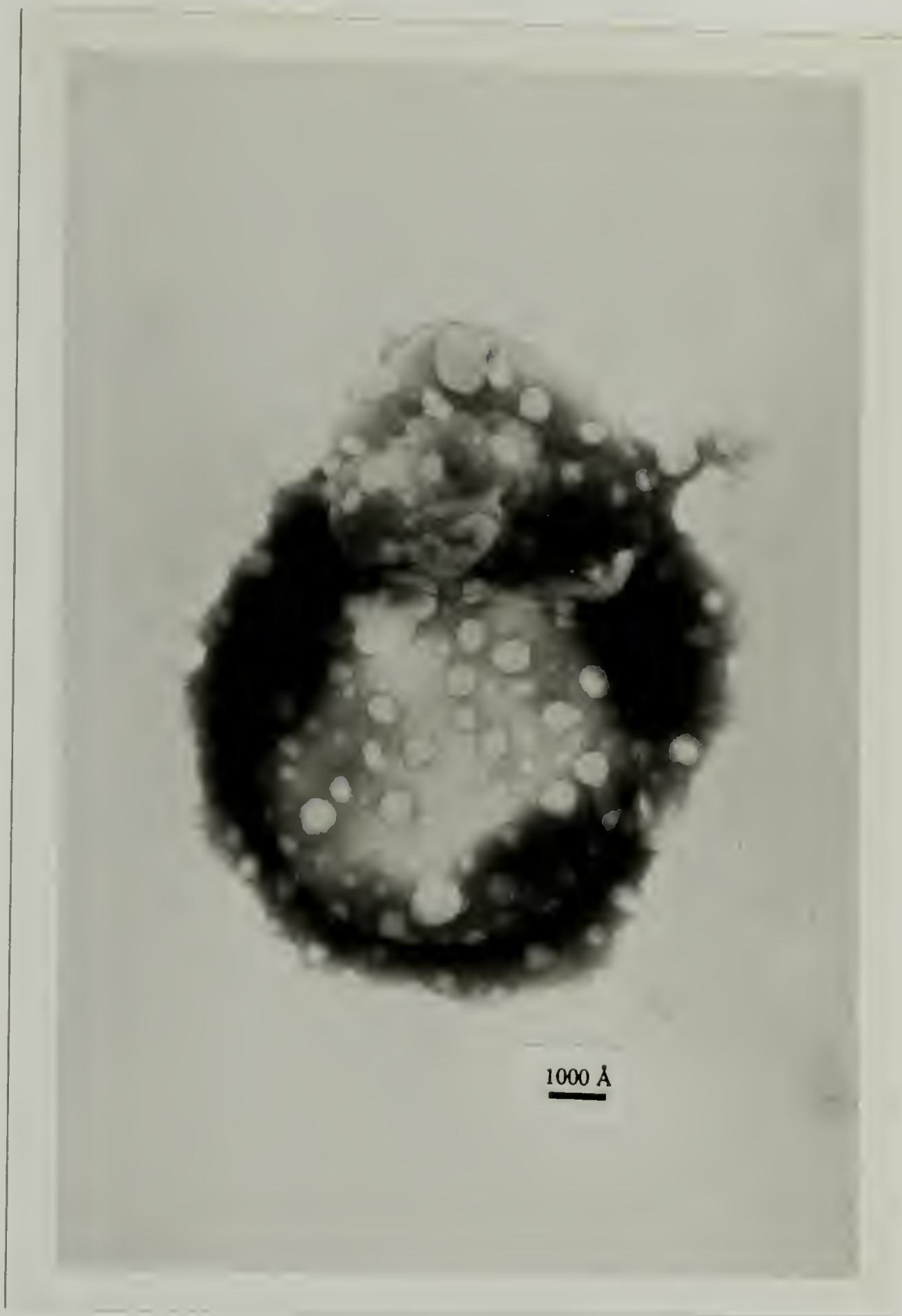


Figure 3.3 Negative-stain electron micrograph of DPPC (1 mg/ml) suspended in phosphate-buffered (0.02 M) aqueous PEAA (1 mg/ml), pH 7.6.



Figure 3.4 Negative-stain electron micrograph of a PEAA-free phosphate-buffered (0.02 M) aqueous suspension of DPPC (1 mg/ml), pH 7.1.



Figure 3.5 Negative-stain electron micrograph of DPPC (1 mg/ml) suspended in phosphate-buffered (0.02 M) aqueous PEAA (1 mg/ml), pH 7.1.

molecule [67]. To accommodate the interfacial area expansion while maintaining the close chain packing, phospholipid molecules are vertically displaced with respect to one another. This results in the formation of the $P_{\beta'}$ ripple phase. In the PEAA-DPPC system, the interaction of PEAA with DPPC may act to increase the effective interfacial cross-sectional area, which could then be accommodated through formation of a rippled phase.

In the micrographs of samples at pH 6.4 (see Figure 3.6) we notice many of the stacked disk structures seen for the pH 5.7 samples. However, we also find quite a few large vesicular structures, which display the rippled surface texture. It has been observed that reorganization of DPPC vesicles in PEAA solutions is dependent on the solution pH, temperature, and time [13]. The vesicle reorganization in mixtures of PEAA and DPPC occurs to a significant extent only when the temperature of the sample is greater than or equal to the T_m of DPPC, which is 41 °C [68]. As a consequence of the time and temperature dependence of the PEAA-DPPC interaction, our experiments are carried out at pseudoequilibrium conditions. The microscopic observation of vesicles and mixed micelles at pH 6.4 may be a consequence of the pseudoequilibrium conditions. Quasi-elastic light scattering [69] shows a bimodal size distribution for the PEAA-DPPC system at pH 6.4, in accordance with microscopic observations. The size distribution becomes unimodal below solution pH values of 6.2.

A particularly intriguing image was obtained by slowing the vesicle-to-mixed micelle transition by maintaining an acidified (pH 6.4) sample below the T_m of DPPC (41 °C). Structural reorganization is very slow under these conditions, which may permit observation of early stages of the process. The micrograph for a sample of this type (see Figure 3.7) shows two large

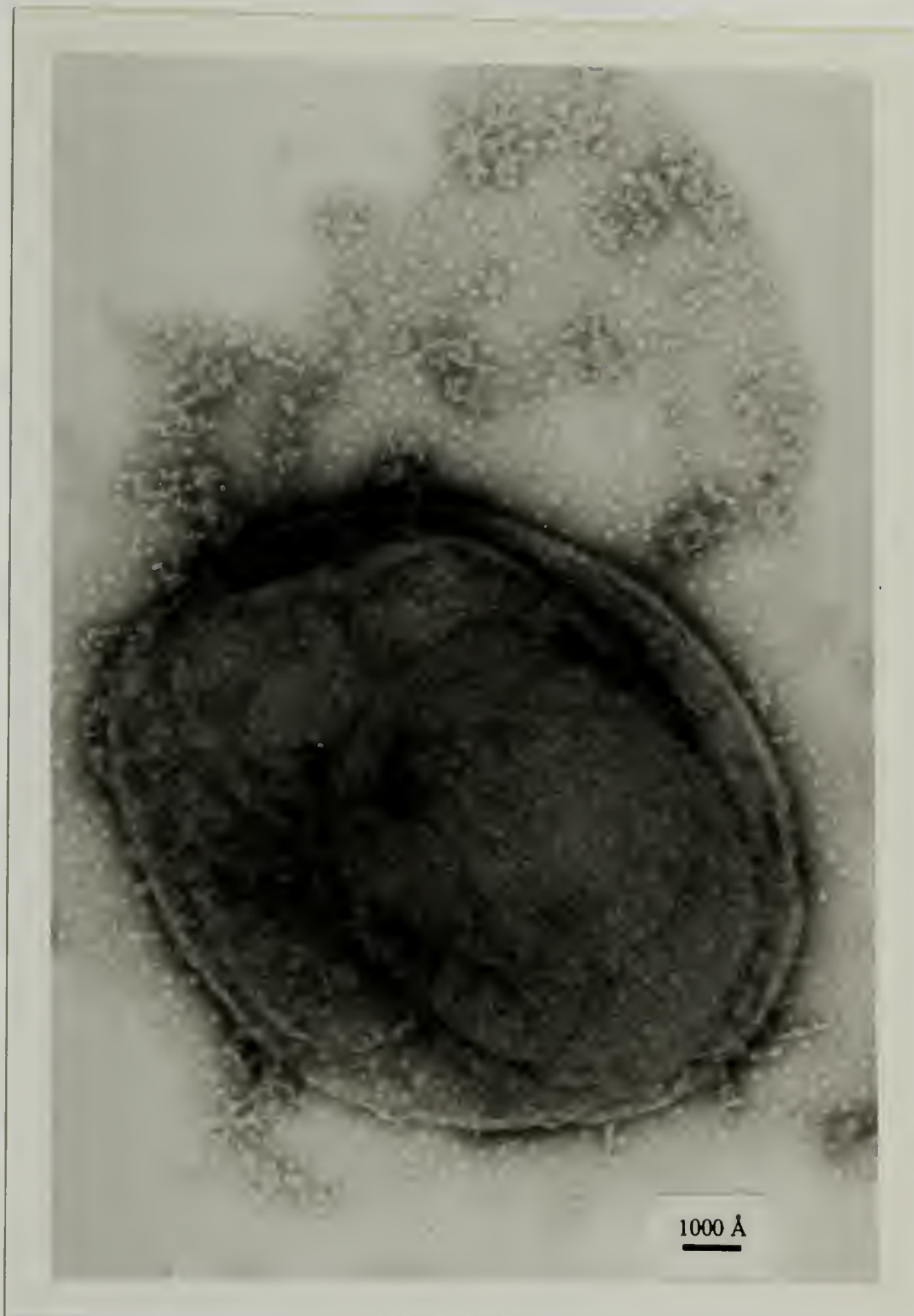


Figure 3.6 Negative-stain electron micrograph of DPPC (1 mg/ml) suspended in phosphate-buffered (0.02 M) aqueous PEAA (1 mg/ml), pH 6.4.



Figure 3.7 Negative-stain electron micrograph of DPPC (1 mg/ml) suspended in phosphate-buffered (0.02 M) aqueous PEAA (1 mg/ml), pH 6.4, temperature of sample maintained at 25 °C (below the main phase transition temperature of DPPC, 41 °C).

intact vesicles with small stacks of mixed micelles protruding from the vesicle surface. Since the sample preparation involved dehydration, it is uncertain if this juxtaposition of the vesicles and mixed micelles is mechanistically significant or only the result of the drying process bringing them together.

C. Conformational Behavior of PEAA in Aqueous Solution.

We used pyrene as a photophysical probe to detect the conformational transition of PEAA. Figure 3.8 shows the fluorescence emission spectra of 5×10^{-6} M pyrene in a series of phosphate buffered (0.02 M) PEAA solutions (1 mg/ml) of varying pH. The molar ratio of pyrene to PEAA is 1 to 10, based on $\overline{M}_n = 20,000$ g/mol. We see that the intensity of emission increases as the solution pH is decreased. A plot of the fluorescence intensity at 374 nm is plotted against solution pH in Figure 3.9. We observe a dramatic increase in fluorescence intensity at low pH, indicating that the PEAA collapses from an expanded conformation at high pH to a hydrophobic, globular coil at low pH. Under this particular set of experimental conditions the midpoint of the conformational transition occurs at pH 6.1. In addition to the intensity change, we see differences in the fine structure of the pyrene emission spectrum in PEAA solutions (see Figure 3.8). In solutions at high pH the peak 1(374 nm)/peak 3(383 nm) ratio is 1.9, which corresponds to the peak 1/peak 3 ratio measured in water, and is indicative of a highly polar environment [47, 48]. In solutions at low pH, where PEAA is in the collapsed conformation, the measured ratio is 1.35, which is similar to the ratio found in CH_3OH [47, 48]. The change in the ratio of

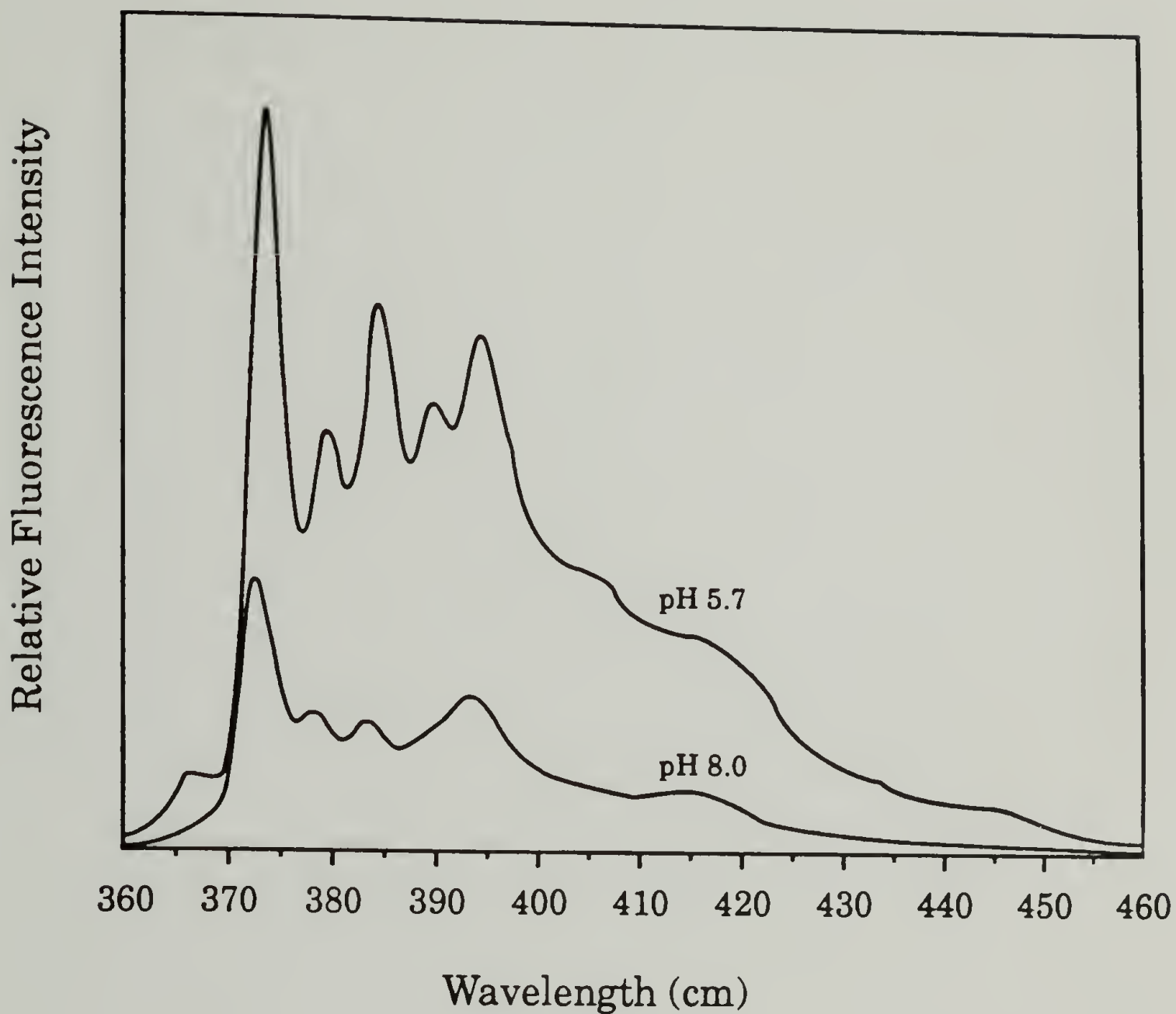


Figure 3.8 Fluorescence emission spectra for pyrene (5×10^{-6} M) in phosphate-buffered (0.02 M) solutions of PEAA (1 mg/ml). Spectra were recorded using 337 nm excitation at 23 °C.

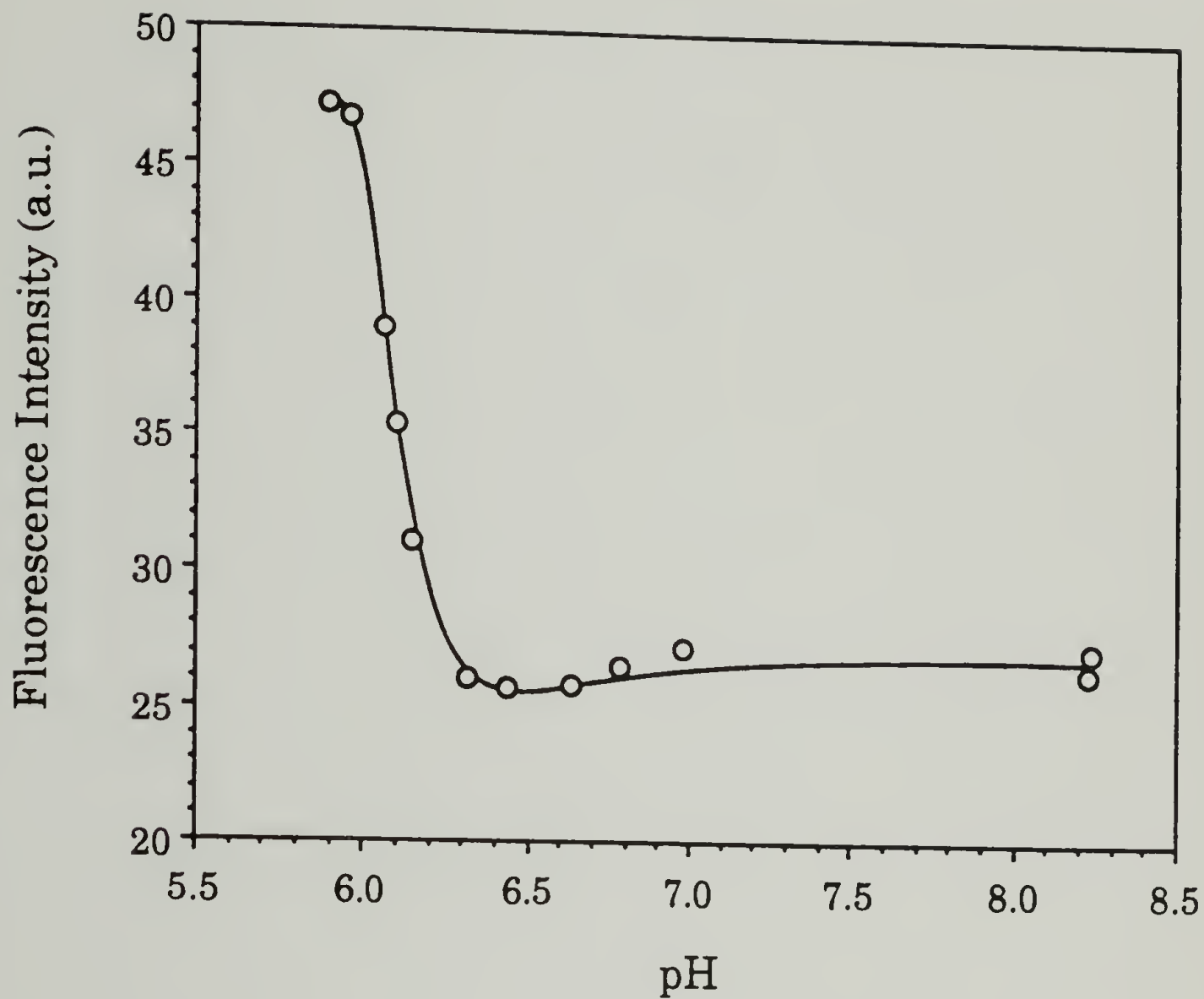


Figure 3.9 Fluorescence intensity (374 nm) emitted by pyrene (5×10^{-6} M) in phosphate buffered (0.02 M) solutions of PEAA (1 mg/ml) as a function of pH. Excitation wavelength 337 nm, temperature 23 °C.

peak 1 to peak 3 ratio suggests the conformational transition of PEAA in solutions at low pH leads to the formation of domains which shield the solubilized pyrene molecule from the aqueous medium. The measured peak 1/peak 3 ratio of pyrene has been found to be sensitive to O₂ dissolved in the solvent, specific interactions between pyrene and the solvent, and also instrumental parameters such as the excitation and emission slit widths. As a consequence, comparison of peak 1/peak 3 ratios from experiment-to-experiment and from lab-to-lab must be made cautiously.

We have also examined the excitation spectra of pyrene in PEAA solutions. It is seen in Figure 3.10 that the wavelength of maximum intensity in the excitation spectrum ($\text{ex } \lambda_{\text{max}}$) shifts from 335 nm in PEAA solution at high pH to 339 nm in PEAA solutions at low pH. So, as the solution pH is lowered and the PEAA undergoes a conformational transition, we observe a shift in $\text{ex } \lambda_{\text{max}}$ to longer wavelength (a red shift).

The absorption of light by a fluorophore results in the formation of an electronically excited state. The absorption occurs on a time scale of 10^{-15} sec, which is too short for significant displacement of the nuclei of the fluorophore. This is the Franck-Condon principle, and it simply states that immediately upon absorption of light, the fluorophore is in the same structural environment in the excited state as in the ground state. Therefore, if there is a certain orientation of the ground state fluorophore with solvent molecules, immediately upon excitation this arrangement of molecules does not change. For fluorophores such as pyrene, the absorption of light results in the instantaneous formation of a dipole, which perturbs the surrounding "ground state" environment. The solvent molecules can respond to the perturbation through a reorganization of the solvent cage of the fluorophore. This process of solvent relaxation results in

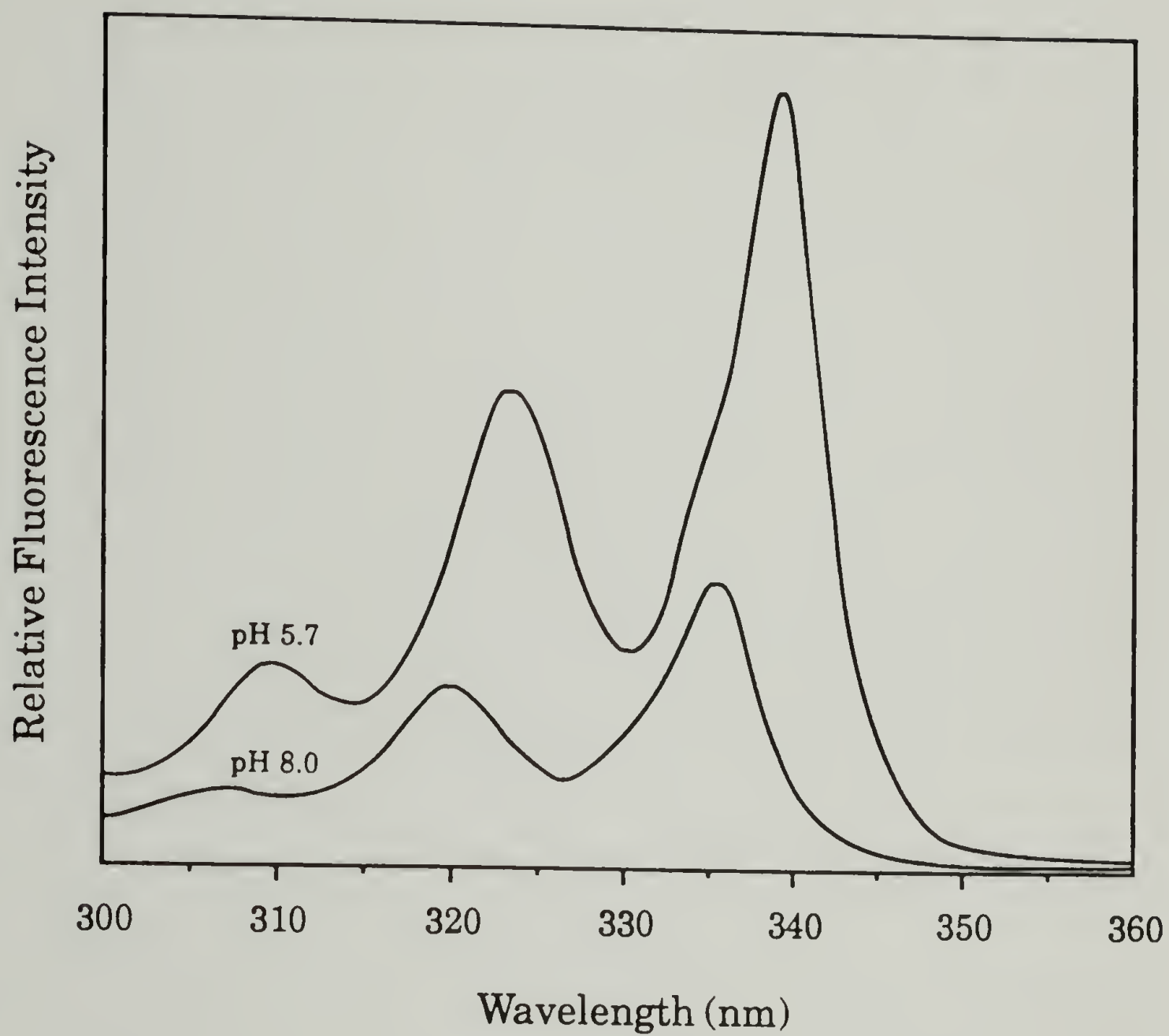


Figure 3.10 Fluorescence excitation spectra for pyrene (5×10^{-6} M) in phosphate-buffered (0.02 M) solutions of PEAA (1 mg/ml). Spectra were recorded using 374 nm emission at 23 °C.

a lowering of the energy of the initial excited state. As the nature of the solvent is changed, there may be a change in the relative energy differences between the ground state, the initial excited state, and the equilibrium excited state. The effects of the nature of the solvent on solvent-fluorophore interactions would be observed as wavelength shifts in the emission and/or excitation spectra. The effect of a fluorophore, which has no dipole in the ground state and an induced dipole in the excited state, moving from a polar solvent to a nonpolar solvent is schematically shown in Figure 3.11. The energy of the initial excited state will be lower in nonpolar solvents (S_1') than in polar solvents (S_1), since there are no unfavorable incorrectly oriented dipole-dipole interactions. In the polar solvent, solvent relaxation leads to a lower energy equilibrium excited state (S_{1E}). In the nonpolar solvent, the equilibrium excited state (S_{1E}') will have a lower energy than the initial excited state (S_1') if the solvent may be sufficiently polarized. In Figure 3.11 it is assumed the ground state energies are unchanged in the different solvents ($S_0' = S_0$). For the case depicted in Figure 3.11, as the polarity of the solvent is decreased one would observe a red shift in the excitation and emission spectra of the fluorophore ($h\nu_{A'} < h\nu_A$, $h\nu_{F'} < h\nu_F$). The magnitude of the shift in the excitation spectra depends on the relative energies of the initial excited state in the different solvents (S_1' to S_1), while the magnitude of the shift in the emission spectra depends on the relative energies of the equilibrium excited state in the different solvents (S_{1E}' to S_{1E}). The magnitude of the emission red shift will also be affected if the time required for solvent relaxation is longer than the excited state lifetime in the different solvents, since the equilibrium excited state will not be attained.

Nonpolar Solvent

Polar Solvent

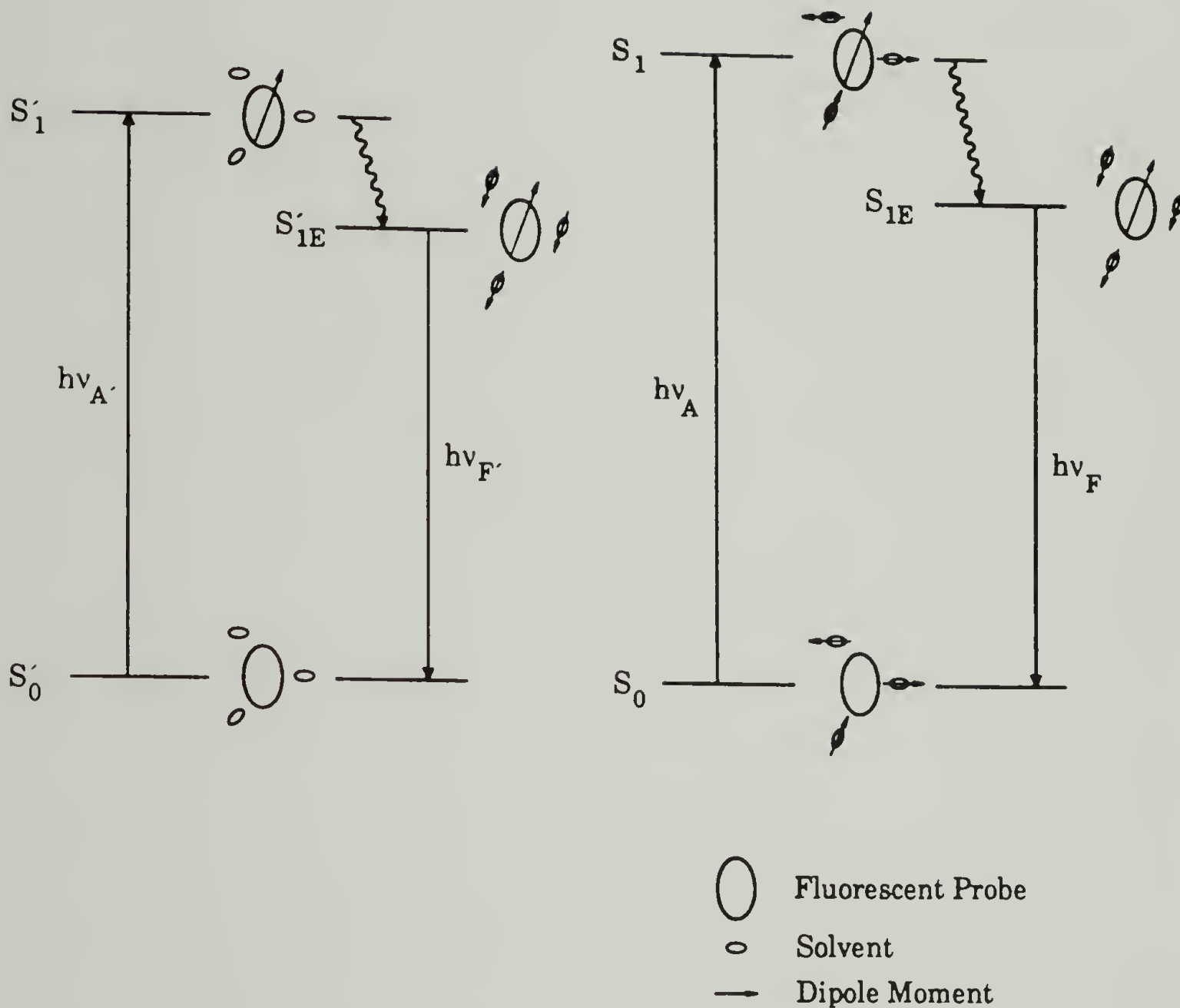


Figure 3.11 Origin of solvent-induced spectral shifts for nonpolar fluorophores. This model shows the fluorophore exhibiting red shifts in the excitation and emission when going from a polar to a nonpolar solvent. From A.J. Pesce, C.-G. Rosen, T.L. Pasby, Fluorescence Spectroscopy, Marcel Dekkar : New York, NY, 1971.

Figure 3.11 may explain the observed red shift in the excitation spectra of pyrene in PEAA solutions as the pH is lowered. The peak 1/peak 3 measurements indicate that when the PEAA adopts a collapsed conformation at low pH, domains are formed which are less polar than water and solubilize pyrene. As the pyrene moves to a less polar environment, a red shift in the excitation spectrum is observed. In addition to the general solvent effects of polarity which result from changes in refractive index and dielectric constant, specific interactions between the solvent and fluorophore may influence the relative energy levels of the ground and excited states. Therefore, interpretation of the experimentally observed wavelength shifts may not be as simple as proposed in Figure 3.11.

The conformational behavior of PEAA with covalently attached pyrene (PEAA-py) was also analyzed using fluorescence spectroscopic techniques. The emission spectra of PEAA-py₂ (1 mg/ml, 2×10^{-7} M bound pyrene) in phosphate buffered solutions (ionic strength 0.40 M) of varying pH is shown in Figure 3.12. As for unbound pyrene we observe an increase in emission intensity as the solution pH is lowered. A plot of the emission intensity at 377 nm versus solution pH is given in Figure 3.13. Again we notice the same dramatic change in intensity occurring over a narrow range of pH as found with the unbound pyrene. The midpoint of this intensity change occurs at pH 6.3, a slight shift from the value of 6.1 found with the unbound pyrene (5×10^{-6} M). In the study with PMAA, Thomas saw a shift from pH 5.0 to 5.7 when changing from unbound (1×10^{-5} M) to bound (7×10^{-6} M) pyrene [41], which is somewhat larger than the change we observe for PEAA, but the change is in the same direction. Thomas's interpretation of this shift is that there are two stages to the PMAA conformational transition. The first stage is an initial opening of the polymer chain, which

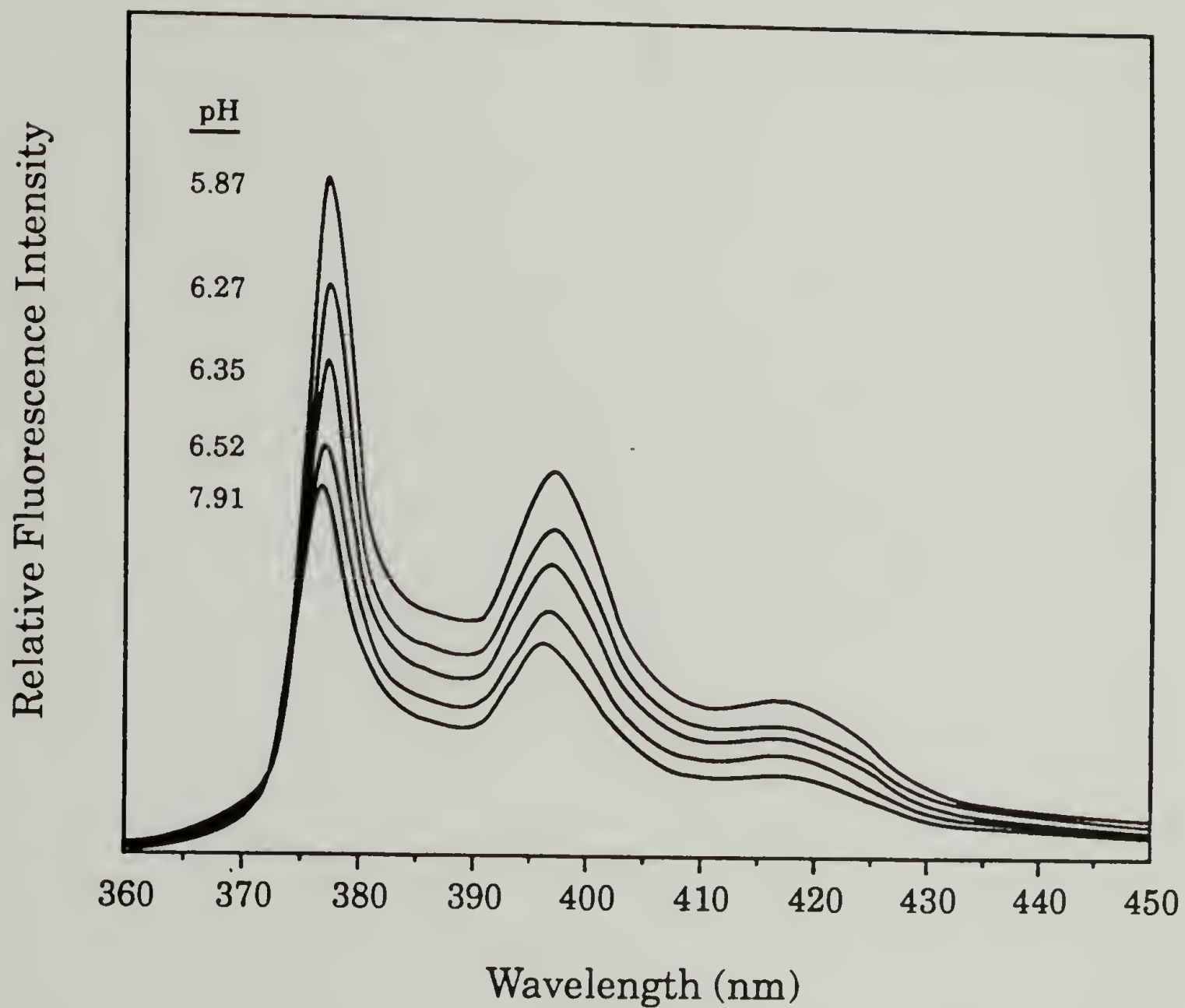


Figure 3.12 Fluorescence emission spectra for PEAA-py2 copolymer (1 mg/ml) in phosphate-buffered (0.40 M) aqueous solution. Spectra were recorded using 345 nm excitation at 23 °C.

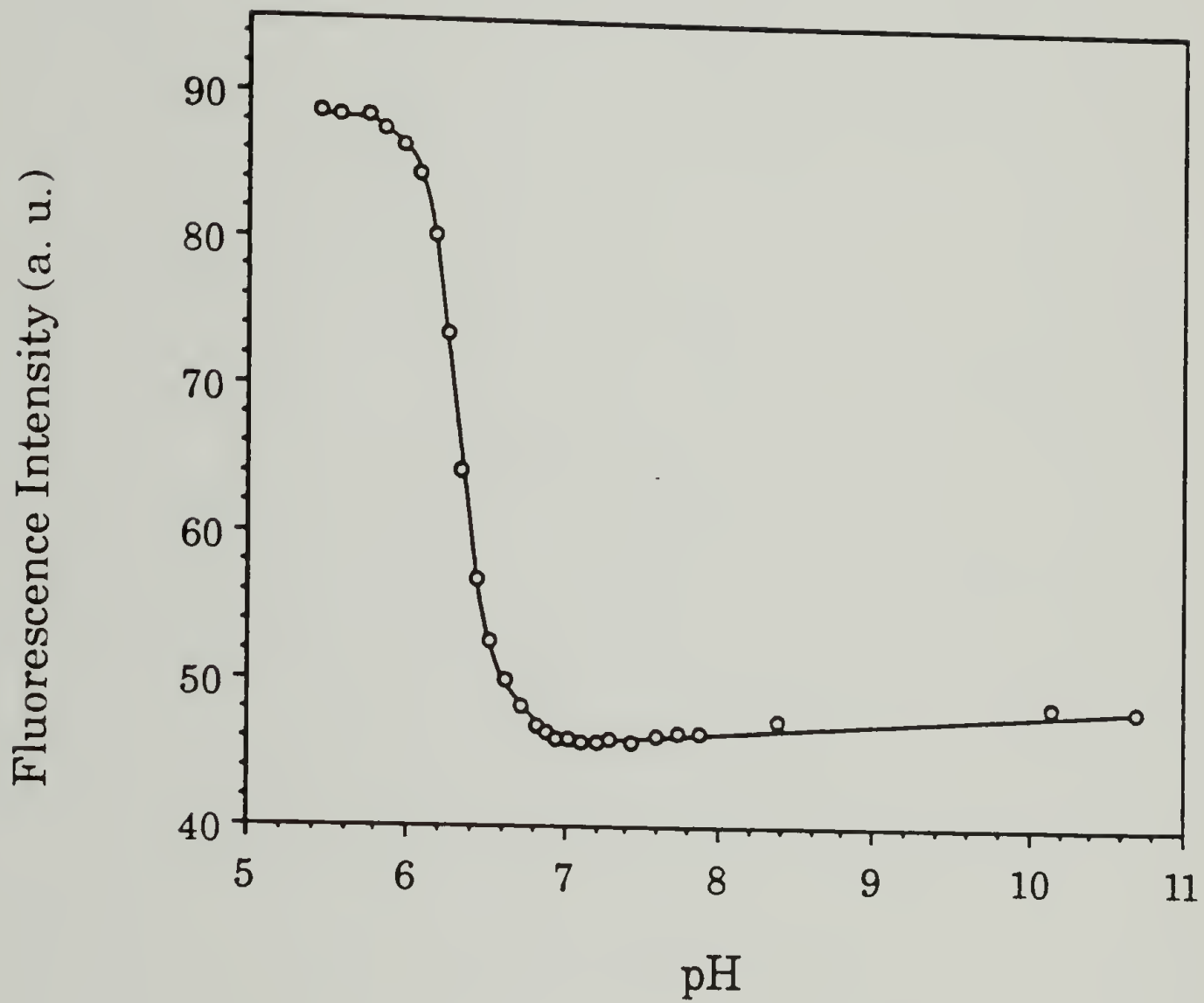


Figure 3.13 Fluorescence intensity (377 nm) emitted by PEAA-py2 (1 mg/ml) in phosphate-buffered (0.40M) aqueous solution as a function of pH. Excitation wavelength 345 nm, $T = 23\text{ }^{\circ}\text{C}$.

results in the ejection of unbound pyrene in the aqueous medium. In this first stage the bound pyrene is partially screened from interaction with water. In the second stage the polymer coil expands further and results in increased contacts between the bound pyrene and water.

In addition to the change in emission intensity, we observe a pH-induced shift in the peak position in the emission spectrum. This phenomenon is presented in Figure 3.14 as a plot of the wavelength of maximum intensity in the emission spectrum ($\text{em } \lambda_{\text{max}}$) against solution pH. The spectral precision of the fluorescence spectrometer is ± 0.1 nm for the wavelength axis, so within each experiment we may determine λ_{max} to within ± 0.1 nm. For solutions at high pH with PEAA-py2 in an expanded conformation, $\text{em } \lambda_{\text{max}}$ is 376.8 nm, while in solutions with collapsed PEAA-py2 we find a $\text{em } \lambda_{\text{max}}$ of 377.6 nm. The $\text{em } \lambda_{\text{max}}$ change occurs over a narrow range of pH (~ 0.8 pH units), the midpoint of which occurs at pH 6.5. For this particular series of samples the midpoint of the intensity change occurs at pH 6.3, so as the solution pH is lowered, the change in $\text{em } \lambda_{\text{max}}$ precedes the change in intensity.

A red shift was observed in the excitation spectra of these PEAA-py2 samples as the solution pH was lowered (see Figure 3.15), which is similar to the effect found with unbound pyrene in PEAA solutions (see Figure 3.10). A plot of $\text{ex } \lambda_{\text{max}}$ versus pH is presented in Figure 3.16. The $\text{ex } \lambda_{\text{max}}$ is 342.8 nm for samples with PEAA-py2 in the expanded conformation, and is 346.6 nm for PEAA-py2 in the collapsed form. The change happens over a very narrow pH range (~ 0.5 pH units) with the midpoint at pH 6.3, which is identical to the midpoint of the change in emission intensity. The second derivatives of the excitation spectra show that the shift is due to the

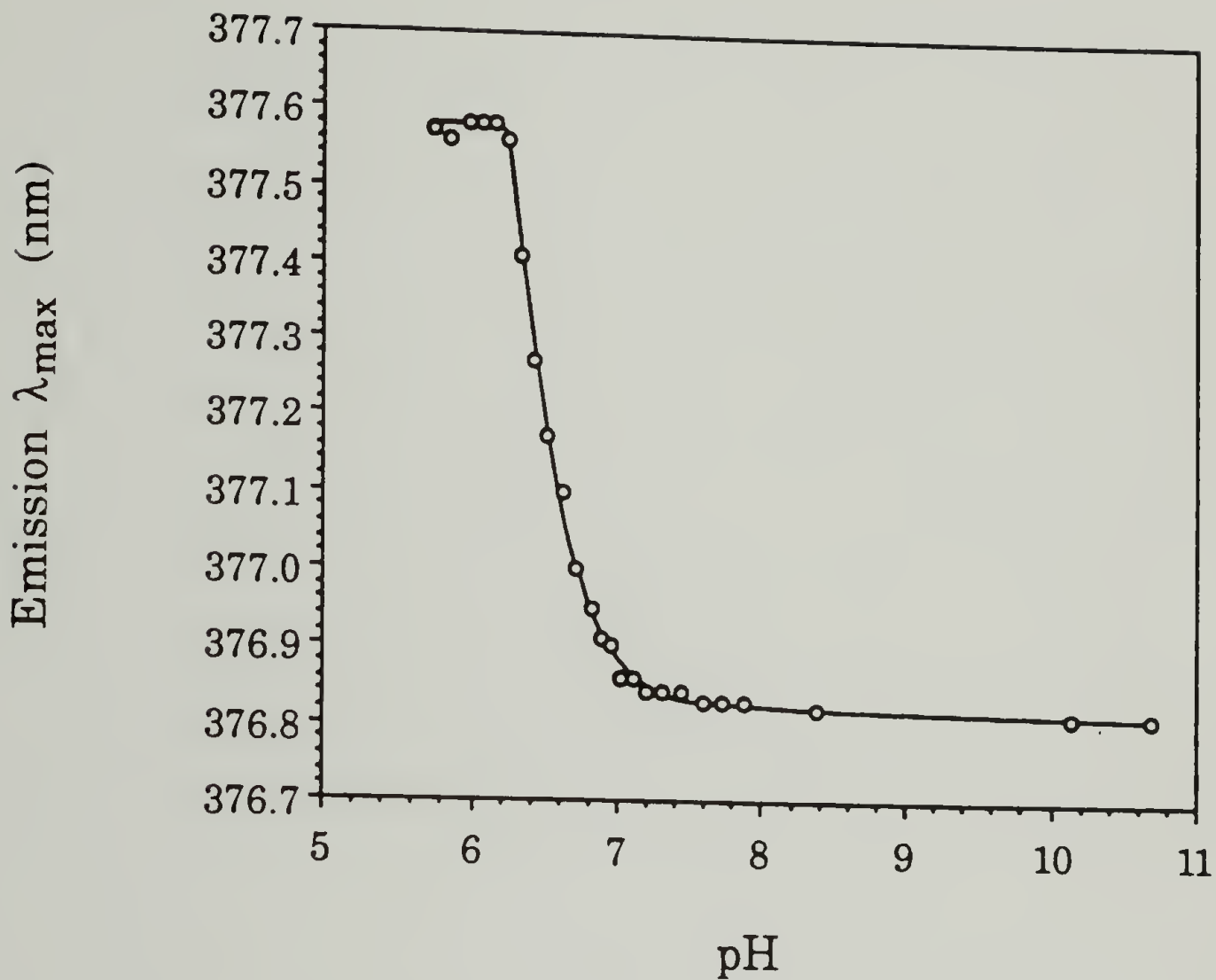


Figure 3.14 Wavelength of maximum intensity in the emission spectrum of PEAA-py2 (1 mg/ml) in phosphate-buffered (0.40M) aqueous solution as a function of pH. Excitation wavelength 345 nm, T = 23 °C.

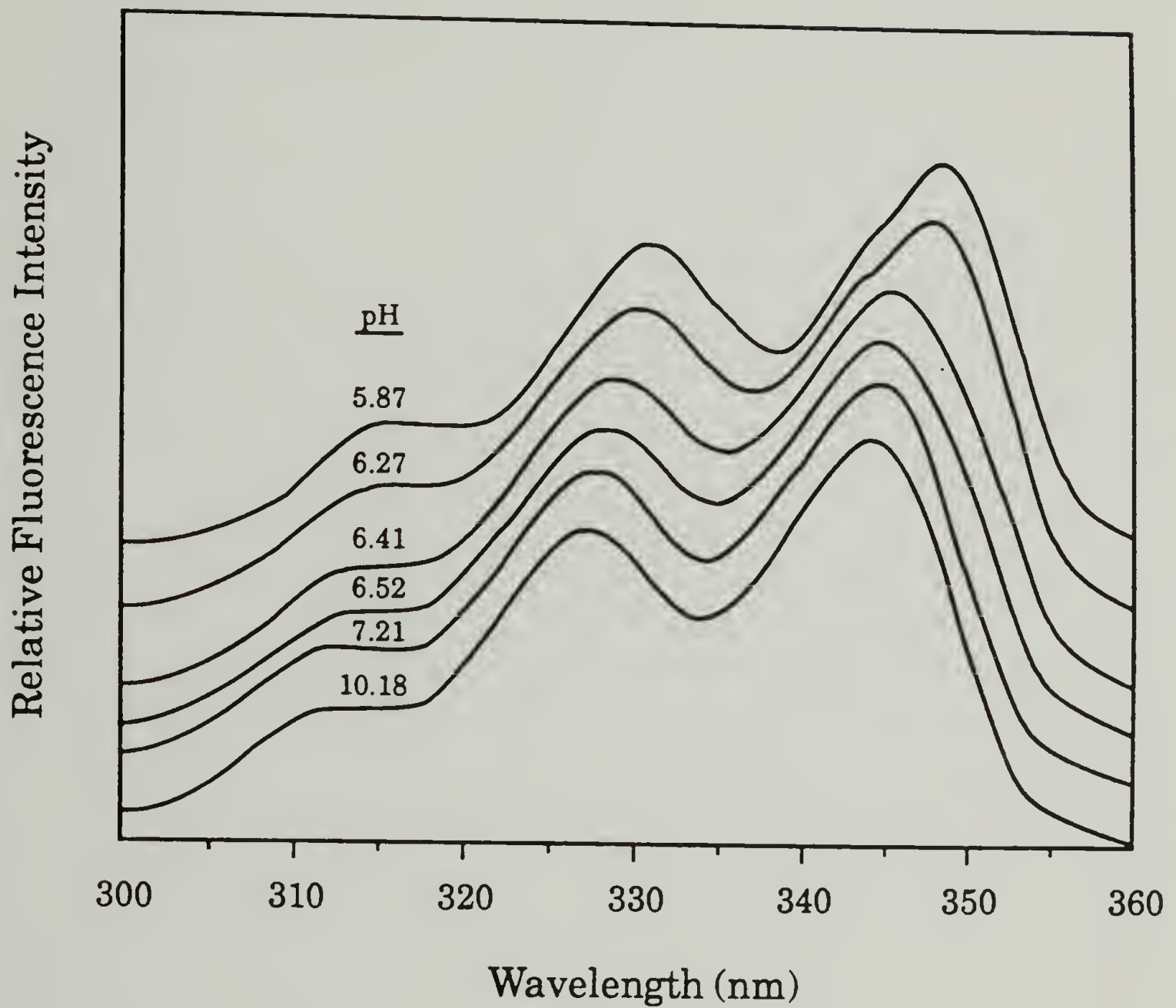


Figure 3.15 Fluorescence excitation spectra for PEEA-py2 copolymer (1 mg/ml) in phosphate-buffered (0.40 M) aqueous solution. Spectra were recorded using 377 nm emission at 23 °C.

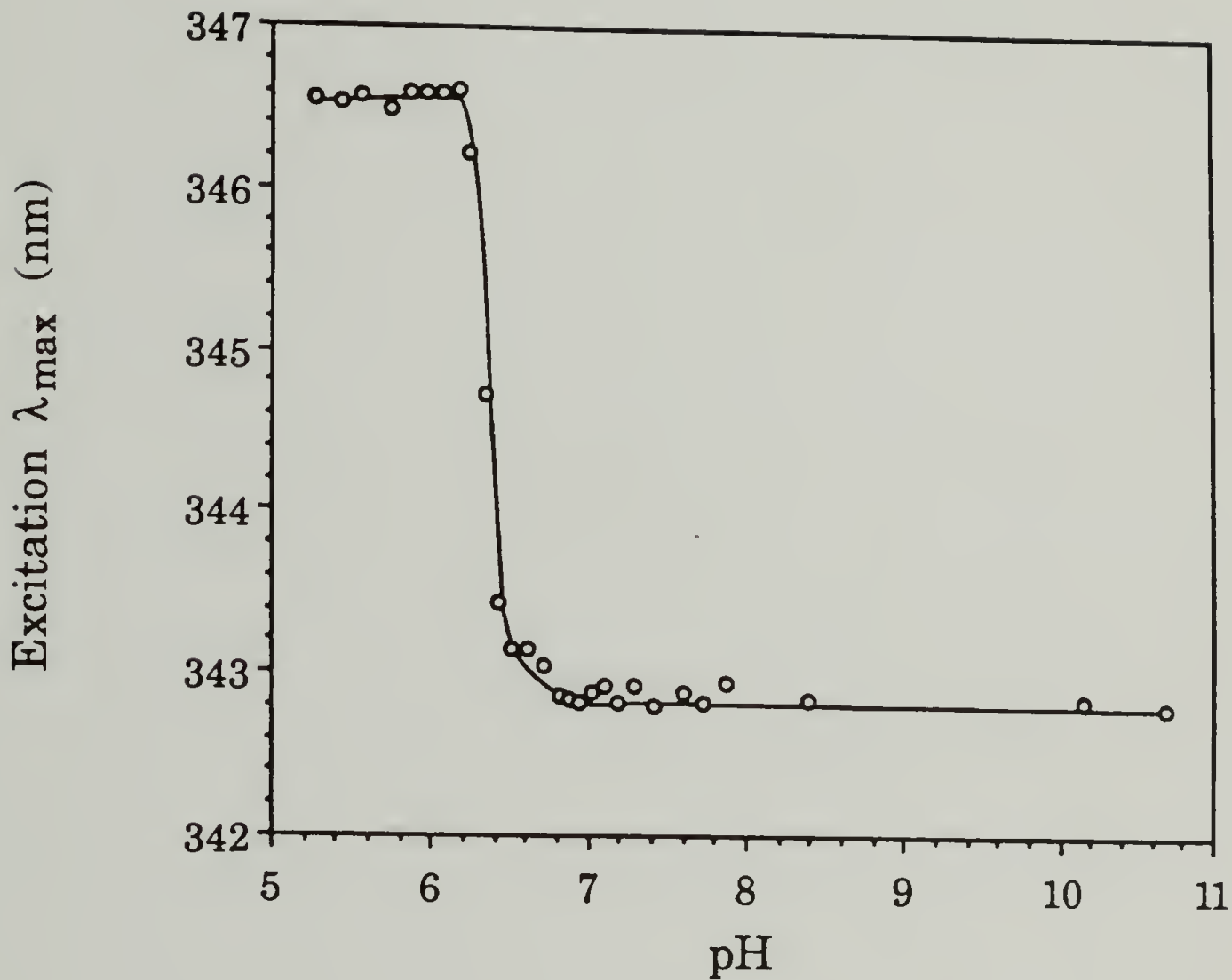


Figure 3.16 Wavelength of maximum intensity in the excitation spectrum of PEAA-py2 (1 mg/ml) in phosphate-buffered (0.40M) aqueous solution as a function of pH. Emission wavelength 377 nm, T = 23 °C.

distribution of the pyrene moiety between two different sites. In Figure 3.17 we see that as the pH is decreased there is a change from a pyrene population with an excitation maximum at 342.8 nm (PEAA expanded state, pyrene in aqueous environment) to a pyrene population with an excitation maximum at 347.8 nm (PEAA collapsed state, pyrene in hydrophobic domains of PEAA).

The ionic strength of the solution has been shown to influence the conformational transition of PMAA and PEAA [24, 27, 28, 32]. It has been found that as the ionic strength of the solution increases, the polyelectrolyte becomes a stronger acid, i.e. the conformational transition occurs at lower pH due to screening of the polymer charge repulsion by ions in solution. We investigated the effect of ionic strength on the conformational transition of PEAA using fluorescence spectroscopy. Figure 3.18 shows the pH-dependent change in pyrene intensity for PEAA-py1 (1 mg/ml) in phosphate buffered solutions at 0.02 M, 0.10 M, and 0.40 M ionic strength. We find that as the ionic strength increases the conformational transition is shifted to lower pH. This observation is consistent with the reported ionic strength effects on PEAA and PMAA [24, 27, 28, 32, 51].

D. Conformational Behavior of PEAA in DPPC Suspensions.

The PEAA-py2 copolymer was used to study the effect of DPPC vesicles on the conformational transition of PEAA. Again we simply measure the emission intensity as a function of sample pH. The results of this experiment are shown in Figure 3.19, where the pyrene fluorescence intensity is plotted against pH for phosphate buffered (0.40 M) solutions of

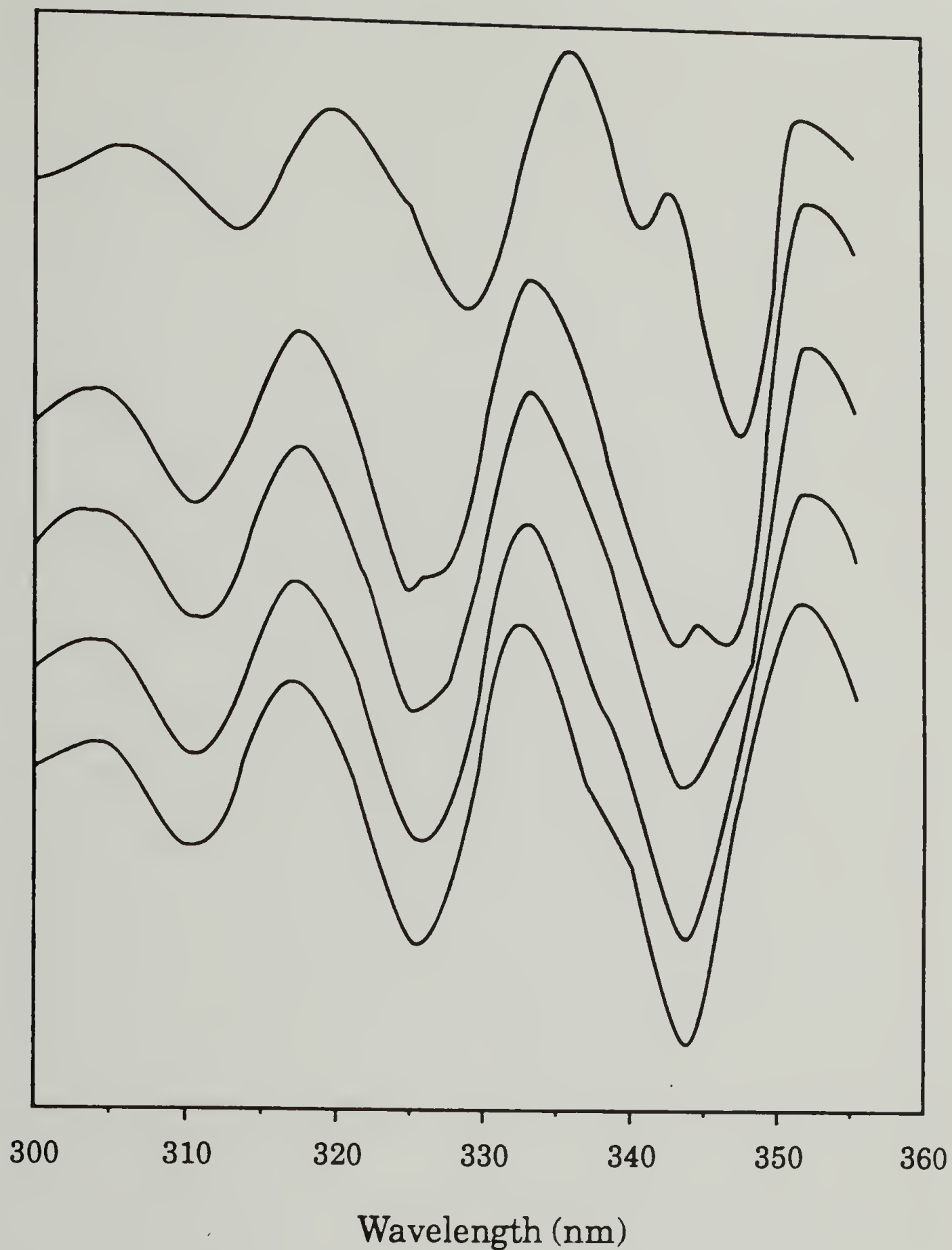


Figure 3.17 Second derivative excitation spectra for PEAA-py2 copolymer (1 mg/ml) in phosphate-buffered (0.40 M) aqueous solution. Spectra were recorded using 377 nm emission at 23 °C. The second derivatives of the excitation spectra were calculated using the derivative function of the Perkin-Elmer MPF-66 fluorescence spectrometer.

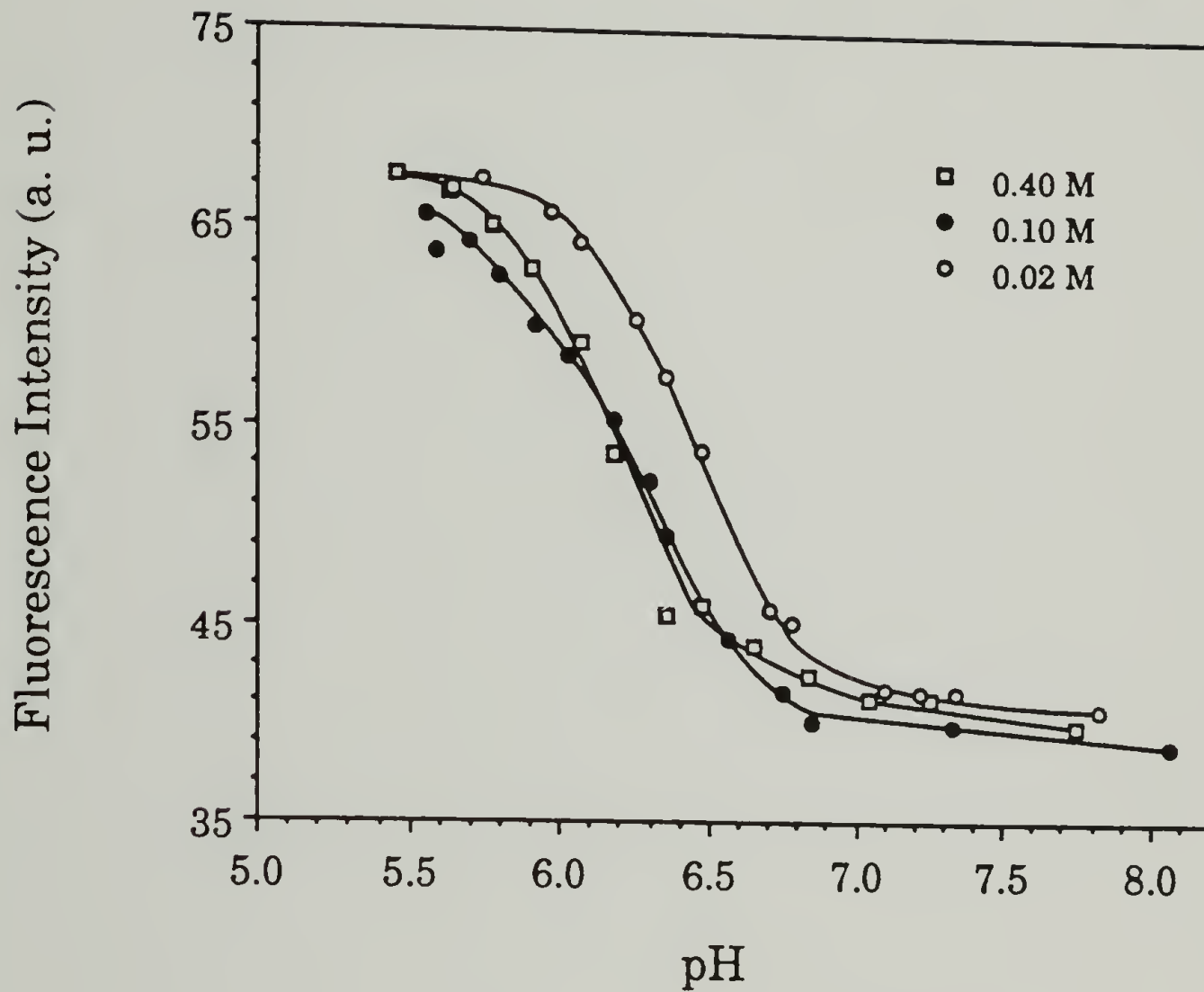


Figure 3.18 Fluorescence intensity (377 nm) emitted by PEAA-pyl copolymer (1 mg/ml) in 0.02 M, 0.10 M, and 0.40 M phosphate-buffered solutions as a function of pH. Excitation wavelength 345 nm, T = 23 °C.

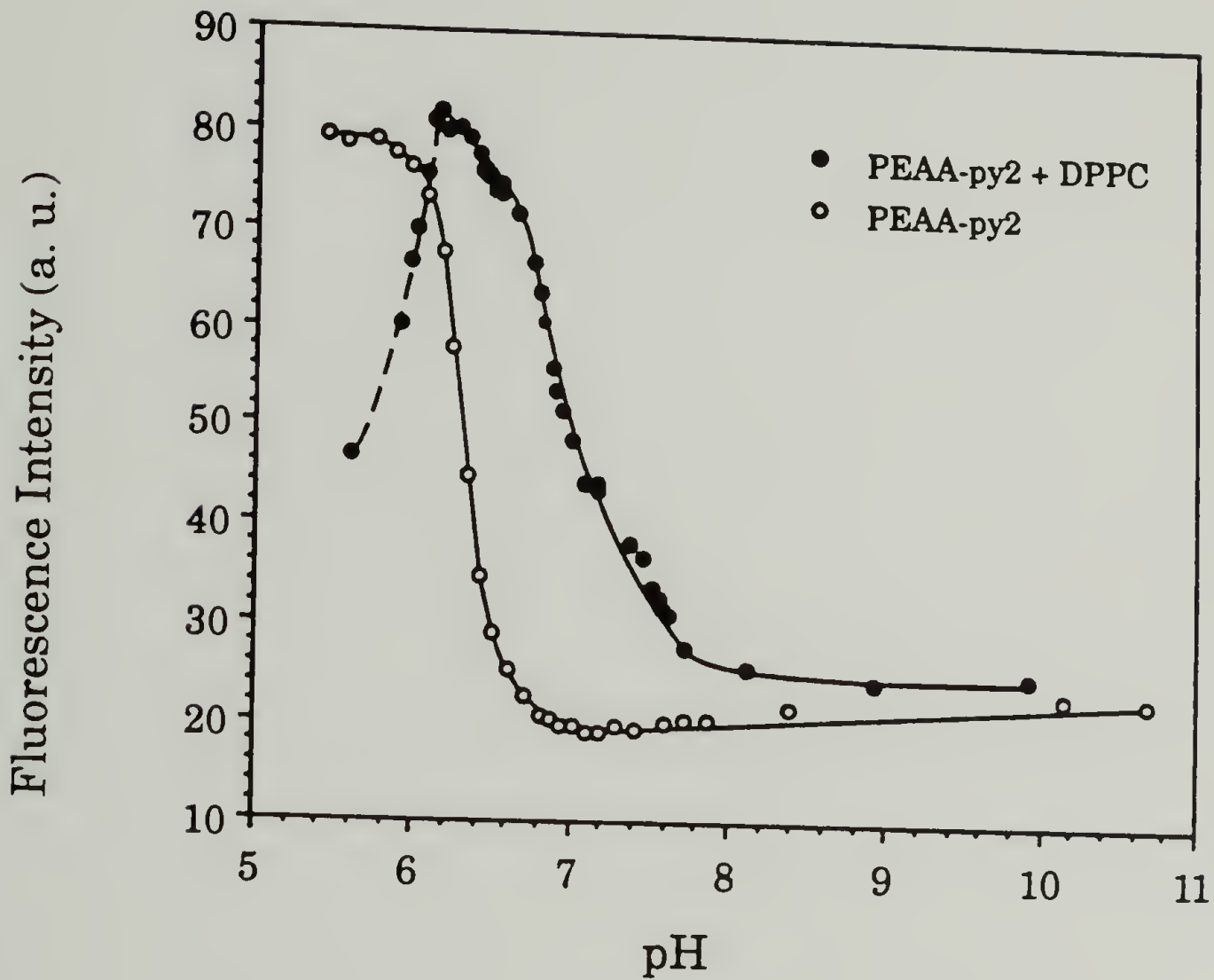


Figure 3.19 Fluorescence intensity (377 nm) emitted by PEAA-py2 copolymer (1 mg/ml) in phosphate-buffered (0.40 M) aqueous solution and suspensions of DPPC (1 mg/ml) as a function of pH. Excitation wavelength 345 nm, $T = 23\text{ }^{\circ}\text{C}$. The curves have been modified to span a similar range of intensity.

PEAA-py2 alone (1 mg/ml) and of PEAA-py2 (1 mg/ml) in the presence of DPPC multilamellar vesicles (1 mg/ml). The same dramatic change in intensity is observed for PEAA-py2 in suspensions of DPPC as for PEAA-py2 alone in solution, however the midpoint of the transition has shifted to a higher pH. In the presence of the DPPC vesicles the transition occurs over a much wider pH range (~2 pH units) than found in simple PEAA-py2 solutions. However, the observed intensity change in the high pH region is due to changes in the optical density of the samples and not to a change in the conformational state of PEAA-py. For samples of PEAA-py2 and PEAA-py2+DPPC at high pH with identical concentrations of PEAA-py2, a lower fluorescence intensity is observed for the DPPC containing samples. The samples containing DPPC multilamellar vesicles are highly turbid with optical densities near 2. The intensity of the exciting light decreases as it travels through a turbid sample. This relationship can be shown with the equation for optical density :

$$OD_x = \log \frac{I_0}{I_x} \quad (\text{Eq. 3.1})$$

where OD_x is the optical density, I_0 is the intensity of incident light and I_x is the intensity of exciting light at a distance x into the sample. Since the observed fluorescence emission intensity is proportional to the intensity of the exciting light, the measured fluorescence from turbid samples will be less than for optically clear samples. As the optical density of the samples is reduced, the observed emission intensity increases. This effect can be demonstrated by presenting the fluorescence intensity versus pH plot for PEAA-py2 alone and PEAA-py2+DPPC with the intensity axis in absolute units, as in Figure 3.20. Superimposed on this graph is the plot of optical

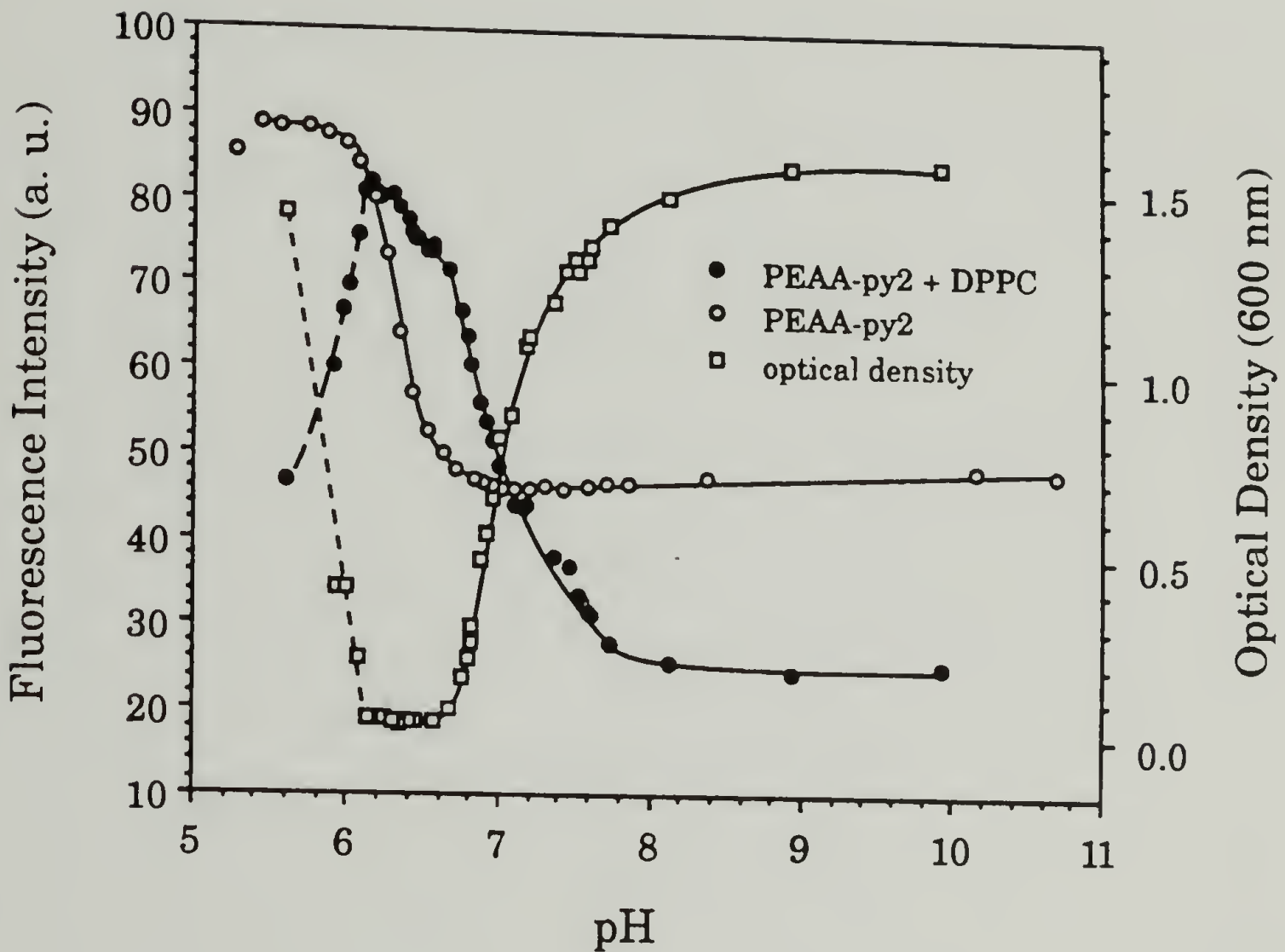


Figure 3.20 Effect of optical density on intensity of fluorescence emitted by PEAA-py2 in suspensions of DPPC. Fluorescence intensity (377 nm) from PEAA-py2 copolymer (1 mg/ml) in phosphate-buffered (0.40 M) aqueous solution and suspensions of DPPC (1 mg/ml) was measured as a function of pH, as well as the optical density (600 nm) for the mixtures of PEAA-py2 and DPPC. Excitation wavelength 345 nm, $T = 23\text{ }^{\circ}\text{C}$.

density versus pH for the PEAA-py2+DPPC samples. Solutions of PEAA-py2 are optically clear over the pH range of the experiment. All samples have identical concentrations of PEAA-py2, but we see that for the DPPC series the observed intensity is artificially low above pH 7.2.

We see that there is a decrease in fluorescence intensity and a corresponding increase in optical density as the solution pH is lowered below 6.1 in the series of PEAA-py2+DPPC samples (see Figure 3.20). The decrease in intensity and increase in optical density is a result of the formation of large aggregate structures below pH 6.1, which precipitate out of solution.

We can gain further insight into the effect of DPPC interaction on the conformational transition of PEAA-py through examination of the shifts in the emission and excitation wavelength maxima for these mixtures of PEAA-py2 and DPPC. We can see in Figure 3.21 that there is a small shift in the emission spectra of PEAA-py2 in mixtures with DPPC as the pH is varied. A plot of $\text{em } \lambda_{\text{max}}$ against pH is presented in Figure 3.22. We find a shift in the emission wavelength maximum from 376.8 nm at high pH to 377.6 nm at low pH, which is similar to the red-shift seen with PEAA-py alone. However, the change now takes place over a wider pH range (midpoint at pH 7.5). The optical density does not seem to affect the observed $\text{em } \lambda_{\text{max}}$, since we see identical values of $\text{em } \lambda_{\text{max}}$ for highly turbid PEAA-py+DPPC samples and optically clear PEAA-py samples at high pH. Therefore, this experiment provides information on the environmental state of the pyrene moiety and is free from complications of turbidity, unlike the experiment where we monitor the change in intensity.

Further evidence for a change in the pyrene environment as the solution pH is altered can be seen in the excitation spectra of PEAA-py2 in

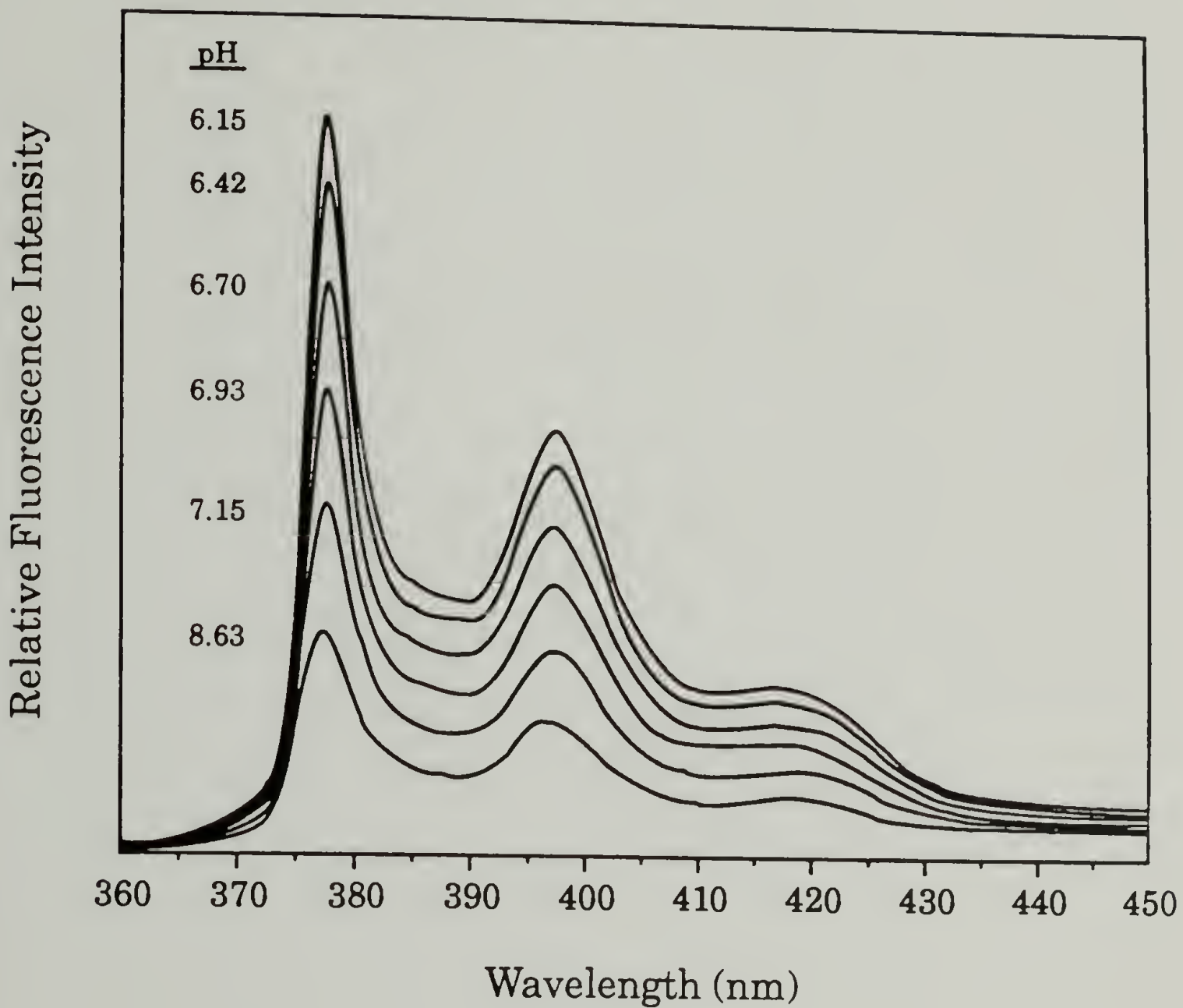


Figure 3.21 Fluorescence emission spectra for PEAA-py2 copolymer (1 mg/ml) in phosphate-buffered (0.40 M) suspensions of DPPC (1 mg/ml). Spectra were recorded using 345 nm excitation at 23 °C.

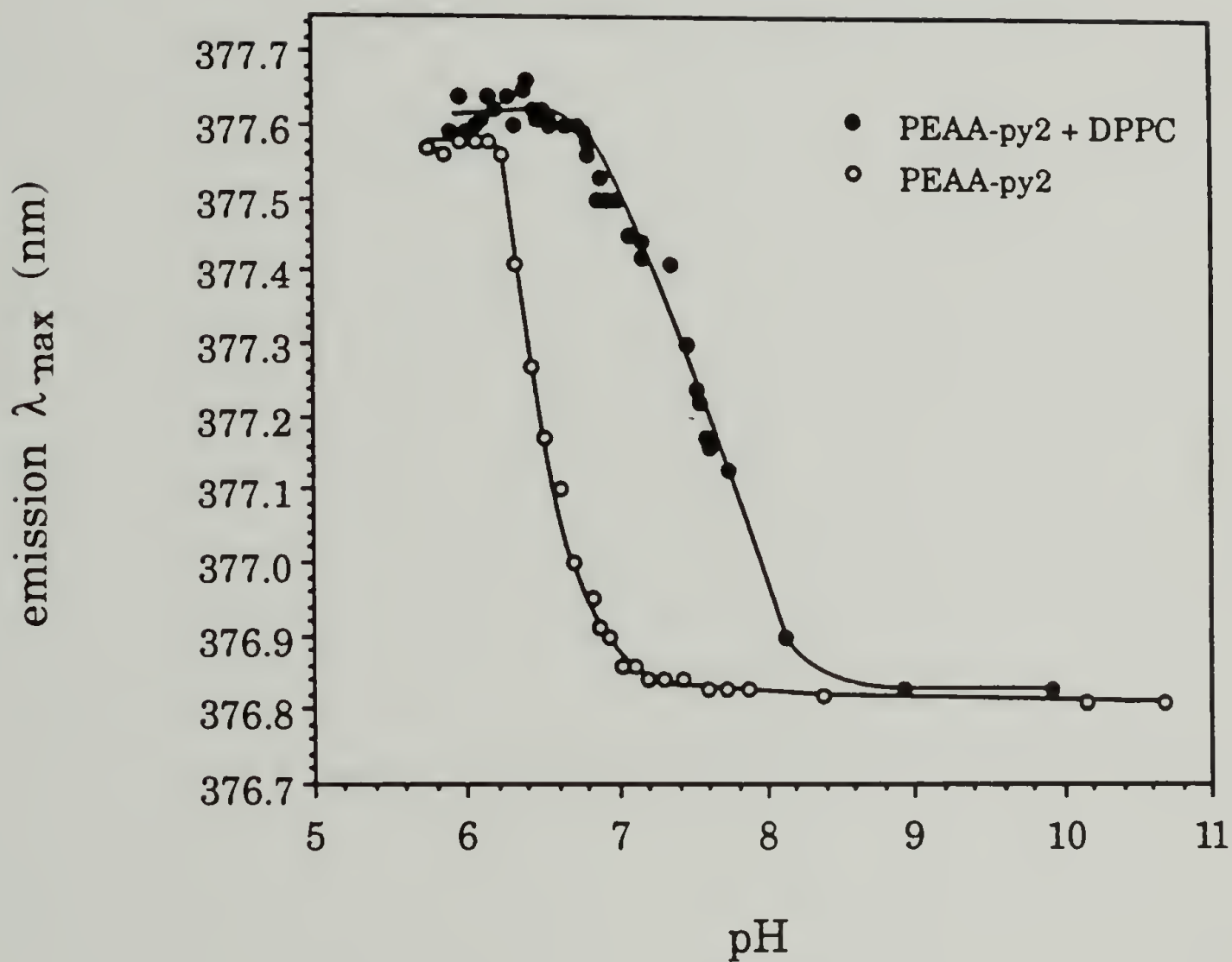


Figure 3.22 Wavelength of maximum intensity in the emission spectrum of PEAA-py2 (1 mg/ml) in phosphate-buffered (0.40M) aqueous solution and suspensions of DPPC (1 mg/ml) as a function of pH. Excitation wavelength 345 nm, T = 23 °C.

mixtures of DPPC, which are shown in Figure 3.23. A plot of $\text{ex } \lambda_{\text{max}}$ versus pH for the PEAA-py2+DPPC samples (see Figure 3.24), shows the samples at high pH have an $\text{ex } \lambda_{\text{max}}$ of 342.9 nm, which is similar to the value found for PEAA-py2 alone at high pH. As the pH is lowered the $\text{ex } \lambda_{\text{max}}$ increases, reaching a plateau value near 346.3 nm below pH 7. The observed change in $\text{ex } \lambda_{\text{max}}$ occurs over a pH range of 1 unit, with the midpoint at pH 7.25. The lack of correspondence between the $\text{em } \lambda_{\text{max}}$ and $\text{ex } \lambda_{\text{max}}$ experiments is deceiving, because the experimentally recorded peaks are really combinations of two components and the measured $\text{em } \lambda_{\text{max}}$ and $\text{ex } \lambda_{\text{max}}$ values are averages which are dependent on the relative amounts of each component. Consequently, the measured λ_{max} depends not only on the environment, but also on the relative amounts of the components. For the $\text{em } \lambda_{\text{max}}$ experiment this effect seems to be negligible because the λ_{max} values of the components are very close and cannot be resolved. The different components can be resolved in the excitation study, and if one could determine the relative amounts of each component, a plot of component concentration versus pH would reveal a transition that occurs over a pH range similar to that found in the $\text{em } \lambda_{\text{max}}$ versus pH plot. A quantitative determination of the relative amount of components is not possible from our data, however a qualitative representation is provided in Figure 3.25. In this stacked plot we can detect the growth of the 347.5 nm component beginning at pH 8.11. We recall that in the $\text{ex } \lambda_{\text{max}}$ plot an increase in the λ_{max} value is not detected until pH 7.6 (see Figure 3.24).

The excitation spectra of PEAA-py allow us to clearly distinguish the PEAA-py molecules which are bound to DPPC from the non-interacting PEAA-py molecules in solution. Samples containing phosphate buffered solutions (0.40 M) of PEAA-py2 (0.5 mg/ml) and DPPC (0.5 mg/ml) in were

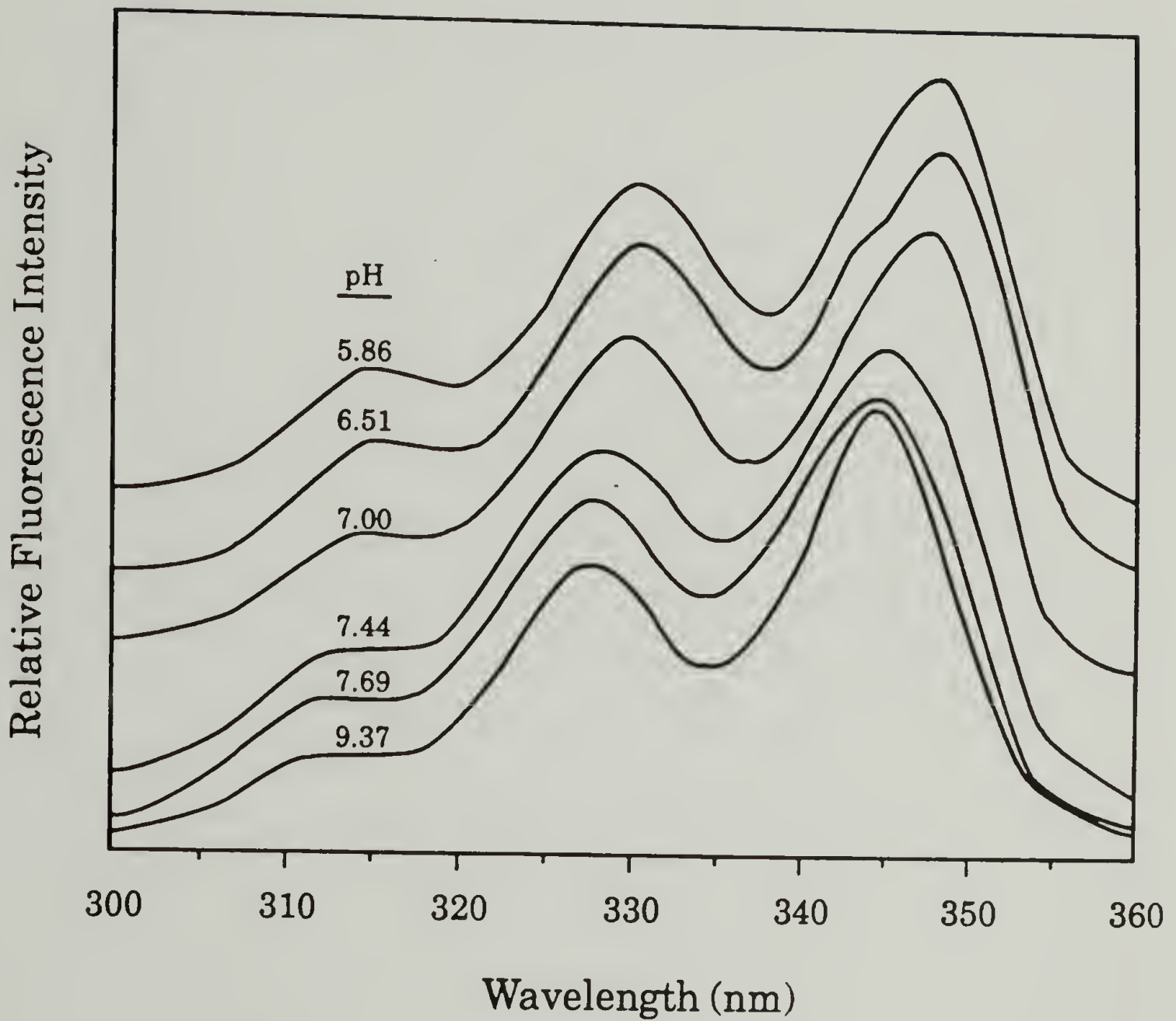


Figure 3.23 Fluorescence excitation spectra for PEAA-py2 copolymer (1 mg/ml) in phosphate-buffered (0.40 M) suspensions of DPPC (1 mg/ml). Spectra were recorded using 377 nm emission at 23 °C.

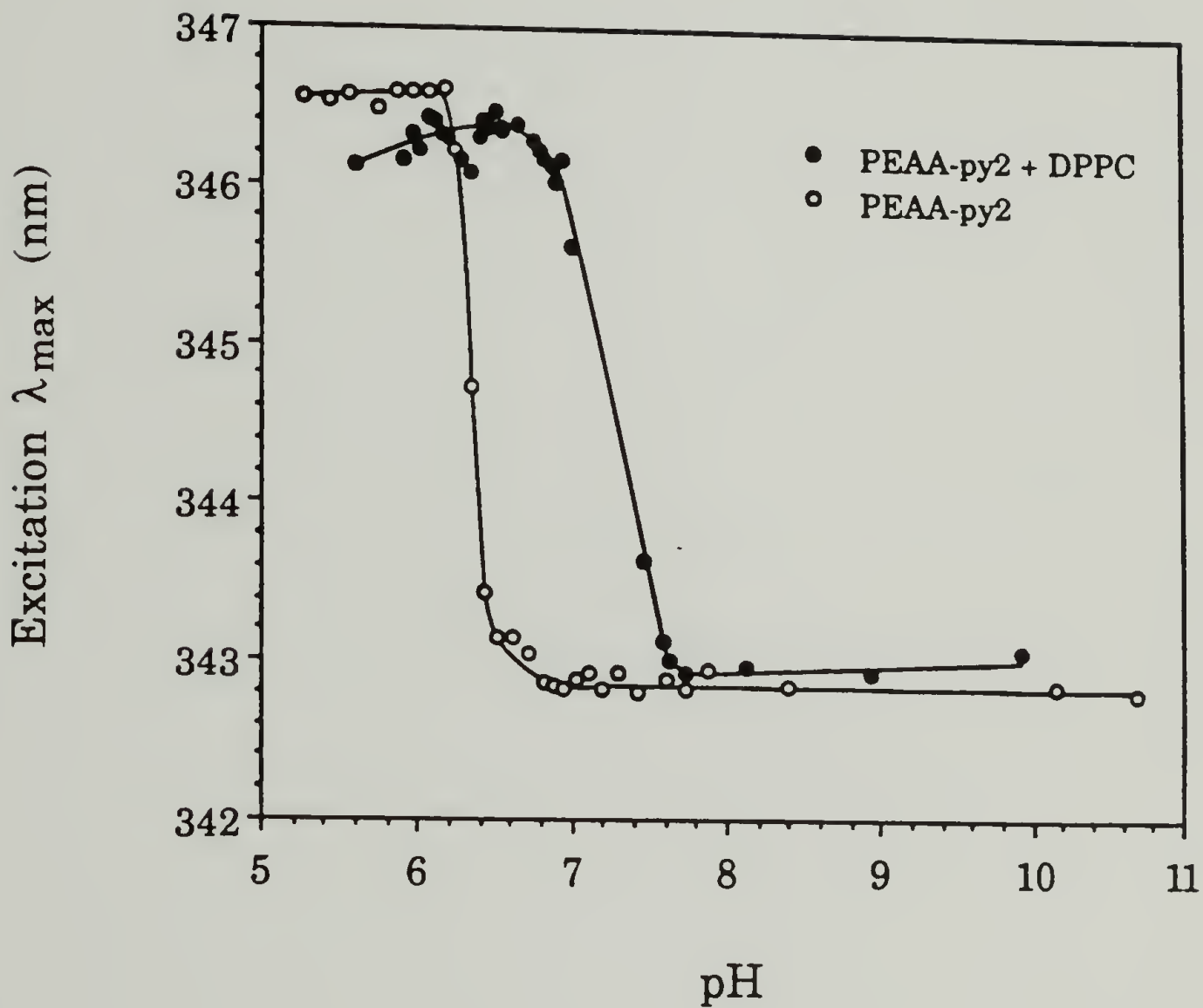


Figure 3.24 Wavelength of maximum intensity in the excitation spectrum of PEAA-py2 (1 mg/ml) in phosphate-buffered (0.40M) aqueous solution and suspensions of DPPC as a function of pH. Emission wavelength 377 nm, T = 23 °C.

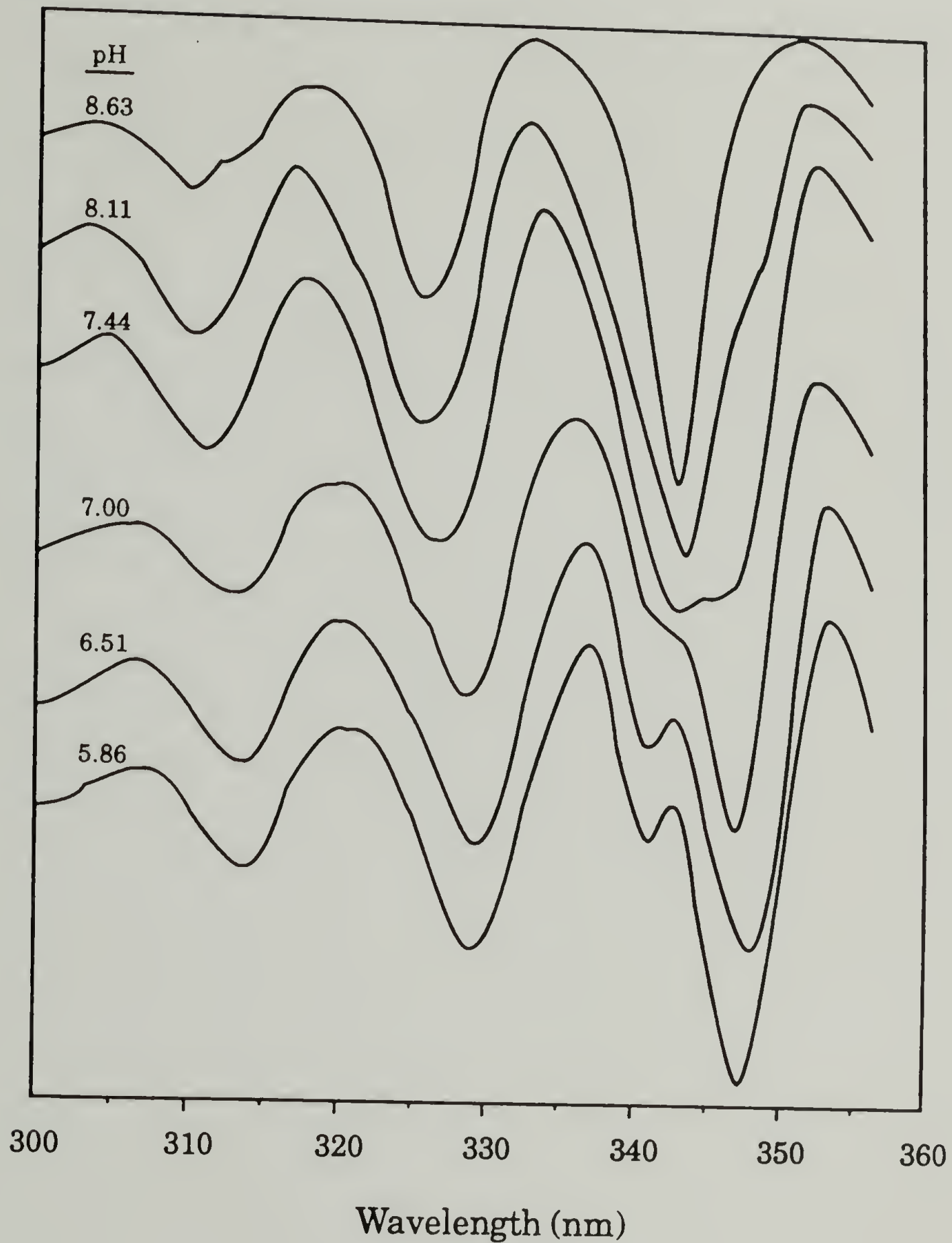


Figure 3.25 Second derivative excitation spectra for PEAA-py2 copolymer (1 mg/ml) in phosphate-buffered (0.40 M) suspensions of DPPC (1 mg/ml). Spectra were recorded using 377 nm emission at 23 °C. The second derivatives of the excitation spectra were calculated using the derivative function of the Perkin-Elmer MPF-66 fluorescence spectrometer.

centrifuged at ~ 2500 rpm in an IEC Model CL centrifuge for 1.5 hours to sediment the DPPC vesicles along with complexed PEAA-py2. Figure 3.26 shows the excitation spectra and their second derivatives for a PEAA-py2+DPPC sample at pH 6.93 before and after sedimentation. The supernatant PEAA-py2 exhibits a single component peak in the excitation spectrum at 343.3 nm, which is identical to the peak found in samples of PEAA-py2+DPPC above pH 8.5 (see Figures 3.23 and 3.25). The unsedimented sample shows a main peak in the excitation spectrum at 347.8 nm, corresponding to collapsed PEAA-py which is complexed with the DPPC vesicles.

Similar red shifts in the emission and excitation spectra have been observed when various derivatives of pyrene are moved from aqueous solution to a bilayer membrane [70]. These researchers investigated the interaction of pyrenebutyrylhydrazide and several pyrene-linked derivatives of oligosaccharides and glutathione with ghost erythrocyte membranes. In each derivative, pyrene is linked to a bulky hydrophilic substituent which does not permeate into the bilayer. The hydrophobic pyrene moiety prefers to locate in the hydrophobic domains of the bilayer. For five of the six probes investigated, a red shift in $ex \lambda_{max}$ (from 2 nm to 6 nm) was observed when the probe was moved from aqueous solution (0.03 M phosphate buffer, pH 7.4) to a suspension of ghost membranes. All of the probes exhibited a red shift in $ex \lambda_{max}$ (from 1 nm to 12 nm) when the solvent was changed from water to less polar solvents (tetrahydrofuran, hexane, 1-butanol). The pyrene probes demonstrated disparate behavior in the observed shifts for $em \lambda_{max}$ as they moved from water to the membranes. Two probes showed a red shift in $em \lambda_{max}$ (1 nm), two showed a blue shift (1 nm), and two remained unchanged. The greater sensitivity of the $ex \lambda_{max}$ to changes in

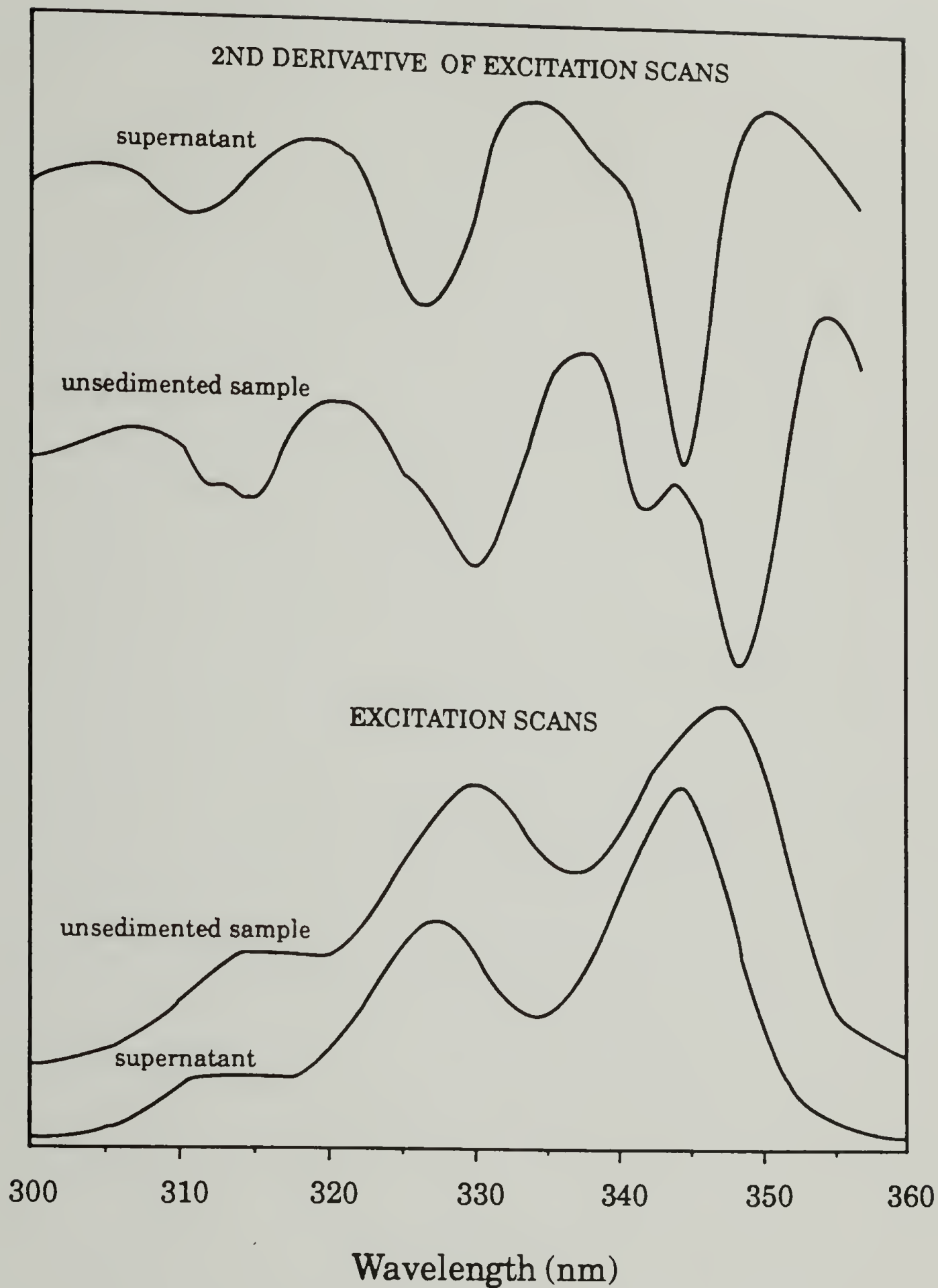


Figure 3.26 Excitation spectra and their second derivatives for PEEA-py2 (1 mg/ml) in sedimented and un-sedimented suspensions of DPPC (1 mg/ml) at pH 6.93. Excitation spectra were recorded at 23 °C using 377 nm emission wavelength. Second derivatives of the excitation spectra were calculated with the derivative function of the Perkin-Elmer MPF-66 fluorescence spectrometer.

environment than $\text{em } \lambda_{\text{max}}$ for these pyrene probes is the same behavior we have found for pyrene and PEAA-py2 in the PEAA-DPPC system.

A precise, quantitative comparison of the conformational transition of PEAA-py alone and in the presence of DPPC is not possible, since the observed emitted fluorescence intensity is dependent on changes in fluorophore environment and changes in the excitation spectrum. The emission spectra are recorded at a fixed excitation wavelength over the entire pH range. However, since the excitation spectrum shifts as the pH is varied in the mixtures of PEAA-py2 and DPPC, the fixed excitation wavelength does not yield invariant emission intensities over the experimental pH range. The different contributions to the observed emission intensity are not easily separated, which complicates the analysis of the change in intensity occurring in the PEAA-py samples. However, all of the fluorescence experiments show a pronounced shift to higher pH for the conformational transition of PEAA-py in the presence of DPPC. This suggests that interaction with DPPC vesicles causes the PEAA-py to become a weaker acid, and promotes the formation of the collapsed coil conformation.

The relation between the conformational state of the polyelectrolyte and the structural order of the surfactant bilayer membrane can be determined through comparison of the pH-dependent changes in fluorescence intensity and optical density. Such a comparison is presented in Figure 3.27 for PEAA-py1+DPPC samples of low initial optical density in order to minimize the effects of optical density on the observed fluorescence. The midpoints of the two transitions correspond, which indicates that the formation of collapsed PEAA coincides with the reorganization from a vesicular to a mixed micellar structure.

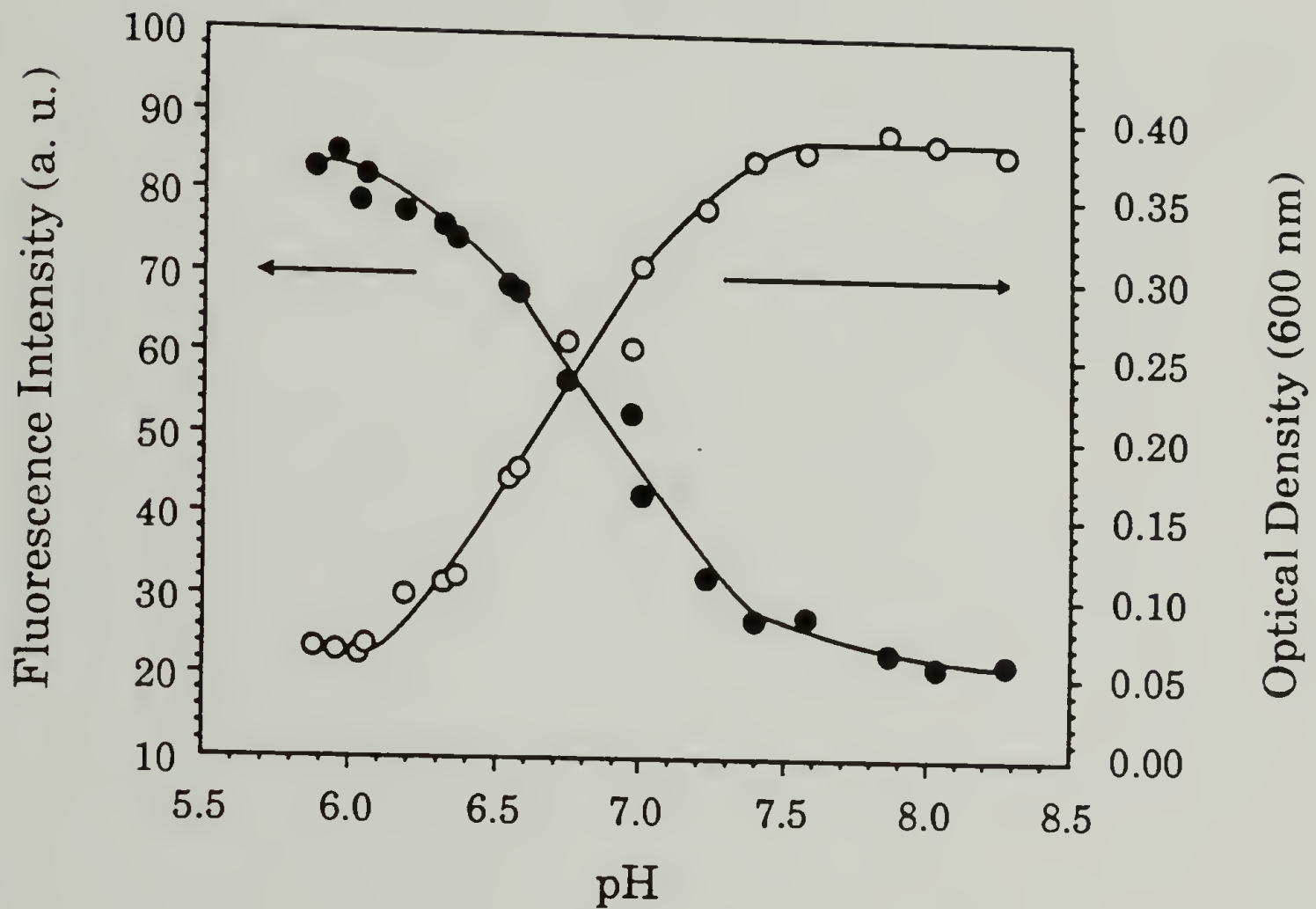


Figure 3.27 Emission intensity (378 nm) and optical density (600 nm) for phosphate-buffered (0.02 M) mixtures of PEAA-py1 (0.1 mg/ml) and DPPC (0.1 mg/ml). Excitation wavelength 345 nm, T = 23 °C.

It has been found for polyelectrolytes such as PMAA and PEAA that as the ionic strength of the solution increases, the conformational transition is shifted to lower pH. This effect has been demonstrated for PEAA solutions (see Figure 3.18) and can also be seen for PEAA in the presence of DPPC. A representative example of the ionic strength effect is provided in Figure 3.28 as plots of optical density versus pH for phosphate buffered solutions of PEAA-py1 (1 mg/ml) and DPPC (1 mg/ml). As the ionic strength is increased from 0.02 M to 0.40 M the midpoint of the optical density transition shifts from pH 6.8 to pH 6.45. For each ionic strength series, there is good correspondence between the conformational transition midpoint as detected by the fluorescence probe method and the structural transition midpoint from optical density measurements.

The results discussed so far have dealt with systems containing multilamellar DPPC vesicles. When one looks at the optical density behavior of a PEAA-DPPC system containing sonicated vesicles a somewhat different effect is observed. Figure 3.29 shows a comparison of the pH-dependent optical density behavior for multilamellar and sonicated vesicle systems. For the multilamellar vesicle series, the midpoint of the optical density change is located at pH 6.8. For the sonicated vesicle series, two transitions are observed with midpoints at 7.7 and 6.85. We know from the fluorescence experiments that the PEAA begins to interact with the DPPC vesicle near pH 8 (see Figures 3.22 and 3.25). Sonicated vesicles are highly strained as result of their severe surface curvature, and consequently are not thermodynamically stable [71]. It seems that the initial interaction of PEAA in the expanded conformation at high pH acts to destabilize the sonicated vesicle structure. The second transition may be

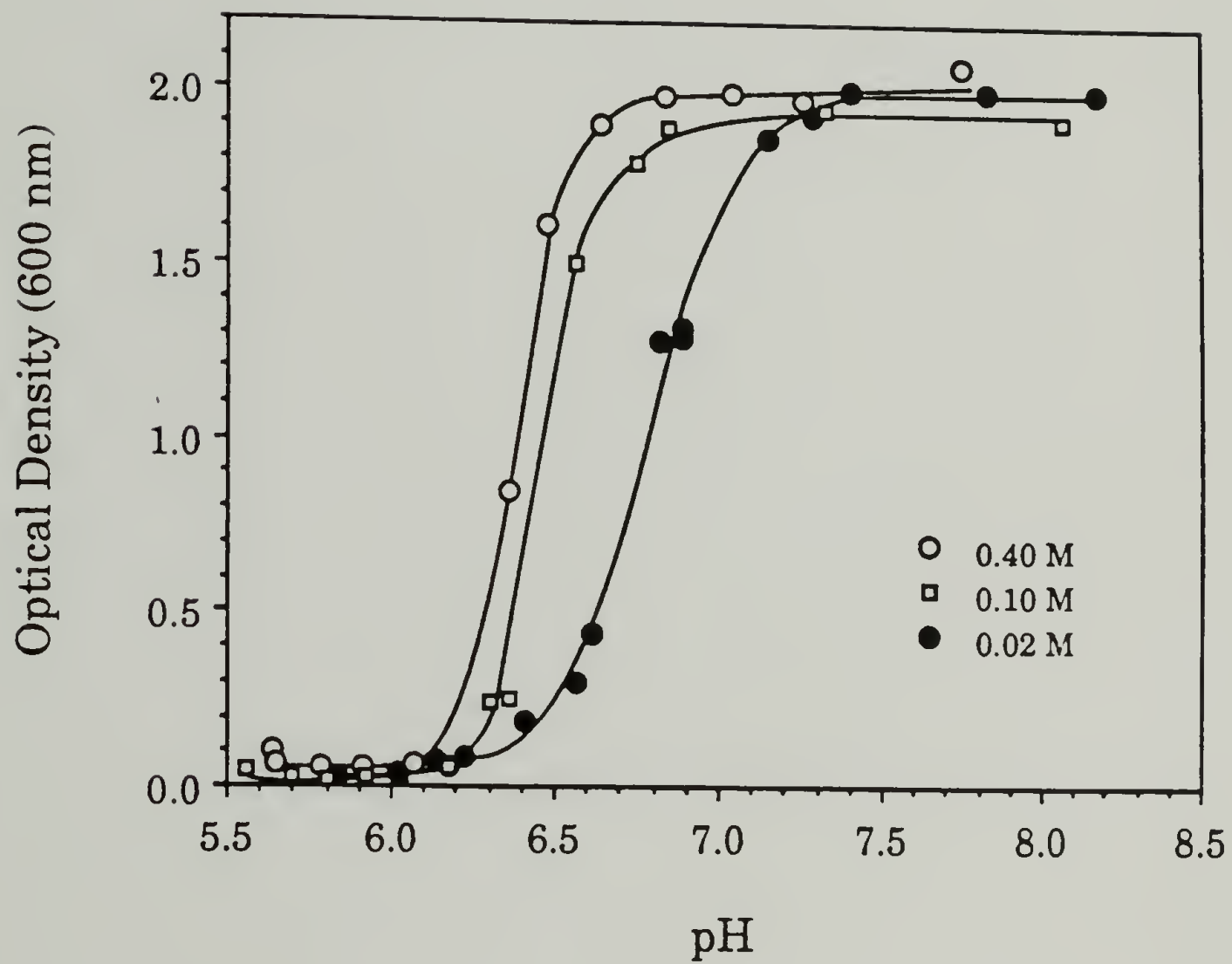


Figure 3.28 Optical density (600 nm) of 0.02 M, 0.10 M, and 0.40 M phosphate-buffered mixtures of PEAA-py1 (1 mg/ml) and DPPC (1 mg/ml).

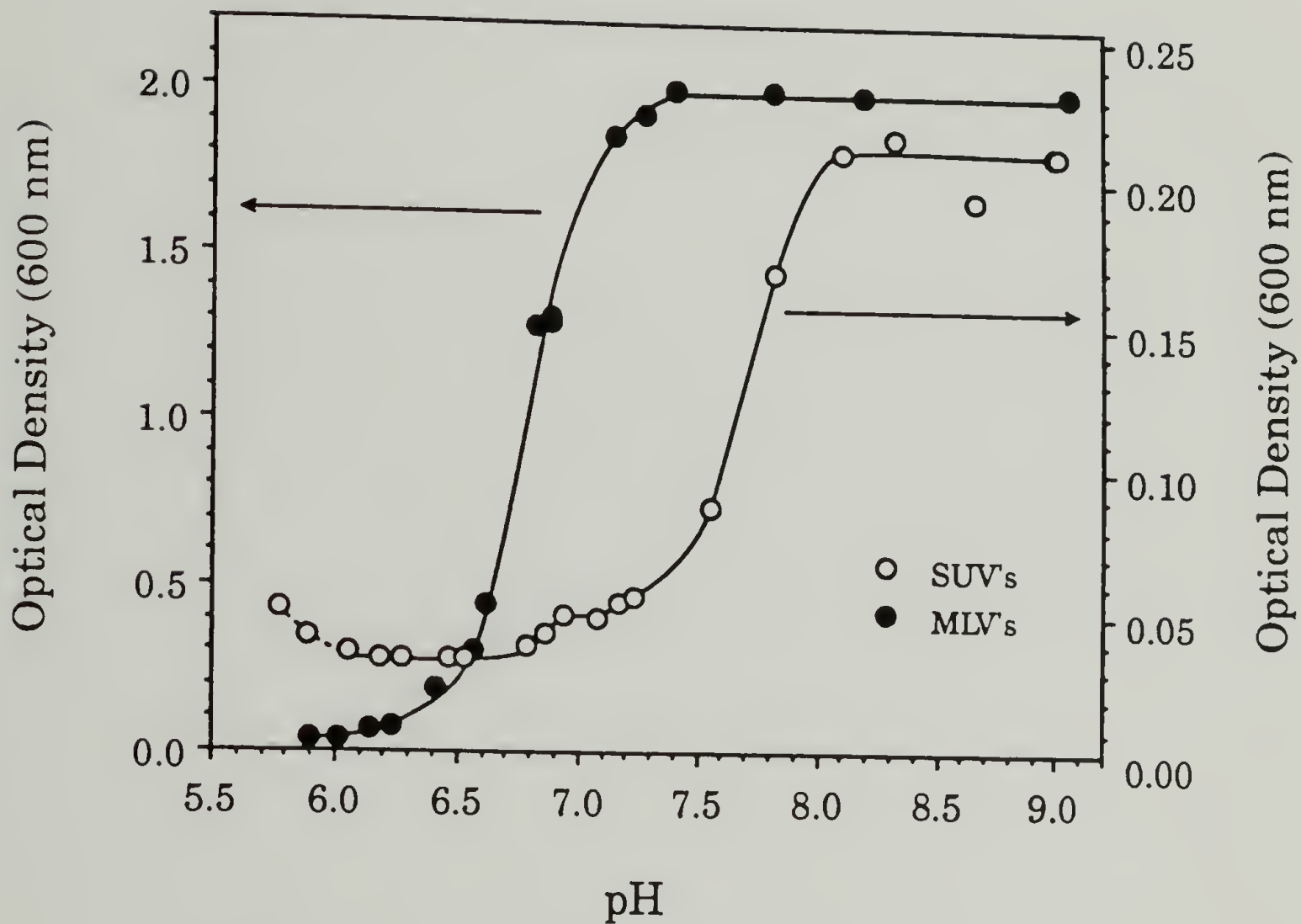


Figure 3.29 Optical density (600 nm) for PEAA (1 mg/ml) in phosphate-buffered (0.02 M) suspensions of multilamellar and sonicated DPPC vesicles (1 mg/ml).

due to the presence of residual multilamellar structures [71] which undergo structural reorganization when the PEAA adopts a collapsed conformation.

E. Potentiometric Titration of PEAA and PEAA-py Solutions.

Potentiometric titration studies have demonstrated that the pK_{app} of polyelectrolytes increases as the extent of ionization increases [27, 28, 32]. This behavior has been attributed to the increased difficulty of removing protons from a charged polymer chain as the charge increases. As the extent of ionization increases there is a continuous increase in the dimensions of the polymer coil due to charge repulsions. For PMAA and PEAA there is resistance to chain expansion, which presumably originates from hydrophobic interactions between the alkyl side chains [22-24, 28]. These hydrophobic interactions cause these polymers to exist in a compact globular conformation at a low degree of ionization in aqueous solution. The alkyl side chains are protected from contact with water in the interior of the globular structure, while the ionized carboxyl groups on the exterior of the structure are solvated by water molecules. At a certain degree of ionization, the resistance to chain expansion is overcome by the charge repulsion, and the polymer chain undergoes a transition from a compact to an expanded coil. This conformational transition has been frequently observed as a discontinuity or plateau in a plot of the degree of ionization (α) versus pH or pK_{app} [22-28, 30-36].

The change in pH for a solution of PEAA-py₂ (1 mg/ml, ionic strength 0.40 M) with added HCl is shown in Figure 3.30. The titration was carried

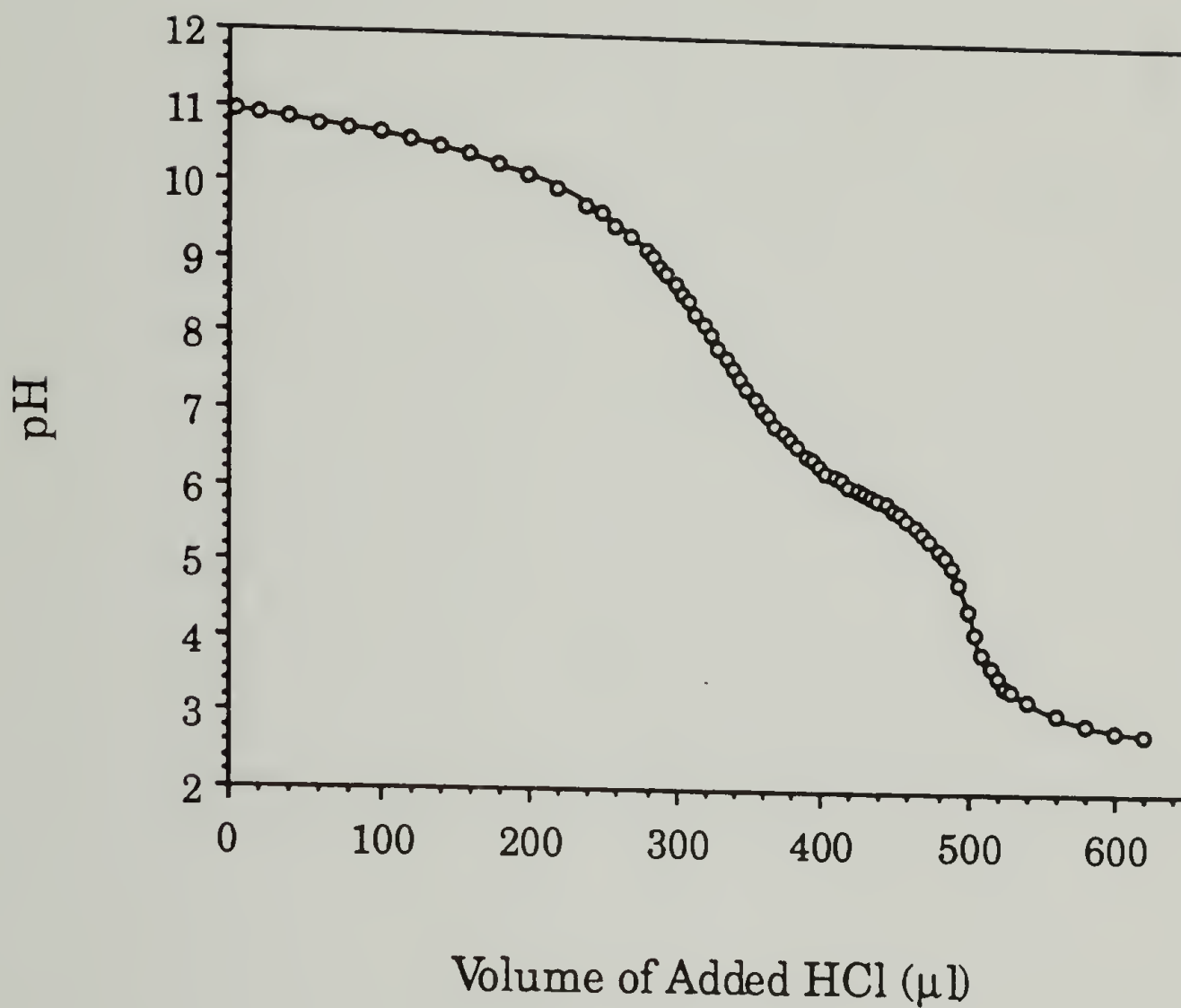


Figure 3.30 The pH of a solution containing PEAA-py2 (1 mg/ml) and 0.40 M NaCl as a function of added 0.100 N HCl. Measurements were made at 55 °C.

out as described in Chapter II. The extent of ionization, α , is calculated from the electroneutrality condition [72]:

$$\alpha = \frac{[C_{\text{Na}^+} + C_{\text{H}^+} - C_{\text{OH}^-} - C_{\text{Cl}^-}]}{C_{\text{M}}} \quad (\text{Eq. 3.2})$$

where C_{Na^+} , C_{H^+} , C_{OH^-} , and C_{Cl^-} represent the concentrations of the sodium, proton, hydroxyl, and chloride ions, respectively, and C_{M} is the monomer repeat unit concentration. A plot of α versus pH is given in Figure 3.31 for PEAA-py2. We see an abrupt change in α between pH 6.8 and pH 5.8 with an inflection point near pH 6.1 corresponding to an α of 0.25. Comparison of the titration curve with the fluorescence intensity curve shows that the most abrupt changes in intensity and α occur over the same pH range (see Figure 3.32). However, the inflection points are slightly different, pH 6.3 for the fluorescence curve and pH 6.1 for the α curve. The fluorescence experiment detects the conformational transition at a higher pH than potentiometric titration. The fluorescent probe senses changes in its local micro-environment, while the titration reports on the macroscopic behavior of the polymer chain. The two experiments are communicating different information, and this may be the reason we find a difference in the critical pH values. Over the pH range 6.8 to 5.8, α decreases from 0.4 to 0.15. The inflection point pH of the fluorescence experiment corresponds to an α of 0.32.

In the presence of DPPC vesicles (1 mg/ml) the inflection point of the α versus pH curve is shifted to higher pH. In Figure 3.33 we see a shift in the inflection point from \sim pH 6.1 for PEAA-py alone (1 mg/ml, ionic strength 0.40 M) to pH 6.4 for a sample containing PEAA-py2 and DPPC (1 mg/ml each, ionic strength 0.40 M). The interaction between the PEAA-py2 and

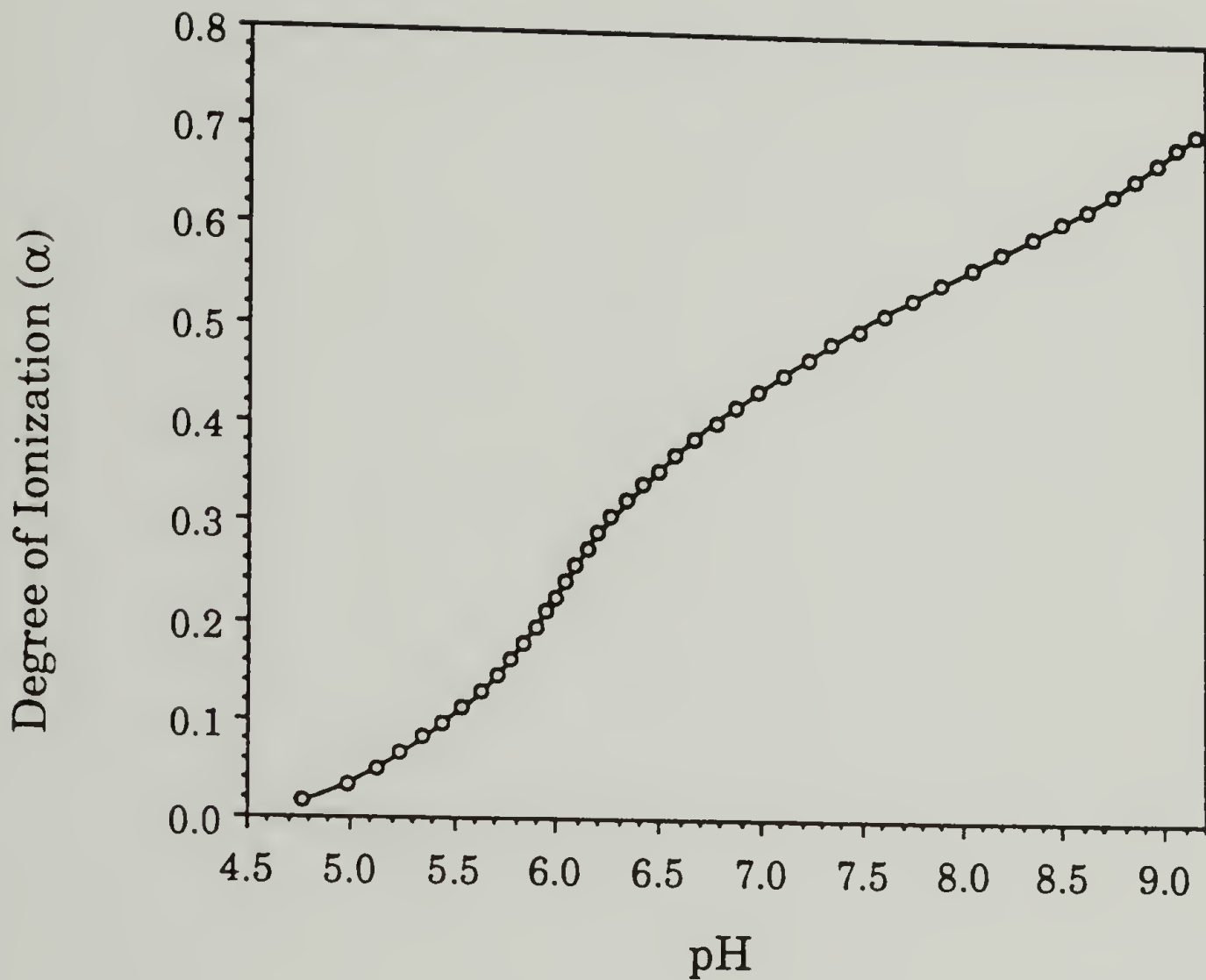


Figure 3.31 Degree of ionization of PEAA-py2 (1 mg/ml) in 0.40 M NaCl solution as a function of pH. Measurements were made at 55 °C.

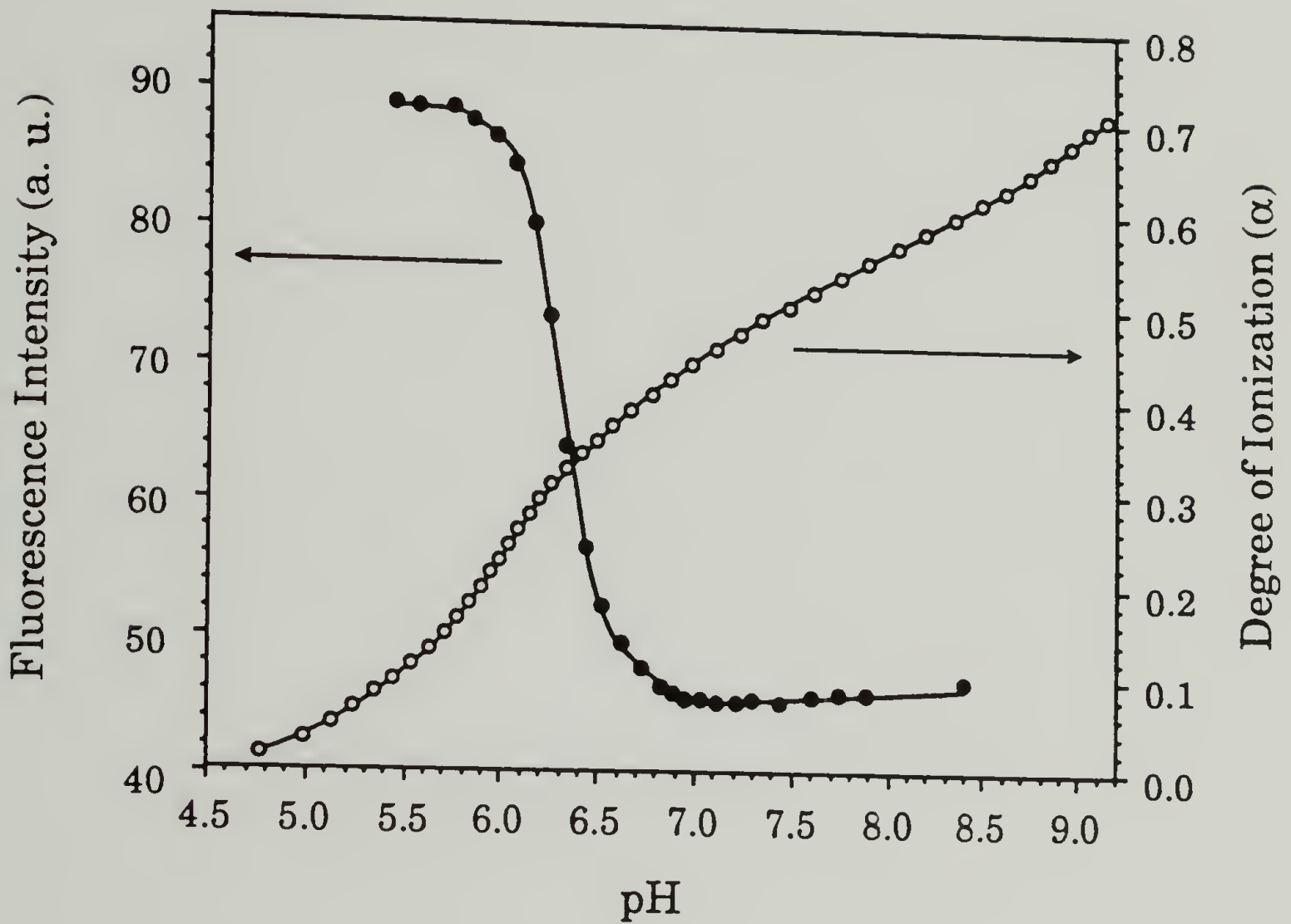


Figure 3.32 Fluorescence emission intensity (377 nm) for phosphate-buffered (0.40 M) solutions of PEAA-py2 and degree of ionization of PEAA-py2 in 0.40 M NaCl solutions. Concentration of PEAA-py2 was 1 mg/ml in each experiment. Fluorescence was recorded using 345 nm excitation at 23 °C. Degree of ionization was measured for sample at 55 °C.

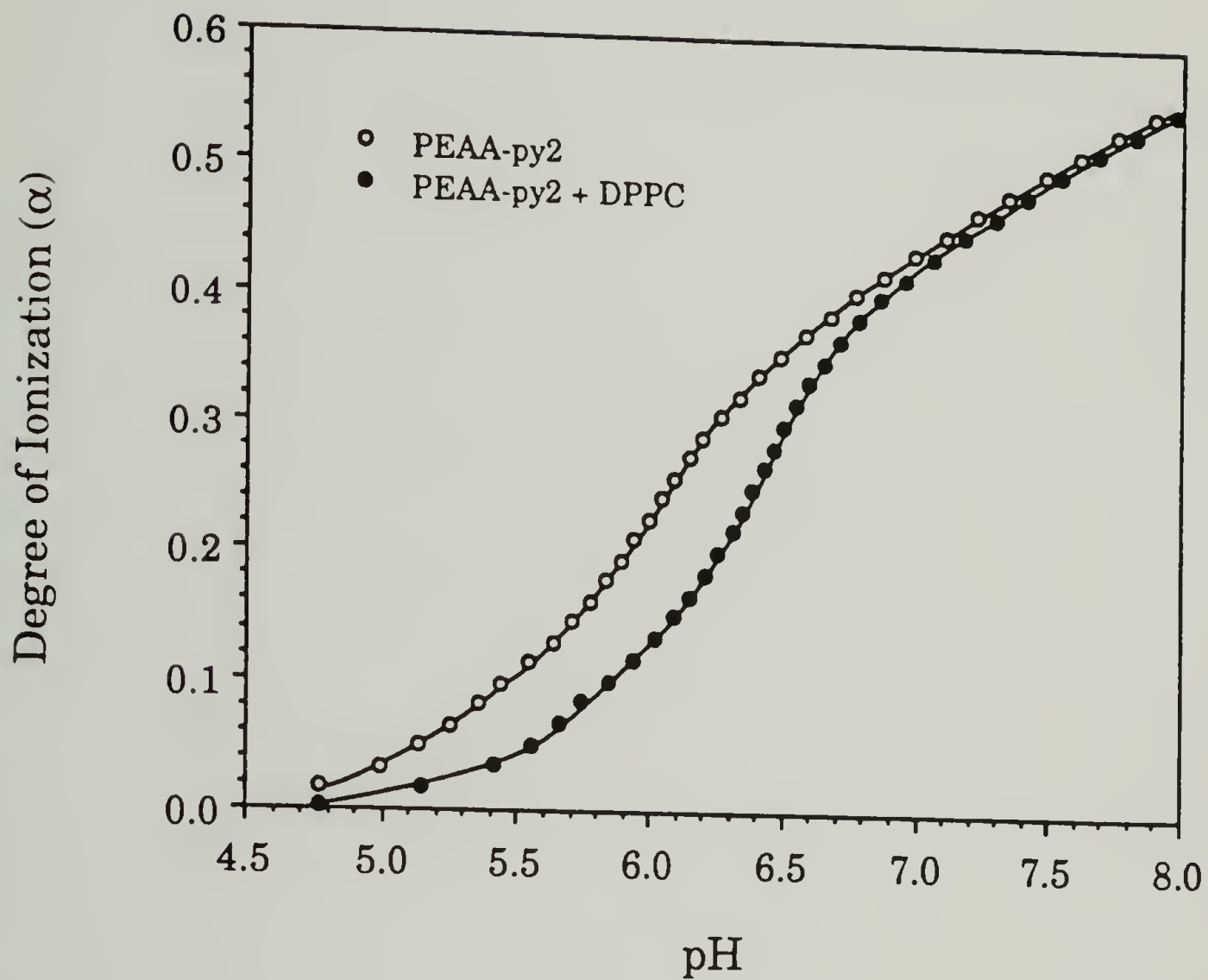


Figure 3.33 Degree of ionization of PEAA-py2 in aqueous solution and suspensions of DPPC (1 mg/ml). Samples contained 0.40 M NaCl, measurements were made at 55 °C.

DPPC causes the polymer to become a weaker acid. This is consistent with the result from the fluorescence intensity experiment (see Figure 3.19). If we assume the measured titration curve is a composite of titration curves for an expanded coil and a collapsed coil, then we can calculate the fraction of each conformation in the crossover region as a function of pH via the method of Nagasawa and Holtzer [73]. The method is graphically outlined in Figure 3.34 for a sample of PEAA-py2. Curve I is the measured titration curve, while curves II and III are the postulated titration curves of wholly collapsed and expanded coils. In the transition region the polymer contains portions of each conformation. For example, at point 'a' the PEAA-py2 has an average degree of ionization α_a , which corresponds to a mixture of collapsed coils and expanded coils with degrees of ionization of α_c and α_e . The fraction of PEAA-py2 in the collapsed coil conformation (f_c) is calculated as:

$$f_c = \frac{\alpha_e - \alpha_a}{\alpha_e - \alpha_c} \quad (\text{Eq. 3.3})$$

We can calculate f_c for every point within the transition region. The calculated values of f_c are plotted versus pH for PEAA-py2 alone and in the presence of DPPC (see Figure 3.35). We see that above pH 7.2 there are no collapsed coil domains for either PEAA-py2 alone or with DPPC. The collapsed coil regions are formed at higher pH values when there are interactions with DPPC. For example, an f_c of 0.50 is found at pH 6.05 for the PEAA-py2 chain alone, while in the presence of DPPC the corresponding pH is 6.4. This is consistent with the shift found in the α versus pH plots (see Figure 3.33). The PEAA-py2 achieves complete collapse below pH 5.2 in solution and below pH 5.6 in the DPPC suspension.

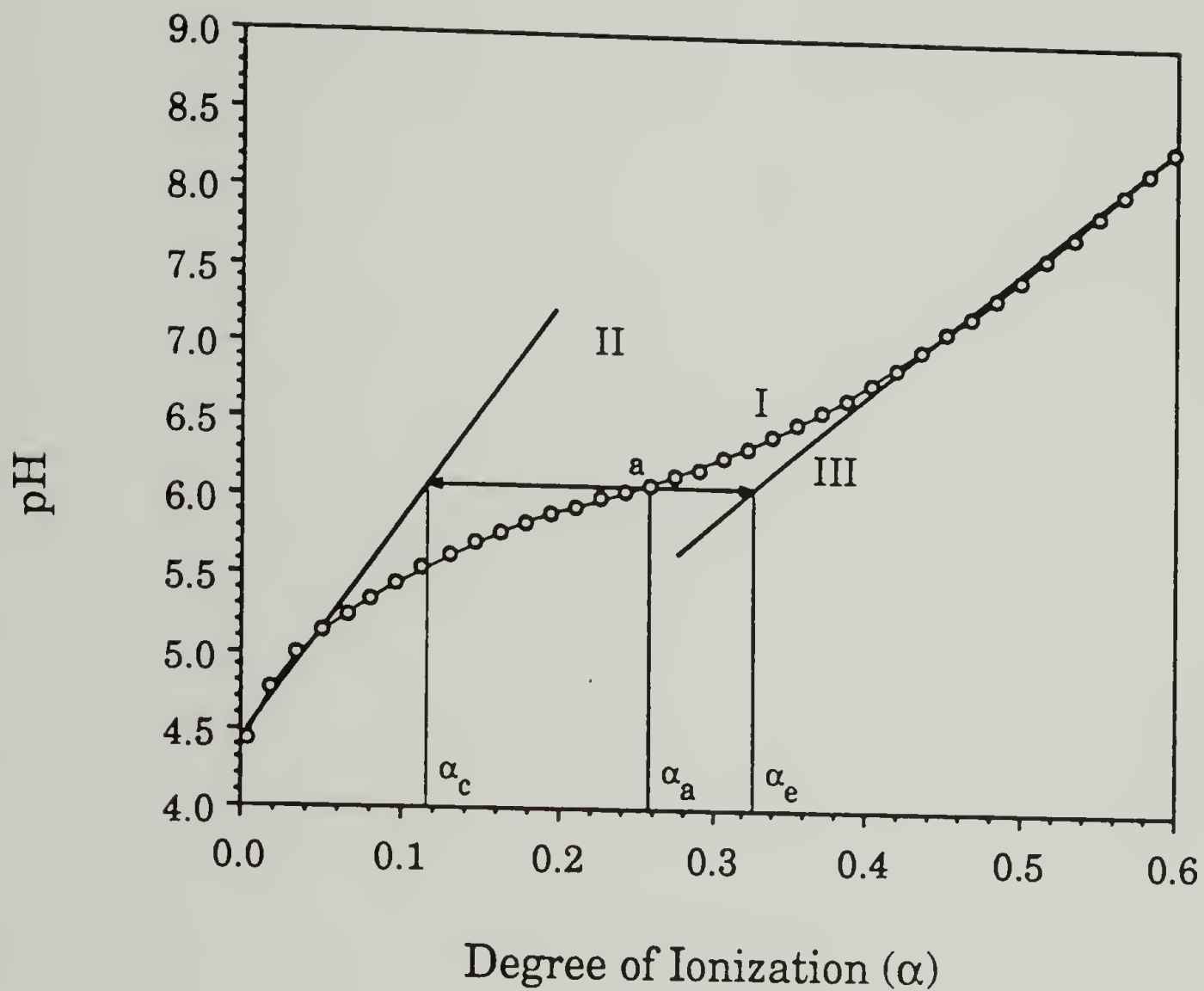


Figure 3.34 Determination of the fraction of collapsed coils (f_c) in the conformational transition region of PEA. From M. Nagasawa and A. Holtzer, *J. Am. Chem. Soc.*, 1964, 86, 538.

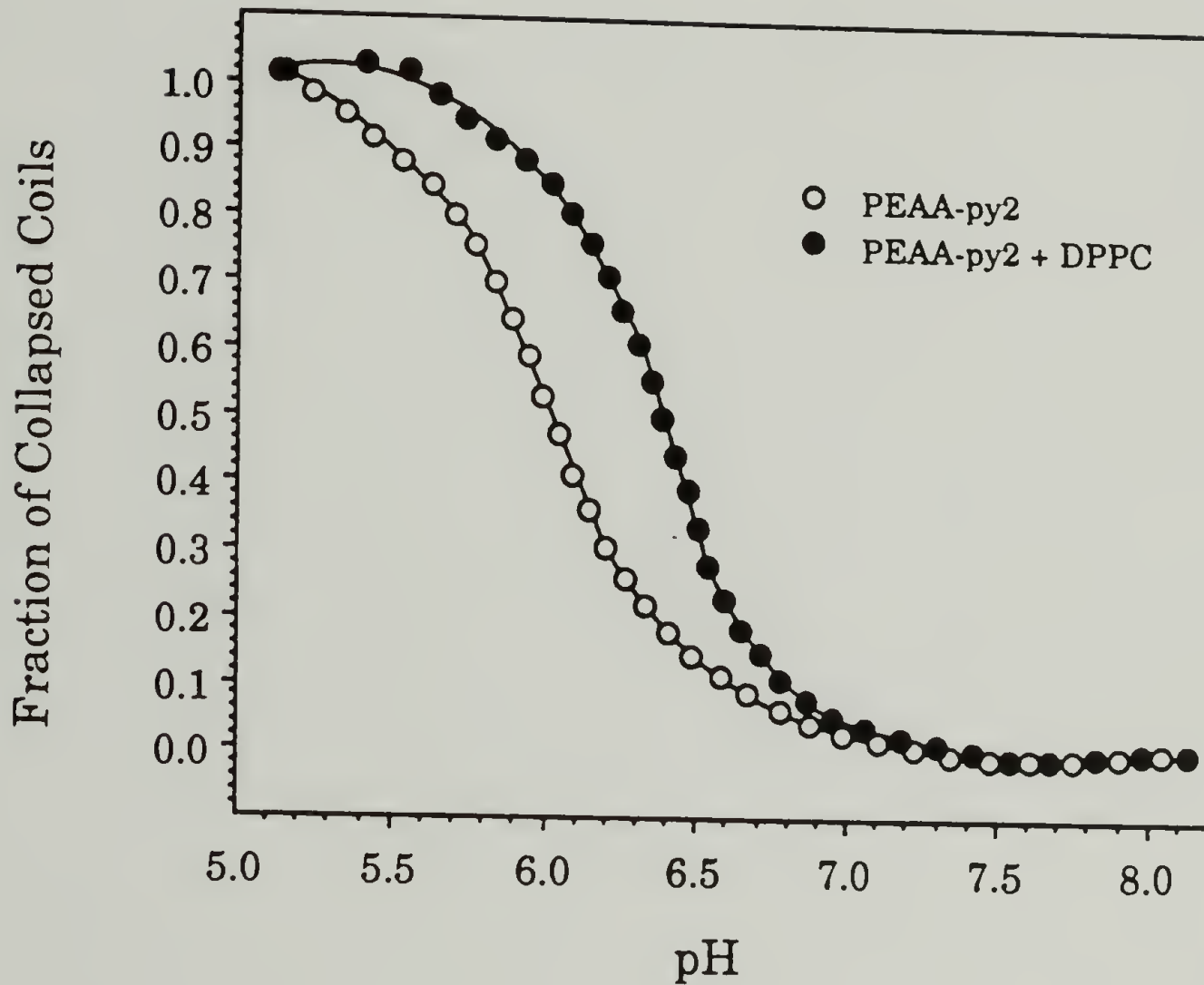


Figure 3.35 Fraction of collapsed coils of PEAA-py2 (1 mg/ml) in aqueous solution and suspensions of DPPC (1 mg/ml) as a function of pH. Samples were at 55 °C and contained 0.40 M NaCl.

A comparison of the derived f_c and fluorescence intensity versus pH for PEAA-py2 in solution (see Figure 3.36) reveals that the midpoint of the transition as reported by pyrene corresponds to a collapsed coil fraction of 22%. A change in f_c from 0.05 to 0.75 corresponds to the total intensity change of the fluorescence study.

The calculation of f_c requires the extrapolation of the presumed titration curves of completely collapsed and expanded coils (curves II and III in Figure 3.34). The extrapolation for curve III seems to be quite reliable, however the extrapolation for curve II is somewhat uncertain due to the small number of data points used. The calculated values of f_c over the transition region are sensitive to the slopes of the extrapolated curves. It was found that an increase in the slope of curve II resulted in a shift of the f_c versus pH curve to lower pH. The maximum shift possible was 0.1 pH units, which corresponded to a twofold increase in the slope of curve II.

The titration data discussed so far has been obtained at 55 °C, in order to detect the full measure of DPPC interaction on the ionization behavior of the PEAA chain. We have mentioned that the interaction between PEAA and DPPC is sensitive to temperature, and occurs extensively only at temperatures greater than or equal to the T_m of DPPC (41 °C) (see Section B of this Chapter). We have compared the ionization behavior of PEAA-py2 to its corresponding fluorescence intensity behavior, even though the fluorescence measurements are recorded at 23 °C after initially heating to 50-60°C. The ionization behavior of PEAA is sensitive to temperature [23], with PEAA becoming a stronger acid as the temperature is increased, however the effect is small for a change from 25 °C to 55°C (see Figure 3.37). The inflection point in the pH versus α plot shifts from pH 6.15 at 25 °C to pH 6.05 at 55 °C. This small shift can account for part of the discrepancy

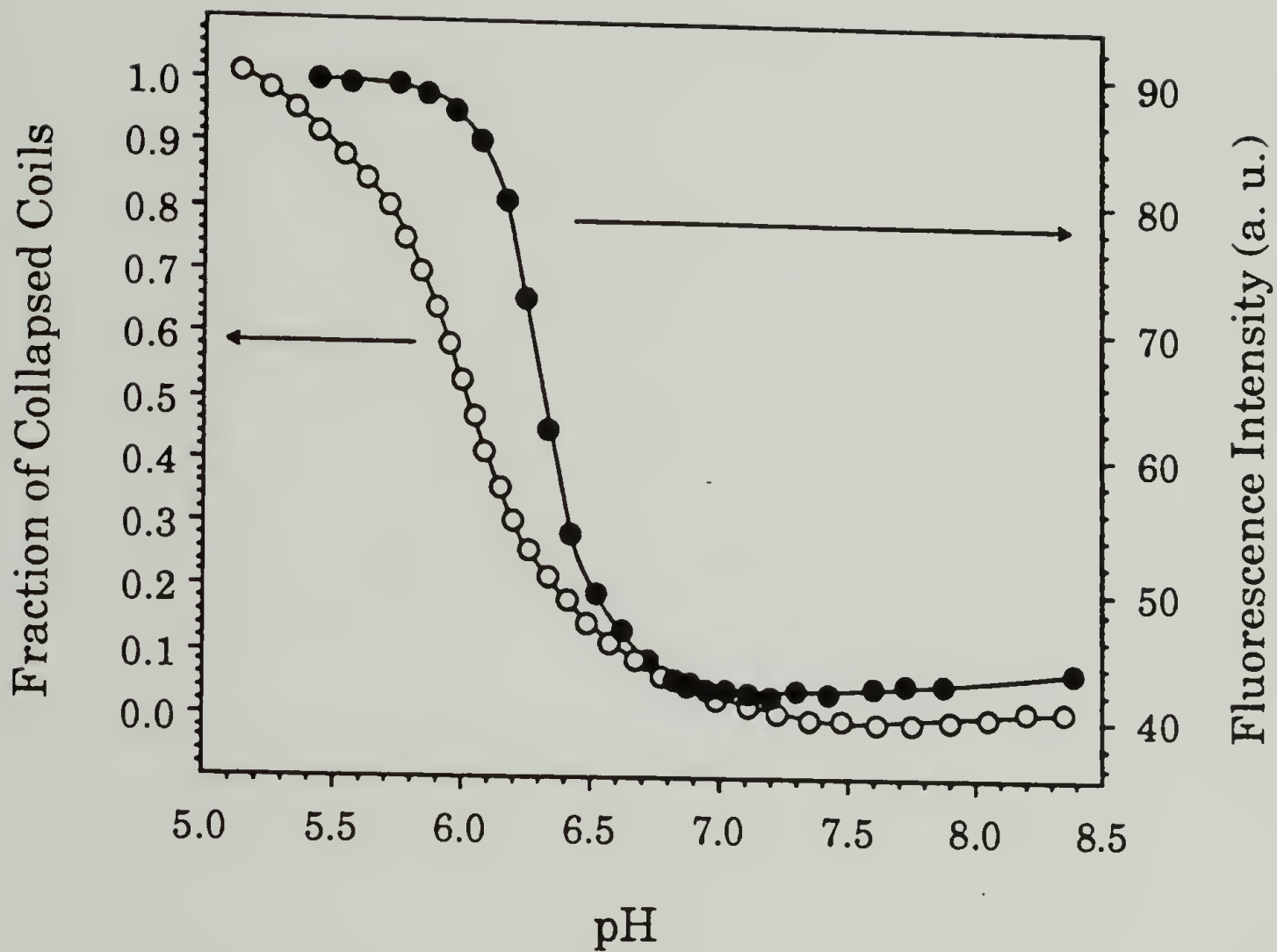


Figure 3.36 Fraction of collapsed coils and emitted fluorescence intensity (377 nm) for aqueous solutions of PEEA-py2 (1 mg/ml) as a function of pH. Fluorescence measurements were made on phosphate-buffered (0.40 M) samples at 23 °C using 345 nm excitation. The fraction of collapsed coils was determined for samples at 55 °C containing 0.40 M NaCl.

between the conformational critical pH values from the titration and fluorescence experiments (see Figure 3.32). In the titration experiments, after addition of dilute HCl the mixtures of PEAA and DPPC were equilibrated for 2 to 3 minutes at 55 °C before recording the solution pH. The pseudoequilibrium state attained in the titration samples may not be equivalent to that found in the samples from the fluorescence experiments, and may be an additional source of discrepancy between the results of the different experiments.

There was some variance observed in the titration curves at high pH for corresponding samples of PEAA with and without DPPC. If there is no interaction between PEAA and DPPC the two curves should coincide for samples of identical ionic strength. This should be the case for mixtures of PEAA and DPPC above pH 8, however the coincidence of the two curves was not always observed. It is believed this is a consequence of the small amounts of PEAA (3 mg) used in each titration experiment and the relatively large uncertainty in the measured mass. The high pH region of the titration curves can be shifted by varying the value of C_M in the calculation of α . Varying the mass of PEAA by ± 0.1 mg (which is the uncertainty of the measurement) was adequate to cause coincidence of the titration curves of PEAA and PEAA+DPPC in the high pH region. The middle and low pH regions of the titration curves were not significantly affected by this artificial variation in PEAA mass. The extreme sensitivity of the high pH region of the titration curve is presumably a consequence of the inability to accurately measure pH changes in this region which are due to the ionization behavior of PEAA [51].

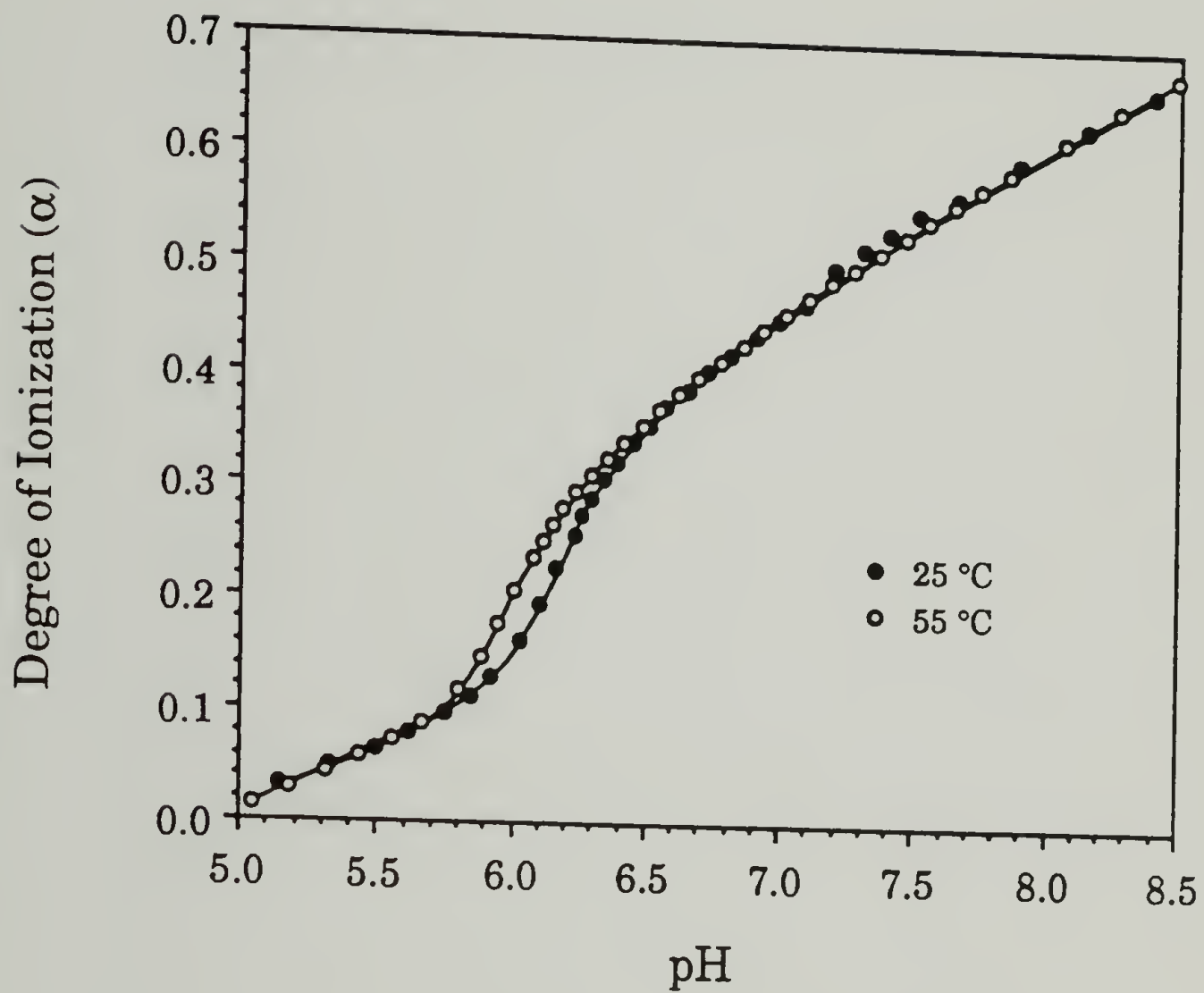


Figure 3.37 Degree of ionization of PEEA (1 mg/ml) in aqueous solution as a function of pH for samples at 25 °C and 55 °C.

F. The pH-Dependent Binding of PEAA and DPPC.

We are interested in obtaining a quantitative description of the pH-dependent interaction between PEAA and DPPC. In order to accomplish this, we must be able to distinguish the non-interacting and interacting species. Multilamellar DPPC vesicles can be easily sedimented by centrifugation at ~2500 rpm in an IEC Model CL centrifuge. Any PEAA that is bound to the DPPC vesicle will be sedimented with the vesicles, while unbound PEAA will remain in solution. We determined the extent of PEAA binding by using fluorescence spectroscopy to measure the concentration of PEAA-py2 in the supernatant of samples at a range of pH that had been centrifuged to sediment the DPPC vesicles. Separate samples containing PEAA-py2 (0.5 mg/ml) and DPPC (0.5 mg/ml) were prepared in 0.02 M phosphate buffer at a range of solution pH (see Chapter II, Section C). After heating to 55 °C for 2 hours and centrifugation at ~2500 rpm for 1.5 hours in an IEC Model CL centrifuge, the concentrations of PEAA-py2 and DPPC in the supernatant were determined as described in Chapter II, Section C. The data obtained from the experiment is shown in Figure 3.38 as a plot of the amounts of PEAA-py2 and DPPC in the supernatant against solution pH. No binding of PEAA-py2 to DPPC vesicles is detected above pH 7.8. Below pH 7.8 there is a dramatic increase in the amount of PEAA-py2 bound to the DPPC vesicles. The supernatant concentration of PEAA-py2 reaches a minimum at pH 7.05, and then begins to increase as the pH is lowered. Below pH 7, PEAA-py2/DPPC mixed micelles are formed. The mixed micelles are not sedimented from solution under the centrifugation conditions we used, consequently as they are formed we observe a relative increase in the supernatant concentration of PEAA-py2. A simultaneous

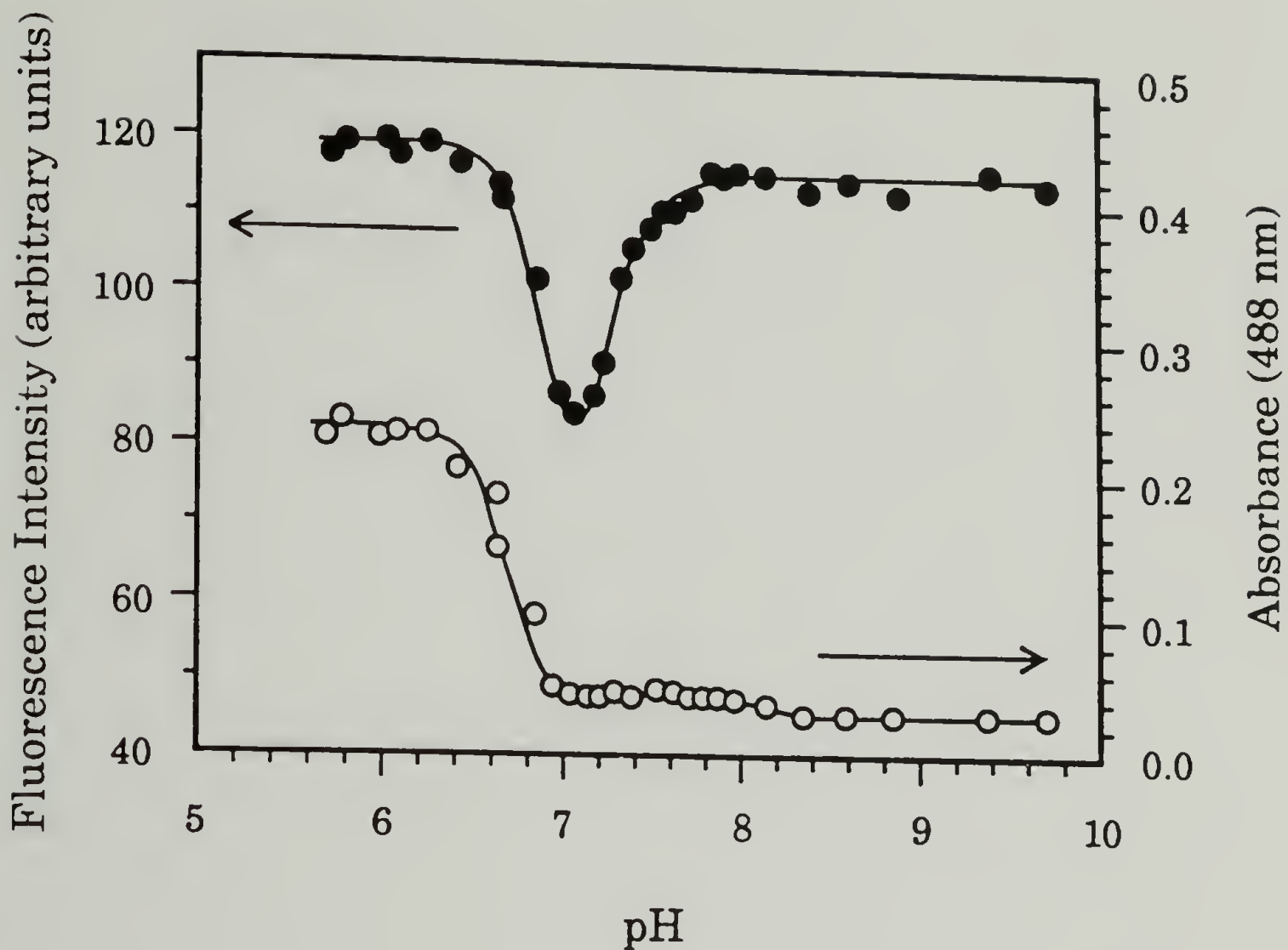


Figure 3.38 Supernatant concentrations of PEAA-py2 and DPPC as a function of pH for 0.02M phosphate-buffered samples after centrifugation. Unsedimented samples were made from phosphate-buffered solutions of PEAA-py2 (0.5 mg/ml) and DPPC (0.5 mg/ml). Supernatant PEAA-py2 was determined from emitted fluorescence intensity (377 nm) at 23 °C using 345 nm excitation. Supernatant DPPC was determined from absorbance of DPPC•Fe(SCN)₃ complex (488 nm) at 23 °C.

increase in the supernatant concentration of DPPC is observed, as shown in Figure 3.38. We find the same pH-dependent binding behavior for samples at 0.40 M ionic strength that we saw for the 0.02 M ionic strength samples. The data from this experiment is shown in Figure 3.39. Again we see a large increase in the amount of PEAA-py2 bound to DPPC vesicles as the pH is reduced below 8. We detect a maximum effect of PEAA-py2 binding to vesicles at pH 7, and notice the formation of mixed micelles below pH 7 as an increase in the supernatant concentrations of PEAA-py2 and DPPC. In this series of samples we find that as the pH is lowered below pH 6 there is a decrease in the supernatant concentrations of PEAA-py2 and DPPC. This behavior is attributed to the formation of large aggregates of mixed micelles which precipitate out of solution. This phenomenon was previously observed as a decrease in fluorescence emission intensity and an increase in optical density in vortex agitated samples of PEAA-py2 and DPPC (see Figure 3.20).

From the data one can calculate the pH-dependent extent of binding as the fraction of the total added PEAA-py2 which is bound to DPPC vesicles. Figure 3.40 shows a plot of the fraction of bound PEAA-py2 versus pH for two ionic strength series of PEAA-py2+DPPC samples. The solid curves are fitted to the data from the region where the extent of binding is determined directly from the supernatant measurements. The formation of mixed micellar structures complicates the binding analysis and the extent of binding cannot be directly determined in the range from pH 7 to pH 6. The dashed lines represent an extrapolation into the mixed micellar region. The data points in the mixed micellar region are the expected fractions calculated from the experimentally determined composition of the

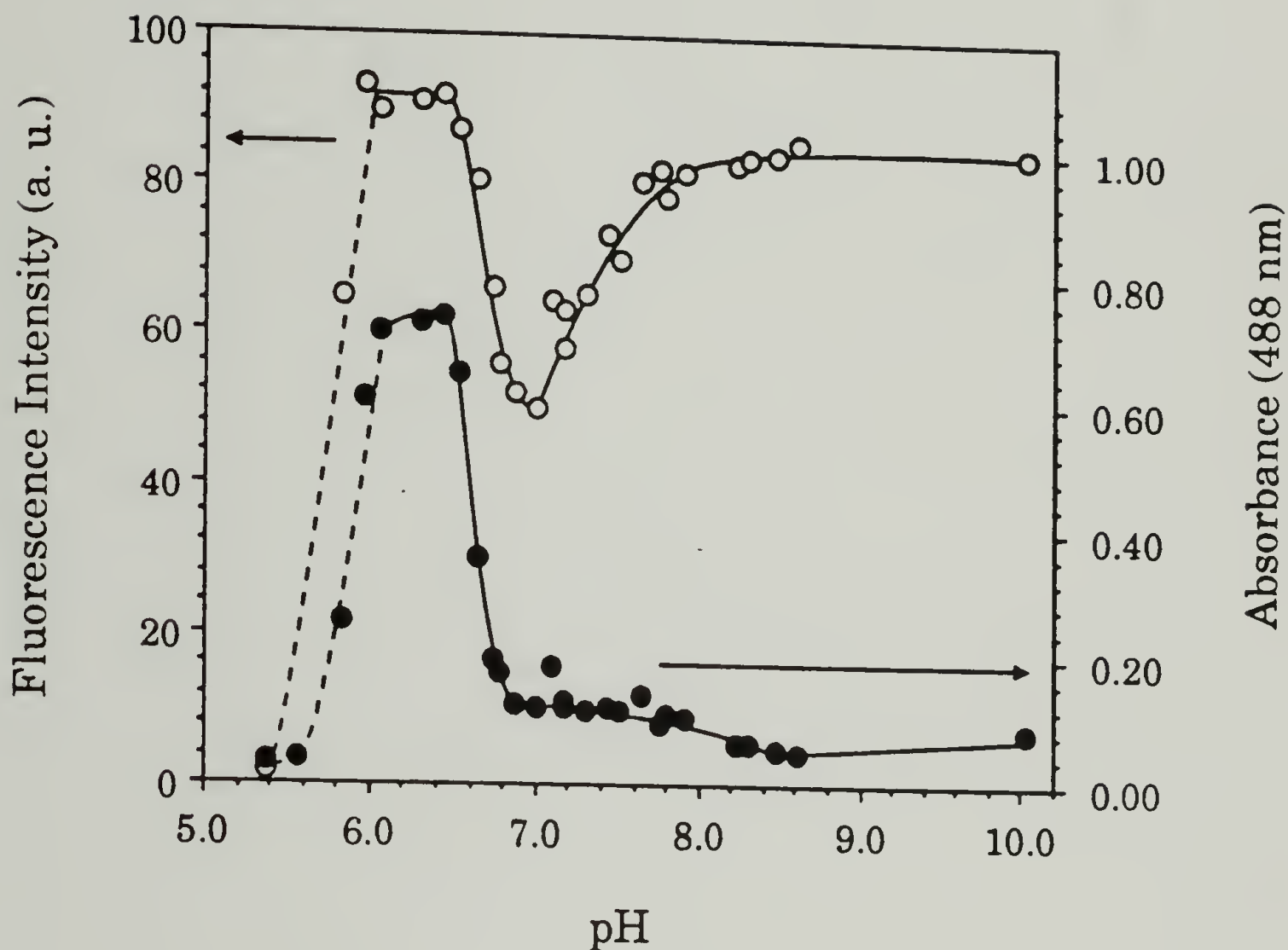


Figure 3.39 Supernatant concentrations of PEAA-py2 and DPPC as a function of pH for 0.40 M phosphate-buffered samples after centrifugation. Unsedimented samples were made from phosphate-buffered solutions of PEAA-py2 (0.5 mg/ml) and DPPC (0.5 mg/ml). Supernatant PEAA-py2 was determined from emitted fluorescence intensity (377 nm) at 23 °C using 345 nm excitation. Supernatant DPPC was determined from absorbance of DPPC•Fe(SCN)₃ complex (488 nm) at 23 °C.

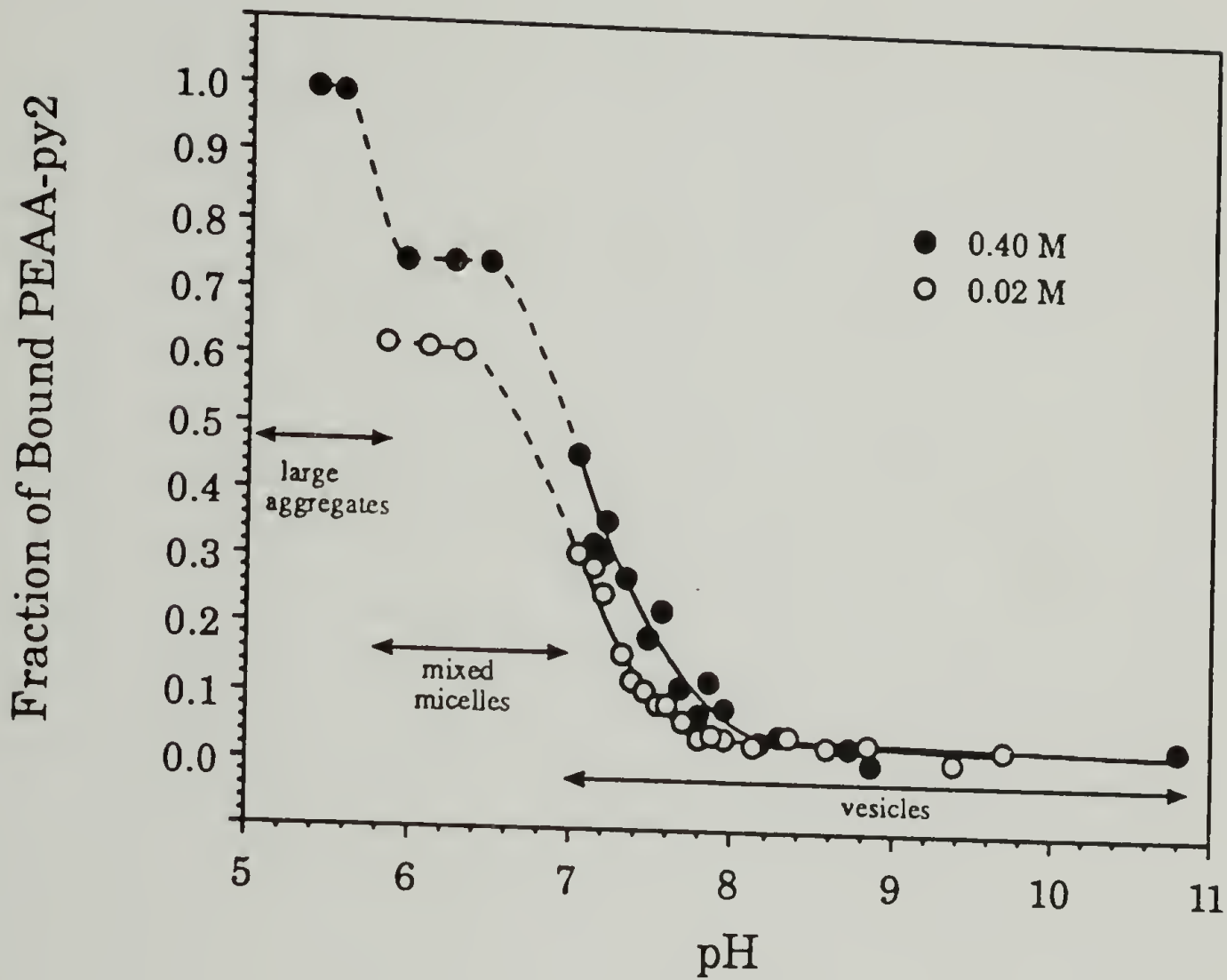


Figure 3.40 Fraction of added PEAA-py2 bound to DPPC aggregates as function of pH for phosphate-buffered (0.02 M and 0.40 M) mixtures of PEAA-py2 (0.5 mg/ml) and DPPC (0.5 mg/ml).

PEAA/DPPC mixed micelles (see Section M of this Chapter). The fraction of PEAA-py2 bound to DPPC vesicles at the onset of the reorganization is found to be 0.30 for the 0.02 M samples and 0.45 for the 0.40 M samples. We also see that the fraction of total added PEAA-py2 in the mixed micelles is 0.65 for the 0.02 M samples and 0.76 for the 0.40 M samples. Evidently, increasing the solution ionic strength promotes the binding of PEAA-py2 to DPPC vesicles. Increased binding with an increase in ionic strength has been observed for the adsorption of polyelectrolytes to neutral surfaces [74]. For the higher ionic strength samples, binding of PEAA-py2 begins at higher pH and the extent of binding is higher than for samples at lower ionic strength. At each ionic strength, there is a significant fraction of the added PEAA-py2 that does not participate in the formation of mixed micelles. Eventually, if the solution pH is lowered far enough, the unbound PEAA-py2 does interact with the mixed micelles to form large aggregate structures. This behavior is found in the 0.40 M series below pH 5.9 as a decrease in the supernatant concentrations of PEAA-py2 and DPPC. All of the added PEAA-py2 is effectively used up in the formation of the large aggregate structures below pH 5.7, since we detect no PEAA-py2 in the supernatant. We did not take the pH low enough in the 0.02 M series samples to observe the formation of large mixed micelle aggregates.

The relationship between the extent of PEAA-py2 binding and the degree of ionization of the PEAA-py2 chain is shown in Figure 3.41. It is seen that the PEAA-py2 is ~50% ionized at pH 7.8 when the binding begins and ~40% ionized when the vesicle-to-mixed micelle reorganization begins at pH 7. The reorganization to mixed micelles is completed well before the inflection point in the titration curve. The titration curve is a composite of

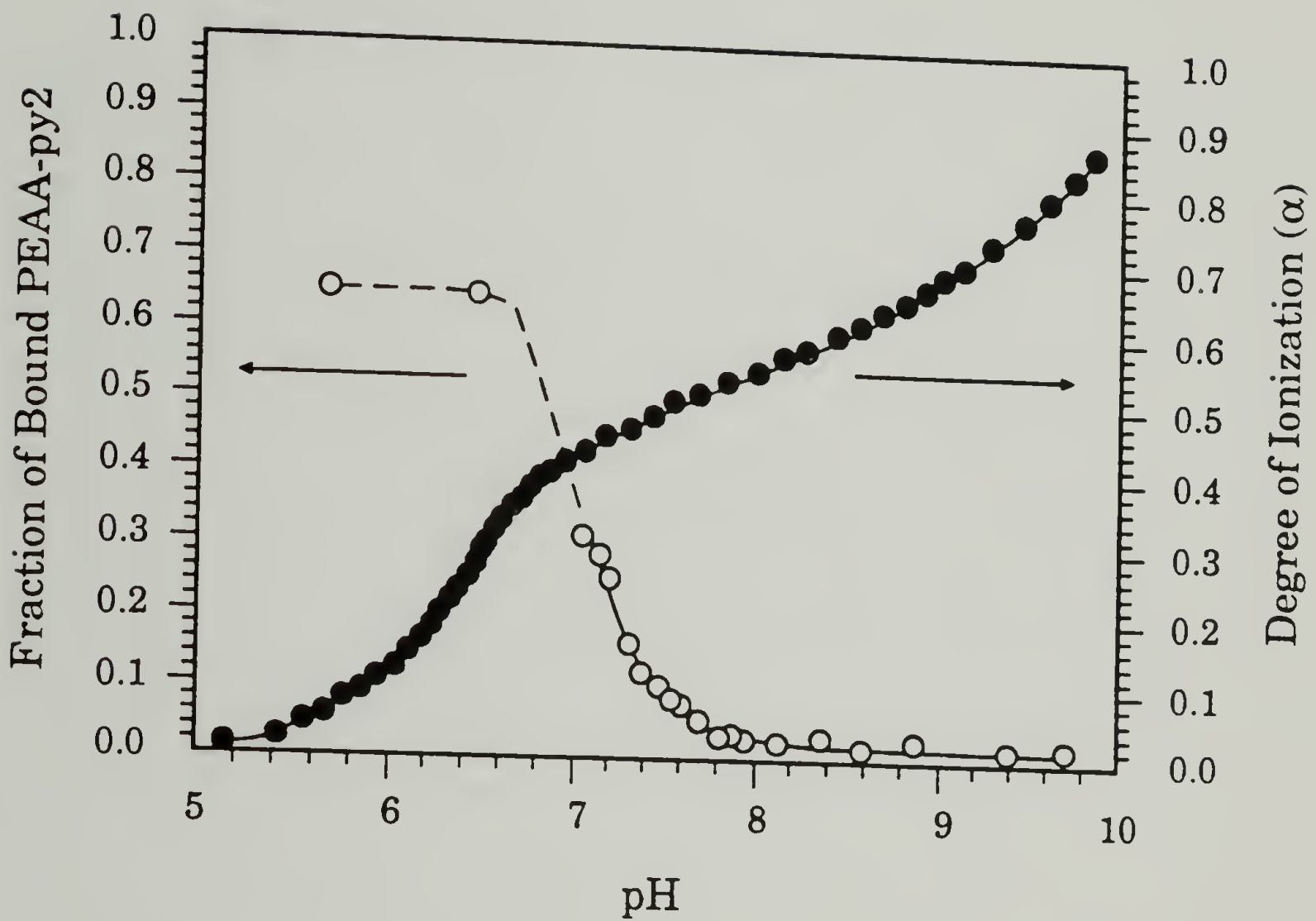


Figure 3.41 Fraction of DPPC bound PEAA-py2 and degree of ionization of PEAA-py2 as a function of pH in aqueous suspensions of DPPC.

the behavior of all the PEAA-py2 chains in the sample. We have determined that a significant fraction of the PEAA-py2 chains are not involved in the formation of mixed micelles. Therefore the titration curve (and also the fluorescence intensity curve) does not reflect only the conformational behavior of the interacting PEAA-py2 chains, but instead includes some contribution from the conformational behavior of unbound PEAA-py2 chains.

The titration curve and fraction bound curve can be combined to show the relation between the fraction of bound PEAA-py2 and measured degree of ionization. This relation is derived for each ionic strength series and the comparison between the two is presented in Figure 3.42. As the ionic strength increases, binding of PEAA-py2 begins at a higher average degree of ionization. In general, the curve is shifted along the α axis to higher values of α as the ionic strength is increased.

The effect of DPPC concentration on the pH-dependent extent of PEAA-py binding was examined. Figure 3.43 shows the effect of increasing the DPPC:PEAA-py2 weight ratio from 1:1 to 3.5:1. For the series with the 3.5:1 ratio, ~15% of the added PEAA-py2 is complexed with DPPC vesicles above pH 8.5. The extent of binding increases as the solution pH is lowered below pH 8.5 with ~65% of the added PEAA-py2 bound to DPPC vesicles when the reorganization to mixed micelles begins. At the 3.5:1 ratio, all of the PEAA-py2 is associated with the mixed micellar structures. It is surprising that so much of the PEAA-py2 is associated with the DPPC vesicles at high pH in the 3.5:1 series. No interaction between DPPC vesicles and PEAA was detected by fluorescence measurements of emission intensity, $em \lambda_{max}$, or $ex \lambda_{max}$ on samples at a 1:1 weight ratio. However,

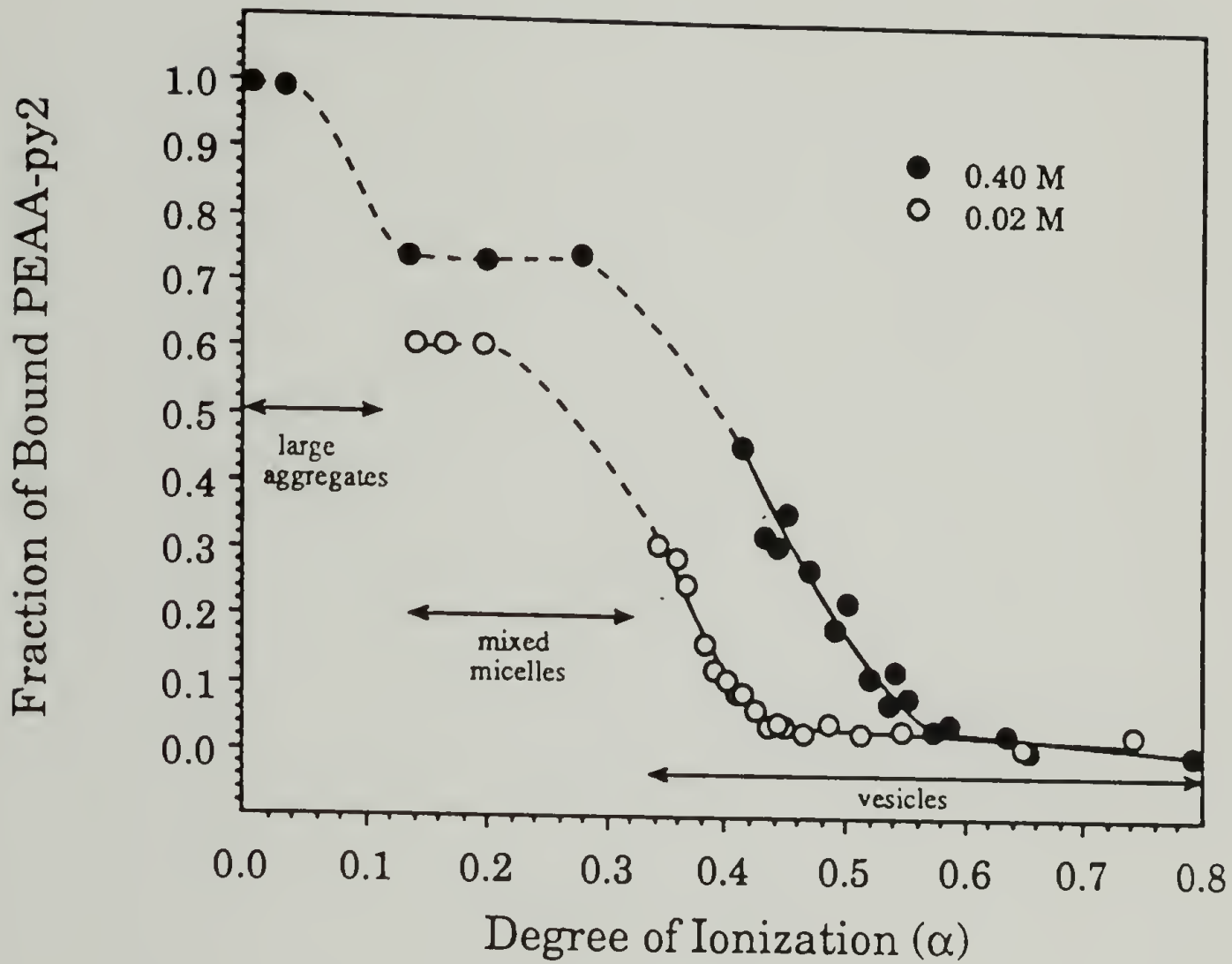


Figure 3.42 Fraction of added PEAA-py2 bound to DPPC aggregates as function of the degree of ionization of PEAA-py2 for 0.02 M and 0.40 M ionic strength solutions of PEAA-py2 and DPPC.

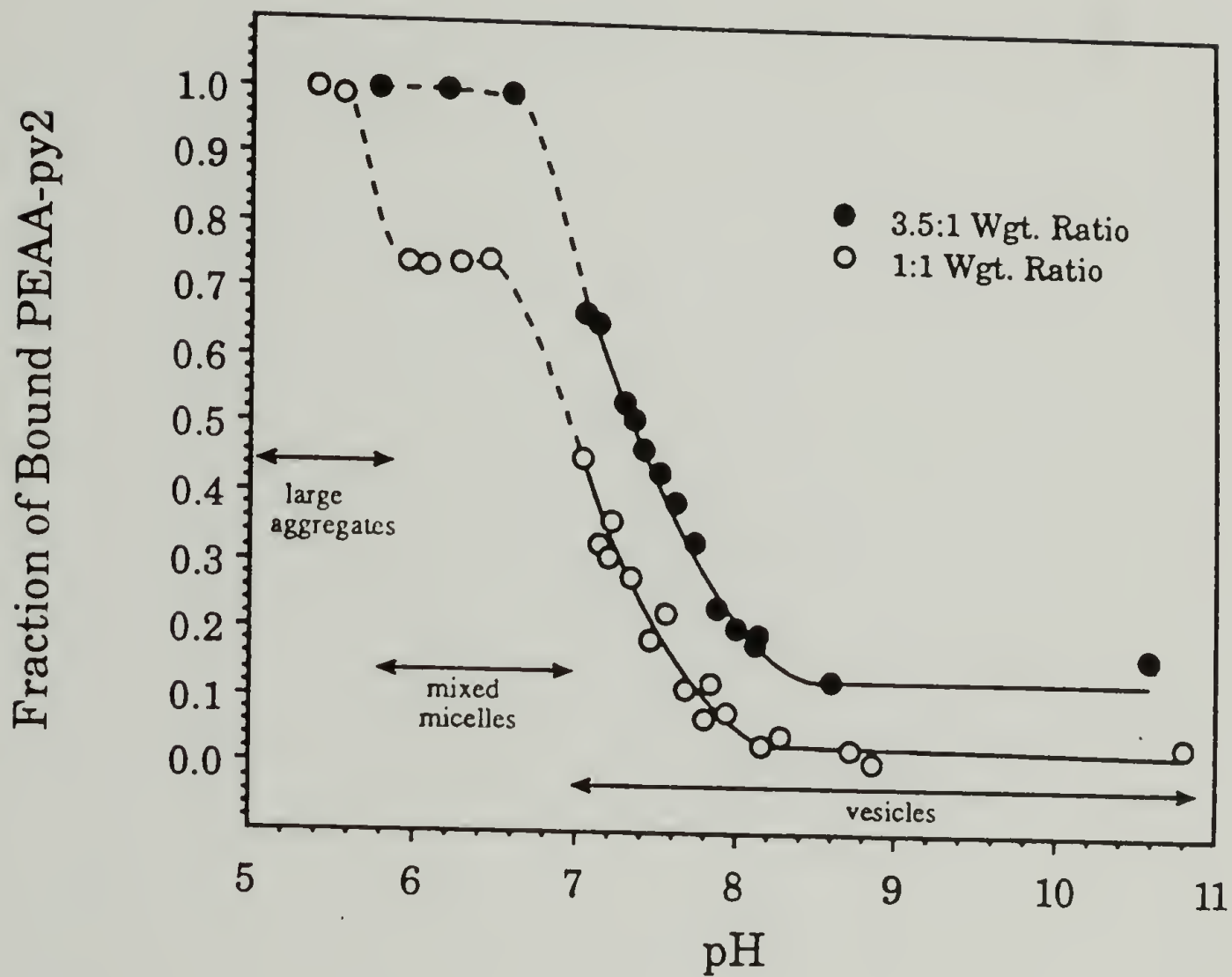


Figure 3.43 Fraction of added PEAA-py2 bound to DPPC aggregates as function of pH for phosphate-buffered (0.40 M) suspensions of PEAA-py2 (0.5 mg/ml) and DPPC (0.5 mg/ml and 1.75 mg/ml).

analysis of the em λ_{\max} versus pH plot reveals an increased level of interaction at high pH for the 3.5:1 ratio samples compared to the 1:1 ratio samples (see Figure 3.44). For the 1:1 ratio samples we observe an increase in em λ_{\max} from 376.8 nm at high pH to 377.6 nm at low pH. However, for the 3.5:1 ratio samples em λ_{\max} changes from 377.4 nm to 377.9 nm as the pH is lowered. There is a shift of 0.6 nm in the em λ_{\max} of samples at high pH as the amount of added DPPC is varied. The 3.5:1 DPPC:PEAA weight ratio experiment reveals that even when the PEAA is highly ionized there exists some type of interaction between the PEAA and the DPPC vesicles. The exact nature of this high pH interaction is uncertain. Hydrophobic interactions between the ethyl side chains and the DPPC bilayer may be possible, as well as a hydrogen bonding interaction between un-ionized carboxyl groups and the phosphodiester moiety of DPPC.

G. Concentration-Dependent Binding of PEAA-py2 to DPPC Vesicles.

As noted in the previous section, the fraction of bound PEAA-py2 depends on the ratio of DPPC to PEAA-py2. We can investigate this effect by measuring the fraction of bound PEAA-py2 as a function of added DPPC for samples at a fixed pH. In this experiment, varying amounts of DPPC vesicles are added to phosphate buffered (0.02 M, pH 7.1) solutions of PEAA-py2. After heating to 55 °C for 2 hours the samples are centrifuged at ~2500 rpm for 1.5 hours and the supernatant is analyzed for PEAA-py2 and DPPC as described in Chapter II, Section C. Figure 3.45 shows how the amount of bound PEAA-py2 increases as the concentration of DPPC is

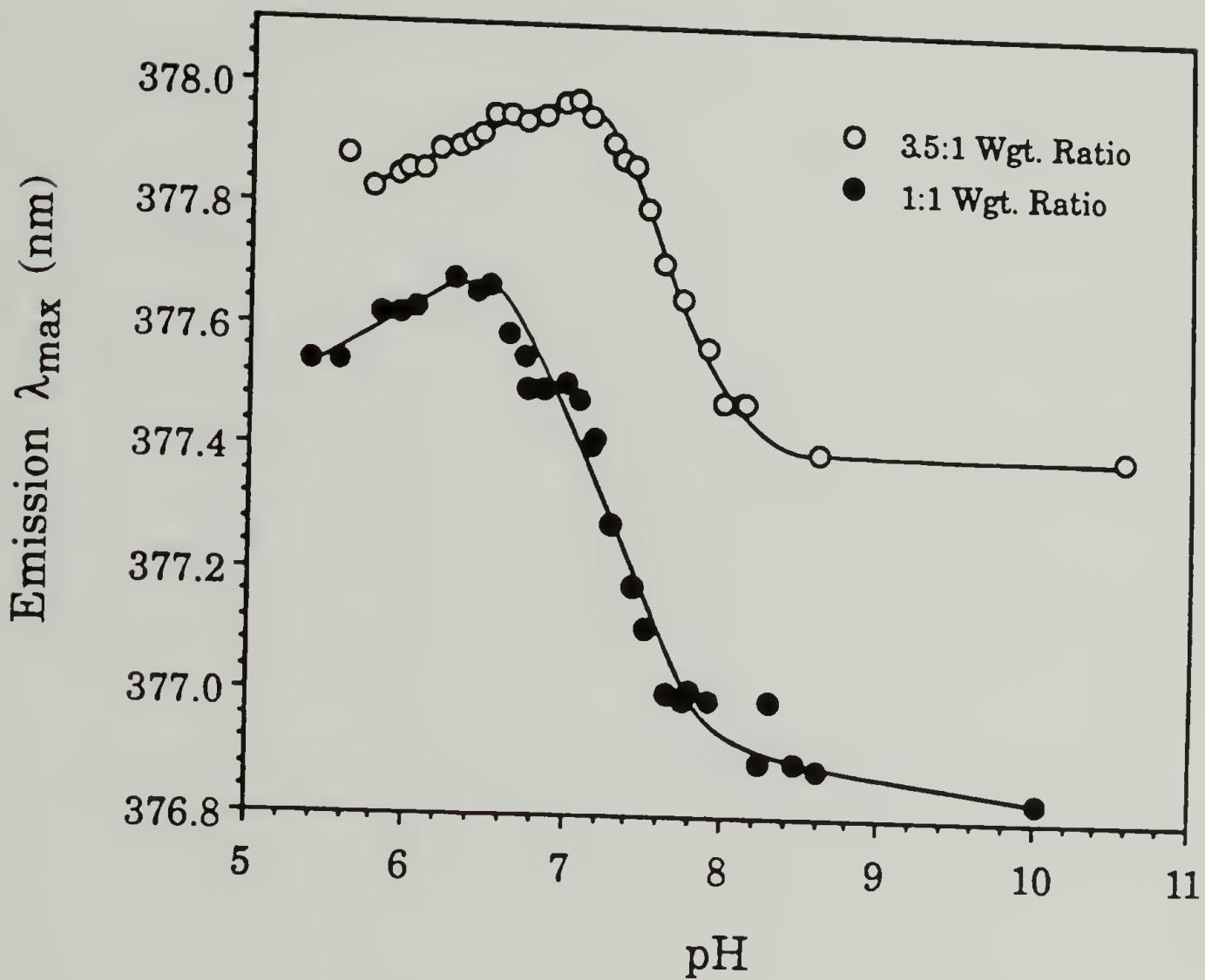


Figure 3.44 Wavelength of maximum intensity in the emission spectrum of PEAA-py2 (0.5 mg/ml) in phosphate-buffered (0.40M) aqueous suspensions of DPPC (0.5 mg/ml and 1.75 mg/ml) as a function of pH. Excitation wavelength 345 nm, T = 23 °C.

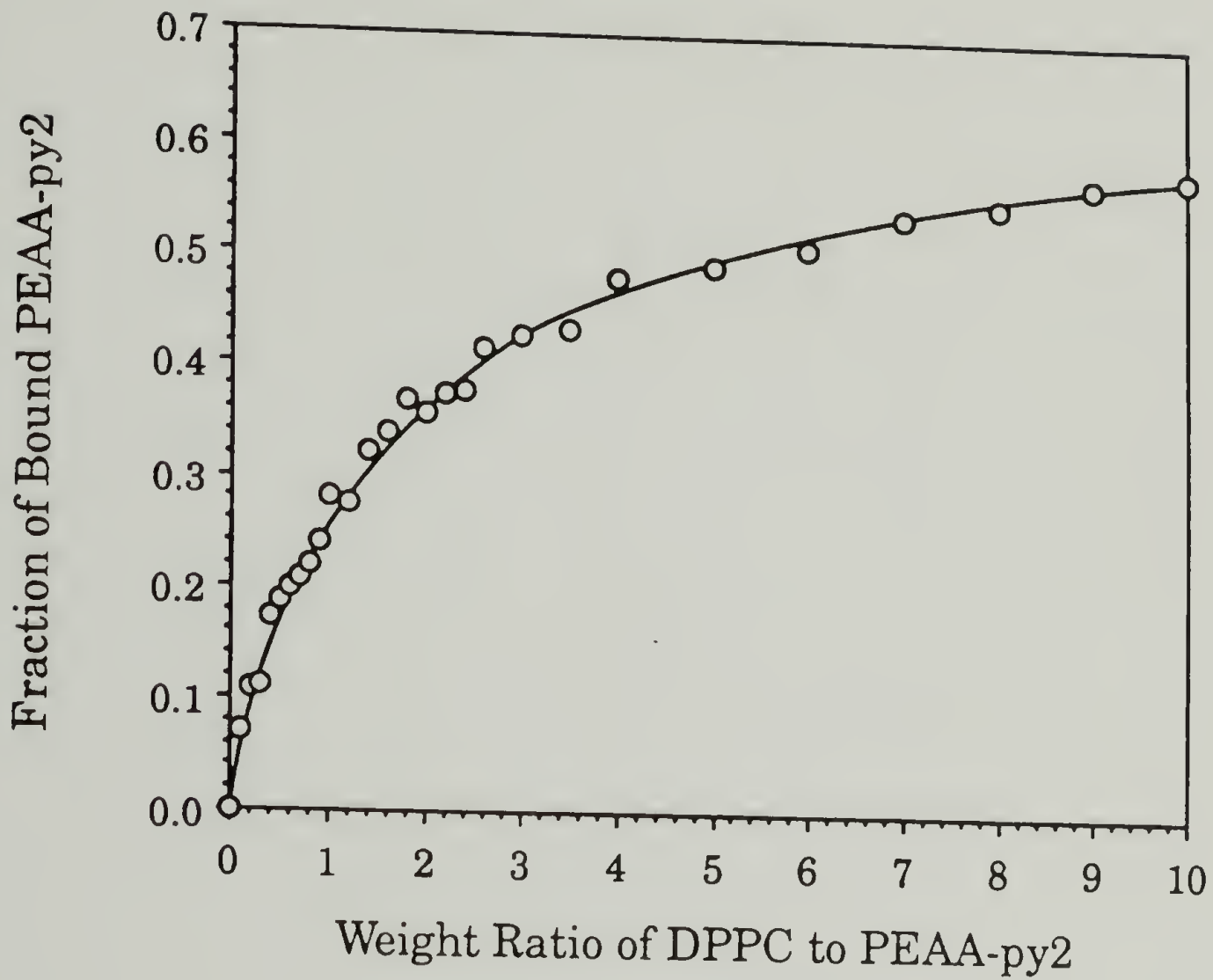


Figure 3.45 Fraction of PEAA-py2 bound to DPPC vesicles in 0.02 M phosphate-buffered suspensions at pH 7.1 as a function of the ratio of added DPPC to PEAA-py2. Concentration of PEAA-py2 was constant at 0.5 mg/ml.

increased. There is a rapid initial increase in the curve, which starts to level out for DPPC concentrations above 1 mg/ml (weight ratio 2:1).

The fraction of bound PEAA-py2 was determined as a function of added DPPC for series of samples at pH 7.1, pH 8.6, and pH 10.3. The results of these experiments are given in Figure 3.46 for samples at 0.40 M ionic strength. For each pH series studied there is an increase in the fraction of bound PEAA-py2 as the concentration of DPPC is increased. We see that as the pH of the samples is raised for a given concentration of DPPC, the fraction of bound PEAA-py2 is diminished. We find that even at pH 10.3 there is a measurable interaction between the DPPC vesicles and PEAA-py2. This correlates with the observations made in the previous section on the effect of an increased DPPC:PEAA-py2 ratio on the amount of PEAA-py bound at high pH. These binding studies have been carried with PEAA chains with attached pyrene moieties. There is some concern that observed binding of PEAA to DPPC vesicles at high pH is the result of the pyrene groups embedding into the DPPC bilayer. This concern may be addressed by comparing the excitation spectra of PEAA-py at pH 10.3 in solution alone and in the presence of DPPC (at the 10:1 ratio). The excitation spectra and their second derivatives are shown in Figure 3.47. We see that the two excitation spectra and their second derivatives are identical. From Figure 3.46 we see that ~20% of the added PEAA-py2 is bound to DPPC vesicles at pH 10.3 for a DPPC to PEAA-py2 ratio of 10:1. If insertion of the pyrene moieties into the bilayer were occurring to a significant extent, we would notice the presence of two components in the excitation spectrum of the 10:1 weight ratio sample, because the embedded pyrene has a different λ_{\max} than the aqueous pyrene (see Section D of this Chapter). Since only one component is seen in the excitation spectrum and

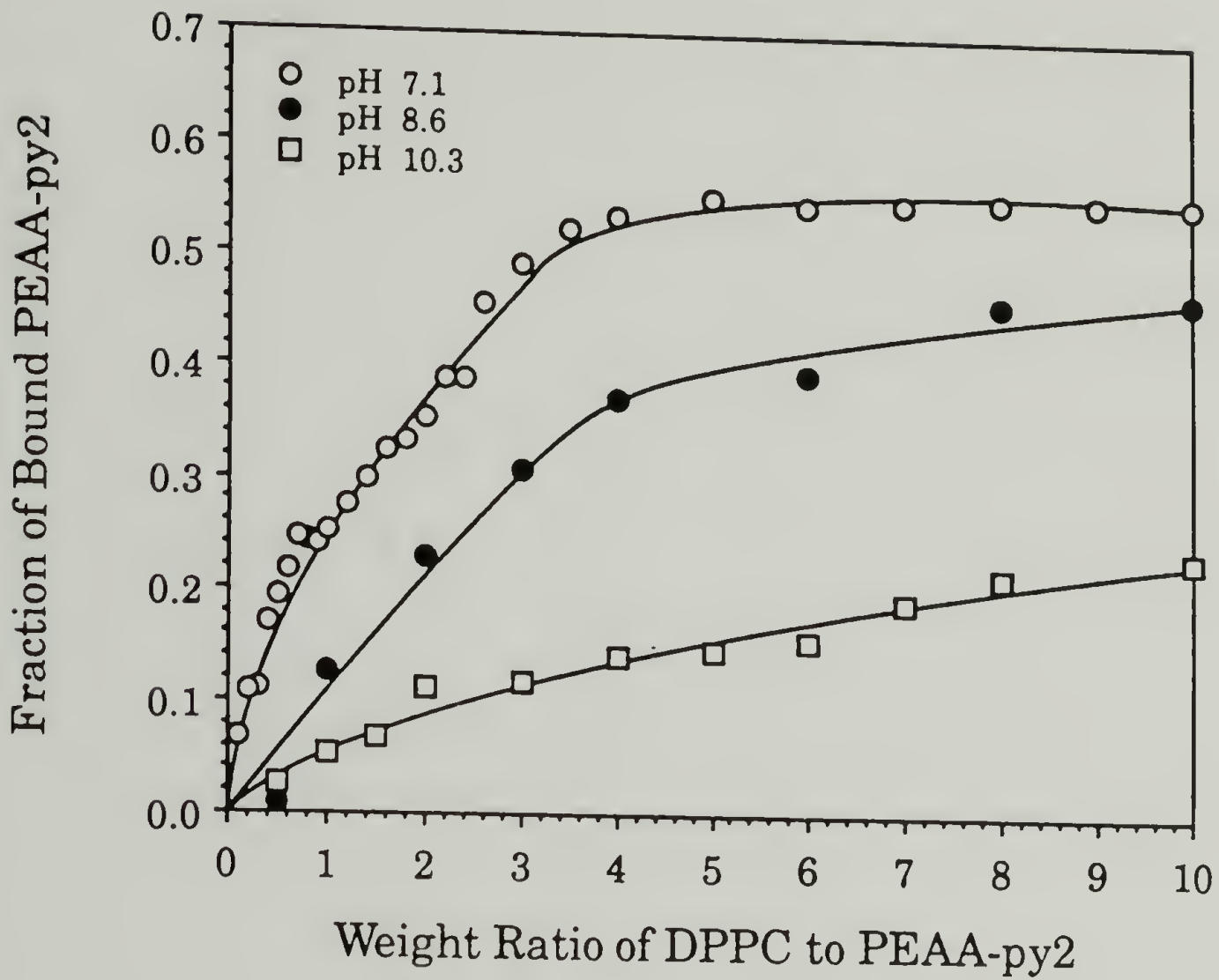


Figure 3.46 Fraction of PEAA-py2 bound to DPPC vesicles in 0.40 M phosphate-buffered suspensions at pH 7.1, pH 8.6, and pH 10.3 as a function of the ratio of added DPPC to PEAA-py2. Concentration of PEAA-py2 was constant at 0.5 mg/ml.

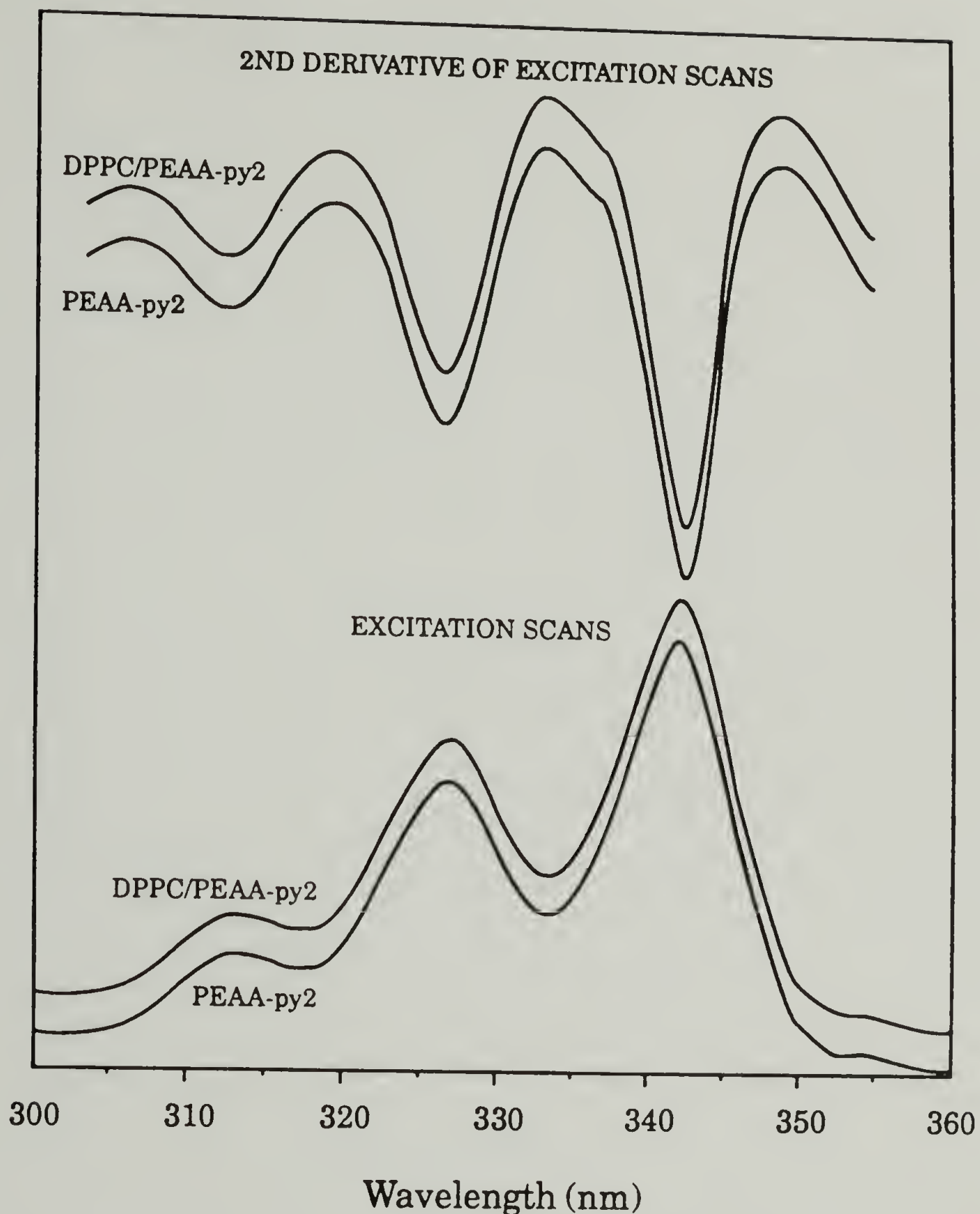


Figure 3.47 Excitation spectra and their second derivatives for PEAA-py2 (0.5 mg/ml) in phosphate-buffered (0.40 M) aqueous solution and suspensions of DPPC (0.5 mg/ml) at pH 10.3. Excitation spectra were recorded at 23 °C using 377 nm emission wavelength. Second derivatives of the excitation spectra were calculated with the derivative function of the Perkin-Elmer MPF-66 fluorescence spectrometer.

it is identical to the component observed for PEAA-py2 alone in solution, we can assume that pyrene insertion into the bilayer is not an important factor in the binding of PEAA to DPPC vesicles.

If we monitor the change in $\text{em } \lambda_{\text{max}}$ in the samples at pH 7.1 (ionic strength 0.40 M) as a function of DPPC concentration we obtain the plot shown in Figure 3.48. The $\text{em } \lambda_{\text{max}}$ is 376.4 nm for PEAA-py2 alone at pH 7.1, and increases to 377.3 nm at weight ratios above 2:1, when the extent of PEAA-py2 binding levels out.

H. Fluorescence Polarization Experiments.

The binding experiments have shown that PEAA interaction with the DPPC vesicles dramatically increases when the solution pH is decreased below pH 8. The interaction between PEAA and DPPC is expected to affect the physical properties of the DPPC bilayer. Fluorescence polarization measurements have proven to be a highly sensitive technique for characterizing changes in the physical state of bilayer membranes, and therefore should be useful in detecting the effect of the pH-dependent interaction of PEAA on the DPPC bilayer. We carried out fluorescence polarization experiments with probes incorporated into the hydrophobic and headgroup regions of the DPPC bilayer as a means of characterizing the pH-dependent interaction between PEAA and DPPC.

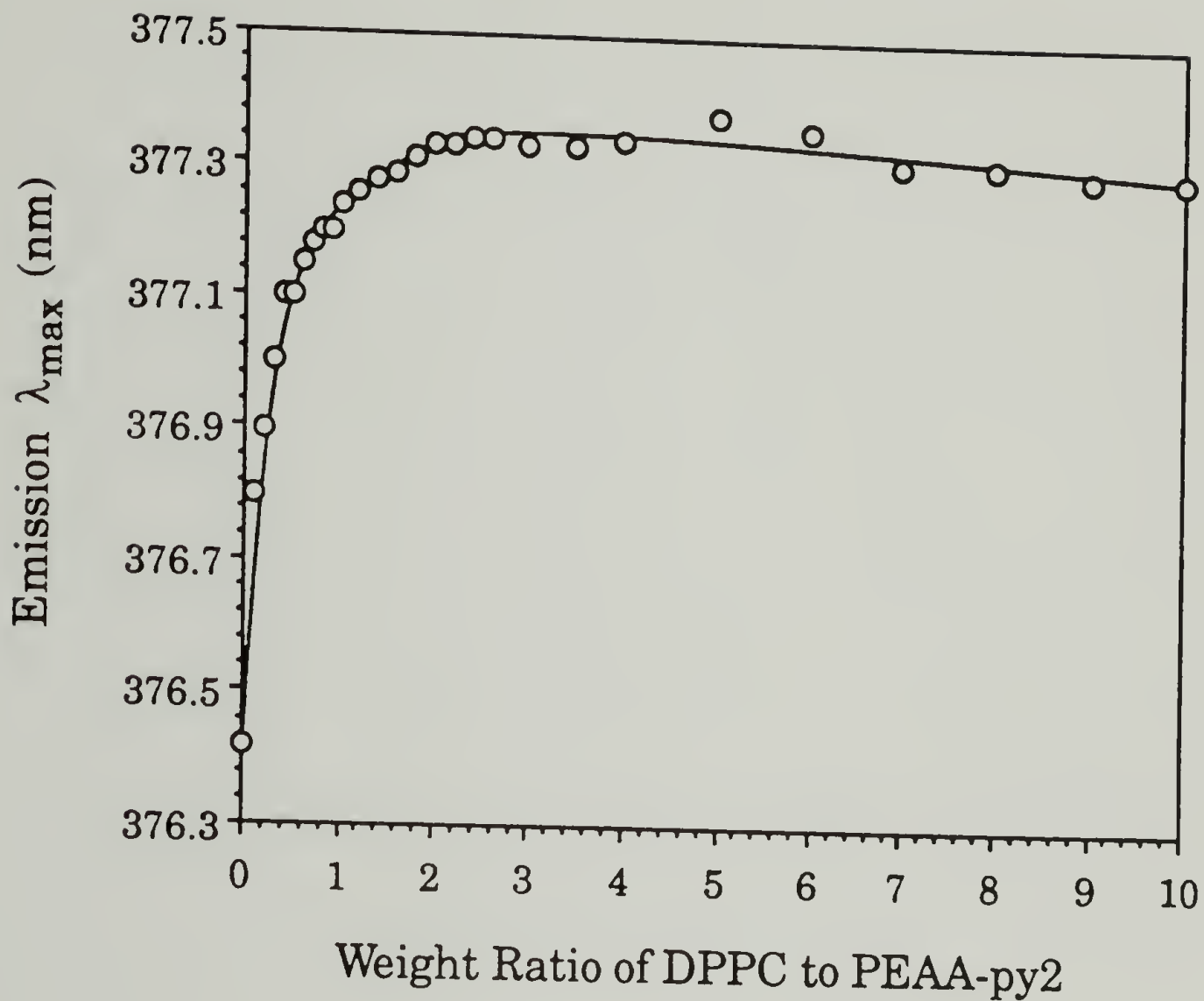


Figure 3.48 Wavelength of maximum intensity in the emission spectrum of PEAA-py2 (0.5 mg/ml) in phosphate-buffered (0.40M) aqueous suspensions of DPPC at pH 7.1 as a function of the ratio of added DPPC to PEAA-py2. Concentration of PEAA-py2 was constant at 0.5 mg/ml. Emission spectra were recorded at 23 °C using 345 nm excitation wavelength.

1. Use of Diphenylhexatriene.

Diphenylhexatriene (DPH) has been widely used for fluorescence polarization studies of biological and model membranes. DPH has been shown to orient with its symmetry axis normal to the plane of the bilayer in the ordered gel phase of phospholipids [75, 76]. Since even small displacements of the DPH symmetry axis result in depolarization of emitted fluorescence (see Chapter I, Section F), DPH is an excellent probe for monitoring changes in the acyl chain packing order of phospholipid bilayers [42, 77-79].

DPH was imbibed into DPPC vesicles (0.25 mg/ml, DPH to DPPC molar ratio 1:1000), PEAA (0.25 mg/ml) was added, and the polarization of emitted fluorescence was measured as a function of solution pH as described in Chapter II, Section C. The experimental results are given in Figure 3.49 as a plot of the fluorescence polarization against pH. As the solution pH is lowered below 8 there is an increase in the measured polarization. The polarization increases from 0.435 above pH 8 to a maximum value of 0.455 at pH 7. Further reduction of pH below 7 results in a sharp decrease in the measured polarization. The measured polarization at pH 6 is 0.40. We find that the polarization of DPH in polymer-free suspensions of DPPC vesicles is unaffected by changes in solution pH, remaining nearly constant at a value of 0.433 over the experimental pH range. The polarization value of 0.433 is similar to that observed for DPH in DPPC vesicles at 23 °C by other researchers [16, 71, 80, 81]. Also, the polarization of DPH in mixtures of PEAA and DPPC above pH 8 is identical to the polarization of DPH in DPPC vesicles. The adsorption of the PEAA chain onto the DPPC vesicle surface leads to an increase in the polarization of the bilayer-embedded DPH. An

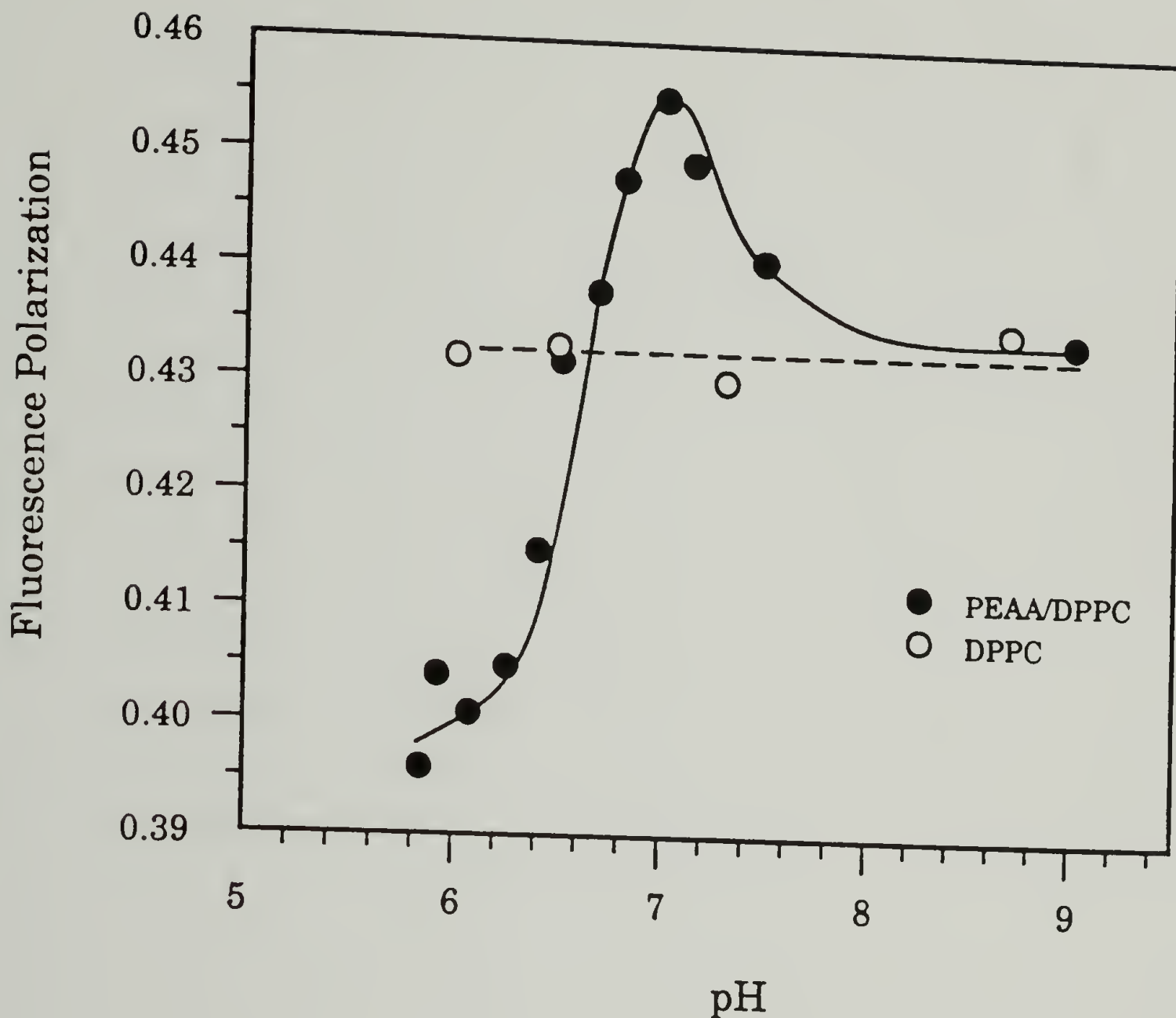


Figure 3.49 Polarization of fluorescence (430 nm) from 3.4×10^{-7} M DPH in 0.02 M phosphate-buffered suspensions of sonicated DPPC vesicles (0.25 mg/ml) and with mixtures of PEA (0.25 mg/ml) as a function of pH. Emission spectra were recorded at 23 °C on deaerated samples using 360 nm excitation. Optical densities were less than 0.10.

increase in polarization is associated with a decrease in the rotational mobility of the probe molecule, assuming no change in lifetime (see Chapter I, Section F). If this is so, then PEAA interaction results in a rigidification of the DPPC bilayer in the sense that the rotational mobility of DPH has been diminished. Similar increases in DPH polarization have been observed for the interaction of α -lactalbumin with DMPC vesicles [82] and for the interaction of sucrose with DOPC and DOPG vesicles [83].

We noted that the sharp decrease in polarization occurs as the pH is lowered below 7. In studies of model membranes a decrease in DPH polarization has been correlated with a decrease in the order of the bilayer [13-18]. The binding experiments (see Section F of this Chapter) showed that mixed micelles are formed when the solution pH is decreased below 7. Therefore, one might assume from the polarization experiment that the mixed micellar structure has a looser bilayer organization than found in vesicles. However, there is a large change in size when the vesicles are reorganized into mixed micelles. Quasi-elastic light scattering measurements have shown there is at least a tenfold decrease in hydrodynamic radius associated with the vesicle-to-mixed micelle transition [57]. The measured polarization is proportional to ϕ/τ , where ϕ is the rotational correlation time of the probe and τ is the fluorescence lifetime. There is a contribution to ϕ from the Brownian rotation of the aggregate in which the probe is embedded. It has been shown that the Brownian rotation of vesicles does not significantly affect the probe rotational correlation time [15], however the mixed micelles are much smaller than vesicles and their rotation may act to reduce ϕ . As noted in Chapter 1, Section F, rotational correlation times for vesicles are on the order of microseconds, while the rotational correlation time for typical

probes are on the order of nanoseconds; therefore the Brownian rotation of vesicles does not affect the measured polarization. The Brownian rotational correlation time is given as:

$$\phi = \frac{\eta V}{kT} \quad (\text{Eq. 3.4})$$

where η is the viscosity of the medium, V is the volume of the rotating aggregate, k is the Boltzmann constant, and T is the temperature. For a tenfold decrease in hydrodynamic radius (with all other parameters remaining unchanged) there is a corresponding 1000 fold decrease in volume, which would put the rotational correlation time of the mixed micelles in the nanosecond range. In this situation the Brownian rotation of the mixed micelles contributes to the time dependent depolarization of the probe. Therefore, it seems plausible that the smaller size of the PEAA/DPPC mixed micelles compared to DPPC vesicles results in the observed decrease in the measured polarization.

In the preceding discussion it was assumed that there was no change in the fluorescence lifetime of DPH. Studies on model membranes show that a decrease in the order of the phospholipid bilayer leads to a corresponding decrease in both the average lifetime and polarization of DPH [14, 15]. We recall that the degree of fluorescence depolarization is inversely proportional to the lifetime (see Eq. 1.5), assuming the rotational correlation time does not change. Therefore, the observance of a decrease in both the polarization and lifetime for these systems suggests that for DPH, a reduction in the order of the bilayer results in a larger decrease in the rotational correlation time than in the lifetime. We were unable to make measurements of DPH lifetimes, consequently we do not know how the vesicle-to-mixed micelle transition affects the lifetime of DPH.

2. Use of 3-Palmitoyl-2-(3-(diphenylhexatrienyl)propanoyl)-L- α -phosphatidylcholine (DPHPC).

In the DPH polarization experiment, there is the possibility that the DPH molecule may be partitioning between the DPPC bilayer and the hydrophobic domains of collapsed PEAA in the mixed micellar structure. We can address the question of possible probe partitioning through the use of a phospholipid-bound DPH analogue for the polarization experiment. We incorporated DPHPC into mixtures of PEAA and DPPC (0.25 mg/ml each, DPHPC to DPPC molar ratio of 1:1000) and measured the fluorescence polarization as a function of solution pH as described in Chapter II, Section C. The results of this experiment are shown in Figure 3.50. We find the same pH-dependent behavior for DPHPC as for DPH. As the solution pH is reduced below pH 8 there is an initial increase in polarization. The measured polarization reaches a maximum value at pH 6.9. Below pH 6.9 there is a sharp decline in the polarization curve. We measured a polarization of 0.45 for DPHPC in mixtures of PEAA and DPPC above pH 8.5, which is similar to the value we and others have found for DPHPC in polymer-free suspensions of DPPC vesicles [84, 85]. The polarization values for DPHPC are slightly higher (0.01 units) than those found for DPH at corresponding points on the polarization versus pH curve. Since the DPH moiety is covalently bound to the phospholipid molecule, which reduces its rotational mobility, it is expected that the measured polarization would be higher than that for unbound DPH. In the mixed micellar structure the DPHPC is found in the phospholipid regions. The polarization behavior of the DPHPC is identical to that of DPH, therefore it does not seem likely that the DPH partitions into the hydrophobic domains of PEAA.

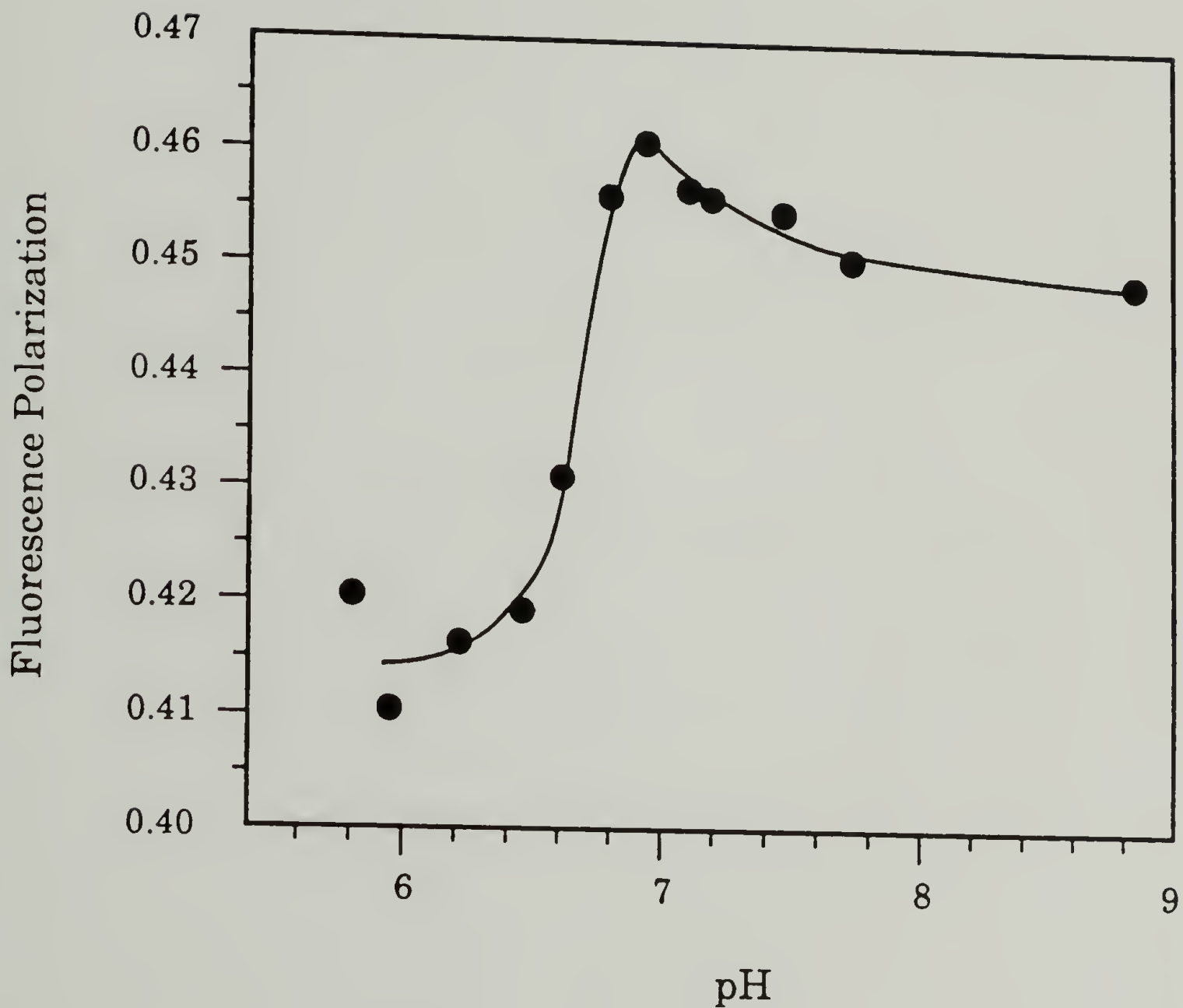


Figure 3.50 Polarization of fluorescence (430 nm) from 3.4×10^{-7} M DPHPC in 0.02 M phosphate-buffered mixtures of PEAA (0.25 mg/ml) and sonicated DPPC vesicles (0.25 mg/ml) as a function of pH. Emission spectra were recorded at 23 °C on deaerated samples using 363 nm excitation. Optical densities were less than 0.10.

3. Use of 3-Palmitoyl-2-(1-pyrenedecanoyl)-L- α -phosphatidylcholine (PyPC).

We noted in Section H that a change in probe lifetime affects the measured polarization, and needs to be considered in the interpretation of measured changes in polarization. We did not have access to instrumentation sensitive enough to measure the fluorescence lifetime of DPH ($\sim 1 \times 10^{-8}$ sec). Pyrene and pyrene-derivatives typically exhibit lifetimes on the order of 10^{-7} seconds. We were able to measure lifetimes of this magnitude with available instrumentation. We employed the use of a pyrene-substituted phospholipid (PyPC) so that we could conveniently measure both the fluorescence polarization and fluorescence lifetime in mixtures of PEAA and DPPC as a function of pH. PyPC was incorporated in mixtures of PEAA and DPPC as described in Chapter II, Section C. The pH-dependent polarization behavior of the bilayer bound pyrene of PyPC in mixtures of PEAA (0.25 mg/ml) and DPPC (0.25 mg/ml, PyPC to DPPC molar ratio of 1:1000) is shown in Figure 3.51. Again we find the same general behavior as found for the other bilayer probes, an initial increase in polarization with reduction in pH which is followed by a sharp decrease. The polarization of PyPC increases from 0.09 in samples above pH 8 to 0.14 at pH 6.9. Below pH 6.9 the polarization decreases, reaching a value of 0.04 at pH 6.2. The polarization of the PyPC in DPPC vesicles is relatively unchanged with variation of the solution pH over the experimental range. The effect of the interaction between PEAA and DPPC on the fluorescence lifetime of PyPC was determined through collaboration with J.S. Tan and P.A. Martic of the Eastman Kodak Research Laboratories and is presented in Figure 3.52. It is found that the lifetime of PyPC increases from 170 nsec in the vesicular structure to 230 nsec in the mixed micellar structure. The

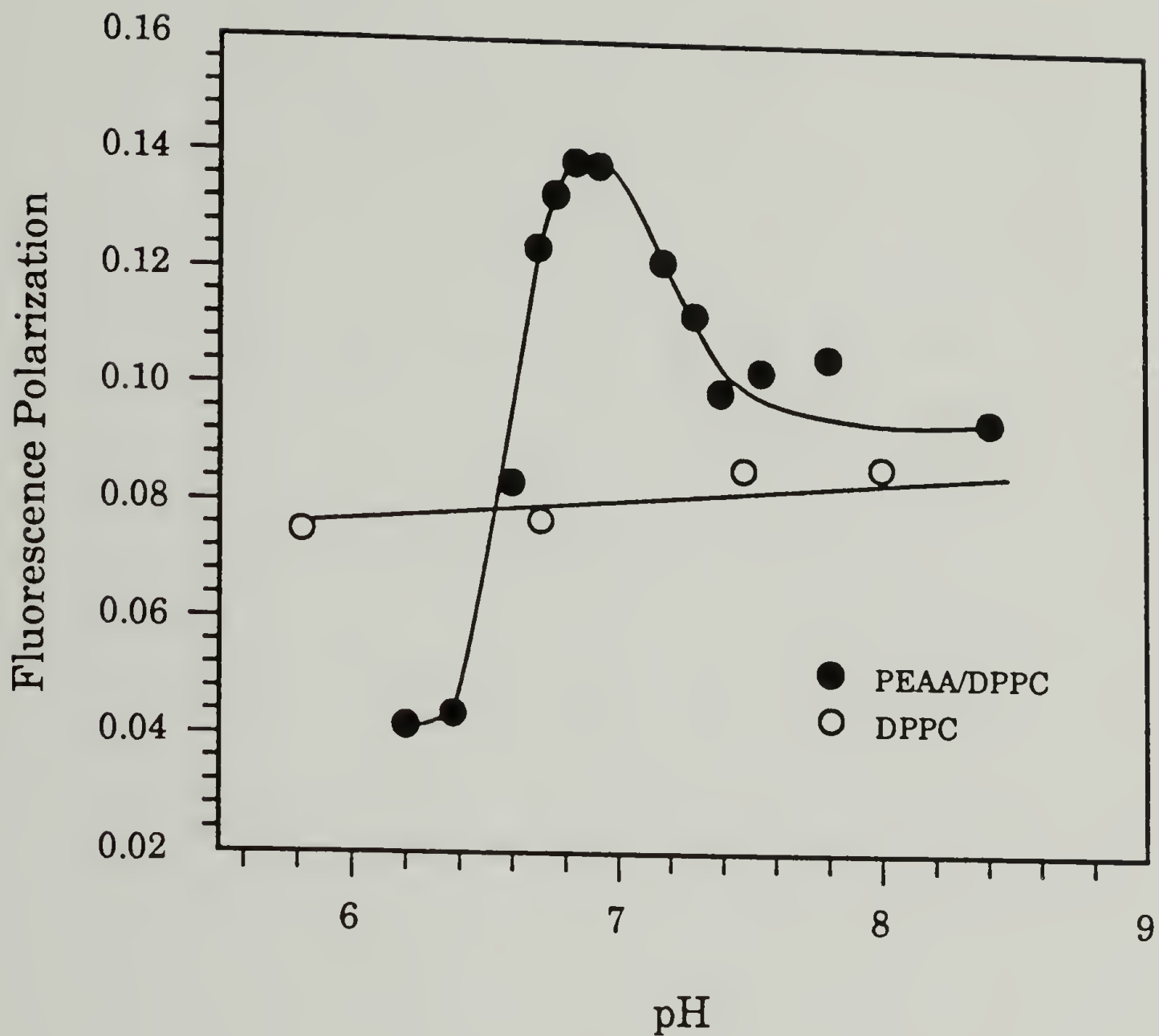


Figure 3.51 Polarization of fluorescence (398 nm) from 3.4×10^{-7} M PyPC in 0.02 M phosphate-buffered suspensions of sonicated DPPC vesicles (0.25 mg/ml) and with mixtures of PEA (0.25 mg/ml) as a function of pH. Emission spectra were recorded at 23 °C on deaerated samples using 347 nm excitation. Optical densities were less than 0.10.

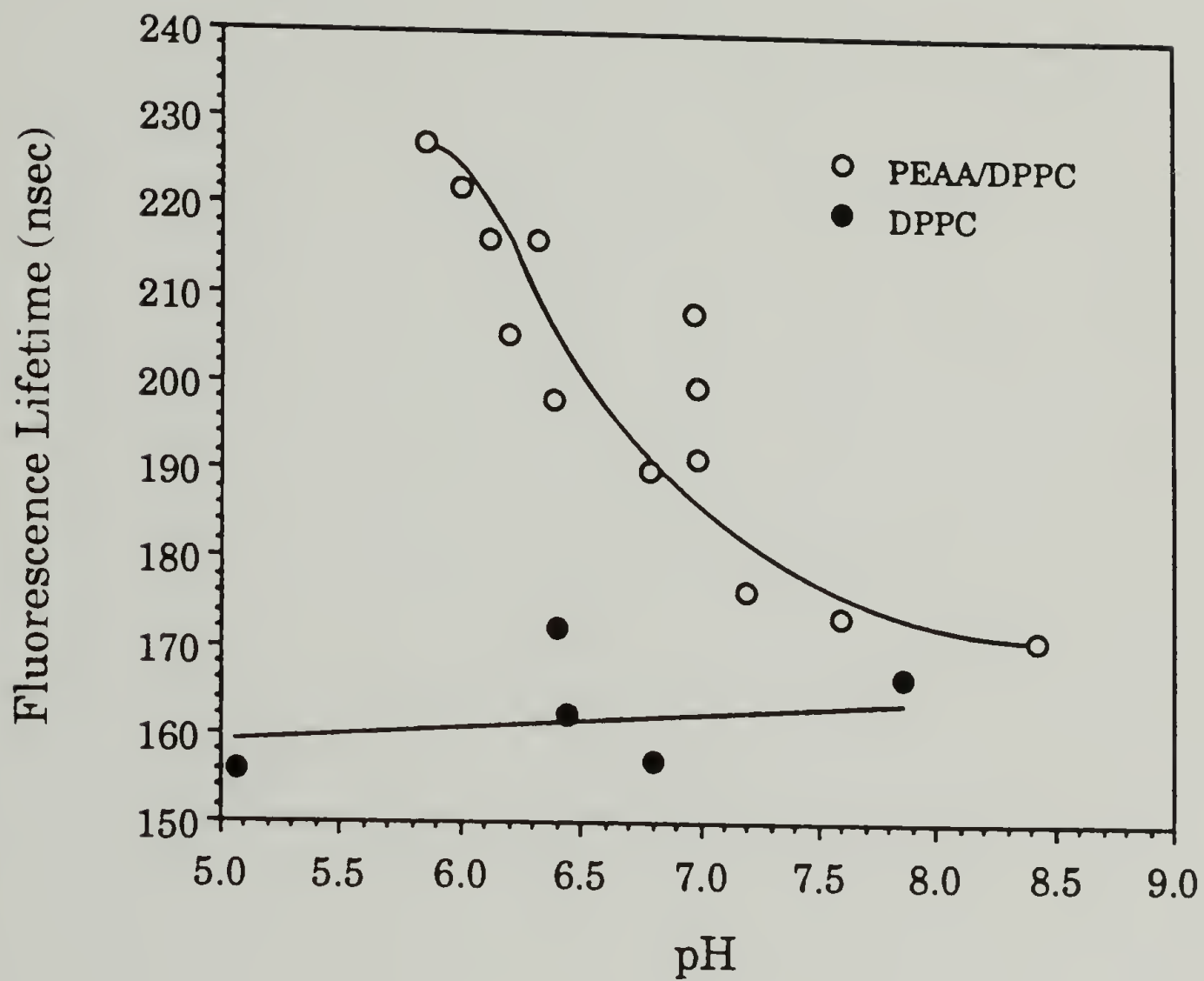


Figure 3.52 Fluorescence lifetime of PyPC in 0.02 M phosphate-buffered suspensions of sonicated DPPC vesicles and with mixtures of PEA as a function of pH. From J.S. Tan and P.A. Martic of the Kodak Research Laboratories.

lifetime of PyPC in DPPC vesicles remains fairly constant at ~165 nsec over the experimental pH range. The change in lifetime of PyPC in PEAA+DPPC mixtures is not continuous with decreasing pH. At the pH where the formation of mixed micelles begins (pH 7), there is a large increase in the PyPC lifetime to 210 nsec, which is immediately followed by a large decrease back to the continuous curve. As noted in Chapter I, Section E, the fluorescence lifetime of a probe molecule is directly influenced by the extent of quenching interactions that deactivate the excited state of the probe. The excited state lifetime decreases as interactions between quenchers and the probe increase. If a change in the environment of the probe results in a change in the relative rates of diffusion of the probe and quencher there will be a change in the excited state lifetime. It has been found for probes in phospholipid bilayers, as the order of the bilayer decreases there is an increase in the diffusion rate of the probe and a corresponding decrease in the fluorescence lifetime [86]. Daems et al. found that as DPPC vesicles went from the ordered gel phase to the disordered fluid phase the lifetime of imbibed pyrene decreased, while the lateral diffusion rate of pyrene increased. They found the lifetime changed from 368 nsec at 25 °C to 333 nsec at 50 °C, while the diffusion coefficient changed from $\sim 1 \times 10^{-8}$ cm²/sec at 25 °C to $\sim 5 \times 10^{-7}$ cm²/sec at 50 °C. Separate studies have shown that as the phospholipid bilayer becomes less ordered there is increased quenching of imbibed pyrene by O₂ [87]. Also, it has been found that O₂ has greater solubility in the fluid phase of phospholipid bilayers than in the gel phase [88]. These experiments show that as the acyl chain packing in the bilayer becomes less ordered there is an increase in probe quenching interactions, which results in a decrease in

fluorescence lifetime. The higher lifetime of PyPC in the PEAA/DPPC mixed micelles compared to that in DPPC vesicles may be interpreted as an increase in the order of the probe bilayer environment in the mixed micellar structure.

In the polarization experiments with DPH and DPHPC the relative changes in the measured polarizations were fairly small. At the maximum in the polarization versus pH plot, we found relative polarization changes of 5% and 2% for DPH and DPHPC, respectively. The sharp decrease at the onset of mixed micelle formation resulted in relative polarization changes of 13% and 11% for DPH and DPHPC, respectively. For the PyPC these two relative changes in polarization were found to be 56% and 71%. The reason for the larger relative change in polarization for the PyPC may be due to its much higher fluorescence lifetime compared to the DPH probes. The DPH probes have lifetimes near 10 nsec, while PyPC has a lifetime near 200 nsec. Larger angular displacements due to rotational diffusion are possible as the excited state lifetime is increased. From Eq. 1.5 we see that if the rotational correlation time is much larger than the lifetime, $\phi \gg \tau$, then $r \approx r_0$. Conversely, if $\tau \gg \phi$, then $r \approx 0$. For DPH in phospholipid bilayers it is found that $r \approx r_0$ ($r = 0.34$, $r_0 = 0.39$), while for PyPC in phospholipid bilayers $r \approx 0$ ($r = 0.05$). If we assume that the rotational correlation times of the probes in each bilayer environment are similar, then a larger change in lifetime for PyPC than for the DPH probes can result in a relatively larger change in polarization.

4. Use of N-(1-pyrenesulfonyl)dipalmitoyl-L- β -phosphatidylethanolamine (Py-DPPE).

The fluorescence polarization experiments discussed so far have involved probes incorporated within the hydrophobic region of the DPPC bilayer. We can obtain additional information about the pH-dependent PEAA-DPPC interaction through the use of a fluorescence polarization probe attached to the headgroup of the phospholipid. In this experiment the probe is at the vesicle surface and should be highly sensitive to polymer adsorption. Py-DPPE is a phospholipid with a pyrene moiety covalently attached to the headgroup, which has been used for investigations on lateral mobility in biological membranes [89, 90]. We present the results of such an experiment using Py-DPPE in the PEAA+DPPC system in Figure 3.53. In mixtures of PEAA and above pH 8 we measure a Py-DPPE polarization of 0.20. As the solution pH is lowered we observe an increase in polarization, which reaches a peak value of 0.29 at pH 7.25. From pH 7.25 to pH 6.55 the polarization decreases from 0.29 to 0.25. Further decrease in solution pH results in an increase in the polarization. At pH 5.9 the measured polarization is 0.34. As in the other polarization experiments, the initial increase in polarization below pH 8 is due to the adsorption of PEAA chains onto the vesicle surface. The midpoint of the polarization decrease occurs at pH 6.9, which is the midpoint of the change in optical density and close to the onset of mixed micelle formation. Despite the change in aggregate size we see an increase in the polarization of Py-DPPE in the mixed micellar structure compared to a vesicular structure, which is contrary to the results from the hydrophobic probes. The interaction of the PEAA with the phospholipid in the mixed micelle

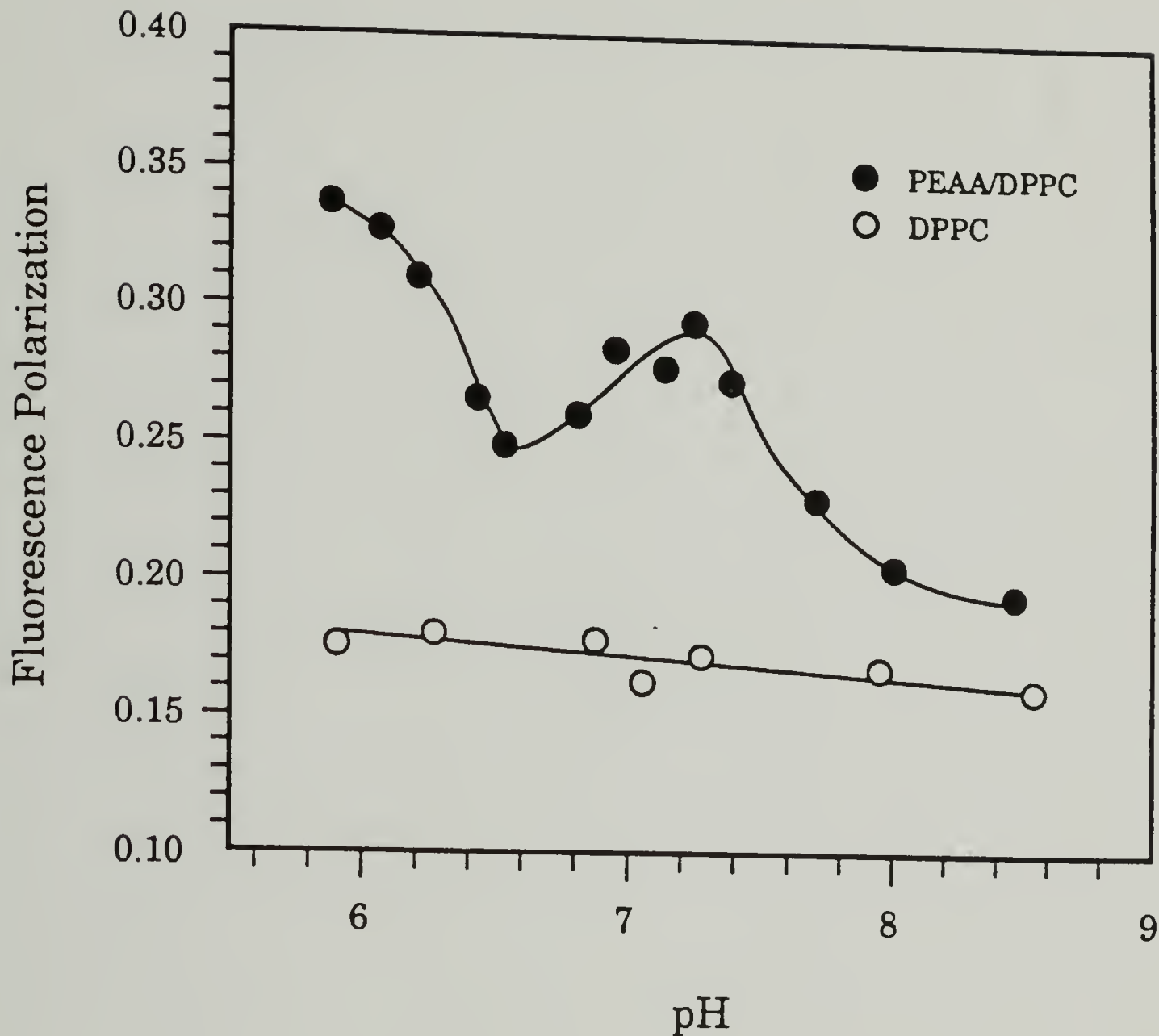


Figure 3.53 Polarization of fluorescence (380 nm) from 4.5×10^{-7} M Py-DPPE in 0.02 M phosphate-buffered suspensions of sonicated DPPC vesicles (0.25 mg/ml) and with mixtures of PEAA (0.25 mg/ml) as a function of pH. Emission spectra were recorded at 23 °C on deaerated samples using 350 nm excitation. Optical densities were less than 0.10.

structure reduces the rotational mobility of the headgroup bound pyrene, and overrides the decrease in polarization due to increased Brownian rotation of the mixed micelle. The control series of Py-DPPE in DPPC vesicles shows little change in polarization with change in solution pH. At high pH the polarizations of the control sample and PEAA+DPPC are not equal (0.17 compared to 0.20), which may be an indication of the high pH interaction we observed in the binding experiments.

I. Monitoring Bilayer Properties with an Intramolecular Excimer Forming Probe: Use of 1,3-bis-(1-pyrene)propane (Py_2C_3).

The change in the polarization of a bilayer bound probe molecule has been associated with a change in the acyl chain order in the bilayer. However, for reasons we have discussed, this relationship is complicated in the PEAA+DPPC system as a consequence of the structural change. Intramolecular excimer forming probes have been used to monitor dynamic properties of biological and model membranes [43-45, 91]. Assuming the rate of excimer complex dissociation is slower than rate of emission, the intensity of excimer fluorescence is determined by the rate of excimer formation. For the intramolecular excimer probes, the rate of excimer formation is dependent on the viscous resistance of the medium. Fluorescence from the monomeric excited state competes with excimer fluorescence, so that the monomer to excimer intensity ratio can be used to monitor changes in the viscous resistance of the probe environment (see Chapter I, Section H). Unlike the depolarization of fluorescence, the formation of intramolecular excimers is not dependent on the rotational

properties of the host structure. We incorporated Py₂C₃ into mixtures of PEAA and DPPC and measured the ratio of monomer to excimer fluorescence intensity for samples as a function of pH as described in Chapter II, Section C. We see in Figure 3.54 that as the pH is lowered the monomer peak (396 nm) grows at the expense of the excimer peak (488 nm). The plot of the ratio of monomer to excimer intensities (I_M/I_E) against pH is shown in Figure 3.55. For mixtures of PEAA and DPPC above pH 8 and for DPPC vesicles the I_M/I_E ratio is found to be ~2. As the pH is lowered below 7.5 in the PEAA+DPPC system, we see an increase in the I_M/I_E ratio to a value of ~4.6 at pH 7.1. The adsorption of the PEAA chain onto the DPPC vesicle surface leads to a decrease in the rate of excimer formation, which may be interpreted as an increase in the viscous resistance of the bilayer environment of Py₂C₃. Between pH 7.1 and pH 6.6 there is a plateau or perhaps a slight decrease in I_M/I_E . This is the pH region where the vesicle-to-mixed micelle structural reorganization begins to take place. There appears to be little change in the probe environment in this transition region. There is a sharp increase in I_M/I_E as the pH is reduced below pH 6.6, with I_M/I_E leveling out below pH 6.4 at a value of ~6.7. In the mixed micellar structure as the PEAA becomes more hydrophobic, there appears to be an increased interaction with the bilayer which results in an additional decrease in the formation of intramolecular excimers by Py₂C₃. Below pH 6.0 a very sharp increase in I_M/I_E is observed. This is the pH range where we observed the formation of large mixed micellar aggregates in the pyrene fluorescence experiments and in the binding studies (see Figures 3.20 and 3.39). It is not clear why the formation of large aggregate structures should reduce excimer fluorescence, unless an increase in the probe "microviscosity" accompanies the aggregate formation. Figure 3.55

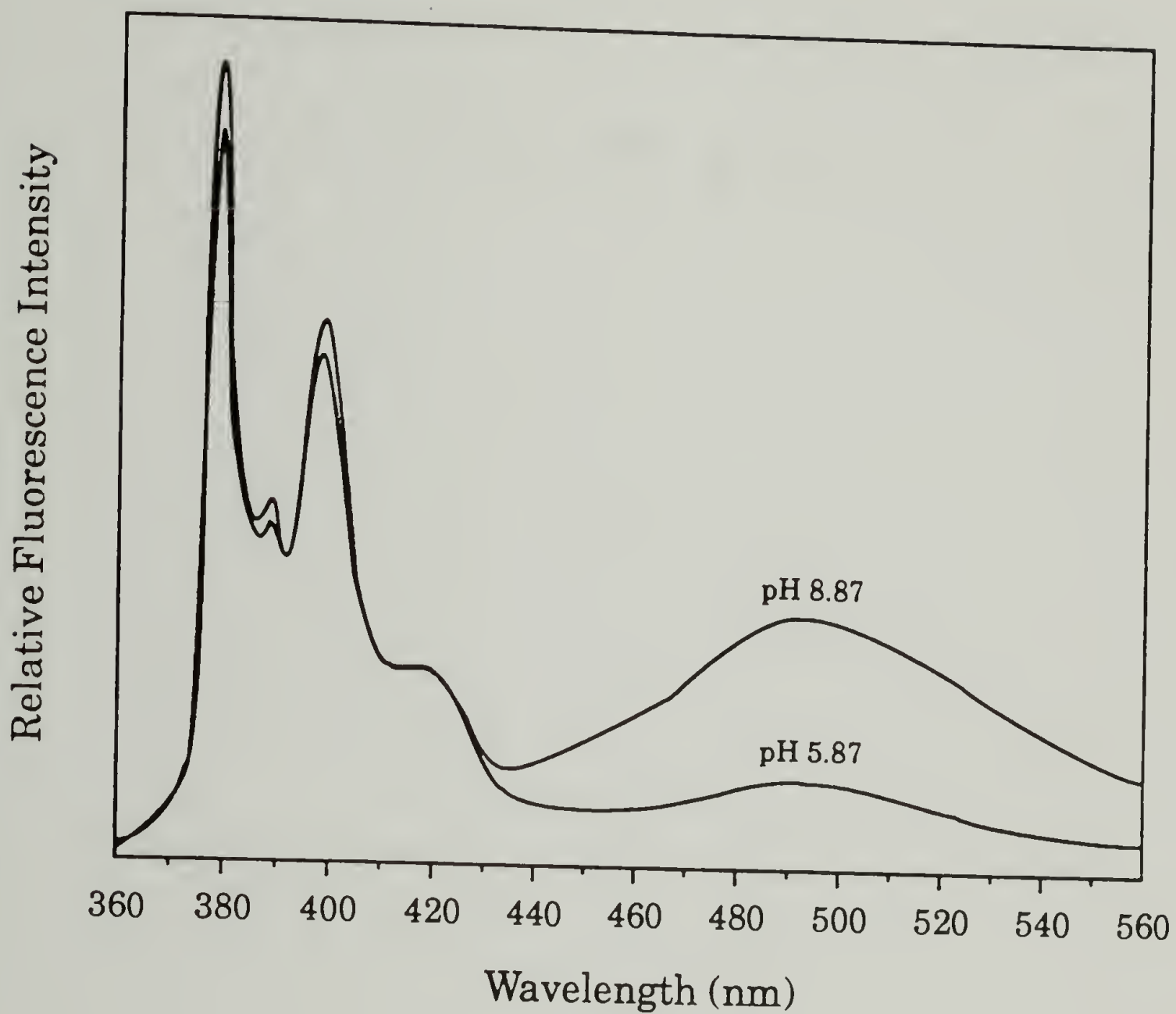


Figure 3.54 Fluorescence emission spectra for 9×10^{-7} M Py_2C_3 in 0.02 M phosphate-buffered mixtures of PEAA (1 mg/ml) and sonicated DPPC vesicles (1 mg/ml). Emission spectra were recorded at 23 °C using 331 nm excitation wavelength.

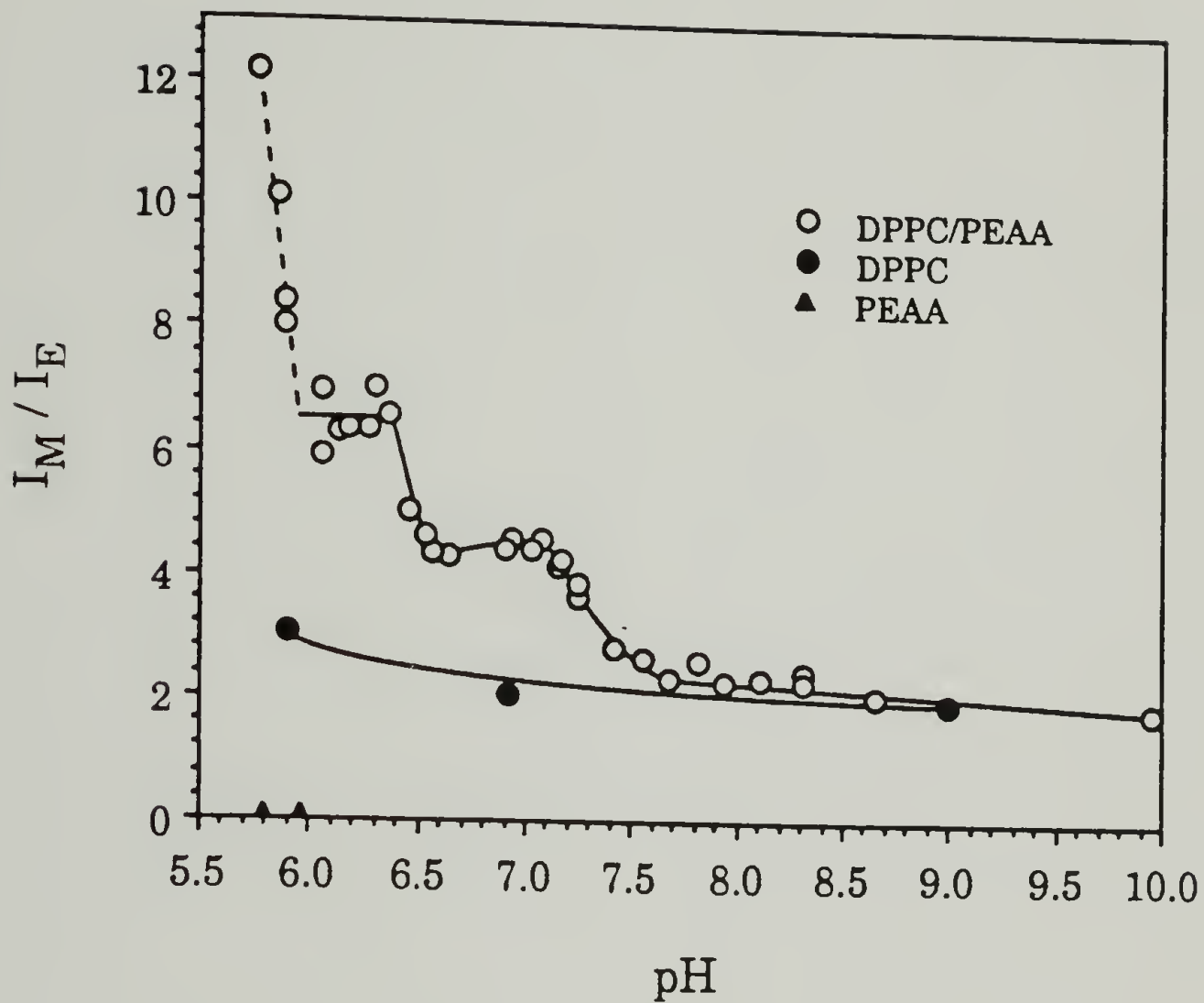


Figure 3.55 Ratio of monomer intensity (396 nm) to excimer intensity (488 nm) (I_M/I_E) for 9×10^{-7} M Py_2C_3 in 0.02 M phosphate-buffered mixtures of PEAA (1 mg/ml) and sonicated DPPC vesicles (1 mg/ml) as a function of pH. Emission spectra were recorded at 23 °C using 331 nm excitation wavelength.

also shows that the I_M/I_E ratio of Py_2C_3 in DPPC vesicles varies little over the experimental pH range ($I_M/I_E \sim 2$, similar to reported value of ~ 1.6 [44]), and that the I_M/I_E ratio of Py_2C_3 in the hydrophobic domains of collapsed PEAA is 0.1. The environment of the hydrophobic domains of PEAA appears to be much more conducive to intramolecular excimer formation than the bilayer environment of the PEAA/DPPC mixed micelles or the DPPC vesicles.

J. Fluorescence Behavior of Pyrene in PEAA/DPPC Mixtures.

It has been shown that the vibrational fine structure of the pyrene emission spectrum is sensitive to solvent polarity (see Chapter I, Section H). We have seen that the peak 1/peak 3 ratio decreases from 1.9 in PEAA solutions at pH 8.5 to 1.35 in PEAA solutions at pH 5.6. The decrease in the peak 1/peak 3 ratio was explained in terms of the formation of collapsed coil PEAA with hydrophobic domains, which could solubilize the hydrophobic pyrene. We used pyrene as a probe of the pH-dependent interaction of PEAA with DPPC vesicles by incorporating the pyrene into DPPC vesicles and measuring the peak 1/peak 3 ratio in the PEAA+DPPC mixtures as described in Chapter II, Section C. The change in the peak 1/peak 3 ratio for 5×10^{-6} M pyrene in phosphate buffered (0.02 M) mixtures of PEAA (1 mg/ml) and DPPC (1 mg/ml) is shown in Figure 3.56 as a plot against solution pH. We see that the peak 1/peak 3 ratio steadily decreases as the solution pH is lowered below pH 8.5. The peak 1/peak 3 ratio is found to be 1.31 at pH 8.5, which is identical to the ratio found in the control sample of DPPC vesicles. The steady decline in the peak 1/peak 3 ratio continues until

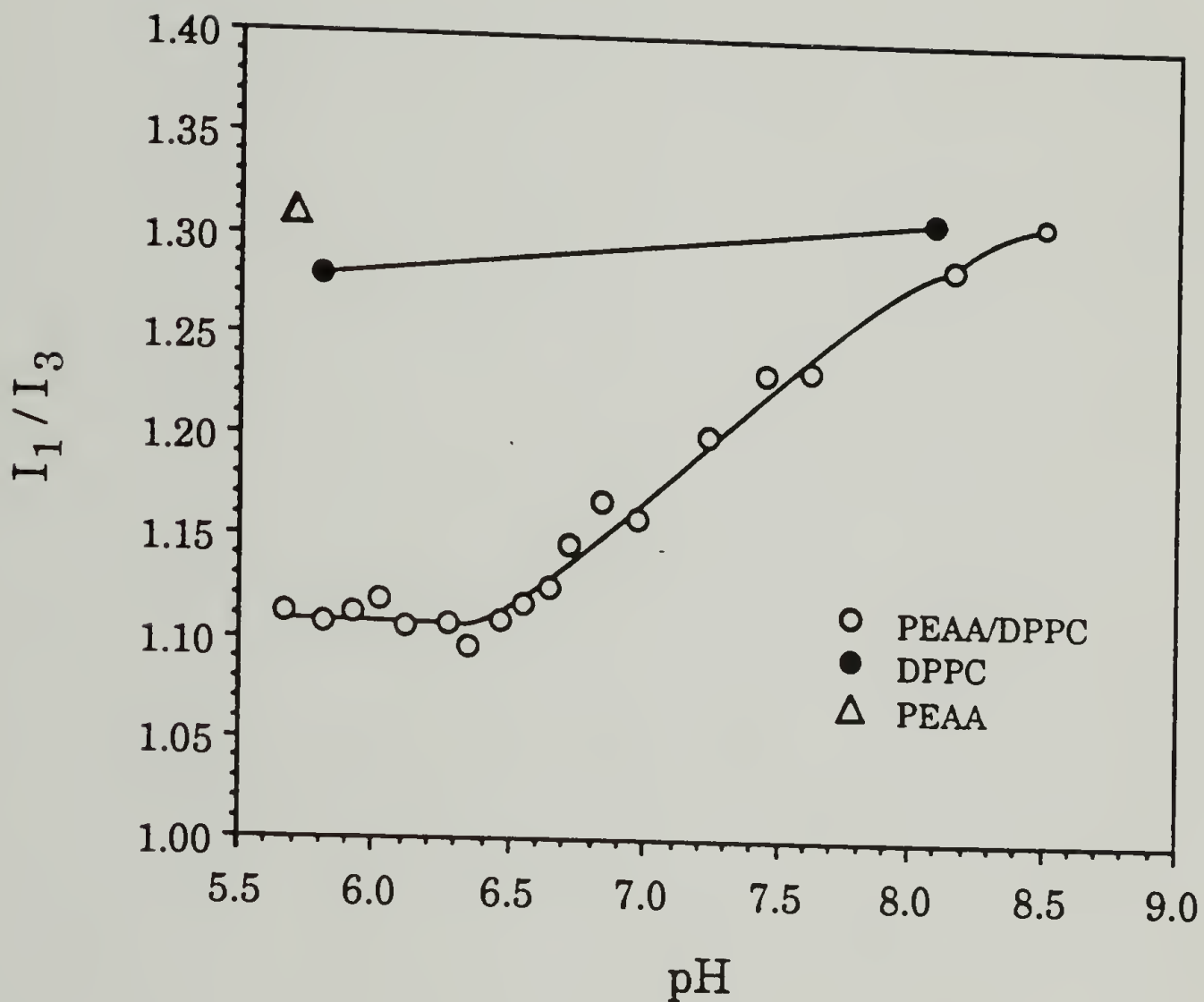


Figure 3.56 Ratio of peak 1 (373 nm) and peak 3 (384 nm) intensities for 5×10^{-6} M pyrene in 0.02 M phosphate-buffered mixtures of PEAA (1 mg/ml) and DPPC (1 mg/ml) as a function of pH. Emission spectra were obtained at 23 °C using 337 nm excitation.

near pH 6.4 to a value of 1.11. Reduction of the solution pH below 6.4 has little effect on the peak 1/peak 3 ratio which remains nearly constant at a value of 1.11 down to pH 5.6. The results of this experiment suggest that the environment of the pyrene in the PEAA/DPPC mixed micelles is less polar than the environment of pyrene in DPPC vesicles or collapsed PEAA.

Through collaboration with J.S. Tan and P.A. Martic of the Kodak Research Laboratories we were able to obtain data on the lifetimes of pyrene in solutions of PEAA, suspensions of DPPC, and mixtures of PEAA+DPPC as a function of pH. This information is shown in Figure 3.57. For the PEAA solutions, we find a sharp change in pyrene lifetime at the conformational transition of PEAA. There is a steady increase in the pyrene lifetime from 160 nsec to 200 nsec as the solution pH is lowered from pH 8.5 to pH 6.3. Below pH 6.3 there is a large increase in lifetime over a narrow pH range. The midpoint of this change is at pH 6.15, which corresponds to the midpoint of the emission intensity change (see Figure 3.9). The pyrene has a lifetime of 380 nsec in the hydrophobic domains of the collapsed PEAA at pH 5.5. For aqueous mixtures of pyrene and PMAA, Thomas and coworkers found that the lifetime of pyrene increased from 140 nsec to 280 nsec as PMAA changed from an expanded coil to a collapsed coil [37]. They also found that the midpoints of the changes in lifetime and emission intensity coincided.

We see that solution pH has little effect on the lifetime of pyrene in DPPC vesicles, since the lifetime is nearly constant at 260 nsec over the entire pH range studied. This value agrees well with the reported lifetime of 280 nsec for pyrene in DPPC vesicles [92]. In the PEAA+DPPC mixtures the pyrene lifetime at pH 8.5 (~250 nsec) is similar to the lifetime found in the control samples of DPPC vesicles (~260 nsec). When the pH is reduced

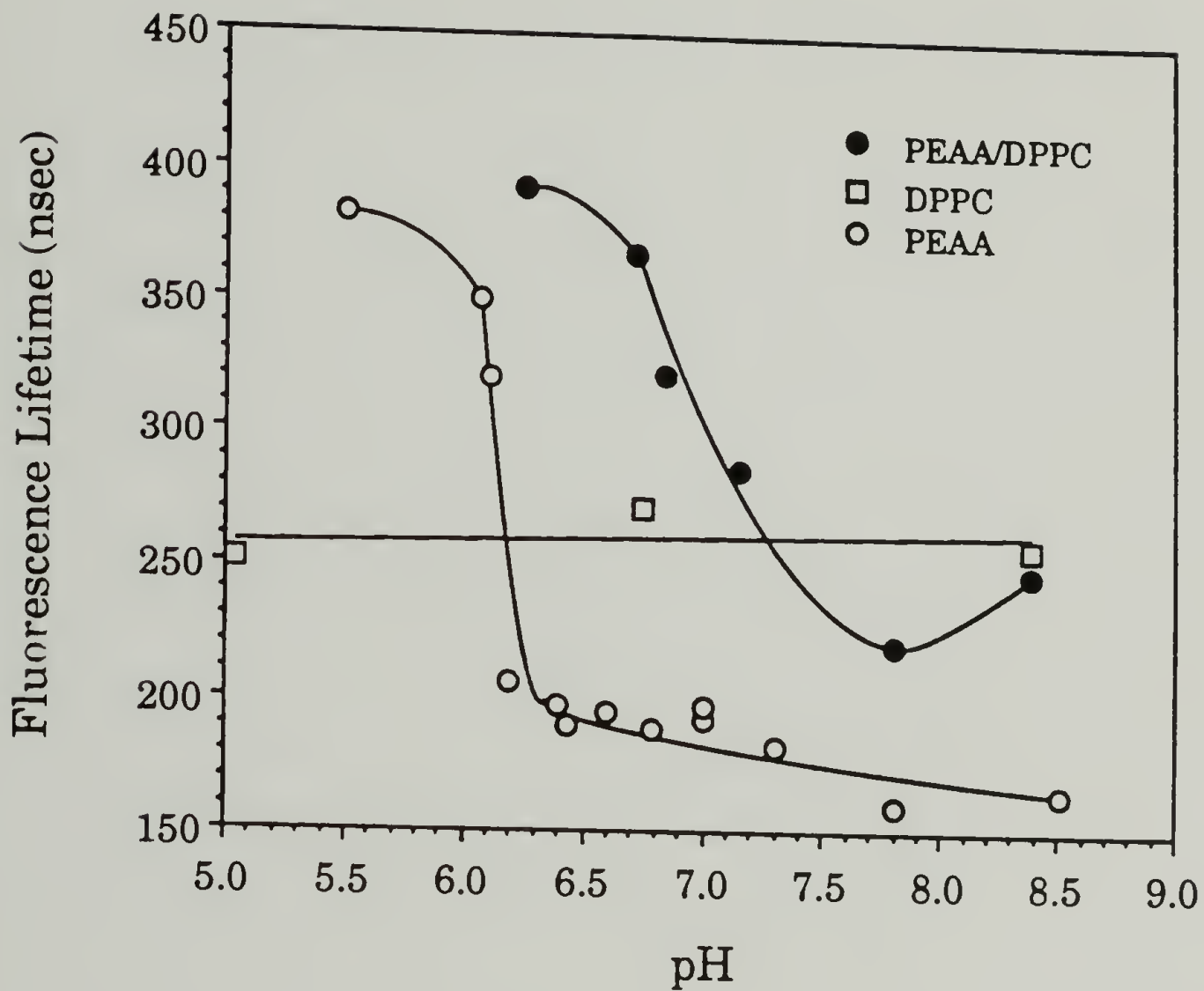


Figure 3.57 Fluorescence lifetime of pyrene in PEAA, DPPC vesicles, and mixtures of PEAA and DPPC as a function of pH. From J.S. Tan and P.A. Martic of the Kodak Research Laboratories.

below 8.5 we observe an initial decrease in lifetime, which is followed by a large increase. A minimum in the lifetime curve is located near pH 7.8 at a lifetime of 220 nsec. Lowering the pH below 7.8 leads to a large increase in pyrene lifetime which levels off below pH 6.5 to a value near 400 nsec. The midpoint of the pH range over which the large change in lifetime occurs is pH 7.05. As discussed in Section H of this Chapter, an increase in lifetime can be associated with a decrease in excited state quenching reactions. The hydrophobic domains of PEAA and PEAA/DPPC mixed micelles seem to provide pyrene molecules with an environment that reduces the extent of quenching reactions experienced in DPPC vesicles or in aqueous solution.

K. Fluorescence Energy Transfer in the PEAA + DPPC System.

Since the extent of energy transfer between a donor molecule and an acceptor molecule exhibits an inverse sixth order relationship, this type of fluorescence experiment provides a highly sensitive means of monitoring the approach of two interacting species. The technique of resonance energy transfer was applied to the PEAA+DPPC system through use of the tryptophan-anthracene donor-acceptor pair. This pair has been successfully used in energy transfer studies of phospholipid-protein interactions in model membranes [93-95]. Tryptophan was covalently attached to the PEAA chain and AMC was incorporated into the DPPC vesicles as described in Chapter II, Section C. The extent of energy transfer from tryptophan to anthracene was measured as the ratio I_F/I_0 as detailed in Figure 3.58 as function of pH for mixtures of PEAA (1 mg/ml) and DPPC (1 mg/ml). The results of this experiment are shown in Figure 3.59 as a

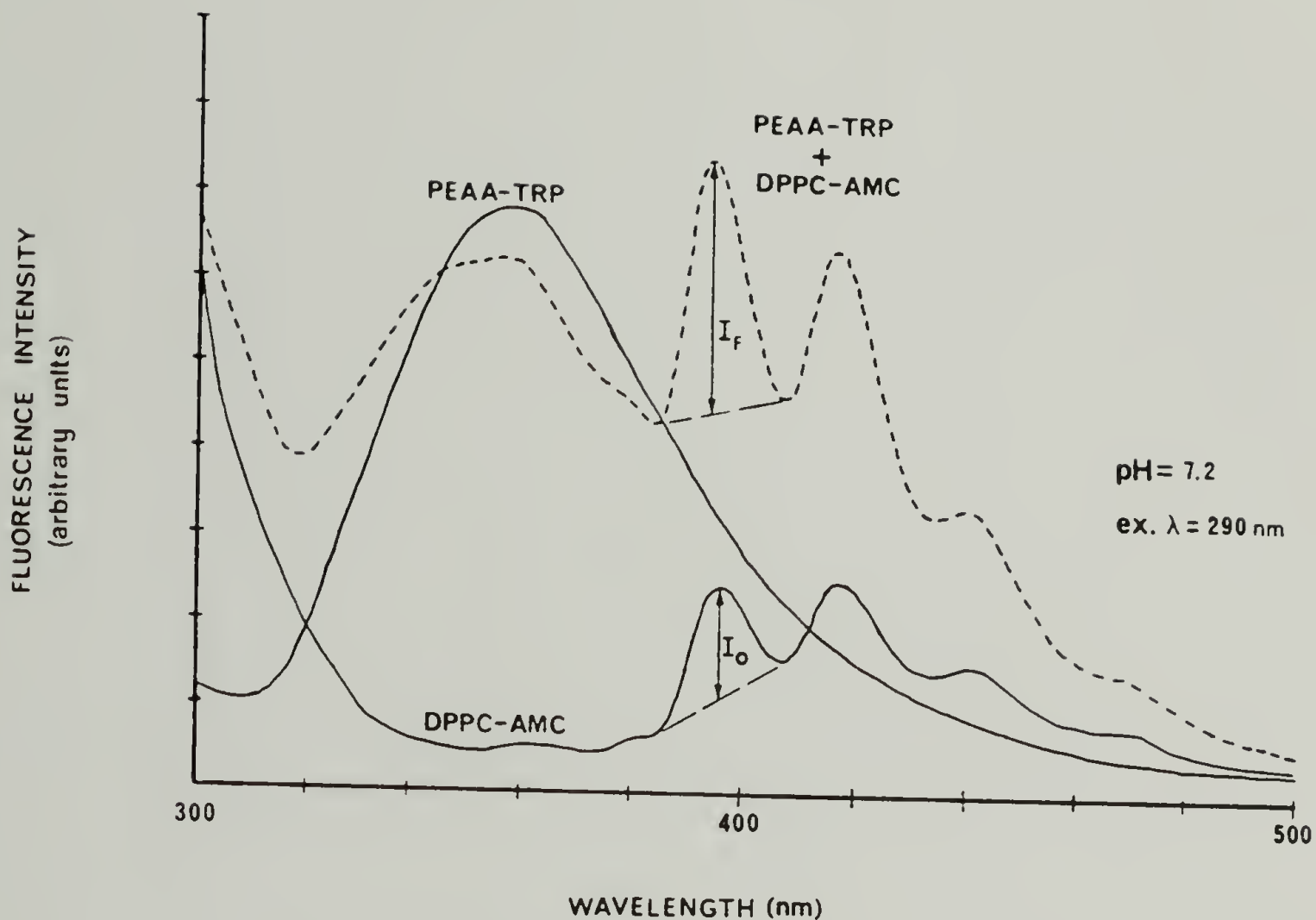


Figure 3.58 Determination of the extent of resonance energy transfer (I_F/I_0) in mixtures of PEAA-trp, DPPC, and AMC. I_F and I_0 were taken as the intensity of AMC fluorescence emission at 395 nm using 290 nm excitation in absence and presence of PEAA-trp, respectively, at 23 °C.

plot of I_F/I_0 versus solution pH. We observe a large increase in the relative extent of energy transfer when the solution pH is lowered below pH 9. The I_F/I_0 ratio reaches a maximum value of 2.5 at pH 7.3, and then decreases with further lowering of the pH below 7.3. The curve has the same general shape as the polarization curves of the bilayer probes.

We do not see a change in the I_F/I_0 ratio until the pH is lowered below pH 9, however we notice that above pH 9 the measured I_F/I_0 ratio is 1.1 and not 1.0 as one would expect if there was no interaction between the donor and acceptor species. This is further evidence of the high pH interaction we observed in the binding experiments (see Sections F and G of this Chapter) and in the fluorescence polarization experiment with the headgroup bound probe, Py-DPPE, (see Section H of this Chapter).

Above pH 9 PEAA is highly ionized, there is little interaction with DPPC vesicles, so we observe little energy transfer between the tryptophan on the polymer and the anthracene embedded in the bilayer. As the pH is lowered, the ionization of PEAA decreases, the chain becomes less hydrated and begins to interact with the surface of DPPC vesicles. In this stage we detect an increase in I_F/I_0 as more PEAA interacts with DPPC. A peak in I_F/I_0 is found at pH 7.3. A peak was also found at this pH in the polarization experiment with the headgroup-bound pyrene probe Py-DPPE (see Figure 3.53). We observe a decrease in I_F/I_0 in the pH range where the vesicle-to-mixed micelle transition has been shown to occur. In this stage PEAA experiences a dramatic decrease in hydration and presumably the hydrophobic domains of the polymer interact with the hydrophobic region of the DPPC bilayer.

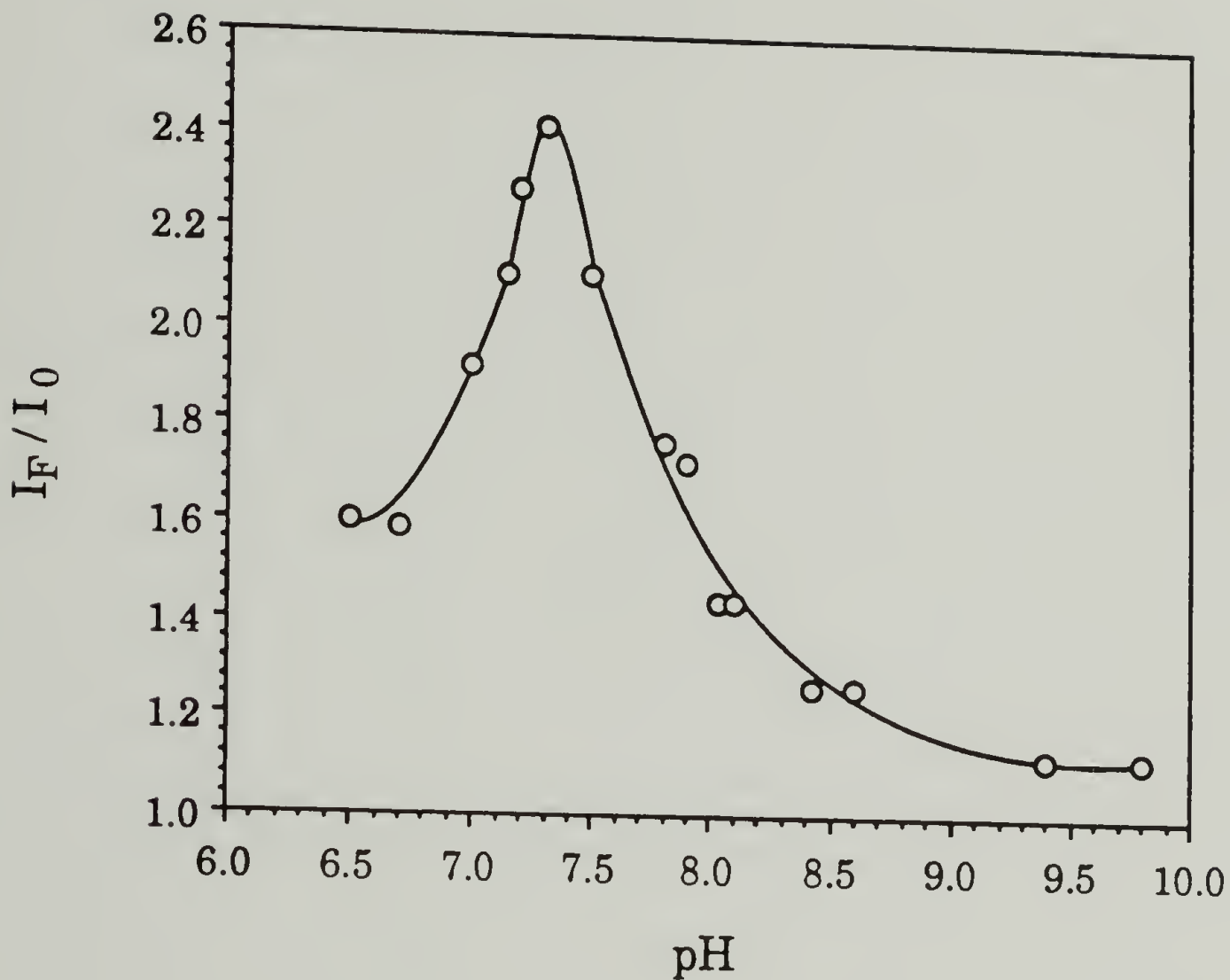


Figure 3.59 Extent of energy transfer (I_F/I_0) as a function of pH in 0.02 M phosphate-buffered mixtures of PEAA-trp (1 mg/ml) and sonicated DPPC vesicles (1 mg/ml) containing AMC (3×10^{-5} M). Emission spectra were recorded at 23 °C using 290 nm excitation. Emission intensity at 395 nm was used for the determination of I_F/I_0 .

As mixed micelles are formed we notice a decrease in I_F/I_0 . The decrease in I_F/I_0 may be indicative of a reorientation of the tryptophan and AMC as mixed micelles are formed. However, the direct correlation between I_F/I_0 and R can be made only if there are no changes in τ_0 and R_0 (see Eq. 1.6). We have seen that the lifetime of pyrene increases dramatically on moving from aqueous solution to the hydrophobic domains of PEAA (see Figure 3.57). Tryptophan may also experience an increase in lifetime as PEAA becomes more hydrophobic. As we see from Eq. 1.6, if R and R_0 remain constant, an increase in τ_0 can lead to a decrease in the extent of energy transfer (I_F/I_0). R_0 depends on the quantum yield of the donor, the spectral overlap of the donor emission and acceptor absorption, and the relative orientation of the transition dipoles of the donor and acceptor [39, 40]. The interaction between PEAA and DPPC to form mixed micelles may influence these factors and thereby alter the observed extent of energy transfer.

L. Differential Scanning Calorimetry of the PEAA + DPPC System.

The various fluorescence experiments have shown that in the sequence of events in the pH-dependent interaction of PEAA with DPPC vesicles there is adsorption of the PEAA chain onto the vesicle surface with initial reduction of solution pH. This is followed by the conformational collapse of the PEAA chain and subsequent structural reorganization of the vesicles to mixed micelles when the pH is reduced further. This sequence of events is also detected through changes in the melting endotherm of the DPPC

molecules. The phase transition behavior of DPPC (1 mg/ml) in phosphate buffered (0.02 M) mixtures of PEAA (1 mg/ml) is presented in Figure 3.60. As the PEAA interacts with the DPPC vesicle surface, we see that the melting endotherm shifts to higher temperature. From pH 7.59 to pH 6.78 the melting temperature is found to be 41 °C, which is identical to the melting temperature of a control sample of DPPC vesicles. However, at pH 6.60 the melting peak has shifted to 42 °C with a small shoulder at 41 °C. This PEAA induced shift in the T_m of DPPC has been previously reported [96]. Adsorption of PEAA onto the vesicle surface may act to dehydrate the phosphate headgroup and increase the melting transition temperature of DPPC. PMAA has been found to cause the same shift in T_m through pH-dependent interaction with DPPC vesicles. Figure 3.61 shows the DSC thermograms for mixtures of PMAA (1 mg/ml) and DPPC (1 mg/ml) in phosphate buffer (0.02 M). The main melting peak shifts from 40.7 °C at pH 7.6 to 42.0 °C at pH 4.3. A small peak at 40.1 °C is also observed at pH 4.3. It should be noted that unlike PEAA, PMAA does not reorganize DPPC vesicles into mixed micelles (samples are not clarified with reduction in pH).

For this series of PEAA and DPPC mixtures, the optical density midpoint occurs at pH 6.5. Beginning with the sample at pH 6.39 in Figure 3.60 we see the effect of mixed micelle formation in the DSC thermogram. As mixed micelles are formed we see the melting peak shift to lower temperatures. In the pH 6.39 sample the melting endotherm consists of overlapping broad peaks at 43 °C and 40.6 °C. Further reduction of the solution pH results in a shift in the melting endotherm to lower temperature. For example, at pH 6.25 the endotherm consists of overlapping broad peaks at 39 °C and 41.3 °C. At pH 6.00 the endotherm has

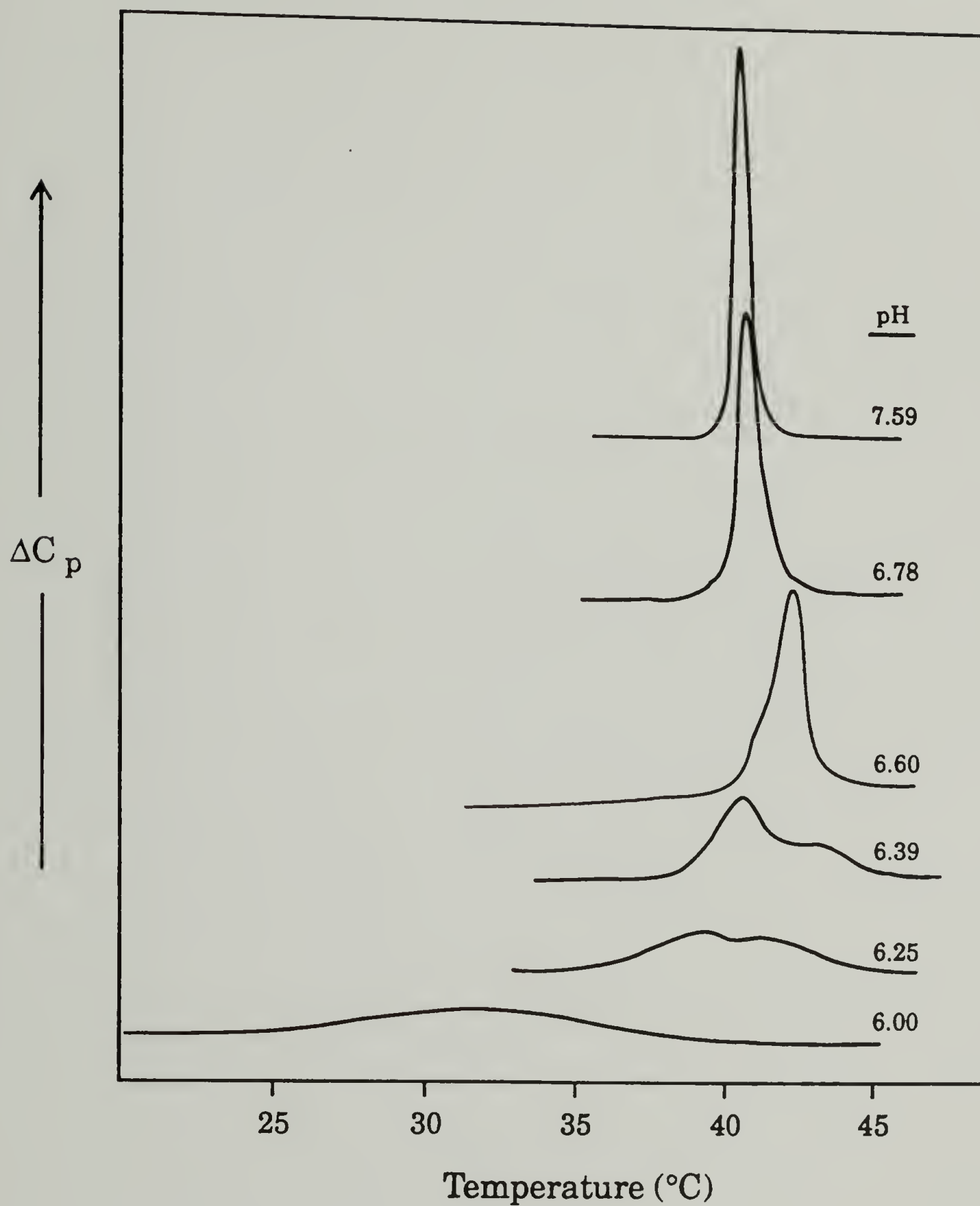


Figure 3.60 DSC thermograms of DPPC (1 mg/ml) in 0.02 M phosphate-buffered solutions of PEAA (1 mg/ml).

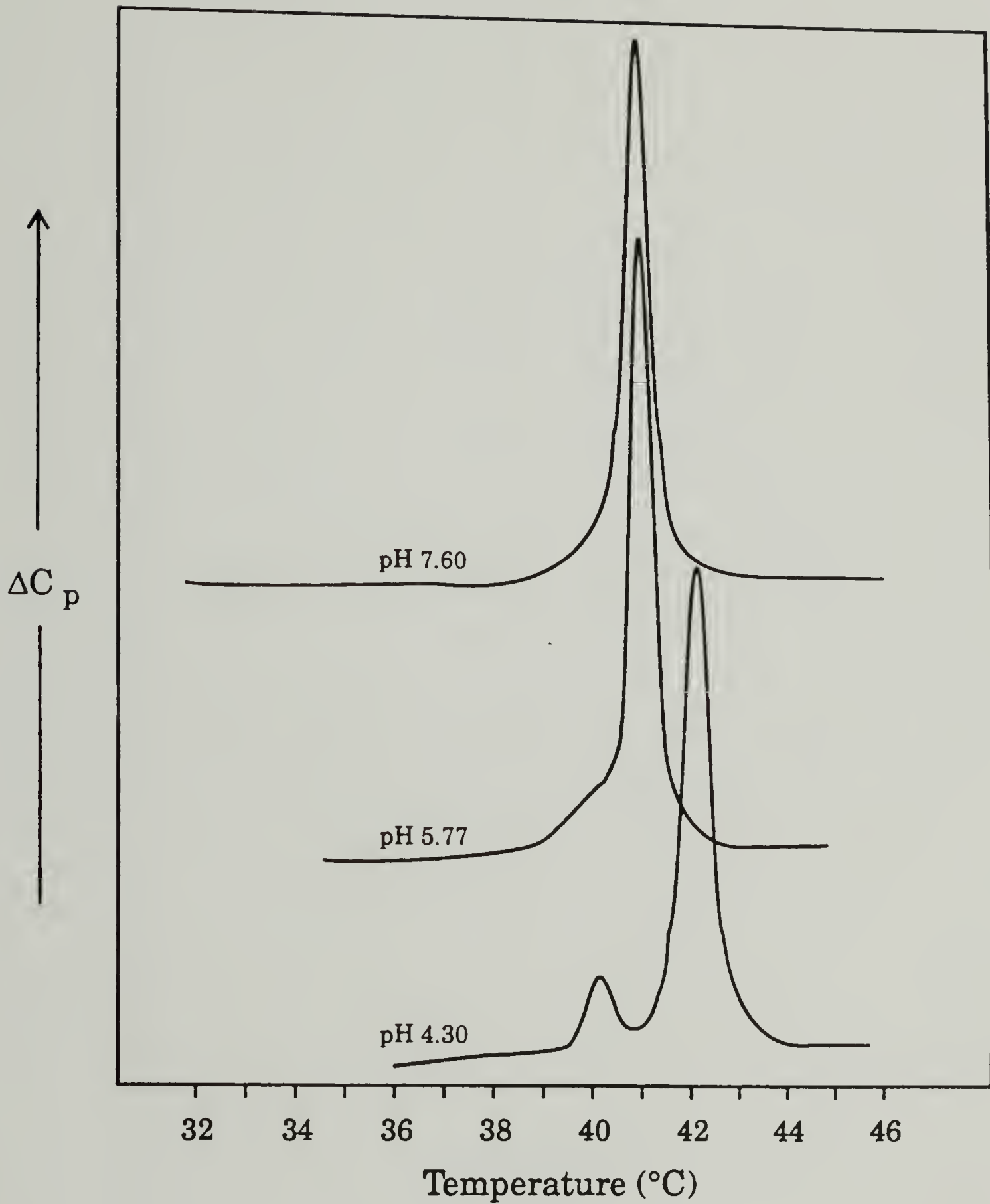


Figure 3.61 DSC thermograms of DPPC (1 mg/ml) in 0.02 M phosphate-buffered solutions of PMAA (1 mg/ml).

one broad peak at 32 °C with $\Delta T_{1/2} \sim 8$ °C. The reorganization to mixed micelles results in a broadening and a shift of the melting endotherm to lower temperature. The change from vesicles to mixed micelles is also accompanied by a decrease in the enthalpy of the melting transition, from 8.7 kcal/mol to 5.0 kcal/mol.

The interaction of apolipoproteins and detergents with phospholipid vesicles has been found to result in similar changes in the phase transition behavior. The interaction of apo A-I with DMPC results in the formation of disk-like mixed micelles which exhibit a broadening of the main melting peak ($\Delta T_{1/2} \sim 8^\circ\text{C}$), a shift in T_m to higher temperature ($\Delta T_m \sim 2^\circ\text{C}$), and a decrease in ΔH_m ($\sim 50\%$ of that found for DMPC vesicles) [93, 97]. The interaction of myelin proteolipid apoprotein with DPPC vesicles lead to an increase in T_m , an increase in $\Delta T_{1/2}$, and a decrease in ΔH_m [98]. Triton X-100 has been shown to interact with DPPC vesicles to form mixed micelles which results in a broadening of the main melting peak ($\Delta T_{1/2} \sim 5^\circ\text{C}$), a shift in the main melting peak to lower temperature ($T_m \approx 35$ °C), and a decrease in melting enthalpy ($\Delta H_m \approx 5$ kcal/mol) [99]. The addition of cholesterol to DPPC vesicles has also been shown to broaden the melting transition peak and reduce the melting enthalpy [100]. It has been suggested that the interaction of these different agents with phospholipid vesicles results in the formation of two domains of phospholipid; a boundary domain comprised of the agent and phospholipid, and a bulk phospholipid domain. The bulk domain exhibits the normal phase transition behavior of the phospholipid, while the boundary phospholipid does not participate in the phase transition. The presence of the boundary domain results in a decrease in the melting enthalpy and a broadening of the transition. This proposed model for the explanation of the observed effects of these agents

has been criticized because it assumes there is ideal mixing between the domains. Morrow et al. [101] have suggested that there is little justification for this assumption, and have proposed a two phase model to account for the observed phase transition of phospholipids in these mixed systems. They proposed a system containing two phases, agent domains (they used an amphiphilic protein), and phospholipid domains. They mention this model is in accordance with ^2H NMR experiments which indicate there is only one domain of phospholipid. The dependence of the transition enthalpy on the agent concentration was shown to account for the observed phase transition behavior.

In the course of the investigation into the thermal behavior of the PEAA/DPPC mixed micelles we observed several interesting features. For most of the studies on the PEAA+DPPC system the typical concentrations used were 1 mg/ml PEAA and 1 mg/ml DPPC. In order to more easily detect the melting transition of the DPPC within the mixed micelles, samples at pH 6 were prepared at concentrations of 5 mg/ml each of DPPC and PEAA. Unlike samples at the typical 1 mg/ml concentration, upon heating up to 50-60 °C the initially highly turbid samples became clear, but soon turned slightly turbid. Within 30 sec after removal from the heating bath the samples became clear again. This temperature dependent change in optical density was repeatedly demonstrated. The samples remained optically clear when left at room temperature for several hours. A sample was injected into the DSC and the thermogram recorded. A very large melting endotherm ($\Delta H \sim 20$ kcal/mol) centered at 39-40 °C with a $\Delta T_{1/2}$ of 3-4 °C was observed. Samples at identical pH with concentrations of 1 mg/ml show broad peaks centered near 32 °C with a $\Delta T_{1/2}$ of ~ 8 °C. When the 5 mg/ml sample was removed from the DSC immediately after the scan

($T = 50\text{ }^{\circ}\text{C}$) it was still optically clear. After sitting at room temperature for 24 hrs the sample became slightly turbid, and after a few days a gel had formed. A sample of PEAA at an identical concentration did not exhibit the temperature-dependent turbidity or the gelation behavior either at similar or lower solution pH values. The turbidity change and gelation appear to be concentration dependent phenomena, since equivalent samples at 1 mg/ml do not behave in a similar manner. These samples remain optically clear at high temperature and at room temperature for weeks.

We did observe curious behavior of the 1 mg/ml mixed micellar samples in the DSC thermogram. We mentioned that samples at pH 6 exhibited a broad melting endotherm centered near $32\text{ }^{\circ}\text{C}$. However, repetitive scans of these samples over the course of several days, shows the growth of a second peak near $36\text{ }^{\circ}\text{C}$. This second peak could be enhanced through the introduction of additional DPPC to the sample, and is somewhat reminiscent of the melting endotherm of small unilamellar DPPC vesicles ($T_m = 37\text{ }^{\circ}\text{C}$, $\Delta T_{1/2} \sim 3\text{-}4\text{ }^{\circ}\text{C}$, $\Delta H \sim 4\text{ kcal/mol}$) [71].

M. Characterization of PEAA/DPPC Mixed Micelles.

1. Comparison to Other DPPC Mixed Micelles.

In Section B of this Chapter we mentioned that disk-like mixed micelles similar to those found on this work have been observed as the recombinant products of phospholipid vesicles and various agents, such as apolipoproteins, bile salts, and synthetic detergents. In an attempt to characterize the physical structure of the PEAA/DPPC mixed micelles we

have compared these to other DPPC mixed micellar structures through the use of fluorescent probes. We compared the PEAA/DPPC mixed micelles to mixed micelles composed of DPPC and the following agents: sodium dodecyl sulfate (SDS), Triton X-100, sodium deoxycholate, sodium cholate, and 3-palmitoyl-lysophosphatidylcholine (lysoPC). Comparison of the different mixed micelles was carried out with the use of fluorescence polarization probes (DPH, DPHPC, and Py-DPPE), an intramolecular excimer forming probe (Py₂C₃), and transmission electron microscopy.

All of the compounds which form mixed micelles with DPPC, also form micellar structures without DPPC. A comparison of the various micellar structures is presented in Table 3.1. The Py₂C₃ probe finds that the micelle structures rank as SDS \geq PEAA > lysoPC > sodium cholate > sodium deoxycholate > Triton X-100 in terms of the degree of excimer formation. The SDS appear to form the most fluid micelles, while Triton X-100 forms the least fluid micelles of the compounds studied. The polarization of DPH, which is sensitive to several factors as discussed in Section H of this Chapter, in the various micelle structures does not follow the same trend as found with Py₂C₃. The order of increasing DPH polarization was found to be PEAA > Triton X-100 > sodium deoxycholate \geq lysoPC > SDS. An unambiguous interpretation of the DPH polarizations is not possible, since we do not know how the lifetimes and rotational correlation times vary in the different micelle structures.

A comparison of the fluorescence properties of the various probes incorporated into the different DPPC mixed micellar structures is presented in Table 3.2. The polarization of the bilayer bound probes, DPH and DPHPC, in the different mixed micellar structures indicates that the

Table 3.1 Polarization of DPH fluorescence and the ratio of monomer to excimer fluorescence of Py₂C₃ in aqueous solutions of various micelle forming molecules.

| <u>Agent (concentration)</u> | <u>I_M/I_E Py₂C₃</u> | <u>DPH Polarization</u> | <u>Micelle MW^a</u> |
|--------------------------------|--------------------------------------------------------------------|-----------------------------|-------------------------------|
| sodium dodecyl sulfate (69 mM) | 0.1 | 0.07 | 18,000 |
| Triton X-100 (23 mM) | 3.3 | 0.20 | 90,000 |
| sodium deoxycholate (46 mM) | 1.6 | 0.18 | 3,000 |
| sodium cholate (93 mM) | 0.6 | 0.12 | 1,400 |
| lysophosphatidylcholine (1 mM) | 0.2 | 0.18 | 92,000 |
| PEAA (0.05 mM) | 0.1 | 0.35 | 20,000 |

a) From D. Lichtenberg, R.J. Robson, and E.A. Dennis, *Biochim. Biophys. Acta*, 1983, 737, 285.

Table 3.2 Polarization of fluorescence from DPH, DPHPC and Py-DPPE, and the ratio of monomer to excimer fluorescence of Py₂C₃ in aqueous solutions of various DPPC mixed micellar structures.

| <u>Agent (molar ratio)</u> | <u>$\frac{I_M}{I_E}$</u> <u>Py₂C₃</u> | <u>Fluorescence Polarization</u> | | |
|-------------------------------|---------------------------------------------------------------------------|----------------------------------|--------------|----------------|
| | | <u>DPH</u> | <u>DPHPC</u> | <u>Py-DPPE</u> |
| sodium dodecyl sulfate (2:1) | 1.2 | 0.39 | 0.39 | 0.14 |
| Triton X-100 (2:1) | 2.8 | 0.39 | 0.39 | 0.22 |
| sodium deoxycholate (2:1) | 4.1 | 0.44 | 0.45 | 0.21 |
| sodium cholate (2:1) | 6.4 | 0.44 | 0.42 | 0.20 |
| lysophosphatidylcholine (3:2) | 1.6 | 0.32 | 0.37 | 0.08 |
| PEAA (0.04:1) | 6.8 | 0.39 | 0.41 | 0.34 |
| DPPC | 2.1 | 0.43 | 0.43 | 0.18 |

extent of depolarization is greatest in the lysoPC/DPPC mixed micelles. However, all of the mixed micellar structures yield polarization values that are fairly close to one another and the values found in DPPC vesicles, especially with DPHPC. The results of the Py₂C₃ study indicate that DPPC mixed micelles formed with PEAA and sodium cholate have the most restrictive bilayer environments, while the DPPC mixed micelles from SDS and lysoPC have the most fluid bilayer regions. The Triton X-100, sodium cholate, sodium deoxycholate, and PEAA all form mixed micelles with DPPC that demonstrate an increase in the viscosity of the probe environment compared to that for the probe in DPPC vesicles. The lysoPC and SDS mixed micelles show a decrease in probe environment viscosity compared to a DPPC bilayer. The fluorescence polarization of Py-DPPE in these mixed micellar structures provides information on the extent of the agent-headgroup interactions. The SDS and lysoPC mixed micelles show a decrease in headgroup polarization compared to DPPC vesicles. We find the DPPC mixed micelles formed with Triton X-100, sodium cholate, sodium deoxycholate, and PEAA demonstrate an increase in the Py-DPPE polarization compared to DPPC vesicles. These are the same four mixed micelle forming agents that caused an increase in the Py₂C₃ I_M/I_E ratio. Of these four, PEAA shows the highest polarization of Py-DPPE, indicating the PEAA has the greatest interaction with the phospholipid headgroups in the mixed micellar structure.

Transmission electron microscopy reveals that all of the agents studied form disk-like mixed micelles with DPPC.

We have noted that the PEAA-DPPC disk-like mixed micelles found in this work are similar to the disk-like mixed micellar structures formed by various agents and phospholipids. The structure of these mixed micelles

has been proposed to be that of a core of phospholipid bilayer with an annulus of the agent [60, 93]. In this structure the agent hydrophobically interacts with the acyl chains of the phospholipid to screen unfavorable interactions with water. The agent may also form domains within the phospholipid core. It is uncertain whether the PEAA-DPPC mixed micelles have such a structure. However, recent theories on membrane formation suggest that a planar bilayer is the preferred state for phosphatidylcholines, and that interaction of these agents allows the formation of a planar structure [102, 103]. It is proposed that as these compounds interact with the phospholipid vesicle they reduce the edge tension of the structure. A sufficient concentration of the edge-active agent leads to a change from the curved bilayer structure of the vesicle to a planar bilayer structure. The edge-active agents are amphiphilic molecules. At low degrees of ionization PEAA has an amphiphilic structure and may behave as an edge-active agent in suspensions of DPPC. However, we do not have experimental data which reveals the structural arrangement of the PEAA-DPPC mixed micelles.

2. Phase Transition Behavior.

In addition to the previously discussed DSC study, we can characterize the phase transition behavior of the DPPC bilayer region of the mixed micelles by measuring the polarization of added DPH as a function of temperature. The polarization behavior of DPH has been frequently used as a probe for the phase transition in phospholipid bilayers. As the hydrocarbon chains of the phospholipid undergo the order-to-disorder transition there is a corresponding decrease in the measured polarization

of DPH. The result of this experiment for DPPC vesicles and PEAA/DPPC mixed micelles is shown in Figure 3.62. DPH detects a sharp phase transition at 38.5 °C for sonicated DPPC vesicles, while the PEAA/DPPC mixed micelles show a broad transition centered near 34 °C. DSC of sonicated DPPC vesicles reveals a phase transition near 37 °C [71], while DSC of the PEAA/DPPC mixed micelles finds a broad transition centered near 32 °C (see Figure 3.62). Each technique shows that the phase transition in the mixed micellar structure occurs over a wider temperature range than the vesicular phase transition and is shifted to a lower temperature.

DPH has also been used to characterize the phase transition behavior of apolipoprotein A-I/DPPC mixed micelles [80, 81]. It was found that the change from vesicles to mixed micelles resulted in a small decrease in DPH polarization (from 0.44 to 0.42 [81], and 0.42 to 0.40 [80]) and an increase in the melting transition temperature (from 41 °C to 44 °C [81], and 40 °C to 42 °C [80]). The DPH detected increase in T_m was in accordance with calorimetric experiments.

3. Composition of the PEAA/DPPC Mixed Micelles.

The composition of the PEAA/DPPC mixed micelles was determined following the method of Paternostre, Roux and Rigaud [104]. The experimental procedure involves the measurement of sample optical density as a function of added PEAA. We have shown that the addition of PEAA to DPPC vesicles results in the formation of mixed micelles and a decrease in optical density (see Sections B and D of this Chapter). In the experiment, it is assumed that there will be an equilibrium distribution of

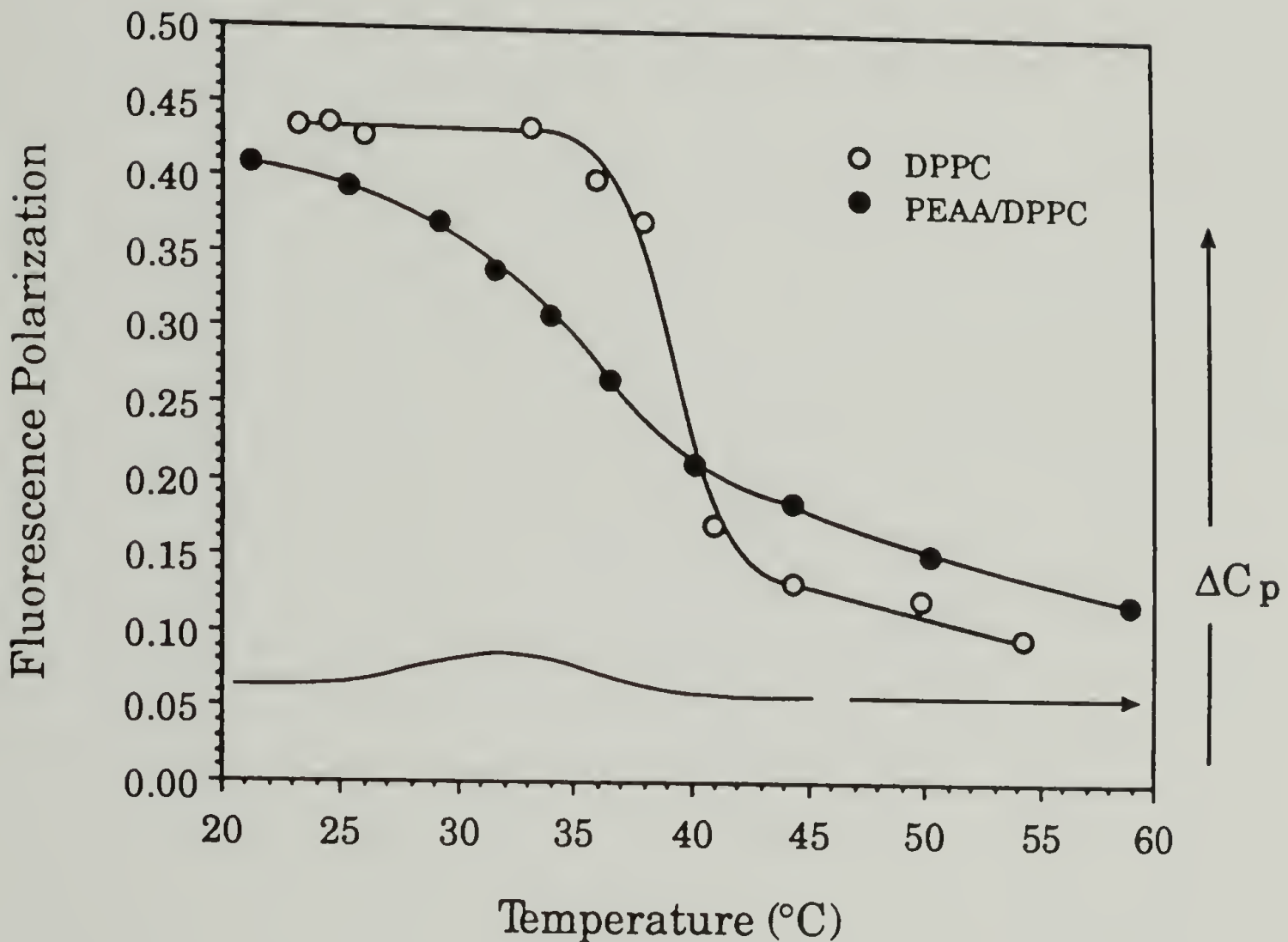


Figure 3.62 Polarization of DPH fluorescence (430 nm) in 0.02 M phosphate-buffered (pH 6) suspensions of sonicated DPPC vesicles and PEAA/DPPC mixed micelles as a function of temperature. The DSC thermogram of the PEAA/DPPC mixed micelles is also presented. Emission spectra were obtained using 360 nm excitation.

the PEAA between the solution and the mixed micelles. One can write the following equation for the concentration of PEAA in the system:

$$[\text{PEAA}]_t = [\text{PEAA}]_w + \left(\frac{[\text{PEAA}]_{\text{mm}}}{[\text{DPPC}]} \right) [\text{DPPC}] \quad (\text{Eq. 3.5})$$

where $[\text{PEAA}]_t$ is the total PEAA concentration needed to form mixed micelles, $[\text{PEAA}]_w$ is the concentration of PEAA in solution, $[\text{PEAA}]_{\text{mm}}$ is the concentration of PEAA in the mixed micelles, and $[\text{DPPC}]$ is the total DPPC concentration. A plot of $[\text{PEAA}]_t$ versus $[\text{DPPC}]$ yields the mixed micelle composition, $[\text{PEAA}]_{\text{mm}} / [\text{DPPC}]$, as the slope. The value of $[\text{PEAA}]_t$ may be determined from the plot of optical density versus added PEAA as shown in Figure 3.63 for a sample at pH 6 with an initial DPPC concentration of 10 mg/ml. This type of optical density versus added PEAA plot was generated for a range of initial DPPC concentrations (2, 5, 10, 15, and 20 mg/ml) in order to determine the mixed micelle composition. The plot of the derived $[\text{PEAA}]_t$ values versus $[\text{DPPC}]$ is shown in Figure 3.64 from which we find the slope of the fitted line to be 0.012. Only the three lower data points were used to fit the line, because the derived values of $[\text{PEAA}]_t$ were suspect for the samples at the high DPPC concentrations due to irregularities in the optical density versus added PEAA curve. For the system initially containing PEAA and sonicated DPPC vesicles, we find an equilibrium mixed micelle composition of 0.012 moles PEAA/mole DPPC or 80 moles DPPC/mole PEAA. This same set of experiments was also carried out for multilamellar DPPC vesicles, from which we determined a composition of 0.025 moles PEAA/mole DPPC or 40 moles DPPC/mole PEAA. The composition of the PEAA/DPPC mixed micelles may be given as 40-80 moles of DPPC per mole of PEAA.

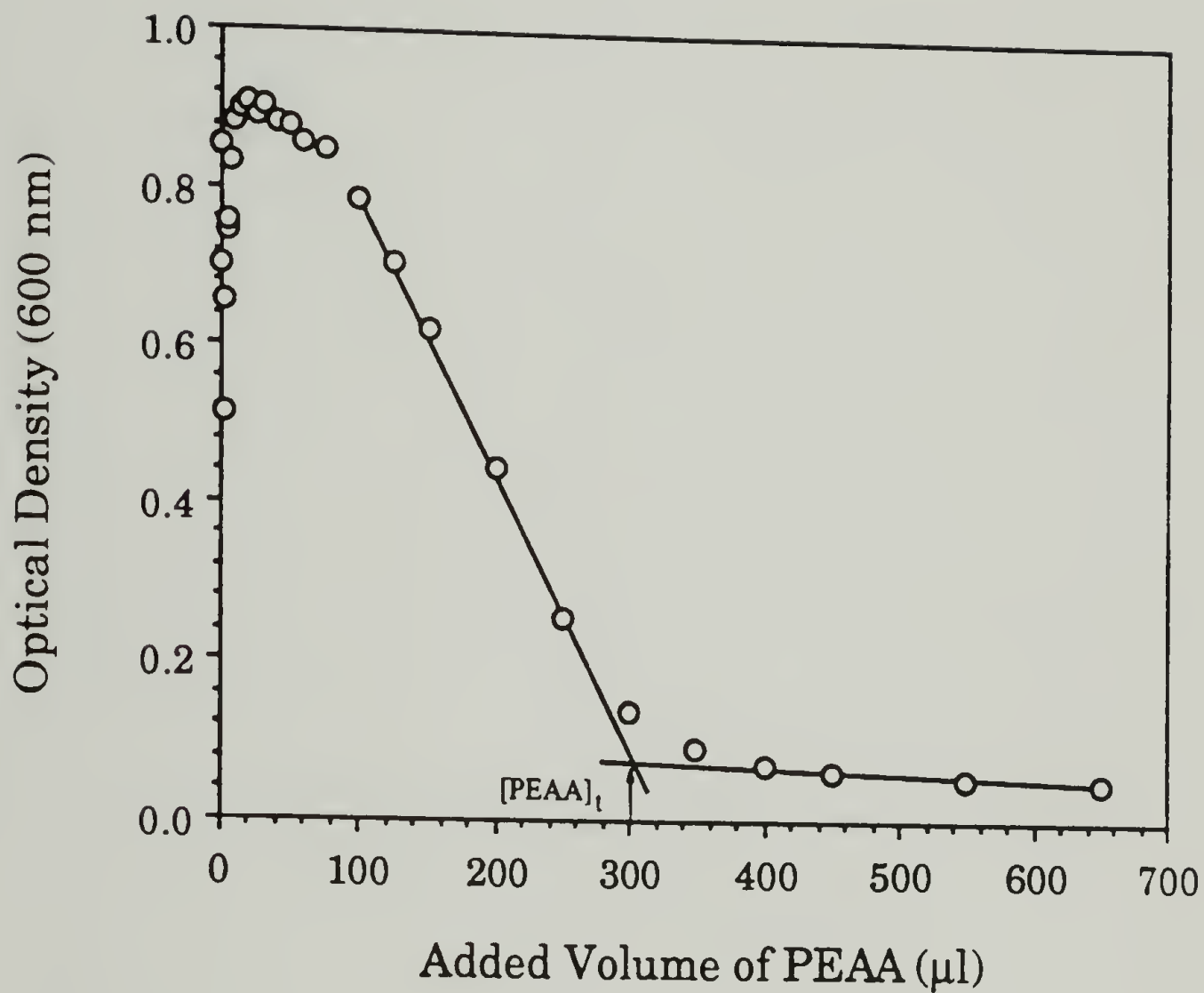


Figure 3.63 Optical density (600 nm) of a 0.02 M phosphate-buffered (pH 6) suspension of DPPC vesicles as a function of the volume of added PEAA and the determination of the concentration of PEAA required to solubilize the DPPC vesicles. The DPPC concentration was 10 mg/ml and the concentration of the PEAA stock solution was 20 mg/ml (0.02 M phosphate buffer, pH 6).

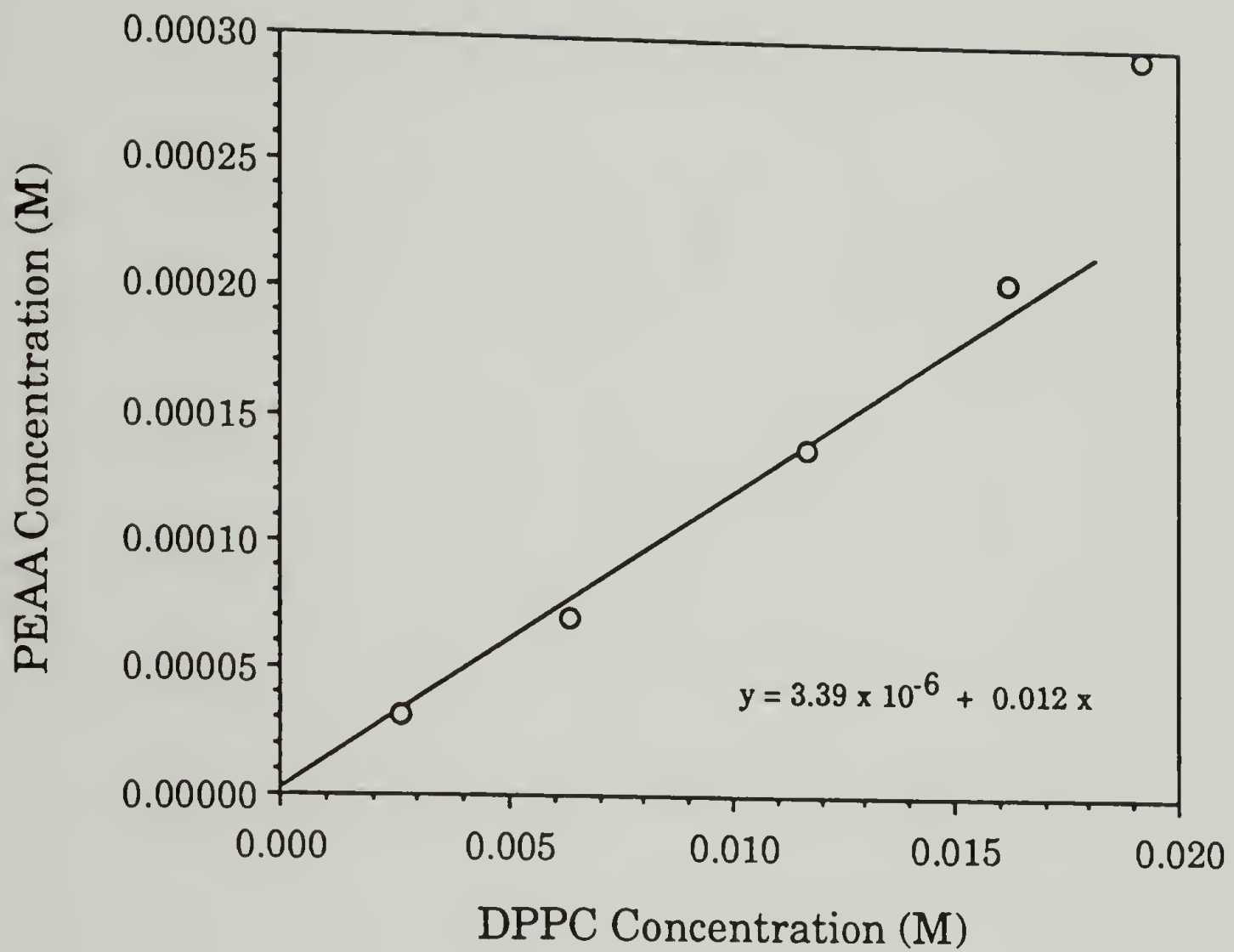


Figure 3.64 Concentration of PEAA required for solubilization of DPPC vesicles as a function of DPPC concentration. The composition of the PEAA/DPPC mixed micelles was determined from the slope of this plot.

From the plot of optical density versus added PEAA for samples at pH 6 (Figure 3.63), we see that the optical density reaches a peak maximum before decreasing with the addition of PEAA. We prepared samples with PEAA and DPPC concentrations corresponding to the peak region of the optical density plot and measured the optical density of these samples as a function of pH. The results of this experiment are shown in Figure 3.65. The optical density decreases from pH 8 to pH 7, and then increases from pH 6.7 to pH 5.8. Above pH 7, the PEAA interacts with the DPPC vesicles in an expanded conformation, as we have determined from the fluorescence experiments. The interaction of PEAA with the surface of the DPPC vesicles seems to affect the integrity of these sonicated vesicles. We noticed this same effect for samples containing PEAA and sonicated DPPC vesicles in Figure 3.29, where we see a initial large decrease in optical density with a midpoint at pH 7.7, followed by a smaller decrease with a midpoint at pH 6.85. However, in the present experiment, the concentration of PEAA is not sufficient to cause structural reorganization of the vesicles to mixed micelles. Under these conditions, in the collapsed coil state the PEAA should simply embed into the vesicle. It appears that PEAA in the expanded state interacts with surface of sonicated DPPC vesicles and causes a decrease in the size of the phospholipid aggregate. At these saturation conditions, PEAA in the collapsed state embeds into the DPPC vesicle and leads to an increase in the aggregate size. Figure 3.65 shows the combined contributions of each form of PEAA. Above pH 7 PEAA is in the expanded state, and we see a decrease in optical density as the interactions between expanded state PEAA and DPPC vesicles increase. Below pH 7 collapsed PEAA is formed, which diminishes the number of

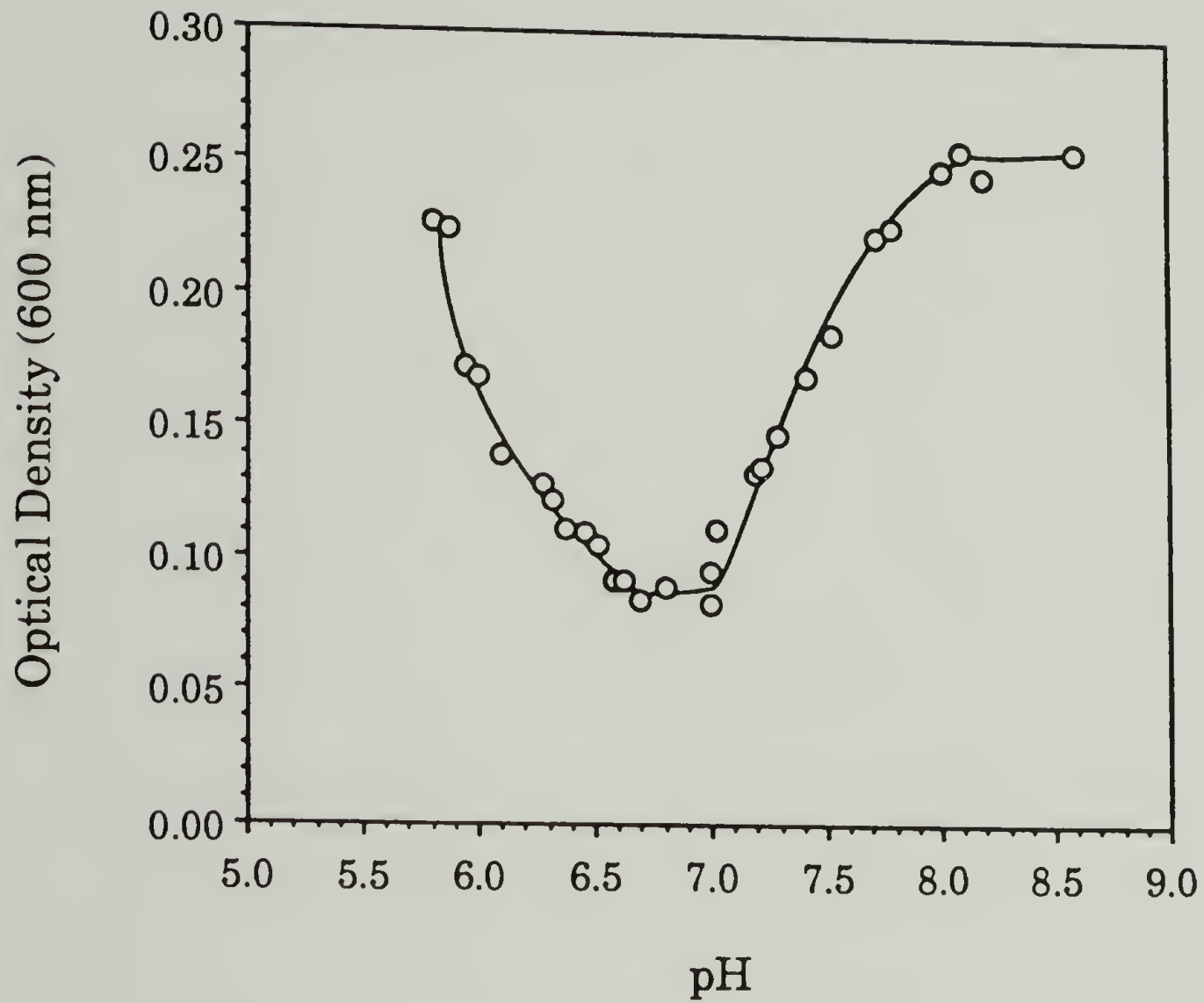


Figure 3.65 Optical density (600 nm) of 0.02 M phosphate-buffered mixtures of PEAA and sonicated DPPC vesicles as a function of pH at subsolubilizing concentrations of PEAA. The concentration of DPPC was 1 mg/ml, and the PEAA concentration was 0.07 mg/ml).

destabilizing expanded state PEAA-DPPC vesicle surface interactions, and thereby results in an increase in the measured optical density. If PEAA in the expanded state did not interact with DPPC vesicles, at subsolubilizing PEAA concentrations a decrease in optical density would not be observed as the solution pH is lowered. Also, when the concentration of embedded collapsed PEAA becomes greater than the concentration required for phospholipid solubilization, reorganization from vesicles to mixed micelles occurs.

CHAPTER IV

CONCLUSIONS

We have discovered that the mechanism for the pH dependent phospholipid vesicle reorganization is the formation of hydrophobic domains within the polyelectrolyte which act to solubilize the phospholipid. We have found that the conformational state of the polyelectrolyte determines the aggregation state of the phospholipid molecules. At high pH when the polyelectrolyte exists in an expanded coil conformation the phospholipid molecules exist in a vesicular structure. At low pH when the polyelectrolyte adopts a collapsed coil conformation the phospholipid molecules assemble with the polyelectrolyte to form mixed micelles. The responsive nature of the polyelectrolyte-phospholipid system to small changes in solution pH is due to fact the conformational transition of the polyelectrolyte occurs over a narrow pH range. It is not necessary for the polyelectrolyte to undergo a conformational change in order for the reorganization process to occur. Only the presence of large hydrophobic domains in a water-soluble molecule is required for reorganization of vesicles to mixed micelles. However, it is the existence of a conformational transition for the polyelectrolyte that enables one to control the interactions necessary for the reorganization. Any means by which one can induce a conformational transition in a hydrophobic polyelectrolyte may be used as a trigger for the formation of responsive polyelectrolyte-surfactant systems.

In the PEAA+DPPC system we have found that the pH-dependent reorganization process occurs in two main stages. The initial stage is adsorption of the PEAA chain onto the DPPC vesicle surface. In this stage

the PEAA chain exists in an expanded coil conformation. In the second stage the PEAA undergoes a conformational transition to a collapsed coil. The hydrophobic domains of the collapsed PEAA interact with the hydrophobic bilayer region of the DPPC vesicles. This hydrophobic interaction results in the reorganization of the aggregation state of the phospholipid molecules from vesicular to mixed micellar. An additional stage has been observed for the PEAA+DPPC system, which is the formation of precipitated mixed micelle aggregates. These large structures form when PEAA present in aqueous solution complexes with mixed micellar structures to form a conglomerate, as if the PEAA were acting as a crosslinking agent for the mixed micelles.

The first stage of interaction is characterized by the microscopic appearance of a rippled surface texture, a shift in the DPPC melting transition to higher temperature, an increase in the fluorescence polarization of bilayer-bound and headgroup-bound probes, an increase in energy transfer between donor groups on PEAA and acceptor groups in the DPPC bilayer, and a decrease in the formation of intramolecular excimers for a probe incorporated into the DPPC bilayer.

The second stage of the interaction between PEAA and DPPC is characterized by the appearance of small disk-like mixed micelles in electron micrographs, a decrease in the average hydrodynamic radius as detected by quasi-elastic light scattering, the clarification of the initially turbid vesicle suspension, a decrease in the fluorescence polarization of bilayer-bound probes, an increase in the lifetime of bilayer-bound probes, an increase in the fluorescence polarization of a headgroup-bound probe, a decrease in the extent of energy transfer between polymer-bound donor and

bilayer-bound acceptor, and a decrease in the intramolecular excimer fluorescence from a bilayer-bound probe.

The experimental data suggest that the first stage interaction results in an increase in the order of the DPPC bilayer. The photophysical experiments suggest that the increased bilayer order is maintained in the PEAA-DPPC mixed micellar structures. However, interpretation of the photophysical experiments is not unambiguous.

CHAPTER V

FUTURE WORK

There are several aspects of the pH-dependent PEAA-induced reorganization of DPPC vesicles which have not been fully addressed. For instance, the structural features of the PEAA/DPPC mixed micelles have not been resolved. It is uncertain how the bilayer organization of the phospholipid differs in the vesicular and mixed micellar structures. One could use the time-dependent decay of fluorescence polarization to provide insight into the organization of bilayers of these structures. The time-dependent decay of polarization reveals the extent of restriction the environment has on the angular displacement of the fluorophore. Therefore, comparison of the time-resolved decay of polarization for a probe incorporated into the phospholipid bilayer region of vesicles and mixed micelles would allow one to determine the relative bilayer order in these structures. In this type of experiment it is important to use a probe whose fluorescence lifetime is comparable to its rotational correlation time. DPH is a probe which meets this requirement, and would be useful for this investigation.

Negative-stain electron micrographs show the PEAA/DPPC mixed micelles with a disk-like structure. Due to the dehydration procedure required to obtain the negative-stain micrographs, there is some uncertainty about the actual structure of the mixed micelles in solution. Structural information may be obtained through the use of freeze-fracture electron microscopy and cryo-fixed electron microscopy. These techniques

would be most useful in providing information on the size and shape of the mixed micelles.

It would be advantageous to isolate the PEAA/DPPC mixed micelles and carry out experiments to determine the mixed micelle composition. Efforts to achieve isolation of the mixed micelles using gel column chromatography failed, due to the inability to separate the unbound PEAA from the PEAA/DPPC mixed micelles. One may attempt to isolate the mixed micelles through ultracentrifugation, which has been successfully used to isolate apolipoprotein/phospholipid mixed micelles. The analysis for PEAA and DPPC may be carried as described in Chapter II or by using ^3H or ^{14}C radio-labelled components. If an experimental technique can be found to isolate the PEAA/DPPC mixed micelles, it would be profitable to determine the mixed micelle composition as a function of solution pH and as a function of the initial ratio of PEAA to DPPC.

It has been discovered that the interaction of PEAA and DPPC to form mixed micelles follows a two-stage sequence. The first stage is interaction of PEAA with the DPPC vesicle surface, which presumably involves hydrogen bonding. The second stage is characterized by a conformational change in PEAA and the formation of mixed micellar structures. It is uncertain whether the first stage interaction is essential for the reorganization or only coincidental. We have mentioned that mixed micellar structures are formed through the interaction of various agents with phospholipid vesicles, and that characteristic to all of these agents is the presence of hydrophobic domains within a water-soluble molecule and the ability to participate in hydrogen bonding. It would be interesting to investigate the reorganization behavior of a hydrophobic water-soluble polymer that is unable to participate in hydrogen bond formation in order to

determine the relative importance of hydrophobicity and hydrogen bonding ability. Alternating copolymers of maleic anhydride and alkyl vinyl ether (with alkyl side chains having eight or ten carbon atoms) are water-soluble polymers which exist in a hypercoiled conformation even at high pH when all the carboxyl groups are ionized. In this state hydrogen bonding is not possible and there are hydrophobic domains present. The hydrophobicity of these polymers can be compared to PEAA using the ratio of pyrene emission intensities of peak 1 to peak 3. The effectiveness of these polymers compared to PEAA in causing vesicle reorganization can be studied by measuring the change in sample optical density as a function of time.

REFERENCES

1. Yatvin, M.B.; Cree, T.C.; Tegmo-Larsson, I.M., in Liposome Technology, Gregoriadis, G., Ed.; CRC Press: Boca Raton, FL, 1984, Vol. 3, pp. 157-175.
2. Tegmo-Larsson, I.M.; Hofmann, K.P.; Kreutz, W.; Yatvin, M.B., *J. Controlled Release*, 1985, 1, 191.
3. Ellens, H.; Bentz, J.; Szoka, F.C., *Biochemistry*, 1984, 23, 1532.
4. Lai, M.Z.; Vail, W.J.; Szoka, F.C., *Biochemistry*, 1985, 24, 1654.
5. Subbarao, N.K.; Parente, R.A.; Szoka, F.C.; Nadasdi, L.; Pongracz, K., *Biochemistry*, 1987, 26, 2964.
6. Okahata, Y.; Seki, T., *J. Am. Chem. Soc.*, 1984, 106, 8065.
7. Okahata, Y.; Ariga, K.; Seki, T. J., *Chem. Soc., Chem. Commun.*, 1986, 1, 73.
8. Nayar, R.; Schroit, A.J., *Biochemistry*, 1985, 24, 5967.
9. Takeyama, N.; Sakaguchi, H.; Shimomura, M.; Nakamura, H.; Kunitake, T., *Chem. Lett.*, 1985, 11, 1735.
10. Toko, K.; Nakashima, N.; Iiyama, S.; Yamafuji, K.; Kunitake, T., *Chem. Lett.*, 1986, 8, 1375.
11. Kunitake, T., *Ann. N. Y. Acad. Sci.*, 1986, 471, 70.
12. Shinkai, S.; Nakamura, S.; Ohara, K.; Tachiki, S.; Manabe, O.; Kajiyama, T., *Macromolecules*, 1987, 20, 21.
13. Seki, K.; Tirrell, D.A. *Macromolecules* 1984, 17, 1692.
14. Tirrell, D.A.; Takigawa, D.Y.; Seki, K., *Ann. N. Y. Acad. Sci.*, 1985, 446, 237.
15. Bangham, A.D.; Standish, N.M.; Watkins, J.C., *J. Mol. Biol.*, 1965, 13, 238.
16. Tanford, C., The Hydrophobic Effect, 2nd Edition, Wiley-Interscience : New York, NY, 1980.
17. Israelachvili, J.N., Intermolecular and Surface Forces, Academic Press: New York, NY, 1985, pp. 229-275.

18. Mabrey-Gaud, S. in Liposomes: From Physical Structure to Therapeutic Applications; Research Monographs in Cell and Tissue Physiology, Vol. 7, Knight, C.G., Ed., Elsevier Biomedical Press: New York, NY, 1981, pp 105-133.
19. Chapman, D., Biol. Membr. 1968, 1968, 1, 125.
20. Janiak, M.J.; Small, D.M.; Shipley, G.G., Biochemistry, 1976, 15, 4575.
21. Luna, E.J.; McConnell, H.M., Biochim. Biophys. Acta, 1977, 466, 381.
22. Fichter, F.; Schonert, H., Colloid and Polym. Sci., 1977, 255, 230.
23. Joyce, D.E.; Kurucsev, T., Polymer, 1981, 22, 415.
24. Sugai, S.; Nitta, K.; Ohno, N.; Nakano, H., Colloid and Polym. Sci., 1983, 261, 159.
25. Katchalsky, A.; Eisenberg, H., J. Polym. Sci., 1951, 6, 145.
26. Katchalsky, A., J. Polym. Sci., 1951, 7, 393.
27. Arnold, R., J. Colloid Sci., 1957, 12, 549.
28. Leyte, J.C.; Mandel, M., J. Polym. Sci., Pt. A, 1964, 2, 1879.
29. Eum, K.M.; Langley, K.H.; Tirrell, D.A., submitted for publication.
30. Anufrieva, E.V.; Birshtein, T.M.; Nekrasova, T.N.; Ptitsyn, O.B.; Sheveleva, T.V., J. Polym. Sci., Pt. C, 1968, 16, 3519.
31. Schaefer, J., Macromolecules, 1971, 4, 98.
32. Nagasawa, M., Pure Appl. Chem., 1971, 26, 519.
33. Crescenzi, V.; Quadrifoglio, F.; Delben, F., J. Polym. Sci., Pt. A-2, 1972, 10, 357.
34. Cutnell, J.D.; Glasel, J.A., Macromolecules, 1976, 9, 71.
35. Lando, J.B.; Koenig, J.L.; Semen, J., J. Macromol. Sci., Phys., 1973, B7, 319.
36. Barone, G.; Crescenzi, V.; Pispisa, B.; Qaudrifoglio, F., J. Macromol. Chem., 1966, 1, 761.
37. Chen, T.S.; Thomas, J.K., J. Polym. Sci., Polym. Chem. Ed., 1979, 17, 1103.

38. Birks, J.B., Photophysics of Aromatic Molecules, Wiley-Interscience: New York, NY, 1970.
39. Lakowicz, J.R., Principles of Fluorescence Spectroscopy, Plenum Press: New York, NY, 1983.
40. Pesce, A.J.; Rosen, C.-G.; Pasby, T.L., Fluorescence Spectroscopy; An Introduction for Biology and Medicine, Marcel Dekkar: New York, NY, 1971.
41. Chu, D.-Y.; Thomas, J.K., *Macromolecules*, 1984, 17, 2142.
42. Dale, R.E.; Chen, L.A.; Brand, L., *J. Biol. Chem.*, 1977, 252, 7500.
43. Dangreau, H.; Joniau, M.; De Cuyper, M., *Biochem. Biophys. Res. Comm.*, 1979, 91, 468.
44. Zachariasse, K.A.; Kuhnle, W.; Weller, A., *Chem. Phys. Lett.*, 1980, 73, 6.
45. Melnick, R.L.; Haspel, H.C.; Goldenberg, M.; Greenbaum, L.M.; Weinstein, S., *Biophys. J.*, 1981, 34, 499.
46. Nakajima, A., *Bull. Chem. Soc. Japan*, 1971, 44, 3272.
47. Kalyanasundaram, K.; Thomas, J.K., *J. Am. Chem. Soc.*, 1977, 99, 2039.
48. Dong, D.C.; Winnik, M.A., *Can. J. Chem.*, 1984, 62, 2560.
49. Thomas, J.K., The Chemistry of Excitation at Interfaces, American Chemical Society : Washington, D.C., 1984.
50. Ferritto, M.S.; Ponticello, I.S.; Tirrell, D.A., *Macromolecular Syntheses*, in press.
51. Schroeder, U.K.O.; Tirrell, D.A., submitted for publication.
52. Elsevier's Encyclopedia of Organic Chemistry, Series III Carboisocyclic Condensed Compounds, Vol. 14 Supplement, Radt, F., Ed., Elsevier Publishing Co.: New York, NY, 1951, p. 442S.
53. Sadtler Standard Ultra Violet Spectra, Sadtler Research Laboratories, Inc.: Philadelphia, PA, 1968, p. 14499.
54. Turro, N.J.; Arora, K.S., *Polymer*, 1986, 27, 783.
55. CRC Handbook of Chemistry and Physics, 60th Edition Weast, R.C., Ed., CRC Press: Boca Raton, FL, 1980, p. C-534.

56. Stewart, J.C.M., *Anal. Biochem.*, 1980, 104, 10.
57. Borden, K.A.; Eum, K.M.; Langley, K.H.; Tan, J.S.; Tirrell, D.A.; Voycheck, C.L., *Macromolecules*, 1988, 21, 2649.
58. Atkinson, D.; Small, D.M., *Annual Rev. Biophys. Biophys. Chem.*, 1986, 15, 403.
59. Carey, M.C.; Small, D.M., *Am. J. Med.*, 1970, 49, 590.
60. Mazer, N.A.; Benedek, G.B.; Carey, M.C., *Biochemistry*, 1980, 19, 601.
61. Galla, H.-J.; Hartmann, W.; Sackmann, E., *Ber. Bunsenges. Phys. Chem.*, 1978, 82, 918.
62. Alonso, A.; Saez, R.; Villena, A.; Goni, F.M., *J. Membr. Biol.*, 1982, 67, 55.
63. Borden, K.A.; Tirrell, D.A., unpublished results.
64. Gebhardt, C.; Gruler, H.; Sackmann, E., *Z. Naturforsch.*, 1977, 32c, 581.
65. Wilkinson, D.A.; Nagle, J.F., in Liposomes : From Physical Structure to Therapeutic Applications; Research Monographs in Cell and Tissue Physiology, Vol. 7, Knight, C.G., Ed., Elsevier Biomedical Press : New York, NY, 1981, pp. 273-297.
66. O' Leary, T.J.; Ross, P.D.; Levin, I.W., *Biophys. J.*, 1986, 50, 1053.
67. Cevc, G.; Marsh, D., Phospholipid Bilayers : Physical Principles and Models, Wiley-Interscience : New York, NY, 1987.
68. Devlin, B.P.; Tirrell, D.A., unpublished results.
69. Eum, K.M., Ph. D. Thesis, University of Massachusetts, 1988.
70. Cogan, U.; Schachter, D., *Biochemistry*, 1981, 20, 6396.
71. Suurkuusk, J.; Lentz, B.R.; Barenholz, Y.; Biltonen, R.L.; Thompson, T.E., *Biochemistry*, 1976, 15, 1393.
72. Mandel, M., *Eur. Polym. J.*, 1970, 6, 807.
73. Nagasawa, M.; Holtzer, A., *J. Am. Chem. Soc.*, 1969, 86, 538.

74. Silberberg, A. in Encyclopedia of Polymer Science and Engineering, 2nd Edition, Vol. 1, Mark, H.E. et al., Eds., Wiley-Interscience : New York, NY, 1985, pp. 577-594.
75. Prendergrast, F.G.; Haugland, R.P.; Callahan, P.J., Biochemistry, 1981, 20, 7333.
76. Barrow, D.A.; Lentz, B.R., Biophys. J., 1985, 48, 221.
77. Tremblay, P.A.; Kates, M., Chem. Phys. Lipids, 1981, 28, 307.
78. Engel, L.W.; Prendergrast, F.G., Biochemistry, 1981, 20, 7338.
79. Pottel, H.; Van der Meer, W.; Herreman, W., Biochim. Biophys. Acta, 1983, 730, 181.
80. Jonas, A.; Mason, W.R., Biochemistry, 1981, 20, 3801.
81. Matz, C.E.; Jonas, A., J. Biol. Chem., 1982, 257, 4535.
82. Herreman, W.; Van Tornout, P.; Van Cauwelaert, F.H.; Hanssens, I., Biochim. Biophys. Acta, 1981, 640, 419.
83. Uso, T.; Rossignol, M., FEBS Lett., 1984, 167, 69.
84. Parente, R.A., Lentz, B.R., Biochemistry, 1985, 24, 6178.
85. Morgan, C.G.; Thomas, E.W.; Moras, T.S., Yianni, Y.P., Biochim. Biophys. Acta, 1982, 692, 196.
86. Daems, D.; Van den Zegel, M.; Boens, N.; De Schryver, F.C., Eur. Biophys. J., 1985, 12, 97.
87. Chong, P.L.-G.; Thompson, T.E., Biophys. J., 1985, 47, 613.
88. Subczynski, W.K.; Hyde, J.S., Biophys. J., 1983, 41, 283.
89. Kido, N.; Tanaka, F.; Kaneda, N.; Yagi, K., Biochim. Biophys. Acta, 1980, 603, 255.
90. Kaneda, N.; Tanaka, F.; Kido, N.; Yagi, K., Photochem. Photobiol., 1985, 41, 519.
91. Dangreau, H.; Joniau, M.; M. De Cuyper, M.; Hanssens, I., Biochemistry, 1982, 21, 3594.
92. Morris, D.A.N.; McNeil, R.; Castellino, F.J.; Thomas, J.K., Biochim. Biophys. Acta, 1980, 599, 380.

93. Massey, J.B.; She, H.S.; Gotto, Jr., A.M.; Pownall, H.J., *Biochemistry*, 1985, 24, 7110.
94. Batenburg, A.M.; Bougis, P.E.; Rochat, H.; Verkleij, A.J.; de Kruijff, B., *Biochemistry*, 1985, 24, 7101.
95. Uemura, A.; Kimura, S.; Imanishi, Y., *Biochim. Biophys. Acta*, 1983, 729, 28.
96. Schroeder, U.K.O.; Tirrell, D.A., *Macromolecules*, in press.
97. Tall, A.R.; Small, D.M.; Deckelbaum, R.J.; Shipley, G.G., *J. Biol. Chem.*, 1977, 252, 4701.
98. Laviaille, F.; Grabielle-Madelmont, C.; Petit, J.; Ollivon, M.; Alfsen, A., *Biochemistry*, 1985, 24, 6170.
99. Goni, F.M.; Urbaneja, M.-A.; Arrondo, J.L.R.; Alonso, A.; Durrani, A.A., *Eur. J. Biochem.*, 1986, 160, 659.
100. Genz, A.; Holzwarth, J.F.; Tsong, T.Y., *Biophys. J.*, 1986, 50, 1043.
101. Morrow, M.R.; Huschilt, J.C.; Davis, J.H., *Biochemistry*, 1985, 24, 5396.
102. Fromherz, P.; Röcker, C.; Rüppel, D., *Faraday Discuss. Chem. Soc.*, 1986, 81, 39.
103. Cornell, B.A.; Middlehurst, J.; Separovic, F., *Faraday Discuss. Chem. Soc.*, 1986, 81, 163.
104. Paternostre, M.-T.; Roux, M.; Rigaud, J.-L., *Biochemistry*, 1988, 27, 2668.

BIBLIOGRAPHY

- Alonso, A.; Saez, R.; Villena, A.; Goni, F.M., *J. Membr. Biol.*, 1982, 67, 55.
- Anufrieva, E.V.; Birshstein, T.M.; Nekrasova, T.N.; Ptitsyn, O.B.; Sheveleva, T.V., *J. Polym. Sci., Pt. C*, 1968, 16, 3519.
- Arnold, R., *J. Colloid Sci.*, 1957, 12, 549.
- Atkinson, D.; Small, D.M., *Annual Rev. Biophys. Biophys. Chem.*, 1986, 15, 403.
- Bangham, A.D.; Standish, N.M.; Watkins, J.C., *J. Mol. Biol.*, 1965, 13, 238.
- Barone, G.; Crescenzi, V.; Pispisa, B.; Qaudrifoglio, F., *J. Macromol. Chem.*, 1966, 1, 761.
- Barrow, D.A.; Lentz, B.R., *Biophys. J.*, 1985, 48, 221.
- Batenburg, A.M.; Bougis, P.E.; Rochat, H.; Verkleij, A.J.; de Kruijff, B., *Biochemistry*, 1985, 24, 7101.
- Birks, J.B., Photophysics of Aromatic Molecules, Wiley-Interscience: New York, NY, 1970.
- Borden, K.A.; Eum, K.M.; Langley, K.H.; Tan, J.S.; Tirrell, D.A.; Voycheck, C.L., *Macromolecules*, 1988, 21, 2649.
- Borden, K.A.; Tirrell, D.A., unpublished results.
- Carey, M.C.; Small, D.M., *Am. J. Med.*, 1970, 49, 590.
- Cevc, G.; Marsh, D., Phospholipid Bilayers : Physical Principles and Models, Wiley-Interscience : New York, NY, 1987.
- Chapman, D., *Biol. Membr.* 1968, 1968, 1, 125.
- Chen, T.S.; Thomas, J.K., *J. Polym. Sci., Polym. Chem. Ed.*, 1979, 17, 1103.
- Chong, P.L.-G.; Thompson, T.E., *Biophys. J.*, 1985, 47, 613.
- Chu, D.-Y.; Thomas, J.K., *Macromolecules*, 1984, 17, 2142.
- Cogan, U.; Schachter, D., *Biochemistry*, 1981, 20, 6396.
- Cornell, B.A.; Middlehurst, J.; Separovic, F., *Faraday Discuss. Chem. Soc.*, 1986, 81, 163.

CRC Handbook of Chemistry and Physics, 60th Edition Weast, R.C., Ed.,
CRC Press: Boca Raton, FL, 1980, p. C-534.

Crescenzi, V.; Quadrifoglio, F.; Delben, F., *J. Polym. Sci., Pt. A-2*, 1972, 10,
357.

Cutnell, J.D.; Glasel, J.A., *Macromolecules*, 1976, 9, 71.

Daems, D.; Van den Zegel, M.; Boens, N.; De Schryver, F.C., *Eur. Biophys. J.*, 1985, 12, 97.

Dale, R.E.; Chen, L.A.; Brand, L., *J. Biol. Chem.*, 1977, 252, 7500.

Dangreau, H.; Joniau, M.; M. De Cuyper, M.; Hanssens, I., *Biochemistry*,
1982, 21, 3594.

Dangreau, H.; Joniau, M.; De Cuyper, M., *Biochem. Biophys. Res. Comm.*,
1979, 91, 468.

Devlin, B.P.; Tirrell, D.A., unpublished results.

Dong, D.C.; Winnik, M.A., *Can. J. Chem.*, 1984, 62, 2560.

Ellens, H.; Bentz, J.; Szoka, F.C., *Biochemistry*, 1984, 23, 1532.

*Elsevier's Encyclopedia of Organic Chemistry, Series III Carboisocyclic
Condensed Compounds, Vol. 14 Supplement, Radt, F., Ed., Elsevier
Publishing Co.: New York, NY, 1951, p. 442S.*

Engel, L.W.; Prendergrast, F.G., *Biochemistry*, 1981, 20, 7338.

Eum, K.M., Ph. D. Thesis, University of Massachusetts, 1988.

Eum, K.M.; Langley, K.H.; Tirrell, D.A., submitted for publication.

Ferritto, M.S.; Ponticello, I.S.; Tirrell, D.A., *Macromolecular Syntheses*,
in press.

Fichter, F.; Schonert, H., *Colloid and Polym. Sci.*, 1977, 255, 230.

Fromherz, P.; Röcker, C.; Rüppel, D., *Faraday Discuss. Chem. Soc.*, 1986,
81, 39.

Galla, H.-J.; Hartmann, W.; Sackmann, E., *Ber. Bunsenges. Phys. Chem.*,
1978, 82, 918.

Gebhardt, C.; Gruler, H.; Sackmann, E., *Z. Naturforsch.*, 1977, 32c, 581.

Genz, A.; Holzwarth, J.F.; Tsong, T.Y., *Biophys. J.*, 1986, 50, 1043.

- Goni, F.M.; Urbaneja, M.-A.; Arrondo, J.L.R.; Alonso, A.; Durrani, A.A., *Eur. J. Biochem.*, 1986, 160, 659.
- Herreman, W.; Van Tornout, P.; Van Cauwelaert, F.H.; Hanssens, I., *Biochim. Biophys. Acta*, 1981, 640, 419.
- Israelachvili, J.N., Intermolecular and Surface Forces, Academic Press: New York, NY, 1985, pp. 229-275.
- Janiak, M.J.; Small, D.M.; Shipley, G.G., *Biochemistry*, 1976, 15, 4575.
- Jonas, A.; Mason, W.R., *Biochemistry*, 1981, 20, 3801.
- Joyce, D.E.; Kurucsev, T., *Polymer*, 1981, 22, 415.
- Kalyanasundaram, K.; Thomas, J.K., *J. Am. Chem. Soc.*, 1977, 99, 2039.
- Kaneda, N.; Tanaka, F.; Kido, N.; Yagi, K., *Photochem. Photobiol.*, 1985, 41, 519.
- Katchalsky, A., *J. Polym. Sci.*, 1951, 7, 393.
- Katchalsky, A.; Eisenberg, H., *J. Polym. Sci.*, 1951, 6, 145.
- Kido, N.; Tanaka, F.; Kaneda, N.; Yagi, K., *Biochim. Biophys. Acta*, 1980, 603, 255.
- Kunitake, T., *Ann. N. Y. Acad. Sci.*, 1986, 471, 70.
- Lai, M.Z.; Vail, W.J.; Szoka, F.C., *Biochemistry*, 1985, 24, 1654.
- Lakowicz, J.R., Principles of Fluorescence Spectroscopy, Plenum Press: New York, NY, 1983.
- Lando, J.B.; Koenig, J.L.; Semen, J., *J. Macromol. Sci., Phys.*, 1973, B7, 319.
- Lavialle, F.; Grabielle-Madelmont, C.; Petit, J.; Ollivon, M.; Alfsen, A., *Biochemistry*, 1985, 24, 6170.
- Leyte, J.C.; Mandel, M., *J. Polym. Sci., Pt. A*, 1964, 2, 1879.
- Luna, E.J.; McConnell, H.M., *Biochim. Biophys. Acta*, 1977, 466, 381.
- Mabrey-Gaud, S. in Liposomes: From Physical Structure to Therapeutic Applications; Research Monographs in Cell and Tissue Physiology, Vol. 7, Knight, C.G., Ed., Elsevier Biomedical Press: New York, NY, 1981, pp 105-133.

- Mandel, M., *Eur. Polym. J.*, 1970, 6, 807.
- Massey, J.B.; She, H.S.; Gotto, Jr., A.M.; Pownall, H.J., *Biochemistry*, 1985, 24, 7110.
- Matz, C.E.; Jonas, A., *J. Biol. Chem.*, 1982, 257, 4535.
- Mazer, N.A.; Benedek, G.B.; Carey, M.C., *Biochemistry*, 1980, 19, 601.
- Melnick, R.L.; Haspel, H.C.; Goldenberg, M.; Greenbaum, L.M.; Weinstein, S., *Biophys. J.*, 1981, 34, 499.
- Morgan, C.G.; Thomas, E.W.; Moras, T.S.; Yianni, Y.P., *Biochim. Biophys. Acta*, 1982, 692, 196.
- Morris, D.A.N.; McNeil, R.; Castellino, F.J.; Thomas, J.K., *Biochim. Biophys. Acta*, 1980, 599, 380.
- Morrow, M.R.; Huschilt, J.C.; Davis, J.H., *Biochemistry*, 1985, 24, 5396.
- Nagasawa, M., *Pure Appl. Chem.*, 1971, 26, 519.
- Nagasawa, M.; Holtzer, A., *J. Am. Chem. Soc.*, 1969, 86, 538.
- Nakajima, A., *Bull. Chem. Soc. Japan*, 1971, 44, 3272.
- Nayar, R.; Schroit, A.J., *Biochemistry*, 1985, 24, 5967.
- O' Leary, T.J.; Ross, P.D.; Levin, I.W., *Biophys. J.*, 1986, 50, 1053.
- Okahata, Y.; Ariga, K.; Seki, T. J., *Chem. Soc., Chem. Commun.*, 1986, 1, 73.
- Okahata, Y.; Seki, T., *J. Am. Chem. Soc.*, 1984, 106, 8065.
- Parente, R.A.; Lentz, B.R., *Biochemistry*, 1985, 24, 6178.
- Paternostre, M.-T.; Roux, M.; Rigaud, J.-L., *Biochemistry*, 1988, 27, 2668.
- Pesce, A.J.; Rosen, C.-G.; Pasby, T.L., Fluorescence Spectroscopy; An Introduction for Biology and Medicine, Marcel Dekkar: New York, NY, 1971.
- Pottel, H.; Van der Meer, W.; Herreman, W., *Biochim. Biophys. Acta*, 1983, 730, 181.
- Prendergrast, F.G.; Haugland, R.P.; Callahan, P.J., *Biochemistry*, 1981, 20, 7333.

- Sadtler Standard Ultra Violet Spectra, Sadtler Research Laboratories, Inc.: Philadelphia, PA, 1968, p. 14499.
- Schaefer, J., *Macromolecules*, 1971, 4, 98.
- Schroeder, U.K.O.; Tirrell, D.A., *Macromolecules*, in press.
- Schroeder, U.K.O.; Tirrell, D.A., submitted for publication.
- Seki, K.; Tirrell, D.A. *Macromolecules* 1984, 17, 1692.
- Shinkai, S.; Nakamura, S.; Ohara, K.; Tachiki, S.; Manabe, O.; Kajiyama, T., *Macromolecules*, 1987, 20, 21.
- Silberberg, A. in *Encyclopedia of Polymer Science and Engineering*, 2nd Edition, Vol. 1, Mark, H.E. et al., Eds., Wiley-Interscience : New York, NY, 1985, pp. 577-594.
- Stewart, J.C.M., *Anal. Biochem.*, 1980, 104, 10.
- Subbarao, N.K.; Parente, R.A.; Szoka, F.C.; Nadasdi, L.; Pongracz, K., *Biochemistry*, 1987, 26, 2964.
- Subczynski, W.K.; Hyde, J.S., *Biophys. J.*, 1983, 41, 283.
- Sugai, S.; Nitta, K.; Ohno, N.; Nakano, H., *Colloid and Polym. Sci.*, 1983, 261, 159.
- Suurkuusk, J.; Lentz, B.R.; Barenholz, Y.; Biltonen, R.L.; Thompson, T.E., *Biochemistry*, 1976, 15, 1393.
- Takeyama, N.; Sakaguchi, H.; Shimomura, M.; Nakamura, H.; Kunitake, T., *Chem. Lett.*, 1985, 11, 1735.
- Tall, A.R.; Small, D.M.; Deckelbaum, R.J.; Shipley, G.G., *J. Biol. Chem.*, 1977, 252, 4701.
- Tanford, C., *The Hydrophobic Effect*, 2nd Edition, Wiley-Interscience : New York, NY, 1980.
- Tegmo-Larsson, I.M.; Hofmann, K.P.; Kreutz, W.; Yatvin, M.B., *J. Controlled Release*, 1985, 1, 191.
- Thomas, J.K., *The Chemistry of Excitation at Interfaces*, American Chemical Society : Washington, D.C., 1984.
- Tirrell, D.A.; Takigawa, D.Y.; Seki, K., *Ann. N. Y. Acad. Sci.*, 1985, 446, 237.

Toko, K.; Nakashima, N.; Iiyama, S.; Yamafuji, K.; Kunitake, T., Chem. Lett., 1986, 8, 1375.

Tremblay, P.A.; Kates, M., Chem. Phys. Lipids, 1981, 28, 307.

Turro, N.J.; Arora, K.S., Polymer, 1986, 27, 783.

Uemura, A.; Kimura, S.; Imanishi, Y., Biochim. Biophys. Acta, 1983, 729, 28.

Uso, T.; Rossignol, M., FEBS Lett., 1984, 167, 69.

Wilkinson, D.A.; Nagle, J.F., in Liposomes : From Physical Structure to Therapeutic Applications; Research Monographs in Cell and Tissue Physiology, Vol. 7, Knight, C.G., Ed., Elsevier Biomedical Press : New York, NY, 1981, pp. 273-297.

Yatvin, M.B.; Cree, T.C.; Tegmo-Larsson, I.M., in Liposome Technology, Gregoriadis, G., Ed.; CRC Press: Boca Raton, FL, 1984, Vol. 3, pp. 157-175.

Zachariasse, K.A.; Kuhnle, W.; Weller, A., Chem. Phys. Lett., 1980, 73, 6.

